GENERAL ATOMIC

GA-A14240
UC-77

GAS-COOLED FAST BREEDER REACTOR

QUARTERLY PROGRESS REPORT
FOR THE PERIOD NOVEMBER 1, 1976 THROUGH JANUARY 31, 1977

by

Project Staff

Prepared under
Contract EY-76-C-03-0167
Project Agreement No. 23
for the
San Francisco Operations Office
U.S. Energy Research and Development Administration

General Atomic Project 3228

Date Published: February 1977

PROGRESS REPORT SERIES

GA-5537	November 1, 1963 through July 31, 1964
GA-6667	August 1, 1964 through July 31, 1965
GA-7645	August 1, 1965 through July 31, 1966
GA-8107	August 1, 1966 through July 31, 1967
GA-8787	August 1, 1967 through July 31, 1968
GA-8895	August 1, 1968 through October 31, 1968
GA-9229	November 1, 1968 through January 31, 1969
GA-9359	February 1, 1969 through April 30, 1969
GA-9639	May 1, 1969 through July 31, 1969
GA-9811	August 1, 1969 through October 31, 1969
GA-9838	November 1, 1969 through January 31, 1970
GA-10517	February 1, 1970 through January 31, 1970
GA-10645	February 1, 1971 through April 30, 1971
GA-A10803	May 1, 1971 through July 31, 1971
GA-A10906	August 1, 1971 through July 31, 1971
GA-A12003	November 1, 1971 through January 31, 1972
GA-A12252	May 1, 1972 through July 31, 1972
GA-A12421	August 1, 1972 through October 31, 1972
GA-A12530	November 1, 1972 through January 31, 1973
GA-A12635	February 1, 1973 through April 30, 1973
GA-A12728	May 1, 1973 through July 31, 1973
GA-A12824	August 1, 1973 through October 31, 1973
GA-A12894	November 1, 1973 through January 31, 1974
GA-A13021	February 1, 1974 through April 30, 1974
GA-A13148	May 1, 1974 through July 31, 1974
GA-A13238	August 1, 1974 through October 31, 1974
GA-A13379	November 1, 1974 through January 31, 1975
GA-A13458	February 1, 1975 through April 30, 1975
GA-A13565	May 1, 1975 through July 31, 1975
GA-A13766	August 1, 1975 through October 31, 1975

GA-A13815	November 1, 1975 through January 31, 1976
GA-A13868	February 1, 1976 through April 30, 1976
GA-A13975	May 1, 1976 through July 31, 1976
GA-A14112	August 1, 1976 through October 31, 1976

ABSTRACT

The tasks of the gas-cooled fast breeder reactor (GCFR) program which are supported by the U.S. Energy Research and Development Administration include development of GCFR fuel, blanket, and control assemblies; development of the pressure equalization system for GCFR fuel; out-of-pile loop facility test programs; fuels and materials development; fuel, blanket, and control rod analyses and development; nuclear analysis and reactor physics for GCFR core design; shielding requirements for the GCFR; reactor engineering to assess the thermal, hydraulic, and structural performance of the core and the core support structure; plant systems control; systems engineering; development of reactor components, including reactor vessel, control and locking mechanisms, fuel handling equipment, core support structure, shielding assemblies, main helium circulator, steam generator, and auxiliary circulator; development of a helium circulator test facility; reactor safety, environment, and risk analyses, including planning and support of an in-pile and out-of-pile safety test program; nuclear island engineering design; and development of a reliability data bank.

CONTENTS

FIGURES

FIGURES (Continued)

FIGURES (Continued)

FIGURES (Continued)

TABLES

TABLES (Continued)

1. INTRODUCTION

The various tasks of the gas-cooled fast breeder reactor (GCFR) program for the period August 1, 1976 through October 31, 1976 sponsored by the U.S. Energy Research and Development Administration (ERDA) are discussed in this quarterly progress report. The GCFR utility program, which is sponsored by a large number of electric utility companies, rural electric cooperatives, and General Atomic (GA), is primarily directed toward the development of a GCFR demonstration plant. The utility-sponsored work and the ERDA-sponsored work are complementary.

Analytical, experimental, and fabrication development is being accomplished under the core assembly development task to establish the basis for the design of GCFR fuel, blanket, and control assemblies. Methods development for structural, thermal-hydraulic, and mechanical analyses is discussed, and the results of structural analysis of the fuel assembly components and thermal-hydraulic analysis of the blanket assembly during low power are presented. Current progress on rod spacer interaction tests, fuel assembly seismic and vibration test planning, and development of assembly fabrication techniques is also presented. The various subtasks of core asembly development and the work accomplished during this reporting period are discussed in Section 2.

The technology to support the design and construction of the pressure equalization system (PES) for GCFR fuel is being developed. This includes (1) the development of analytical models and computer codes which will be verified by test programs and testing of materials and seals and (2) the development of fabrication processes for the PES. These are discussed in Section 3.

To demonstrate the ability of GCFR fuel, control, and blanket assembly designs to meet design goals and verify predictions of analytical models, a

series of out-of-pile simulation tests will be performed. The emphasis of the tests will be on obtaining thermal-structural data for steady-state, transient, and margin conditions using electrically heated rod bundles in a dynamic helium loop. These are discussed in Section 4.

In the fuels and materials development program, thermal flux and fast flux irradiation programs are being conducted to establish conditions and design features specific to GCFR fuel rods, such as vented fuel, fission product traps, and surface-roughened cladding. In addition, a test program of smooth and surface-roughened GCFR cladding specimens is being conducted to determine how materials behave under irradiation. The fuels and materials tests, the analytical studies, and the results to date are presented in Section 5.

Under the fuel rod engineering task, performance of the fuel and blanket rods under steady-state and transient conditions is being evaluated to determine performance characteristics, operating limits, and design criteria. In addition, surveillance of the fuel rod and blanket rod technology of other programs is being carried out. These studies are presented in Section 6.

The objectives of the nuclear analysis and reactor physics task are to verify and validate the nuclear design methods which will be applied to the GCFR core design. Data from a critical assembly experimental program on the ZPR-9 facility at Argonne National Laboratory (ANL) are being used for this purpose. Critical assembly design, analysis, and methods development are discussed in Section 7.

Verification of the physics and engineering analytical methods and the data for design of the GCFR shields is being conducted under the shielding requirements task along with an evaluation of the effectiveness of various shield configurations. The results of radial shield analyses and the work being done on structural analysis are presented in Section 8.

Section 9 discusses systems engineering for the GCFR. This includes systems integration; coordination of interface requirements between plant systems; development and implementation of effective documentation management; and assessment of the thermal-hydraulic performance of the core.

Section 10 presents the evaluation and development of the main components of the GCFR which are currently in progress, including reactor vessel, control and locking mechanisms, fuel handling, core support structure, shielding assemblies, main helium circulator, steam generator, auxiliary circulator, and helium processing components.

Development of control systems and assessment of seismic- and flow-induced vibration behavior for the GCFR demonstration plant are discussed in Section 11.

The reactor safety task, which is discussed in Section 12, includes (1) maintenance of liaison between GA and other organizations and integration of the overall GCFR safety analysis effort; (2) formulation and review of a GCFR safety program plan; (3) performance of detailed safety, environmental, and risk analyses of the GCFR; (4) evaluation of the postaccident fuel containment capability of the GCFR; (5) integration of the results of ERDA safety studies into the licensing reviews; and (6) evaluation of probabilistic design methods for use in the GCFR program.

Section 13 discusses the safety test program, which involves quantification of fuel and cladding behavior during accidents leading to core damage and identification of safety test information required for licensing and commercialization of the the GCFR. The GRIST-2 and duct melting and fallaway test programs are also examined.

Section 14 discusses the nuclear island. The purposes of this task are to accomplish engineering design work on the nuclear island portion of the demonstration plant and to resolve the interface requirements of major nuclear steam supply (NSSS) and balance of plant (BOP) systems.

Section 15 is concerned with the procurement, supplying, and storage of reliability data and estimates in support of probabilistic analyses of accident events being analyzed for gas-cooled reactors.

2. CORE ASSEMBLY DEVELOPMENT (189a No. 00582)

2.1. CORE ASSEMBLY THERMAL-HYDRAULIC ANALYSIS*

2.1.1. Introduction

The analytical basis for the design and development of the GCFR fuel and control assemblies is being developed through evaluation of experimental data. Because complete prototype in-pile tests cannot be conducted, a strong analytical base supported by development tests is required to design the core assemblies. The current effort is devoted to the development of an adequate steady-state and transient analysis capability in the areas of thermal-hydraulic and structural analyses to provide a basis for assembly design criteria and specific test requirements.

During this quarter, the effort to improve thermal-hydraulic correlations and methods of applying the correlations to the design and analysis of GCFR core assemblies was continued. Hot spot analyses for fuel and blanket assemblies have been performed, and scoping analyses to guide the conceptual design of core assemblies have been conducted.

2.1.2. Fuel Assembly Analysis

2.1.2.1. FLOMAX Development. Evaluation of the FLOMAX thermal analysis code continued during this quarter with several calculations of a model of the BR-2 assembly, shown in Fig. 2-1. A very severe power tilt was used, as indicated by the power factors below the rod numbers in Fig. 2-1, to emphasize the differences in the temperatures calculated by FLOMAX and COBRA. For comparison, the factors corresponding to the maximum GCFR power tilt (1 kW per rod per row or a 1.35 maximum to average tilt for

*The nomenclature in this section is given in Table 2-1.

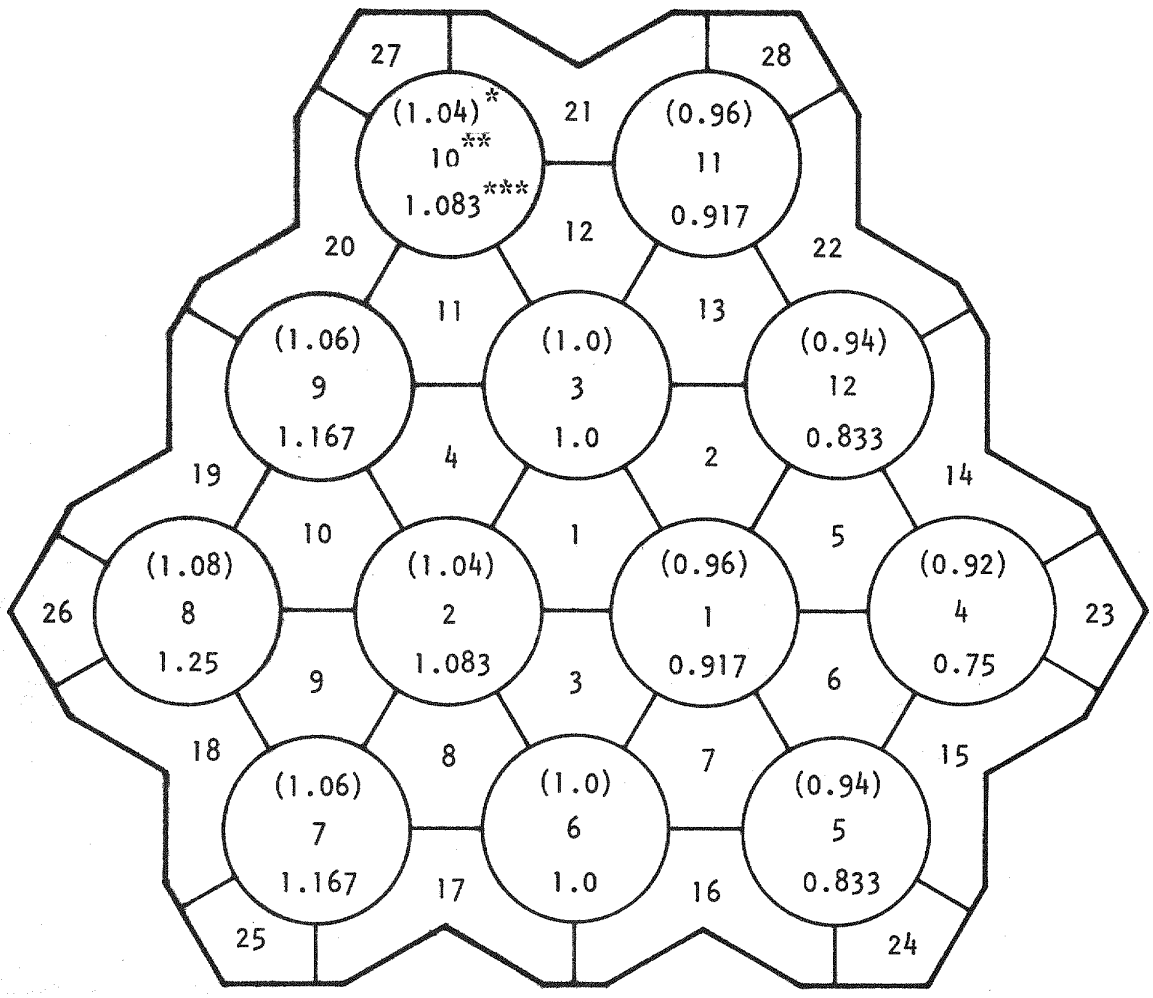

Fig. 2-1. Subchannel model of the BR-2 assembly for evaluation of FLOMAX

TABLE 2-1
NOMENCLATURE

A	area (mm^2)
D	diameter (mm)
f	friction factor
h	rib height (mm)
K_2	empirical factor in Warburton-Pirie transformation (Eq. 2-2)
K_3	empirical factor in Warburton-Pirie transformation (Eq. 2-2)
L	length (mm)
Δp	differential pressure (N/m^2)
Re	Reynolds number
r_1	rod radius (mm)
r_2	tube radius (mm)
St	Stanton number
U	velocity (m/s)
X	parameter in K_3 equation
ε	relative roughness
ρ	density (kg/m^3)

Subscripts

a	whole annulus
h	hydraulic
s	smooth
x	ratio
1	inside radius of zero shear
2	outside radius of zero shear

the whole assembly) are shown in parentheses above the rod numbers. It can be seen that in this model the hottest rods are on the left and the coolest on the right. Thus, subchannel 26 is the hot channel, 23 is the cold channel, and 1 is the average channel.

The results of the calculations with FLOMAX and COBRA are shown in Fig. 2-2. The agreement between the two codes is excellent for the hot channel (26) and the average channel (1). The agreement is not so good for the cold channel (23). Since FLOMAX uses an approximate integration (the Galerkin method) for computational efficiency, an empirical eigenvalue factor was built into the code and adjusted to give better agreement for channel 23. A 10% change in this factor resulted in better agreement without changing the other temperatures too much; however, considerable disagreement still persisted. It is possible that this disagreement is not due to an inaccuracy in FLOMAX but due to an error in COBRA. The latter code always exhibits a negative heat balance error.

Calculations are in progress with more realistic power tilts (the bracketed numbers in Fig. 2-1) which will result in smaller differences. It is possible that with the realistic power tilts, the agreement between the codes will be adequate for design calculations. These calculations were done for a flat axial power profile, and, calculations are now in progress for a chopped cosine axial power profile.

2.1.2.2. Inverse Transformation for Assembly Subchannel Thermal-Hydraulic Analysis. Subchannel thermal-hydraulic analysis computer codes such as FLOMAX and COBRA use correlations of friction factor (f) and Stanton (St) or Nusselt (Nu) numbers to calculate pressure drops and surface temperatures. Correlations of friction factor and Stanton number were developed from test data for single, heated, roughened rods mounted in annular flow tubes. The test data were first "transformed" to separate the effects on the flow field on the smooth outer tube wall from those of the rough inner rod. The procedure for correlating the friction factor and Stanton number data is described in Refs. 2-1 and 2-2.

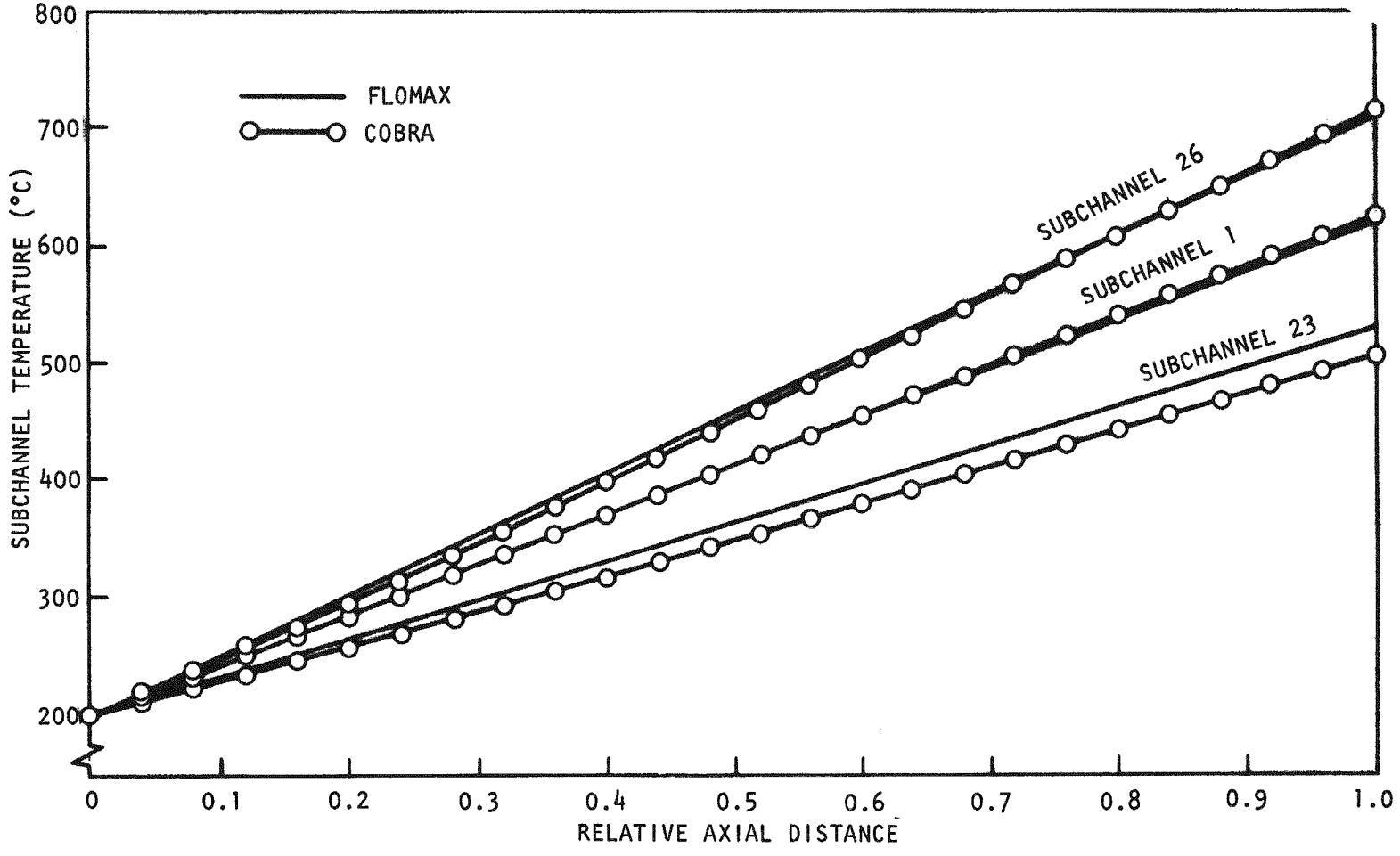

Fig. 2-2. Comparison of subchannel temperatures

A method has been developed for determining the friction factor for the peripheral subchannels of a fuel assembly. The inverse of the Warburton-Pirie transformation has been derived to combine the effects of the rough rod surface and the smooth duct wall into an effective friction factor for the channel. This technique has been programmed and is currently being used in the subchannel analysis codes to predict thermal-hydraulic performance of rod bundles.

The original Warburton-Pirie transformation equations (Ref. 2-3) were derived again using the method of Markoczy (Ref. 2-4) to modify the terms requiring raw pressure drop data, and one of the empirical relationships was modified to provide closer agreement with a transformation technique developed by Dalle Donne (Ref. 2-5). The justification for this approach and the derivation of the transformation equations are given in Ref. 2-1. The resulting equations are as follows:

$$\frac{f_1}{f_a} = \left[1 + A_x(K_2 - 1)\right]^2 \frac{1 - A_x}{1 - P_x} \quad , \tag{2-1}$$

$$\frac{f_a}{f_s} = \frac{K_2^2 K_3 P_x}{\left[1 + A_x(K_2 - 1)\right]^2 A_x} \quad , \tag{2-2}$$

$$\frac{Re_1}{Re_a} = \left[1 + A_x(K_2 - 1)\right]^{-1} \frac{1 - A_x}{1 - P_x} \quad , \tag{2-3}$$

where $A_x = \dfrac{r_2^2 - r_o^2}{r_2^2 - r_1^2}$,

$$P_x = \frac{r_2}{r_1 + r_2} \quad ,$$

$$K_2 = 0.114 r_1/r_2 + 0.97 \quad ,$$

$$K_3 = 1.0194 + 0.02931 f_1/f_s \quad .$$

Solving Eqs. 2-1 and 2-2 for f_a, subtracting one from the other, and dividing out common terms yields

$$F \equiv f_s K_2^2 K_3 \frac{P_x}{A_x} - f_1 \frac{1 - P_x}{1 - A_x} = 0 \quad . \tag{2-4}$$

Knowing the geometry of the subchannel (r_1, r_2, h_{rib}) and the Reynolds number (Re_a), the following procedure is used to calculate the friction factor (f_a):

1. The smooth tube friction factor based on the Drew, Koo, McAdams correlation is calculated by

$$f_s = 0.0056 + 0.5 Re_a^{-0.32} \quad .$$

2. A value for the radius of zero shear (r_o) is assumed.

3. The A_x and P_x functions are calculated along with relative roughness

$$\epsilon_1 = \frac{h_{rib} r_1}{2(r_o^2 - r_1^2)} \quad .$$

4. The transformed Reynolds number is calculated from Eq. 2-3.

5. The transformed friction factor is calculated from the data correlation of the form

$$f_1 = f_1(Re_1, \varepsilon_1) \quad .$$

6. The empirical factor K_3 is calculated.

7. F is evaluated from Eq. 2-4, compared with zero, and iterated from step 2 until adequate convergence is achieved.

8. f_a is calculated from Eq. 2-1 or 2-2.

After the initial calculation, the secant method is used to select r_o for the subsequent iteration. This simple procedure has been found to converge rapidly, usually within five iterations, to a tolerance of 10^{-5}.

A function subprogram called SIDE has been written to calculate f_a using the procedure outlined above. It also calculates the subchannel Stanton number (St_a) from the Nathan-Pirie equation, calling on the function subprograms FCENT and STCENT, which contain the correlations for the transformed parameters. The procedure has been verified using data from the Swiss Federal Institute for Reactor Research (EIR) to calculate known inverse friction factor and Reynolds number values. This new inverse Warburton-Pirie subprogram has been used with FLOMAX and COBRA to predict the pressure drops in the BR-2 bundle for comparison with calibration experiment test results.

2.1.2.3. Hot Spot Analysis for the GCFR Fuel Assembly. Hot spot factors for the GCFR fuel assembly have been defined at the 2σ confidence level to limit the maximum midwall cladding temperature to 700°C. Hot spot subfactors are defined as

$$F_{b_a} = 1 + \left(\frac{\Delta T_b}{\Delta T_n}\right)_a \quad ,$$

where F_{b_a} = subfactor for the effect of parameter b on component a,

ΔT_n = nominal temperature difference of component a,

ΔT_b = temperature deviation of component a due to deviation of parameter b.

The uncertainties affecting the temperature of the coolant, film, and cladding have been divided into two groups. Uncertainties which occur randomly (e.g., manufacturing and assembling tolerances, properties of materials and correlations) are treated as statistical subfactors; nonrandom components (uncertainties in calculations and measurements) are directly added as cumulative subfactors. The statistical subfactors are combined to give a total statistical factor f_{s_a} according to the equation

$$f_{s_a} = \sqrt{\sum_i (f_{i_a} - 1)^2} + 1 \quad ,$$

and the total direct factor f_{c_a} is given by

$$f_{c_a} = \Pi f_{i_a} \quad .$$

The overall hot spot factor for component a is then defined as

$$F_a = f_{s_a} \cdot f_{c_a} \quad .$$

The subfactors for each of the three components are listed in Table 2-2. The group of statistical factors consists of engineering tolerances

TABLE 2-2
HOT SPOT FACTORS FOR 300-MW(e) GCFR FUEL CLADDING[a]

Parameter	Uncertainty 3σ (%)	Channel Factor F_c	Film Factor F_f	Cladding Factor F_{cl}
Statistical factors				
Tolerances				
Fuel rod pitch	0.5	1.011	1.001	1.000
Grid spacer	1.0	1.000[b]	1.000[b]	1.000[b]
Bowing	1.1	1.000[b]	1.000[b]	1.000[b]
Cladding o.d.	0.27	1.003	1.000[b]	1.000
Cladding o.d. } cladding thickness	0.27	1.000	1.000	1.034
Cladding i.d. } cladding thickness	0.31			
Cladding o.d. to i.d. eccentricity	4.8	1.000	1.000	1.030
Pellet o.d. } pellet size	0.64	1.015	1.015	1.014
Pellet i.d. } pellet size	4.0		1.035	1.035
Pellet density } pellet fissile content	3.5, local			
Pellet enrichment } pellet fissile content	0.5, zonal	1.006		
Orifice tolerance	5.0	1.050	1.040	1.000
Rib height	10	1.016	1.000	1.000
Swelling } negligible at location of hot spot		1.000	1.000	1.000
Creep and duct dilation } negligible at location of hot spot				
Correlations and properties				
Specific heat of coolant	0.5	1.000	1.002	1.000
Density of coolant	0.5	1.000	1.002	1.000
Viscosity of coolant	4.5	1.000	1.030	1.000
Conductivity of coolant	7.2	1.000	1.040	1.000
Conductivity of cladding	10.0	1.000	1.000	1.100
Film coefficient	10.0	1.000	1.100	1.000
Friction factor	10.0	1.002	1.007	1.000
Mixing	60	1.000	1.000	1.000
Total				
3σ		1.056	1.125	1.116
2σ		1.037	1.083	1.077
Cumulative factors	Error (%)			
Thermohydraulic analysis	2.0	1.020	1.020	1.020
Radial peaking } physics methods		1.040	1.050	1.050
Axial peaking } physics methods				
Control rod peaking } physics methods				
T-heating				
Inlet flow maldistribution in plenum	0.5	1.005	1.004	1.000
Inlet temperature[c]	6°C	1.005	1.004	1.000
Axial variation of film coefficient	-70	1.000	1.067	1.000
Total		1.071	1.152	1.000
Overall hot spot factors				
3σ		1.131	1.296	1.195
2σ		1.111	1.248	1.153

[a] All values are for full-power steady-state conditions.

[b] Values indicated are insignificantly greater than 1.

[c] In addition, inlet temperature directly raises the temperature of all the components.

and property and correlation uncertainties. The manufacturing and assembly value deviations are assumed to have normal Gaussian distribution with the tolerances at the 3σ confidence level. The overall hot spot factors at the 2σ and 3σ confidence levels are shown in Table 2-2; a design margin of 4% is added to each factor. At 2σ,

channel factor F = 1.155,
film factor F_f = 1.298,
cladding factor F_{cl} = 1.200.

2.1.2.4. Thermal-Hydraulic Design Analysis. Selection of the proper edge spacing for the fuel rods in the fuel assembly is very important owing to its impact on the temperature gradient across the edge fuel rods. The choice of edge spacing is made more difficult by the fact that the temperature gradient across the edge rods changes direction at the elevation of smooth to rough transition of the fuel rod. During this quarter, analysis to select a suitable edge spacing was initiated.

2.1.3. Radial Blanket Assembly Analysis

2.1.3.1. Methods Development. The thermal-hydraulic analysis of the blanket assembly is complicated by the large radial power gradients which exist in this region of the core and by the spiral-wrapped wire spacers, which have two important effects: the wires cause a local coolant sweeping motion to occur between subchannels, and the low rod pitch-to-diameter ratio caused by the use of the wire results in comparatively large temperature gradients around the circumference of the rod. Up to now, these effects have been investigated using the COBRA III-C subchannel analysis code without a wire-wrap mixing model. The effects of flow sweeping have been approximated by increasing the turbulent mixing factor. In addition, the currently used code does not provide for conduction in the cladding and will not adequately handle transient flow problems. For these reasons, a survey is being made of new subchannel analysis codes which have these capabilities; the codes currently under investigation are listed in

Table 2-3. From this survey, a code will be selected for future thermal-hydraulic analysis of the GCFR blanket assembly.

One of these codes, COBRA-IV was received from Battelle Northwest Laboratory (BNWL) during this quarter, and efforts are under way to make it operational on the UNIVAC 1110 system. A number of procedures which are incompatible with the UNIVAC 1110 have been modified, and the code has been successfully compiled and mapped. One of the accompanying sample cases was run, and the results are being evaluated. COBRA-IV is a considerable improvement over the previous version; however, although it provides for axial conduction in the fuel rod cladding, it does not consider circumferential conduction.

For thermal-hydraulic analysis of the radial blanket assembly, the subchannel areas and wetted perimeters must be sized under operating conditions of temperature and pressure and corrected for the presence of the wire spacers. To generate this information, a code entitled PANIC has been written. This code uses specified cladding dimensions and clearances and calculates the parameters necessary for input to the subchannel analysis codes.

2.1.3.2. Preliminary Analysis of Hot Spot Factors for the Radial Blanket Blanket Assembly. Preliminary evaluation of the blanket hot spot factors was carried out for the low-pressure-drop (155 kPa) core; the analysis was conducted in a manner similar to that for fuel hot spot factor analysis. Most of the parameters affecting the fuel assembly temperatures also affect the blanket assembly temperatures. However a few factors are peculiar to the blanket, and these are described below.

1. The pitch of the blanket rods is defined by the sum of the rod and wire diameters.

2. Any one subchannel has a minimum flow area when both diameters are at their minimum tolerance limits.

TABLE 2-3
SUBCHANNEL ANALYSIS COMPUTER CODES

Code Name	Source
COBRA-IV	Battelle Pacific Northwest Laboratories
COTEC	Westinghouse Electric Corporation
ENERGY I, II, III	Massachusetts Institute of Technology
FORCMX	Atomics International
FULMIX	General Electric Corporation
ORRIBLE	Oak Ridge National Laboratory
RETSAC	Rand Corporation
SIMPLE-2	Argonne National Laboratory
SWEEP	Argonne National Laboratory
THI3D	Argonne National Laboratory

3. Pellet fissile content is a manufacturing tolerance and does not apply to the blanket.

4. Flow sweeping is forced mixing in a preferred direction by the wire wrap; uncertainties in the flow sweeping correlation and the wire wrap orientation are included in this analysis.

5. Circumferential variations of the heat transfer coefficient are large in the blanket assemblies owing to the wire wrap and the small pitch-to-diameter ratio.

The overall factors were calculated by the semistatistical method, and the subfactors and overall hot spot factors are presented in Table 2-4. With the 4% design margin, the overall hot spot factors at the 2σ confidence level are

channel factor F_c = 1.197,
film factor F_f = 2.287,
cladding factor F_{cl} = 1.250.

2.1.3.3. Thermal-Hydraulic Design Analysis. The proposed reduction of the GCFR core pressure drop from 293 to 155 kPa has resulted in a redesign of the radial blanket assembly. Scoping studies to re-evaluate the performance parameters for the low-ΔP core design have been continued.

The effects of wire diameter (rod spacing) on assembly temperatures have also been studied. As the wire diameter and rod pitch-to-diameter ratio decrease, the circumferential temperature gradient in the rod cladding increases; this effect is illustrated in Fig. 2-3 for a 61-rod assembly. Similarly, as wire size decreases, the total coolant temperature rise through the assembly increases, as illustrated in Fig. 2-4. In this figure, blanket coolant temperature rise is expressed as a percent of fuel assembly coolant temperature rise; the larger this percentage, the smaller the degradation in the core mixed mean outlet temperature.

TABLE 2-4
HOT SPOT FACTORS FOR 300-MW(e) RADIAL BLANKET[a]

Parameter	Uncertainty 3σ (%)	Channel Factor F_c	Film Factor F_f	Cladding Factor F_{cl}
Statistical factors				
Tolerances				
Cladding o.d. } rod Wire o.d. } pitch	0.06 0.90	1.071	1.013	1.000
Wire-wrap orientation		1.010	1.000	1.000
Bowing	∿1.0	1.000	1.000	1.000
Cladding o.d. } cladding Cladding i.d. } thickness	0.06 0.06	1.000	1.000	1.018
Cladding o.d. to i.d. eccentricity	4.0	1.000	1.000	1.018
Pellet o.d.	0.12	1.003	1.003	1.002
Orifice tolerance	5.0	1.050	1.040	1.000
Swelling Creep and duct } negligible at location of hot spot Dilation		1.000	1.000	1.000
Correlations and properties				
Specific heat of coolant	0.5	1.000	1.002	1.000
Density of coolant	0.5	1.000	1.002	1.000
Viscosity of coolant	4.5	1.000	1.030	1.000
Conductivity of coolant	7.2	1.000	1.040	1.000
Conductivity of cladding	10.0	1.000	1.000	1.100
Heat transfer coefficient	10.0	1.000	1.100	1.000
Friction factor	14.0	1.025	1.040	1.000
Flow sweeping correlation	50.0	1.034	1.000	1.000
Nuclear data		1.080	1.090	1.090
Total				
3σ		1.126	1.150	1.137
2σ		1.084	1.100	1.091
Cumulative factors				
Thermohydraulic analysis	2.0	1.020	1.020	1.020
Axial peaking T-heating Radial peaking } physics methods		1.030	1.080	1.080
Inlet flow maldistribution in plenum	0.5	1.005	1.004	1.000
Inlet temperature[b]	6°C	1.006	1.004	1.000
Circumferential variation of heat transfer coefficient	50	1.000	1.800	1.000
Total		1.062	1.999	1.102
Overall hot spot factors				
3σ		1.196	2.299	1.253
2σ		1.151	2.199	1.202

[a] All values are given for full-power steady-state conditions.

[b] In addition, inlet temperature directly raises the temperature of all the components.

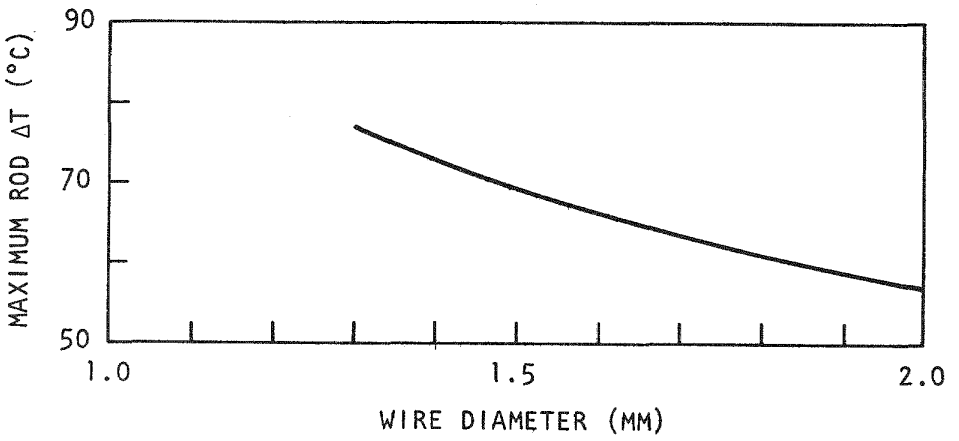

Fig. 2-3. Effect of wire diameter on maximum temperature difference across rod

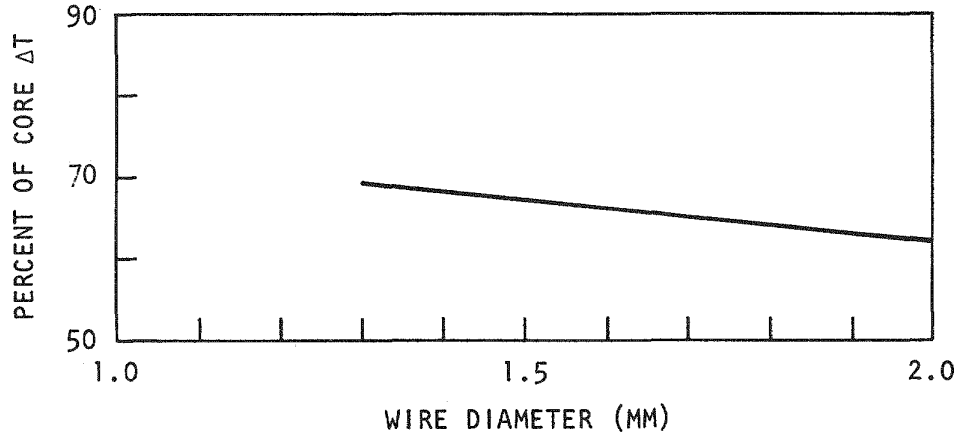

Fig. 2-4. Effect of wire diameter on blanket assembly coolant temperature increase

2.2. CORE ASSEMBLY MECHANICAL ANALYSIS

2.2.1. Introduction

During the previous quarter, three areas of core assembly mechanical analysis were investigated: (1) duct bowing analyses were performed to examine the effect of recent changes in the correlations for irradiation creep and volume swelling; (2) the computer code WRAPUP was made operational to analyze wire-wrap spacer systems in the GCFR blanket assemblies; and (3) a parametric study of the seismic performance of new fuel assembly designs having various duct configurations was completed.

2.2.2. Core Static Analysis

2.2.2.1. Outer Row Fuel Assembly Bowing. A reassessment of the 300-MW(e) GCFR outer row fuel assembly flow duct has been made using the latest irradiation creep and volume swelling correlations. The CRASIB code was used to calculate unrestrained bowing, and the results were compared with those obtained previously. A 50-element model was employed (Fig. 2-5). Figure 2-5 also presents input flux (normalized) and temperature data; temperature is plotted in Fig. 2-6. With the exception of the creep and swelling correlations, these data are the same as those used over the past 2 yr. Some slight dimensional changes have been taken into consideration.

Of primary concern is the maximum deflection for an unrotated assembly which occurs at the assembly outlet at the end of life (18,000 hr). The displacement from the undistorted centerline was calculated to be 57.63 mm (compared with 48.34 mm from earlier analyses). This increase is entirely due to the increased volume swelling based on current material correlations. If a 180-deg rotation is imposed on the assembly, the maximum deflection is reduced to 28.91 mm hot and 20.05 mm cold (in contrast to 21.74 mm and 13.66 mm, respectively, from previous analyses) (Ref. 2-6).

More detailed analyses are necessary for considering possible interference between adjacent assemblies. Since this study was performed with

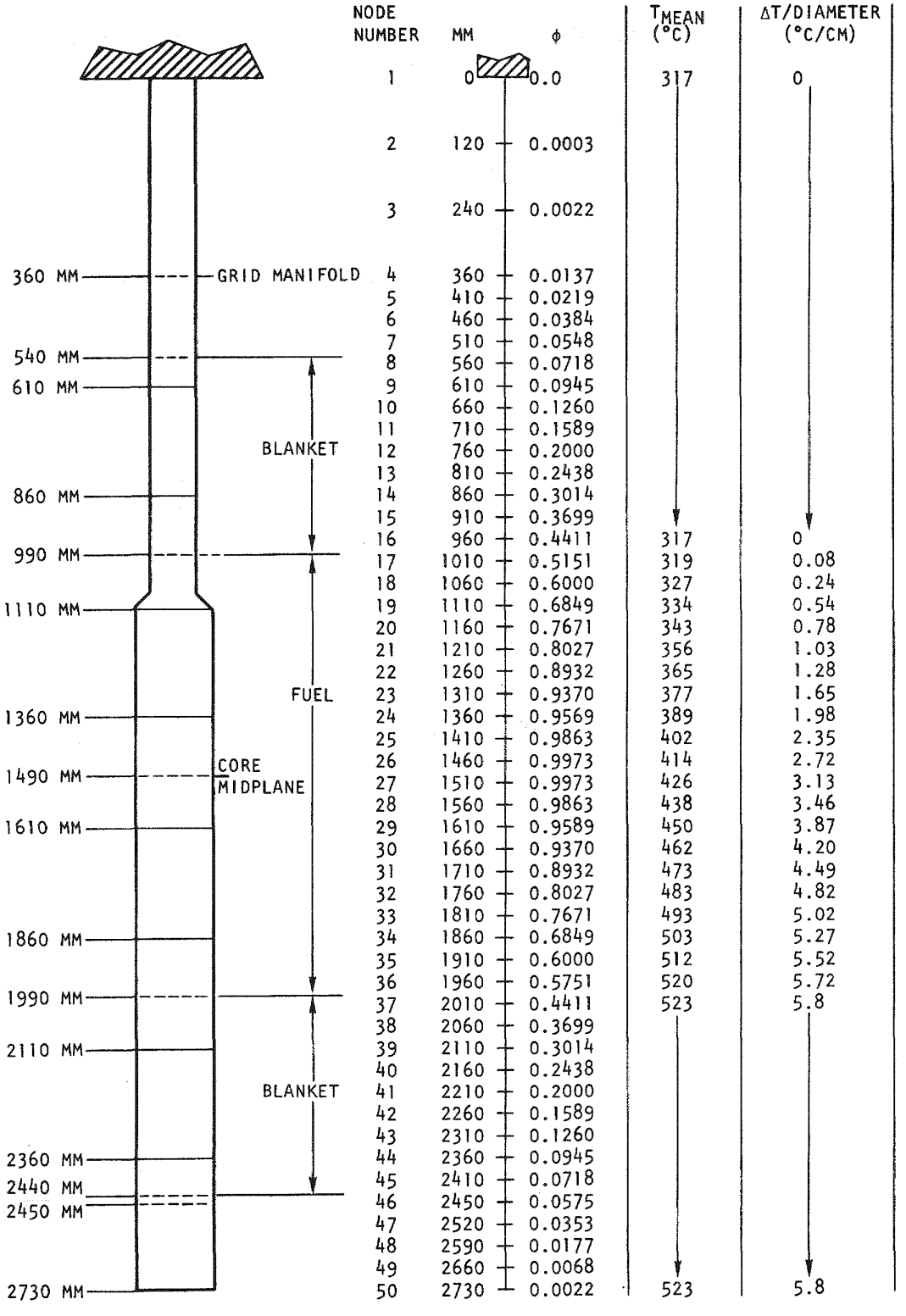

Fig. 2-5. Fifty-element model

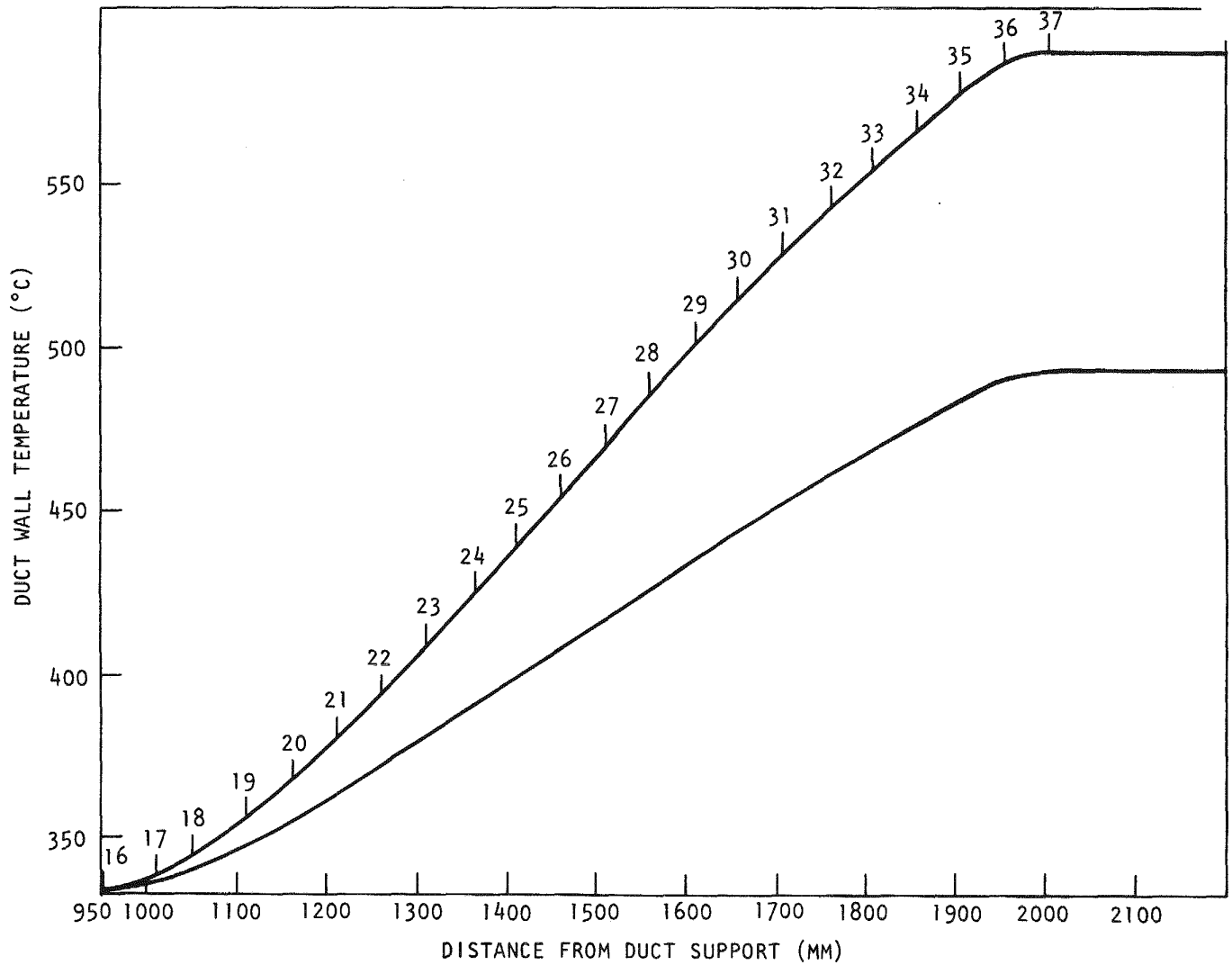

Fig. 2-6. Duct temperature vs axial position

data from an outer row assembly, it is the worst case, because bowing distortion decreases with decreasing distance from the core center. Future efforts will concentrate on predicting combined dilation and bowing distortion and assembly interference.

2.2.2.2. Mechanical Analysis of Wire-Wrapped Systems. Recent changes in the GCFR radial blanket assembly (Ref. 2-7) include the adoption of a wire-wrapped spacer system for the rods. The computer code WRAPUP is being utilized to analyze the performance of the wire wrap and its effects on the cladding. This code was originally developed at Westinghouse to analyze the same conditions on the fast flux test facility (FFTF) fuel rods. The code has been made operational on the GA computer, and a sample problem has been run using GCFR blanket rod dimensions. The results from this sample problem are consistent with those previously obtained for the FFTF rods (Ref. 2-8).

The current version of the code includes swelling, thermal creep, and irradiation-induced creep formulations from 1971, when the code was written and the final FFTF pin design analyzed (Ref. 2-8). Prior to doing a full parametric study for the GCFR blanket rod involving wire-wrap preload, pitch, and wire size, the latest formulations for creep and swelling will have to be incorporated in the code. An effort to do this will be made in the near future.

Figure 2-7 shows the results of the sample problem, and the pertinent input data are shown in Table 2-5. Upon going to power, the wire load increases dramatically from the initial preload of 22.5 N to 187.71 N, giving the highest stress in the wire of 1.225×10^8 Pa. This increase in load is reasonable to expect since the wire temperature always lags behind the cladding, and the differential expansion between the two causes an increase in the wire load. Following the initial rise to power, the load decreases owing to thermal creep to a low value of 1.07 N after 7000 hr. Up to this time, there is an insignificant amount of swelling and irradiation creep, causing all three cases (maximum swelling - maximum creep, nominal swelling - nominal creep, and minimum swelling - minimum

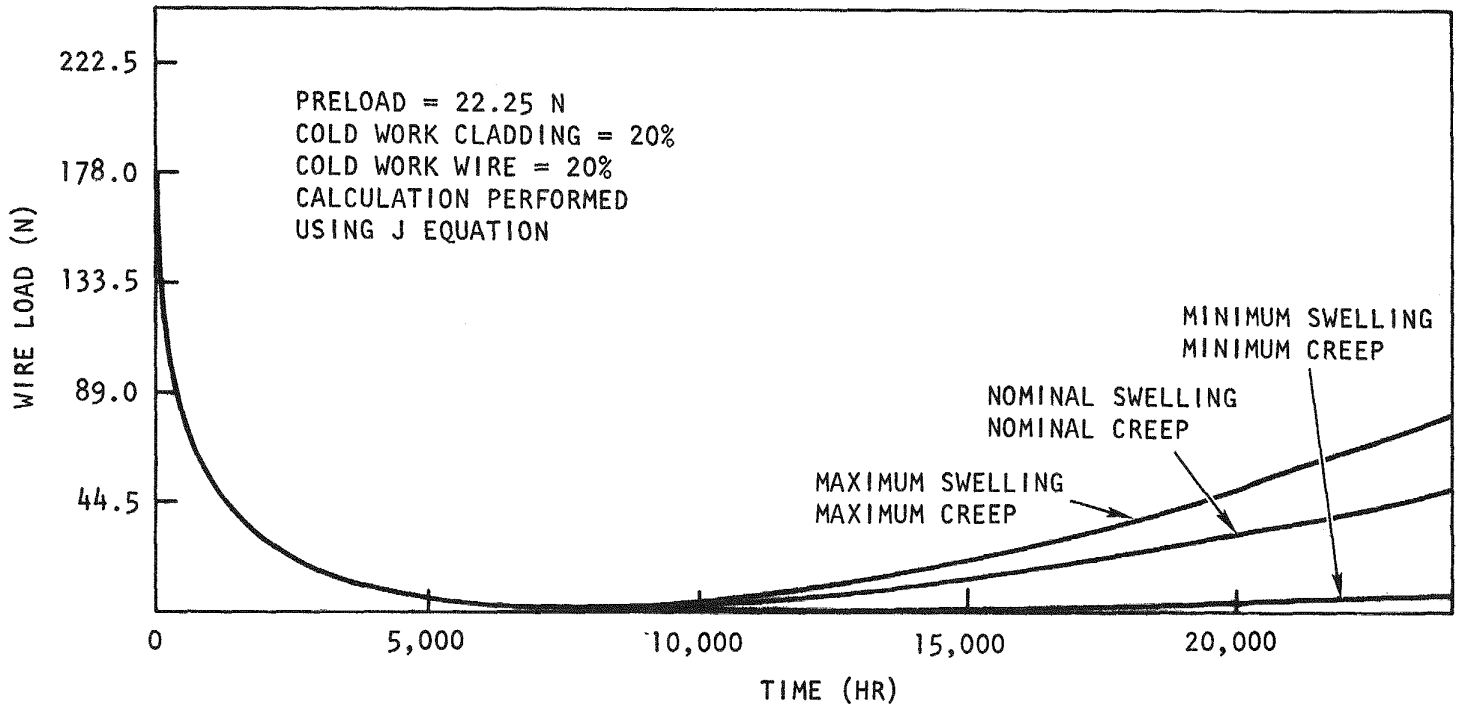

Fig. 2-7. Blanket rod design

TABLE 2-5
BLANKET ROD MECHANICAL DESIGN PARAMETERS

Blanket rod i.d. (mm)	21.60
Cladding thickness (mm)	0.50
Wire diameter (mm)	1.40
Wire preload (N)	22.25
Length of rod, weld to weld of wire wrap (mm)	2,165
Lifetime (hr)	24,000
Number of wire-wrap cycles	7
Cold work of cladding (%)	20
Cold work of wire (%)	20

creep) to follow the same load curve. After this time, the three cases diverge, as expected, to give distinct loading curves for each.

The sample problem is not too unreasonable from a design point of view, given a maximum wire temperature of 500°C and an allowable stress of 1.52×10^8 Pa (Ref. 2-8). This sample problem meets the following two criteria:

1. The maximum stress is well below the allowable stress level (1.225×10^8 versus 1.52×10^8 Pa).

2. The wire never slackens (minimum load of 1.07 N).

Having met these two criteria, there is little left to design. The task now is to obtain a similar design using the latest formulations for swelling and creep.

2.2.3. Core Dynamic Analysis: Fuel Assembly Seismic Response

A study of fuel assemblies having various duct configurations was done using the structural analysis program MODSAP (GA version of SAPIV) to assess assembly seismic response. Duct wall thickness and across-flats width was varied, and consideration was given to stepped- and uniform-thickness ducts. It was necessary to analyze two core lengths: (1) 1000 mm, which was the length used for the Preliminary Safety Information Document (PSID) (Ref. 2-9) reference fuel assembly design and served as the basis for comparison with other designs and (2) 1130 mm, which is the length used in all current assembly designs.

Because reliable input seismic forcing functions (time histories or response spectra) for the core assemblies for the current design of the 300-MW(e) GCFR will not be available until about mid-1977, it is impossible to directly compare the magnitudes of seismic response for different assembly designs. In lieu of this, the assumption was made that the PSID reference high-ΔP design is adequate from a seismic response

standpoint and other assembly designs which have a fundamental frequency near or greater than that of the PSID reference high-ΔP assembly are also adequate. This implies that the effective grid plate response spectrum is relatively flat in the frequency range of interest. Although previous analyses have shown that this may not be the case, until a good determination of the response spectrum is made, the assumption of a flat spectrum is most reasonable.

The MODSAP finite-element structural analysis program was used for this study. The assembly was modeled using 13 linear elastic beam elements (Figs. 2-8, 2-9) whose stiffness was taken to be the local stiffness of the assembly duct (accounting for the temperature dependence of Young's modulus); the small stiffness of the rod bundle was neglected. The mass of the rod bundle was distributed with the local duct mass at each beam, but no attempt was made to include the masses of the grid spacers or the flow control orifice since these masses make up a relatively small fraction of the total assembly mass and will not significantly affect the relative ranking of different designs. The total mass accounted for was 361 kg for the low-ΔP reference design. The assembly was assumed to be clamped at the grid plate, and although the absolute magnitude of the frequencies will vary somewhat if this assumption is changed, the relative rankings should be unaffected.

The first five natural modes of assembly vibration were determined from the models, and the corresponding mode shapes for a typical case are shown in Figs. 2-10 through 2-14. Mode 4 is indicated to be a duct stretching mode and is an erroneous mode introduced by modeling simplifications. This has no effect on the study since the item of primary interest is the fundamental assembly frequency.

Table 2-6 given the fundamental assembly frequencies for the various duct configurations examined. The fundamental frequency of the PSID reference design high-ΔP assembly was found to be 10.4 Hz. As can be seen from the table, low-ΔP designs with ducts having a stepped thickness of 3.8/2.5 mm have a frequency equal to or greater than 10.4 Hz, indicating

ALL DIMENSIONS IN MILLIMETERS

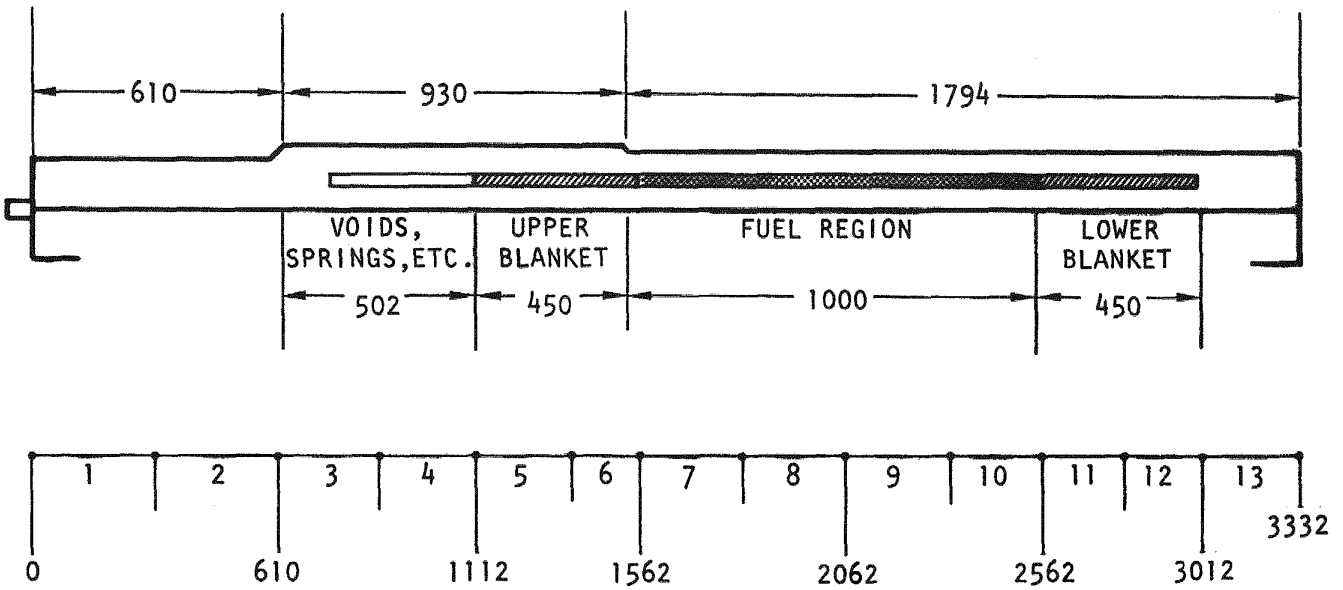

Fig. 2-8. High-ΔP fuel assembly reference design

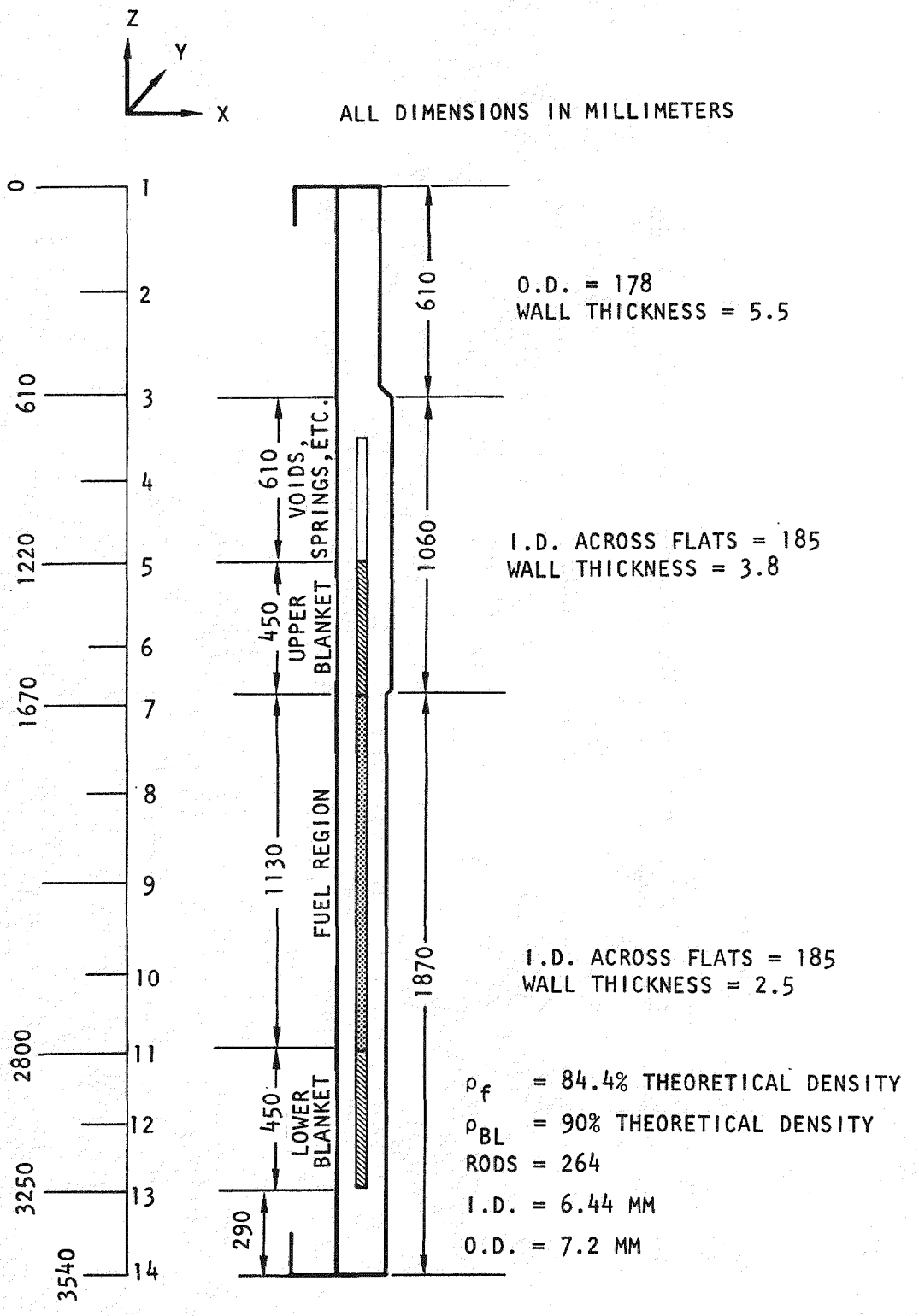

Fig. 2-9. Low-ΔP fuel assembly reference design

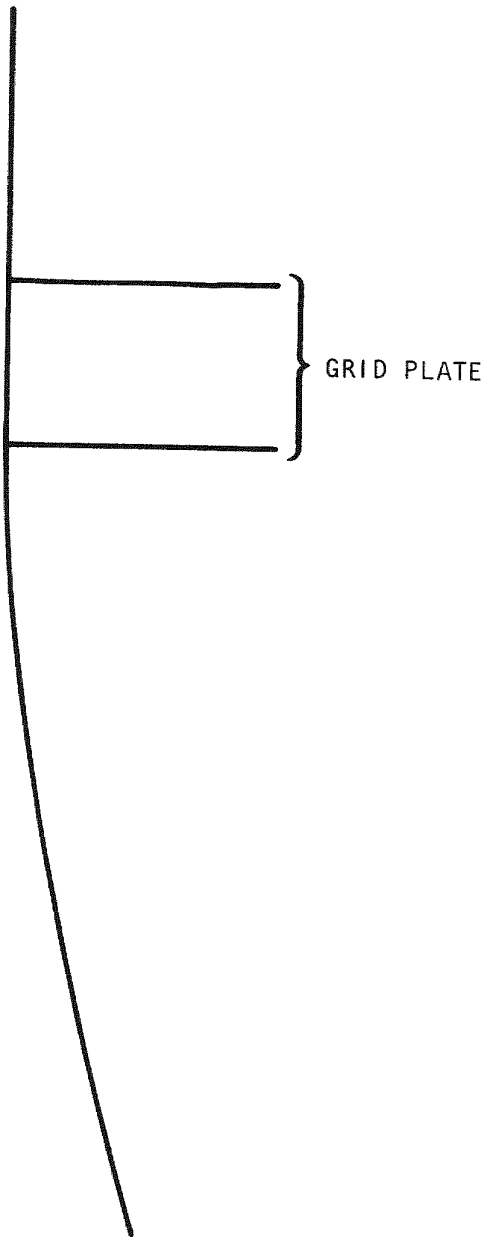

Fig. 2-10. Low-ΔP reference design, mode 1

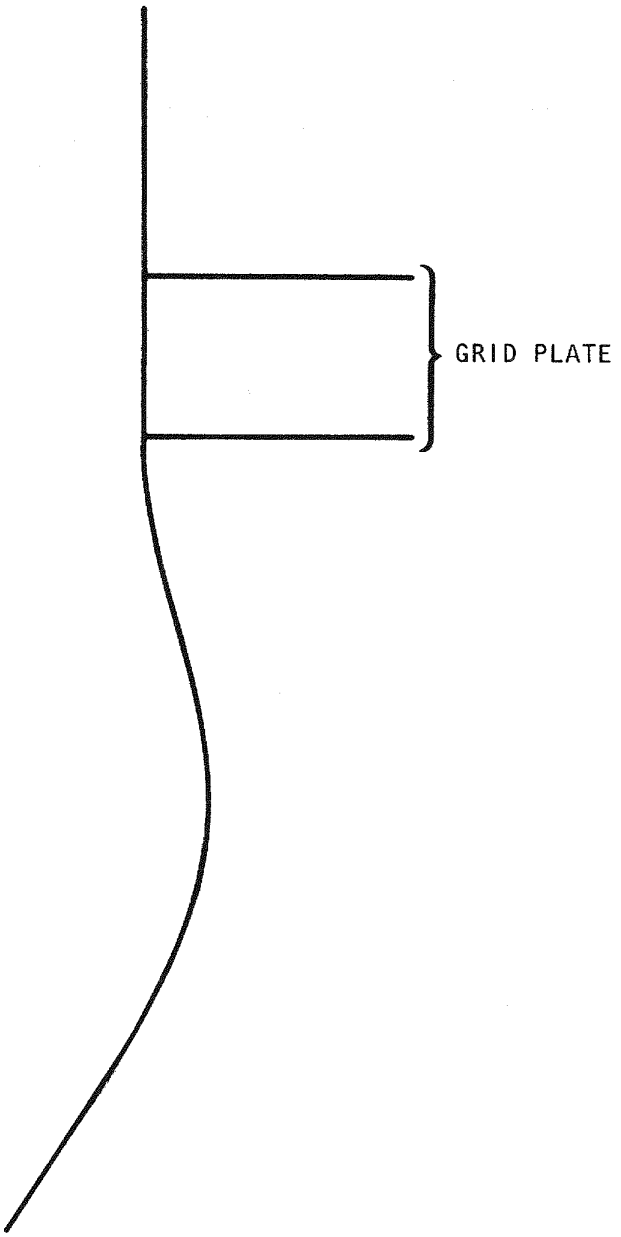

Fig. 2-11. Low-ΔP reference design, mode 2

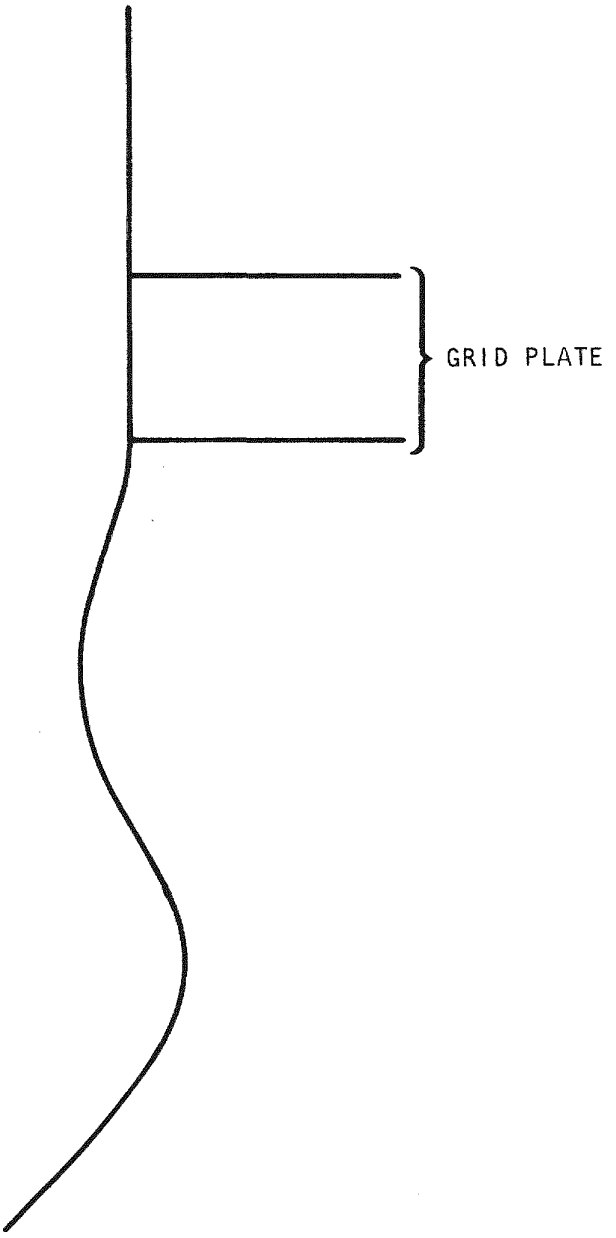

Fig. 2-12. Low-ΔP reference design, mode 3

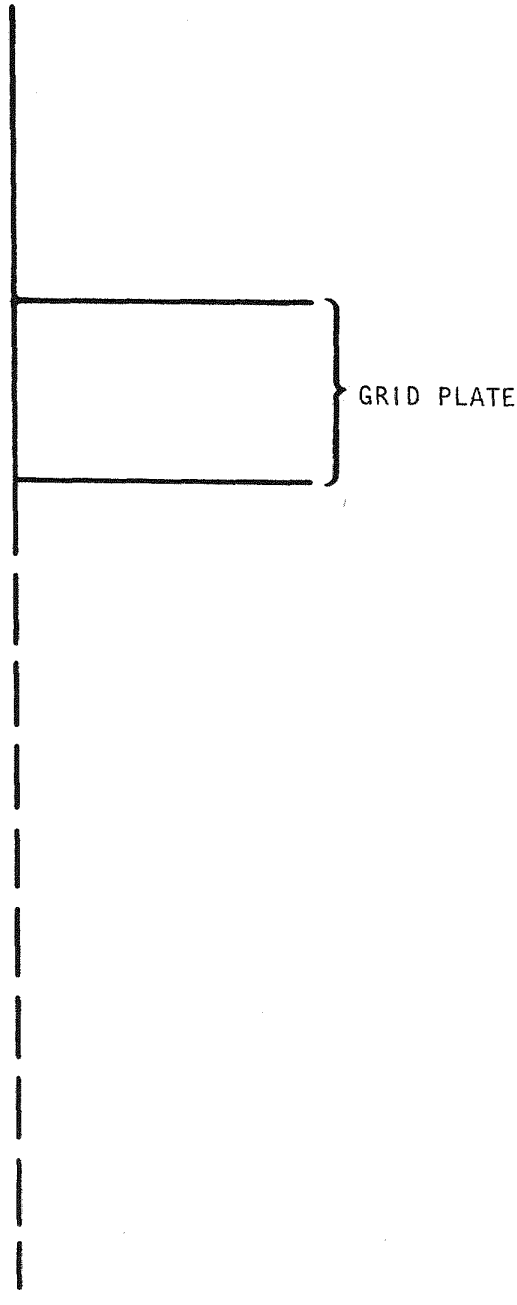

Fig. 2-13. Low-ΔP reference design, mode 4

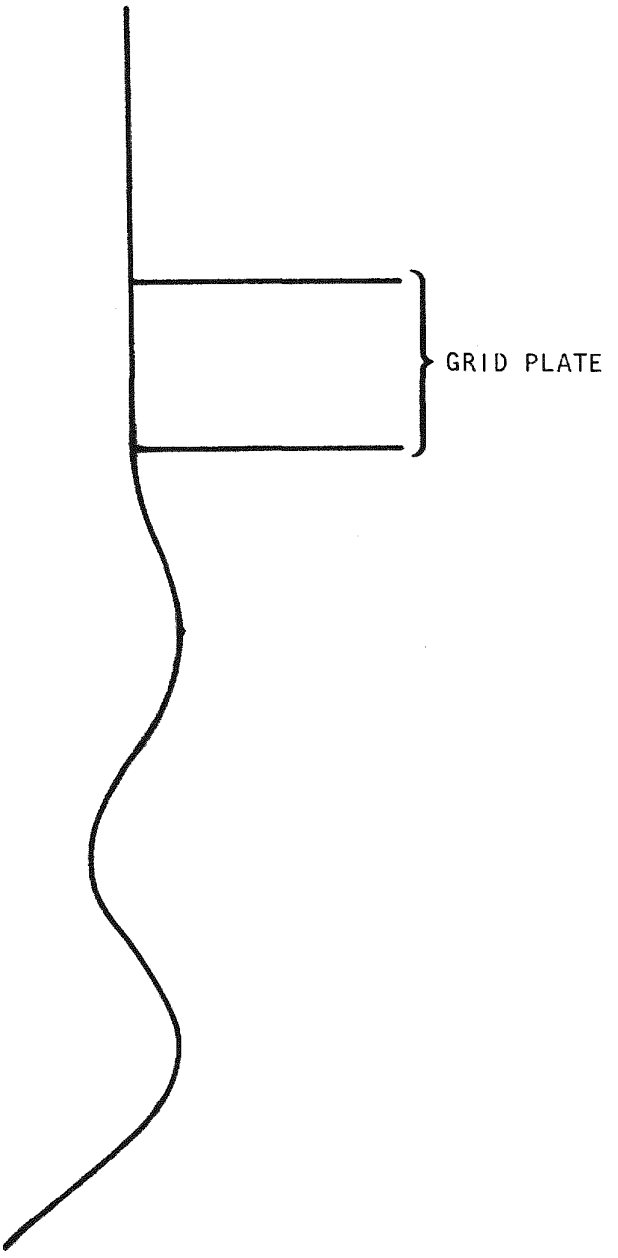

Fig. 2-14. Low-ΔP reference design, mode 5

TABLE 2-6
FUNDAMENTAL ASSEMBLY FREQUENCIES (IN Hz) FOR VARIOUS DUCT CONFIGURATIONS

Stepped ducts (3.8/2.5-mm wall thickness)

Duct Width (mm)	PSID Reference Low ΔP	PSID Reference High ΔP
165	--	10.4
186	10.4	--
188	10.6	--
191	10.8	--

Uniform ducts (low-ΔP core designs)

Duct Width (mm)	Duct Thickness (mm) 2.5	3.0	3.5
185	8.6	9.3	9.9
188	8.8	9.5	--
191	9.0	9.7	--

that such designs are adequate. It appears that low-ΔP designs with a uniform duct wall thickness of 3 mm will also be adequate, particularly for designs with larger across-flats widths. Thus, compared with the high-ΔP reference design seismic response, currently contemplated low-ΔP designs will be adequate. It has also been shown that uniform-thickness ducts may offer an attractive alternative for low-ΔP assemblies. A cost benefit study of such designs will be undertaken in the future.

2.3. CORE ASSEMBLY STRUCTURAL DESIGN CRITERIA

Work continued on the development of the core consumable structural design criteria. In order to justify the selection of these criteria and verify their adequacy for ensuring structural integrity, a trial application program has been undertaken. The work plan for such a program has been completed and reviewed. The work scope was broken into four areas: (1) preliminary activities, (2) fuel rod analysis, (3) fuel assembly flow duct analysis, and (4) documentation (Ref. 2-10). Items 1 and 4 are reported in this Section, item 2 is discussed in Section 6.3, and item 3 is presented in Section 2.2.

The material properties and time-dependent behavior correlations recommended by General Electric for the trial application program have been written into subroutines which are compatible with all the computer codes used for structural analysis. Some revision of the individual codes will be required to output various quantities necessary for application of the criteria. This will be individually done as the need arises.

Because of the modified irradiation creep and swelling correlations, it is doubtful whether prior analysis can be directly used. In addition, since important design changes have occurred since these analyses were performed, most of the analyses will have to be rerun with the current material correlations and design data.

The experience gained and the results obtained from this program will be combined with the National Working Group's activities on improvement of the design criteria. In addition, work on an analysis procedures manual to be used in the application of the design criteria will begin near the end of FY-77.

2.4. CORE ASSEMBLY MECHANICAL TESTING

The objective of this task is to conduct mechanical tests of core assembly components and subassemblies to simulate the mechanical loads expected during normal and abnormal reactor operating conditions. The current phase of the assembly mechanical testing program involves testing of fuel assembly components. The preliminary fuel rod/spacer interaction test using single spacer cells and rods was conducted during FY-76. The reproducibility testing of the hexagonal spacer cells was completed, and testing of a new modified hex design has continued. The design and procurement of blanket assembly components for testing was initiated.

The purpose of the rod/spacer interaction test is to evaluate the effect of interacting forces between the fuel rod and the spacers under the mechanical and environmental operating conditions expected in the GCFR. The interacting forces between the rod and the spacers are primarily caused by bowing induced by temperature gradients and irradiation-induced swelling. Reactor operational transients cause relative motion of the rod and spacer, which results in frictional forces. The frictional forces and relative motion cause wear of the rod and spacer pad surfaces.

Various spacer designs, spacer materials, and smooth or ribbed rods have been investigated in a simulated GCFR operational environment. Additional tests to investigate spacer contact surface geometry, surface roughness, and manufacturing techniques have resulted in specifications for spacer fabrication for optimum performance. Spacers fabricated by the reference technique of electrodischarge machining (EDM) have been subjected to reproducibility tests in a typical GCFR environment. The effects of hydrogen/water content and dwell time between interacting relative

motion on friction and wear have also been investigated. Reproducibility testing of the reference design hexagonal rod spacers was completed in FY-76, and a summary report on these tests is nearly complete.

During FY-76, a cooperative design program was initiated with the Kraftwerk Union (KWU) GCFR design team. One of the design improvements made was changing the spacer design to that of a modified hexagonal cell spacer. In the modified design, the concept of spacing the fuel rods is similar to that for a normal hexagonal spacer; i.e., a flat surface bears against the fuel rods (Fig. 2-15). It was believed that the results from the reproducibility tests could be applied to the new modified hex design. In order to verify this, six spacer cells were tested in three test series. The six cells were cut by EDM from a 37-cell modified hex spacer designed for testing in the AGATHE helium test loop of the EIR (see Fig. 2-12 of Ref. 3-2). The tests were conducted in the rod spacer test rig using the long-stroke test equipment and smooth rods having an 8.41-mm diameter.

The first test resulted in a friction coefficient of $\sim$0.5 (the normal value is $\sim$1) and wear of less than 25×10^{-6} m. The second test, however, resulted in a higher friction coefficient of about 1.2 and wear of 50×10^{-6} m. The parts were examined and measured, and it was concluded that some distortion may have occurred during the test.

Prior to the third test, careful measurements were made on the rod and the spacer. The rod diameter was 8.41 mm, and the spacer cell diameter was 8.46 mm. This provided a clearance of 0.05 mm; the nominal design clearance specification is 0.1 ± 0.01 mm. It was decided to test the spacers to evaluate the effect of the smaller than nominal clearance. The results were similar to those for the prior reproducibility tests. The friction coefficient was $\sim$0.7, and the wear was about 25×10^{-6} m.

Two additional spacers of the AGATHE design were procured. The spacer cell diameters were in the range 8.471 to 8.484 mm. These diameters will

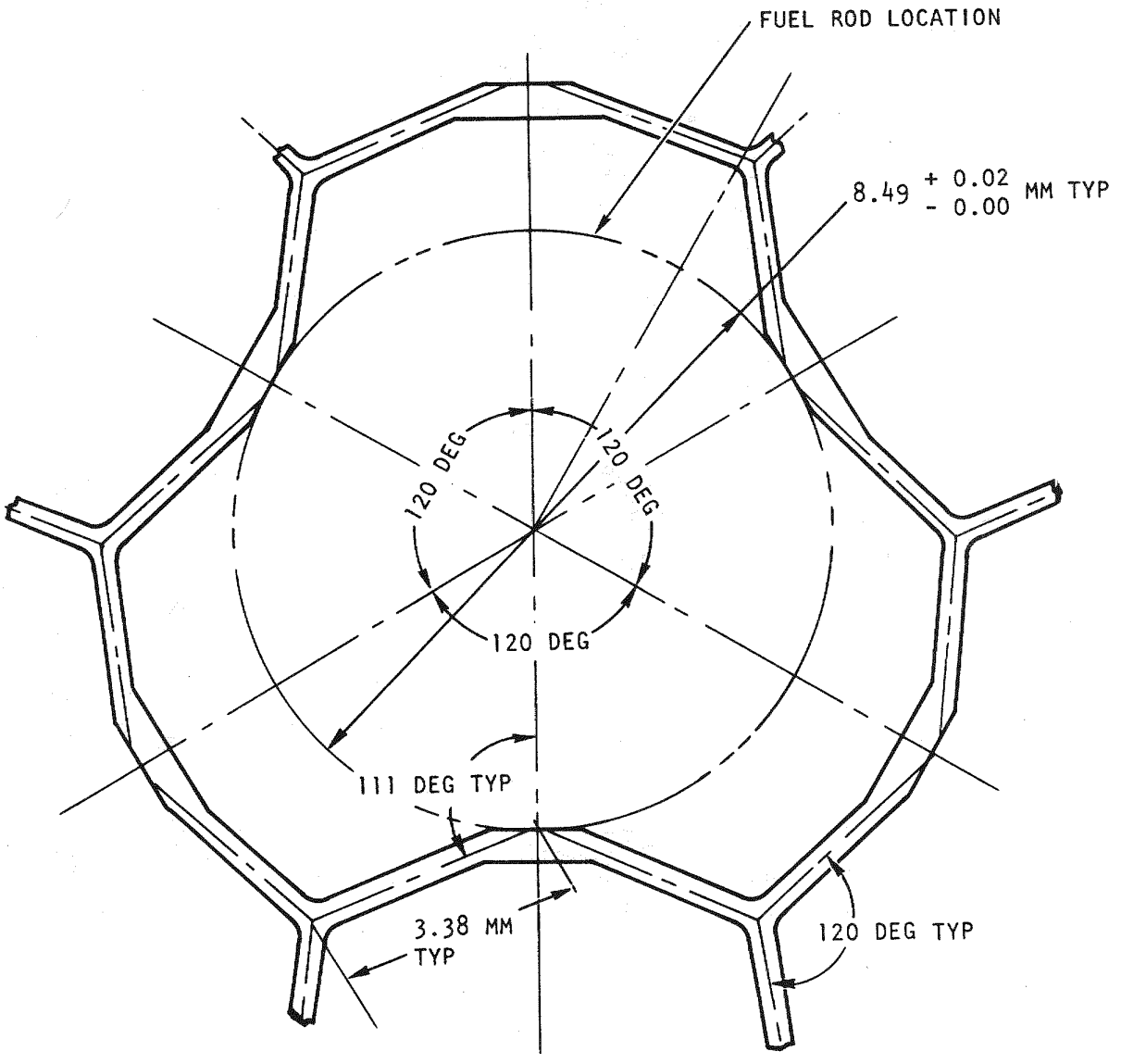

Fig. 2-15. Modified hex fuel rod spacer cell concept

be stress relieved and measured again, after which seven more cells will be cut from the spacer assembly and measured. Six of these cells will be tested against ribbed rods having an o.d. of 8.41 mm.

It is planned to conduct further rod spacer testing on larger spacers with multiple cells to evaluate structural effects. These tests can be conducted on the AGATHE 37-cell spacer designs. In addition, two or three spacers will be tested to simulate the axial spacing effects of a fuel rod bundle. This will require a furnace to accommodate three spacers on a 150-mm pitch, which is the current GCFR spacer pitch in the fueled core region.

2.5. HEAT TRANSFER AND FLUID FLOW TESTING

During this quarter, preliminary air flow testing of the full-scale plexiglass model of the GCFR core fuel assembly inlet nozzle was initiated. The test model design is described in Refs. 3-1 and 3-2. A high-intensity acoustic noise was observed during testing at approximately 30% of full air flow. Owing to the very high noise levels present ($\sim$142 dB near the assembly inlet), testing was suspended until this situation could be remedied, after which testing to higher flow rates was resumed without incident. This acoustic problem, its solution, and its relation to GCFR design are discussed below.

2.5.1. Acoustic Noise

During the initial course of flow testing, a strong acoustic noise developed inside the cylindrical duct at a flow rate corresponding to about 30% of full flow. Measurements made just outside the duct indicated a peak sound pressure level of 142 dB (ref 2×10^{-5} Pa) with a prominent observed frequency of about 2.4 kHz and a second significant frequency of about 1 kHz. This unexpected noise caused suspension of continued testing to higher flow rates until a solution to the problem could be obtained.

The noise was traced to the inlet nozzle, where three struts support a central thermocouple tube. The cross section shape of these struts is shown in Fig. 2-16. Analysis indicated that the primary acoustic mode involved was the (0, 2, 1) mode (0 nodal circles, 2 nodal diameters). It is believed that separation and consequent vortex shedding occurs at the trailing edge of the struts and that this is what excited the acoustic mode. The calculated vortex shedding frequency for this velocity closely corresponds to the 2.4-kHz acoustic frequency, indicating a resonance condition between the acoustic mode and the vortex shedding. A similar problem occurred in British AGRs. The following is an excerpt from Ref. 2-11.

> "An example of damage arising from flow induced sound occurred in the fuel channel already mentioned. During the inspection of damaged fuel stringers at Hinkley early in 1975, cracks were discovered in thin shrouds protecting some sealed gimbal joints in the stringer. A part fuel stringer was set up in the laboratory and atmospheric air blown through it. The liner of the one gimbal was strain gauged and the strain signals monitored. The measurements showed that normal flow turbulence could not have caused the failure, but it was found that at certain flow rates the rig would emit extremely intense pure tone whistles. One of these, at frequencies at 2000 Hz, was found to emanate from spiders supporting the fuel tie bar where vortex shedding was exciting acoustic cross modes in the stringer tube. These vortex shedding frequencies locked onto the acoustic resonance over a short range of flow velocities."

The whistles were eliminated by modifying the spider leg training edges to change their shedding frequencies. Tests carried out in high-pressure facilities verified that the speed of sound changes and Reynolds number changes did not cause these whistles to return.

A temporary measure was taken to alleviate the noise in the GCFR test assembly so that further flow testing could proceed. Pieces of clay were

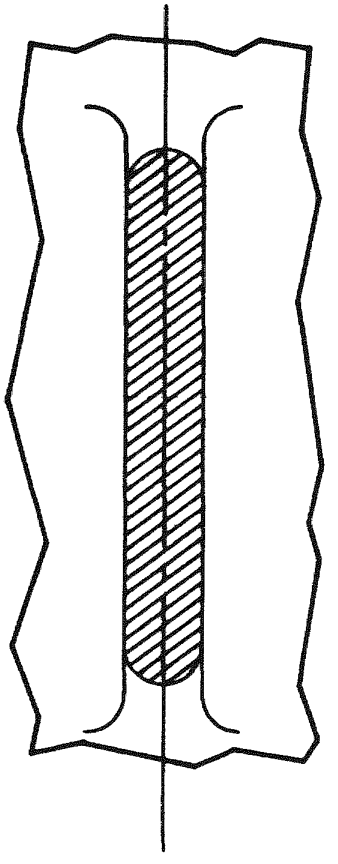

Fig. 2-16. Profile of original strut in inlet model flow test

placed on the upstream side of the struts because this presumably sufficiently disturbs the flow, preventing organized vortex shedding from the struts. A more permanent solution would be to shape the strut so that it has a better aerodynamic profile, i.e., one in which flow separation and vortex shedding are minimized. Any reasonably streamlined shape will probably be adequate so long as the included angle at the trailing edge is less than about 10 deg (Ref. 2-12). A recommended shape is shown in Fig. 2-17.

2.5.2. Impact of Air Flow Test Noise on GCFR Assembly Design

The helium coolant in a GCFR at operating conditions differs significantly from the room temperature air used in the test rig. The speed of sound in helium at reactor inlet temperature is 1430 m/s, or about 4.2 times that of air at standard temperature and pressure. Thus, the frequency of any given acoustic mode is 4.2 times higher in the reactor than in atmospheric air. In addition, the maximum velocity of the coolant in the reactor is at least three times lower than the air flow velocity in the test rig.

The maximum frequency of vortex shedding from the struts will occur at maximum flow velocity and will be about 2.0 kHz. The minimum reactor frequency for the acoustic mode corresponding to the mode found in the test [the (0, 2, 1) mode] will be about 8.8 kHz, over four times higher than the vortex shedding frequency. The frequency of the cross mode with the lowest frequency [the (0, 1, 1) mode] will be at least 4.4 kHz, still more than twice the vortex shedding frequency. This means that coupling between strut vortex shedding and acoustic cross modes is impossible at reactor conditions. Thus, the acoustic noise problem is only a model problem, not a problem with the design.

From the above discussion, it can be seen that no problem is expected from the struts at reactor conditions for two reasons: first, the struts will be aerodynamically shaped so that vortex shedding will not occur,

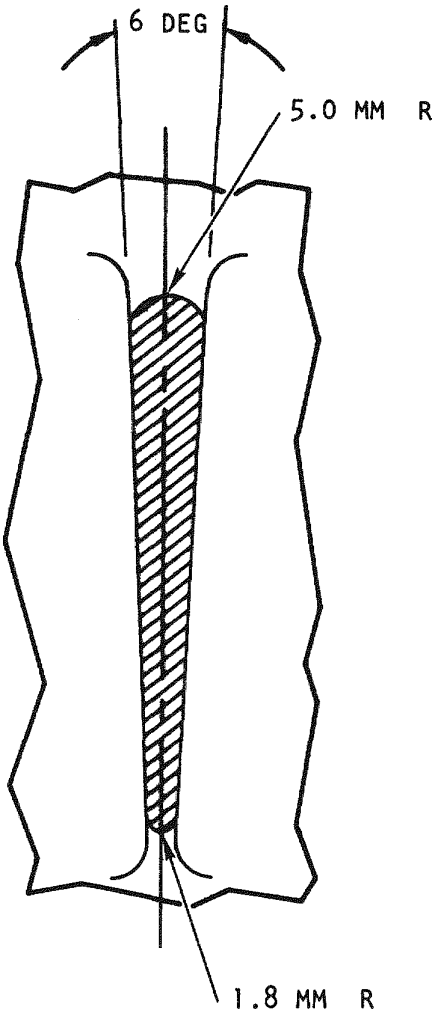

Fig. 2-17. Suggested strut profile

and second, even if vortex shedding were to occur, the frequencies would be such that they could not couple with the acoustic cross modes in the duct. However, owing to the complex geometry involved in the core assembly, it is impossible to analytically determine all the areas which might suffer from undesired acoustic excitations. Such a determination can be made only by conducting tests which correctly simulate the acoustic and flow conditions of the prototype. This can only be accomplished in full-scale tests at prototypical helium temperatures, flow rates, and pressures.

2.5.3. Pressure Drop

During the investigation, it was noted that the noise could be abated by placing a small projection at the inlet between the struts. This was done using putty, enabling continuation of the tests up to about one-half of full air flow test conditions, or about one-half of the GCFR design Reynolds number. The limiting condition was that the total head capability of the air blower system was exceeded. It is likely that the pressure drop for this design exceeds the design value.

Analytical correlation of the data is continuing. The first analysis conducted was for the loss coefficients for the individual nozzle components at various flow rates. These coefficients seemed to be nearly constant at any Reynolds number, which is expected for turbulent flow. This indicates that the error due to the high Mach number of the air flow ($M_{max} \sim 0.4$) was not significant at one-half of the flow rate. The analysis of and correlation between the calculated and measured pressure losses are continuing and will be reported during the next quarter.

The design of the inlet strut supports is being changed, and new supports will be fabricated. The design of the test parts for the new shield and trap configuration is nearly finalized, and the drawings are in review prior to being issued. The materials for fabricating the plastic model components have been procured.

REFERENCES

2-1. "Gas-Cooled Fast Breeder Reactor Quarterly Progress Report for the Period May 1, 1976 Through July 31, 1976," ERDA Report GA-A13975, General Atomic, August 31, 1976.

2-2. "Gas-Cooled Fast Breeder Reactor Quarterly Progress Report for the Period August 1, 1976 Through October 31, 1976," ERDA Report GA-A14112, General Atomic, November 1976.

2-3. Warburton, C., and M. A. M. Pirie, "An Improved Method for Analyzing Heat Transfer and Pressure Drop Tests on Roughened Rods in Smooth Channels," ASME Paper 74-WA/HT-56, November 1974.

2-4. Markoczy, G., "Konvektive Wärmeübertragung in Längsangeströmten Rohr-oder Stabbündeln," Swiss Federal Institute for Reactor Research Report TM-IN-430, April 1970.

2-5. Dalle Donne, M., "Heat Transfer From Rough Surfaces," Gesellschaft für Kernforschung, to be published.

2-6. Heisser, D. J., "Bowing Distortion of an Outer Fuel Element," General Atomic, unpublished data.

2-7. Baxi, C. B., and H. J. Snyder, "Modification of Design and Management Scheme of the 300 Mw(e) GCFR Radial Blanket," General Atomic, unpublished data.

2-8. Sim, R. and A. R. Veca, "FFTF Fuel Pin Final Design Support Document," Westinghouse Report FCF-214, 1972.

2-9. "Gas-Cooled Fast Breeder Reactor Preliminary Safety Information Document," Gulf General Atomic Report GA-10298, February 15, 1971.

2-10. Heisser, D. J., "Design Criteria Trial Application Program Plan," General Atomic, unpublished data.

2-11. Vaughan, R. D., "AGR Experience and Its Relevance to Future Gas-Coolded Reactors," Paper Presented at the 1976 ASME-ANS International Conference on Advanced Nuclear Energy Systems, March 14-17, 1976, Pittsburgh, Pennsylvania.

2-12. Blevins, R. D., "Flow-Induced Vibration, Part 1," General Atomic Report GA-A13380, October 1, 1975, p. 3-43.

3. PRESSURE EQUALIZATION SYSTEM FOR FUEL (189a No. 00582)

3.1. FUEL ASSEMBLY AND VENT CONNECTION SEALS

The core assemblies (fuel, control, and blanket) in the GCFR are clamped at the conical surfaces of the assemblies to the matching surfaces in the grid plate with a force sufficient to support the assembly against side loading. The assemblies are cantilevered downward and must be sealed to the grid plate to limit the coolant flow bypassing the assemblies. The assembly vents must be connected and sealed to matching gas passages in the grid plate, and the seals must function at the coolant pressure difference between the reactor core inlet and exit plenums. The effectiveness of the seals over the life of the core is uncertain, not only because each assembly may be rotated several times over its useful life, but also because the seals must be effective in a high-purity, high-temperature helium environment while subject to mechanical, vibrational, and thermal effects. Most of the uncertainties are expected to be resolved in a two-part program: (1) a materials screening test program for the study of static adhesion of simulated fuel assembly and grid plate parts clamped together and (2) leakage tests of fuel assembly and vent connection seals to the grid plate. Current progress in these activities is described below.

3.1.1. Static Adhesion Tests

The first set of static adhesion tests was conducted in FY-75 on 316 and 304 stainless steel at various matching cone angles, contact loadings, and surface finishes. This was followed in FY-76 by a second set of tests using materials including couples of Inconel 718 - 316 stainless steel, Inconel 718 - 304 stainless steel, and 304 - 316 stainless steel. Preliminary planning of tests for FY-77 is in progress. The third set of tests will be performed using hardened surfaces on the core assembly conical

clamping surface. The hard surfaces will be either coated onto a 316 stainless steel conical surface or placed on this surface in the form of raised inserts. It is planned to include the following material surfaces in the tests:

1. Stellite-6 bar, machined into a conical shape which is similar to the previously tested 316 and 304 stainless steel parts.

2. Stellite-6, flame sprayed onto the surfaces of the 316 stainless steel test specimens.

3. Chromium carbide coatings applied to the surfaces of the 316 stainless steel test specimens.

4. Chromium oxide coatings applied to the surfaces of the 316 stainless steel specimens.

The coated stainless steel specimens will be the same conical test parts fabricated and tested in the prior two tests. They will be chemically cleaned and the conical surface reground before coating. The test procedure and setup will be similar to those for the previous tests.

3.1.2. Fuel Assembly Ring Seal Leakage Tests

An alternative to the conical metal-to-metal core assembly seal design being developed uses piston rings as static sealing members. The test equipment, test grid parts, and core subassembly parts from the conical seal test have been modified, and ring seal tests are in progress. These tests include two ring designs provided by U.S. vendors (Stein Company and Dover Corporation) and one German design (KWU). The KWU design will be fabricated by KWU and two U.S. vendors for performance test comparisons. The piston ring designs are described below.

1. The Stein Company design is a 410 stainless steel single-piece seal ring with a step-cut joint. The design is described in Refs. 3-1 and 3-2.

2. The Dover Corporation design is a three-piece seal ring assembly; i.e., there are two outer rings and one inner ring. This ring assembly is shown in Fig. 3-1 and described below.

3. The KWU design is a double seal ring with straight-cut end joints. Each ring has a safety ring to prevent broken parts from falling out. The design is fabricated from Inconel 718 which has not been chrome plated.

During the previous quarter, the three Stein seal rings were tested at room temperature (Ref. 3-2). During this quarter, the Dover seal rings were tested, and the results are given in Figs. 3-2 through 3-4. The Dover ring assembly (Fig. 3-1) consisted of two outer seal rings, one inner expanding ring, an inner marcel spring for radial force, and a wave spring for axial loading force. The outer ring seal materials were (1) chrome-plated S-Monel, (2) chrome-plated type 410 stainless steel, and (3) nonplated Inconel 718. The inner ring material was 17-4 PH stainless steel, the axial wave spring material was 17-7 PH stainless steel, and the radial spring material was Inconel X-750. The ring design is similar to that of a larger assembly ($\sim$1.22 m diameter) supplied for a high-temperature gas-cooled reactor (HTGR) application.

The test procedure was the same as that used in the test of the Stein Company seals (Ref. 3-2); i.e., the fuel and grid parts were clamped together with a force of 13,300 N, the helium inlet pressure was raised, and leakage measurements were recorded until a ΔP of 340 KPa was achieved. Then the clamping load was reduced to zero, and in all cases, the leakage decreased significantly. The clamping load was again applied, and the leakage followed the curves shown in Figs. 3-2 through 3-4; the maximum leakage measured during the first phase (prior to release of the clamping load) is given at the right of the plotted curves.

The best consistent performance of the Dover ring design was obtained with 410 stainless steel. It is suspected that the bad performance of Inconel 718 (upper curve of Fig. 3-4) was caused by two scratches on the

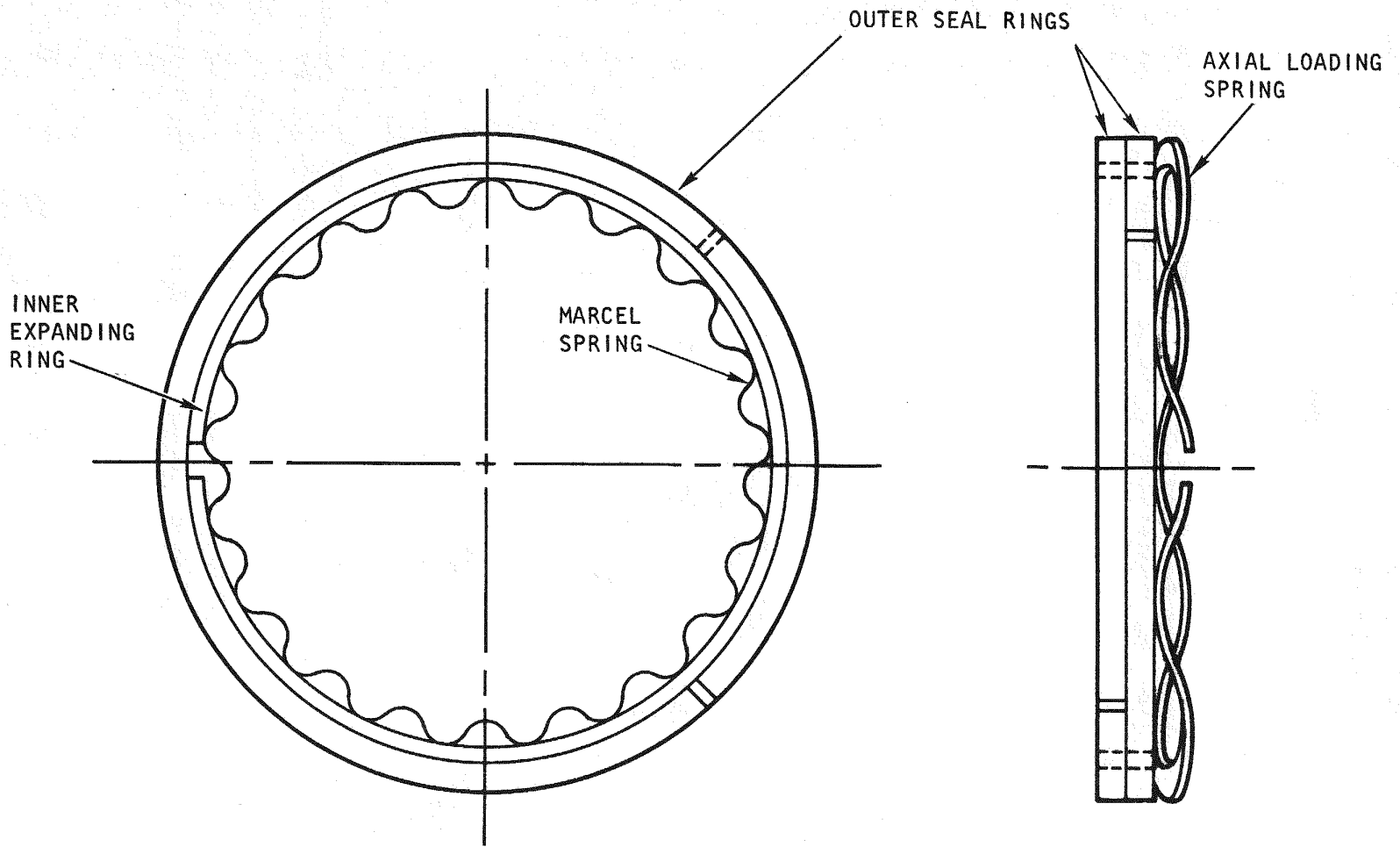

Fig. 3-1. Dover seal design

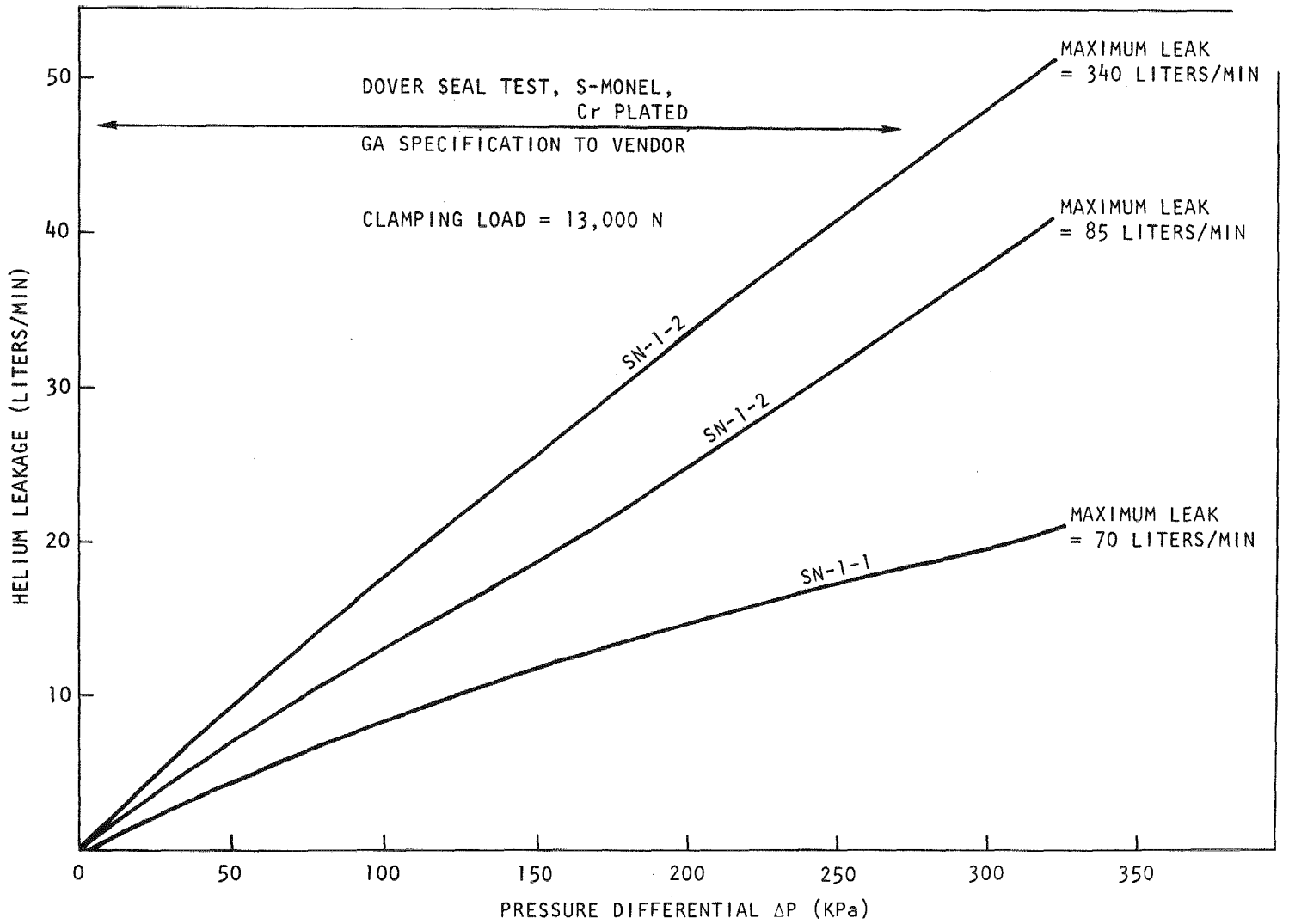

Fig. 3-2. Core assembly piston ring test

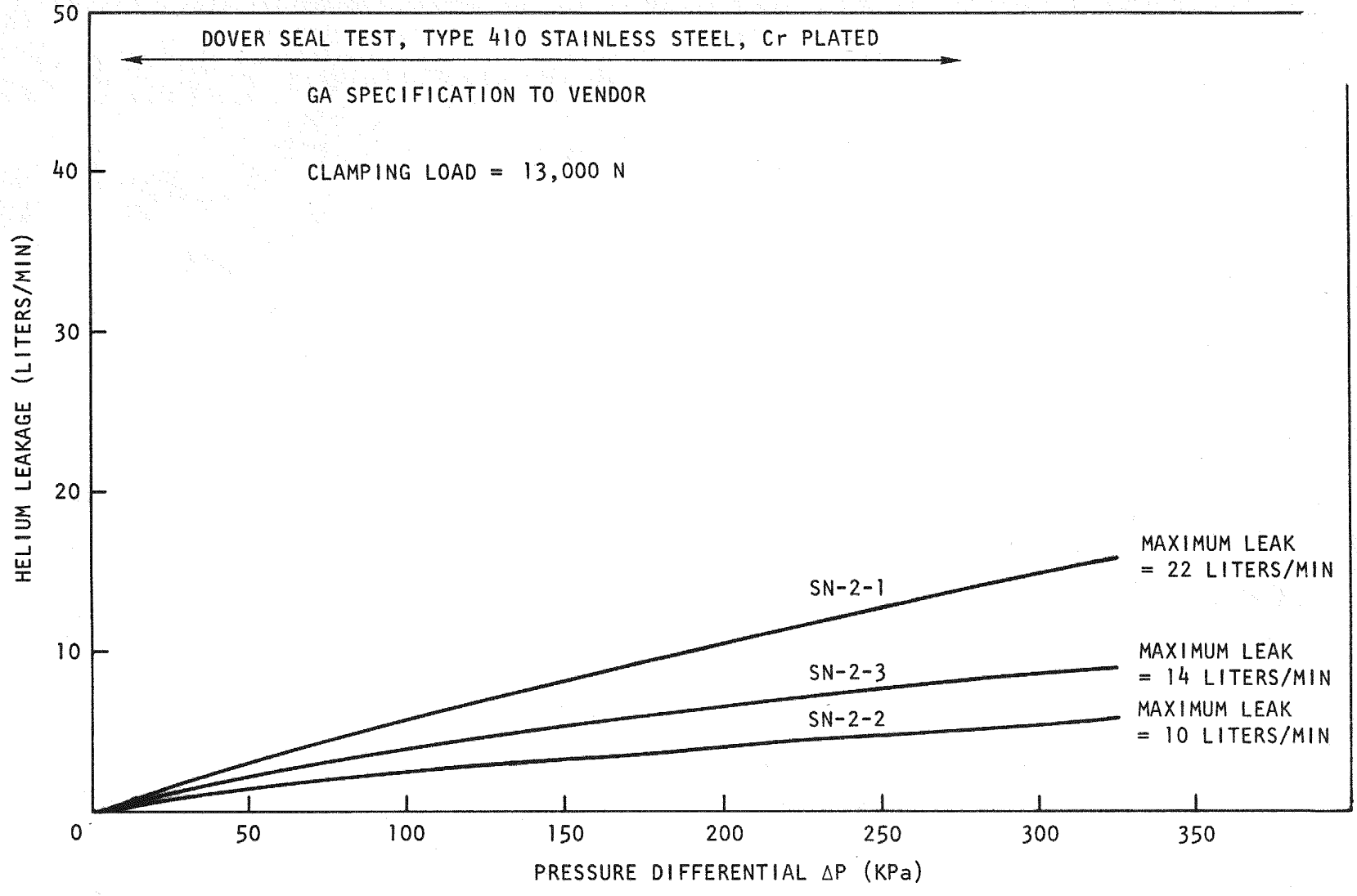

Fig. 3-3. Core assembly piston ring test

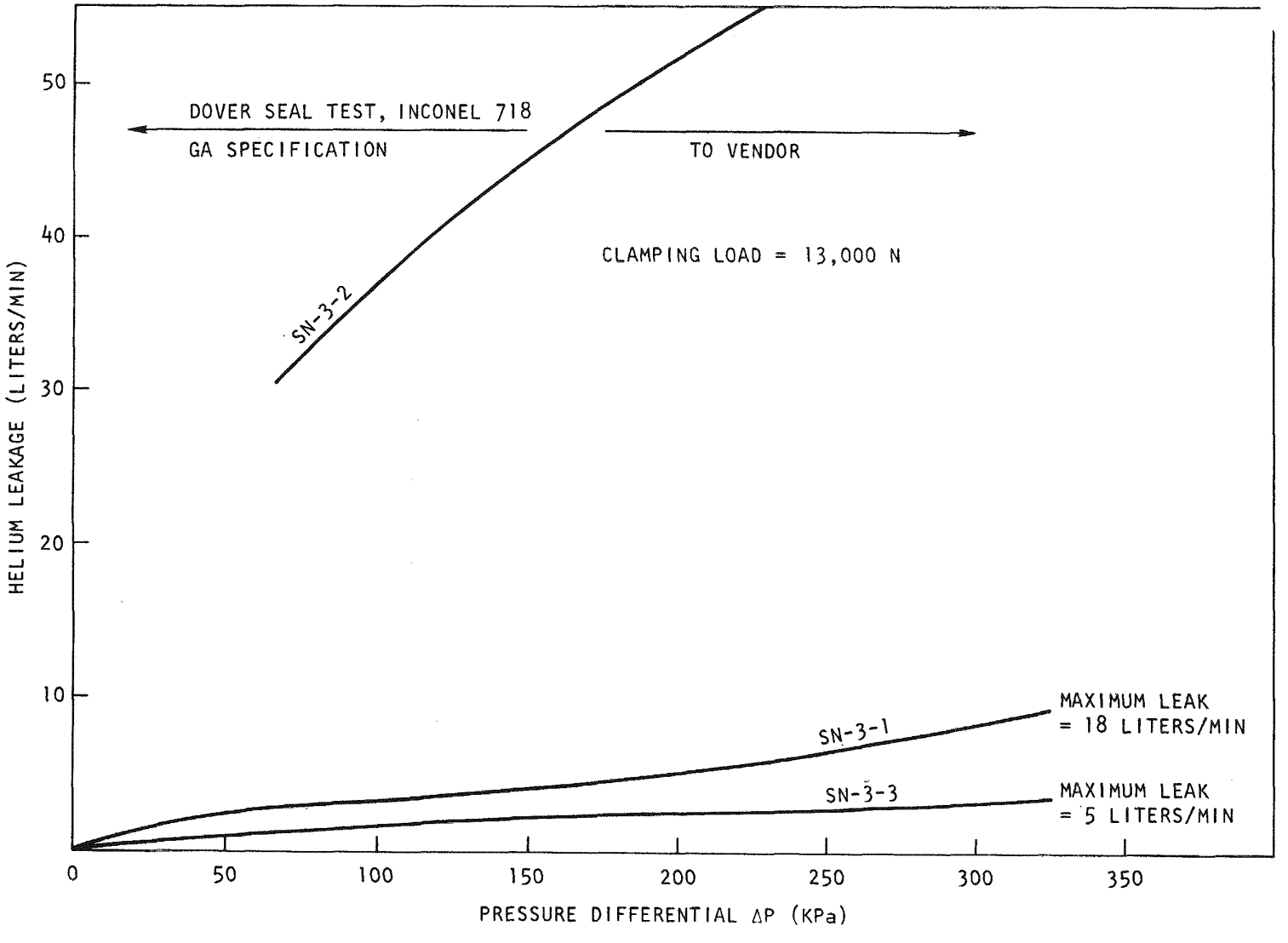

Fig. 3-4. Core assembly piston ring test

outer ring sealing surface. When the ring was turned over, the leakages were reduced to about one-half of those shown in Fig. 3-4, or from 20 liters/min at 50 KPa to 60 liters/min at 300 KPa; this is still bad. Chrome plating of the Inconel 718 would probably improve its performance.

Comparison of the Dover ring leakages with the previous Stein seal leakage tests (Fig. 3-5 from Ref. 3-2) leads to the following preliminary conclusions:

1. Based on performance and economy, the best seal ring material is type 410 stainless steel.

2. The best seal ring design is the Stein seal.

3. The sealing procedure for any ring design may have to specify final clamping of the assemblies into the grid plate after the core pressure differential is reached.

4. The cost of the two seal designs are nearly equal, i.e., $235 each for Stein and $220 each for Dover (type 410 stainless steel). These costs should decrease for large-quantity manufacturing.

5. The Stein design has the obvious advantage of being a single piece compared with the five parts required for the Dover design. This should result in further lowering production costs owing to decreased inspection, quality assurance, and handling.

6. The addition of a safety ring, if required, would be simple for the Stein design.

Testing of the Stein seal design at temperatures up to 350°C is planned. If the performance is still satisfactory, the Dover rings will not be tested further.

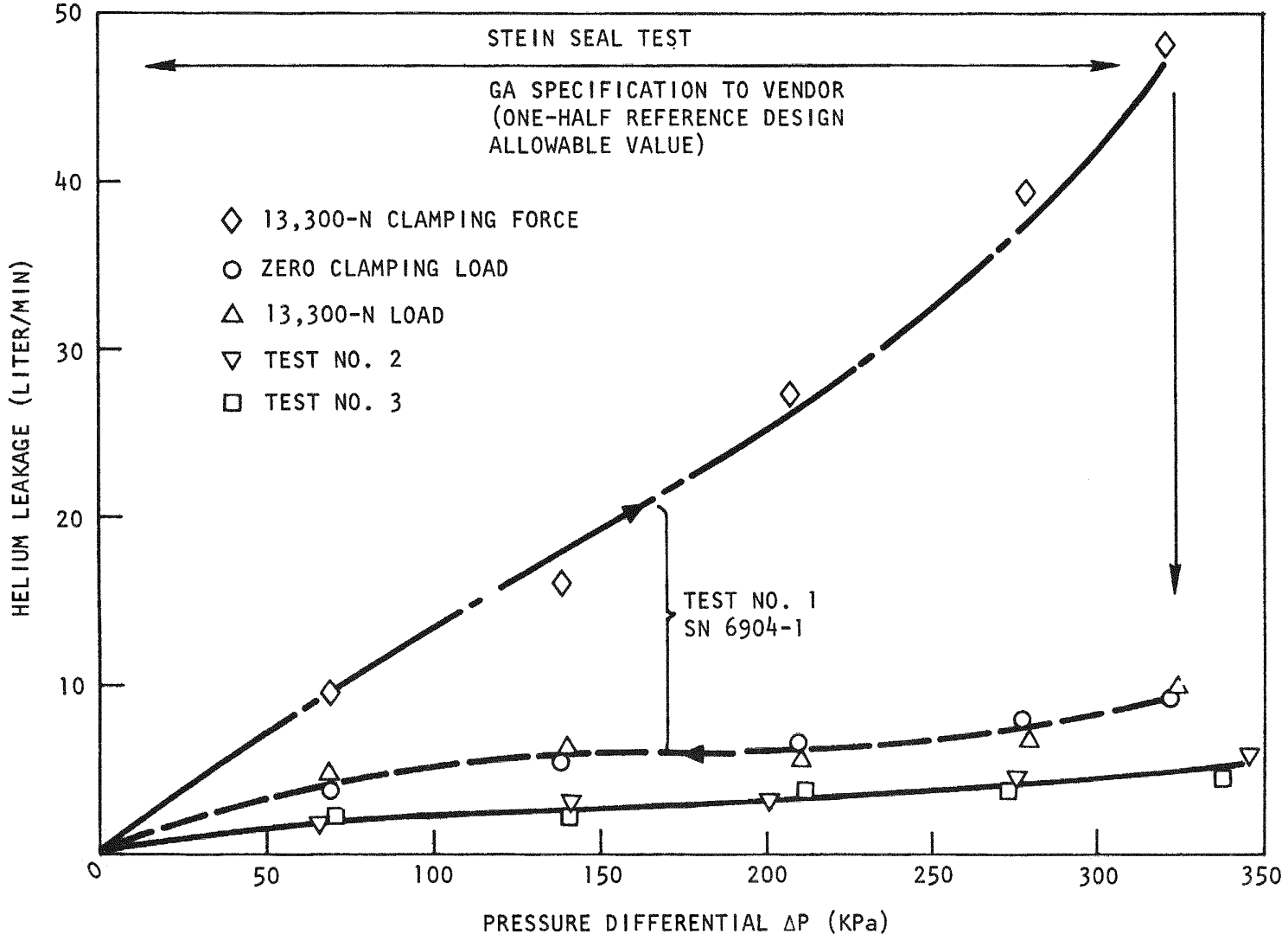

Fig. 3-5. Core assembly piston ring test

3.1.3. Vent Assembly Seals

A vent assembly design concept is being developed for connecting the GCFR core subassembly vents to the passages in the grid plate and sealing the core subassembly vents when the subassemblies are removed from the grid plate for handling, storage, and transport. Two design concepts for installing the vent assembly into the conical clamping surface of the fuel subassemblies were completed: one for radial installation and the other for vertical installation. These devices, described in Ref. 3-2, are being leak tested in the laboratory before being installed in the piston ring seal test apparatus for integral testing. The leak test results are being analyzed and will be reported during the next quarter.

3.2. ANALYSIS, MODELS, AND CODE DEVELOPMENT

The transient analysis of the PES flow network continued during this quarter using the three-node model of the PES reported in Ref. 3-1 and shown in Fig. 3-6. The volumes represented by nodes N_1, N_2, and N_3 were reported (Ref. 3-2) to be 1.02, 0.02, and 3.46 m^3, respectively. These nodes are shown in proportion to their volumes in Fig. 3-6. The loss coefficients of branches K_1 to K_5 were calculated to give the same initial pressure drops and flow rates (Table 3-1) as those in Ref. 3-3. These model parameters are preliminary, but their magnitudes are representative of the PES.

The primary objective of the calculations with this model was to study the capability of the network code to perform the numerical integration. As noted previously (Ref. 3-2), numerical instabilities seem to have prevented the execution of models which are more complex than the basic three-node model. Although the model parameters were selected to represent the PES, the model itself is very preliminary and is deficient in several respects: first, the monitor lines (K_4) will contain check valves which prevent reverse flow through them, and these valves were not included in the present model; second, the volume of gas in the rods of the core does not behave the same way as the single lumped volume in this model (N_1); third,

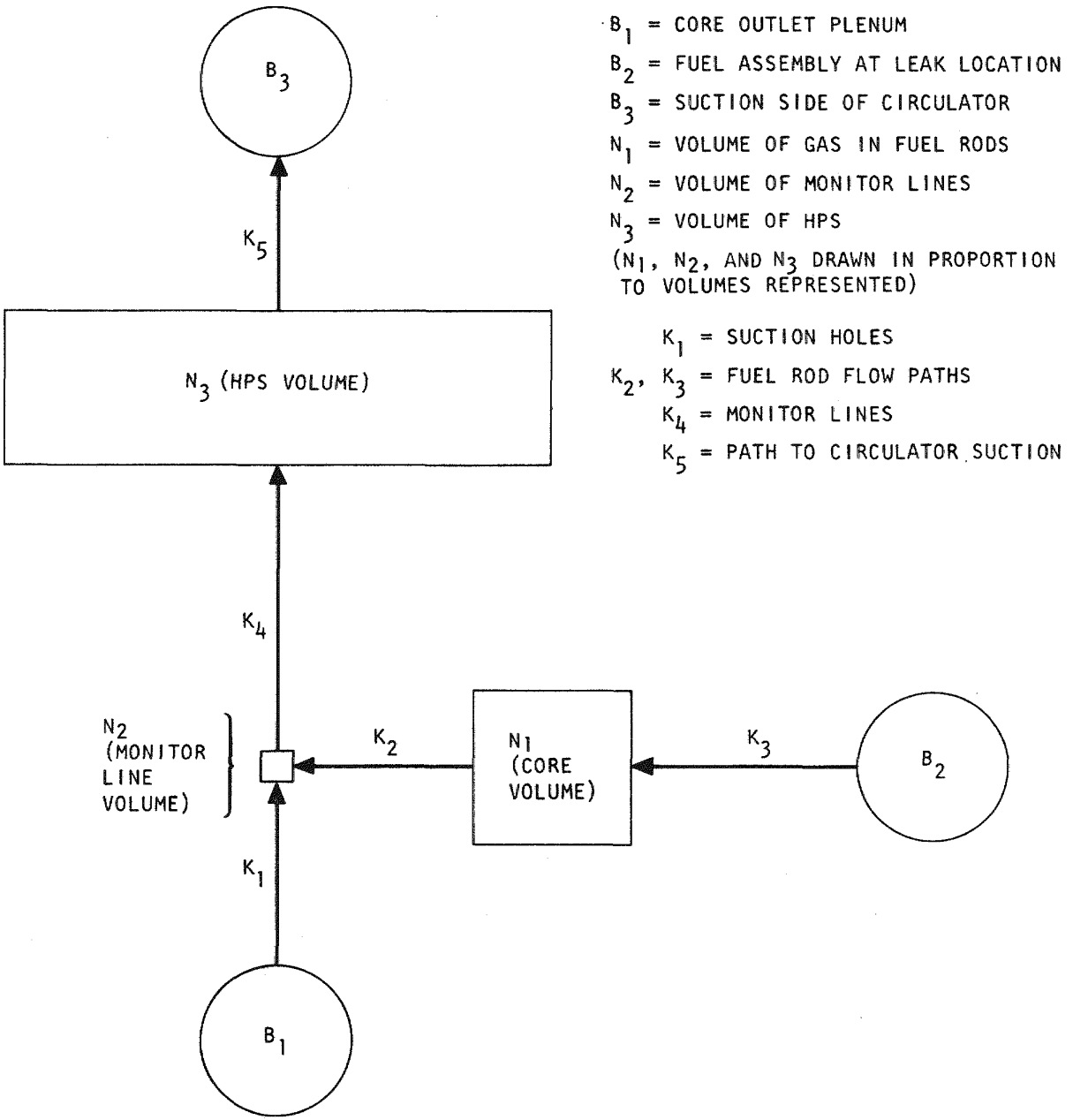

Fig. 3-6. Three-node lumped parameter model of the PES

TABLE 3-1
GEOMETRY OF THE BRANCHES

Branch No.	No. of Lines	Length (m)	Diameter Per Line (mm)	Flow Per Line (g/s)	Pressure Drop (kPa)	Loss Coefficient
1	288	1	1.5	0.289	13.8	5.5
2	300	1	1.38	0.139	110.3	136.7
3	300	1	1.38	0.139	110.3	136.7
4	144	20	3.20	0.578	11.7	24.2
5	1	30	50.0	83.2	37.9	224.7

during a depressurization accident, the temperatures of the rods drop rapidly, so that there will initially be flow into volume N_1 instead of out of it, as this model predicts. Therefore, the results of this analysis represent the behavior of the model in Fig. 3-6 and not necessarily the behavior of the actual PES. Nevertheless, the model is a useful tool in understanding the nature of a depressurization and the numerical integration process.

The initial pressures of boundary nodes N_1, N_2, and N_3 were 9.01, 9.22, and 8.95 MPa, respectively, and these proportions were held fixed during the depressurization. The depressurization function is shown in Fig. 3-7 along with the response of the three volume nodes. In this severe accident transient, the boundary pressures were reduced from 100% to 2% of the initial pressure in 20 s. It can be seen that there is a lag in the decay of the volume pressures, so that the higher pressures at nodes N_1, N_2, and N_3 will drive flow out of the volumes during part of the transient.

During normal operation, the flow in the branches is positive, as indicated by the arrows in Fig. 3-6. The main venting flow is from the lower plenum (B_1) through the suction holes (K_1) and the monitor lines (K_4) to the helium purification system (HPS) and the circulator (B_3), with superposed leakage flow from the fuel assemblies (B_2) through the fuel rods (K_3, K_2) to the monitor lines. During the transient, because of the large volumes of nodes N_3 and N_1, some of these flows reverse, as shown in Fig. 3-8. The strongest changes in the flow rates occur in the first 25 s, when the boundary pressures are still changing, after which there is a decay toward the steady state at the 2% pressures. It can be seen (Fig. 3-8, curve A) that there is a rapid flow reversal through the suction holes, discharging gas from the HPS volume and the core volume [the flow in branch K_2 is positive (Fig. 3-8, curve B)]. In addition, there is a reverse flow through the assumed 300 leaking rods into the main coolant [the flow in branch K_3 is negative (Fig. 3-8, curve C)]. The consequences of these flow reversals on isotope transport require further study.

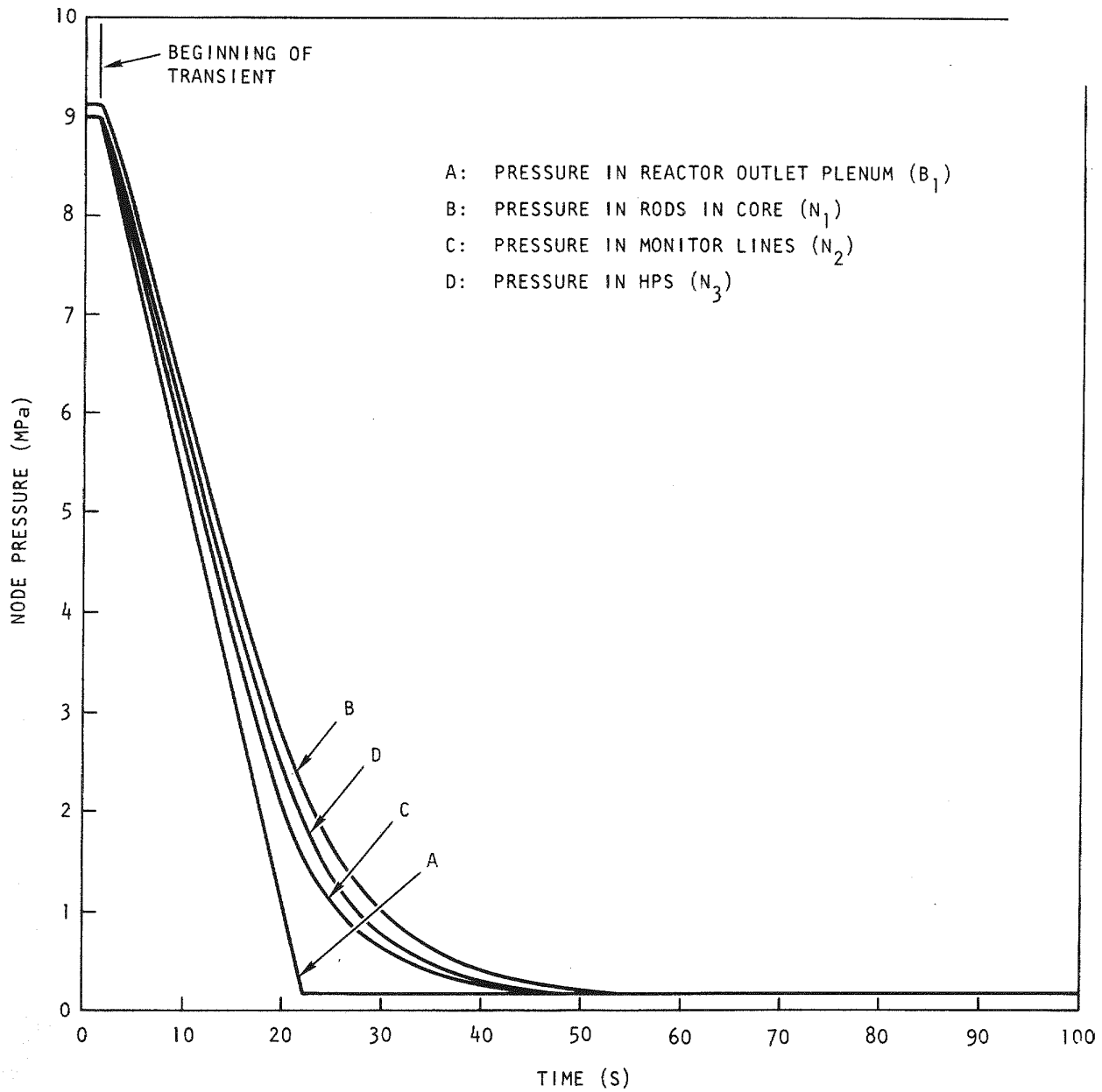

Fig. 3-7. Node pressures during a depressurization accident

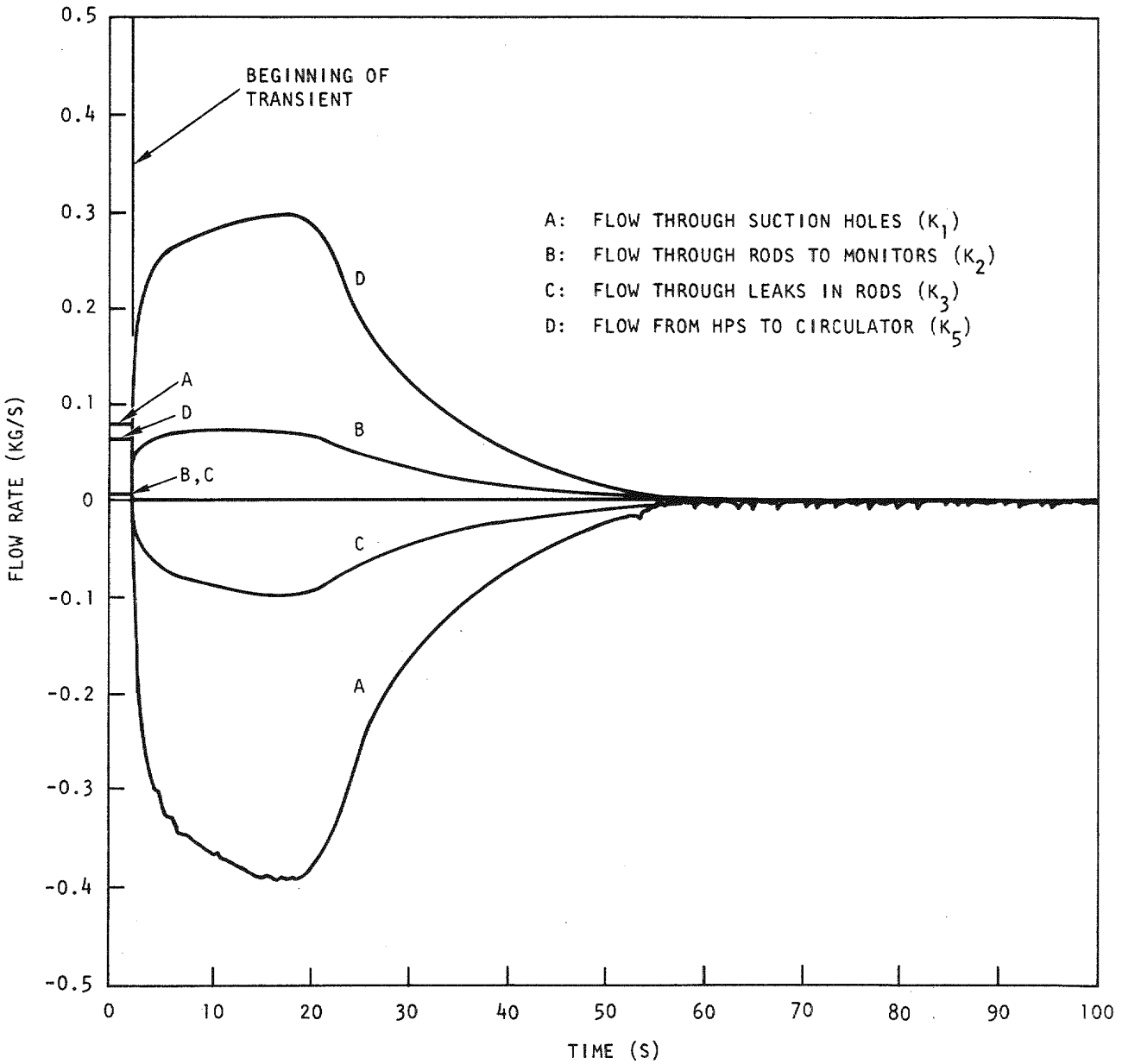

Fig. 3-8. Branch flow rates during a depressurization accident

From a numerical standpoint, the very rapid changes exhibited in Fig. 3-8 followed by slower decays are typical of so-called stiff equations. Such equations are among the most difficult to integrate numerically, and special procedures are often required. The stiffness of the equations was also evidenced by the vastly different initial eigenvalues of the system; these eigenvalues ranged from -6×10^{2} to 1×10^{-1}. Because of this varied character of the solution, the time steps had to be small so that the 100-s transient would take about 200 s of computer time. Even with small time steps, flow oscillation instabilities occurred after 60 s, as shown in Fig. 3-8. Since integration difficulties have been experienced for complex models and instabilities are present in the three-node model, it is planned to make the descriptive equations of the network system nondimensional such that the numerical stability of the equations will be improved. For instance, the network code must presently deal with small differences of large pressures, which can introduce instabilities owing to round-off errors in the computer. From Fig. 3-7 it appears that the node pressures can be described as departures from a reference pressure. The possibility of such a description is currently under investigation. There is also a need for an improved description of the elements of the PES network, and such improvements are being investigated in conjunction with making the variables nondimensional.

3.3. PLATEOUT AND PLUGGING

Volatile fission products, particularly cesium and iodine, vented from the core assemblies and produced by gaseous precursor decay of fission products vented from the core assemblies may plate out on the walls of the monitor lines. These fission products are swept through the monitor lines into the HPS traps by helium entering at the core subassembly vent connections. Accumulation of deposited material may constrict the sweep gas flow passages and could potentially lead to plugging of the lines. The conditions under which plateout and plugging could occur in the GCFR, the means of minimizing or eliminating it, and the methods for removing deposits are being investigated. A small high-pressure loop has been built and is being used for this purpose. Development of components for injection,

control, and measurement of impurities in the helium (i.e., H_2 and H_2O) and sources for simulating venting of the volatile fission products and their compounds is being examined.

3.3.1. High-Pressure Loop

The circulator pumps experienced a failure when the square-wave generator used to drive the pump actuator coils malfunctioned. This event allowed a high-current surge of direct current to the coils, which caused overheating. New pumps were installed and checked, and an in-line charcoal trap (which can be interposed in the main circulating flow) was fabricated and installed. This allows for rapid cleanup of the loop gas when the loop has been depressurized and opened to the atmosphere. A small cooldown heat exchanger which will be used to trap cesium vapor after it has passed through the test section is currently under construction. This improvement will localize the region for cesium vapor removal and make it easier to evaluate the quantity of cesium which has passed through the test segment.

3.3.2. Oxygen Potential Analyzer

The effect of an apparent electochemical oxygen leak into the sample side of the ZrO_2 cell from the air reference side was studied. The most straightforward solution of this problem was to construct a reference sleeve around the commercial cell which is "leak free" and permits the use of a low oxygen potential ($pO_2 \sim 10^{-15}$ Pa), well buffered ($\sim$1% H_2, $\sim$2% H_2O in helium) reference gas. A typical calibration curve of log (H_2/H_2O) versus cell emf is given in Fig. 3-9. The performance of this cell, which has a GA-fabricated reference sleeve, has been superior to the commercial cells tested.

3.4. FISSION PRODUCT RELEASE AND TRANSPORT

The purpose of the work on this subtask is to obtain experimental data on the interdiffusion and gas phase and the surface back diffusion of gaseous and volatile fission products. The diffusion coefficient data will be

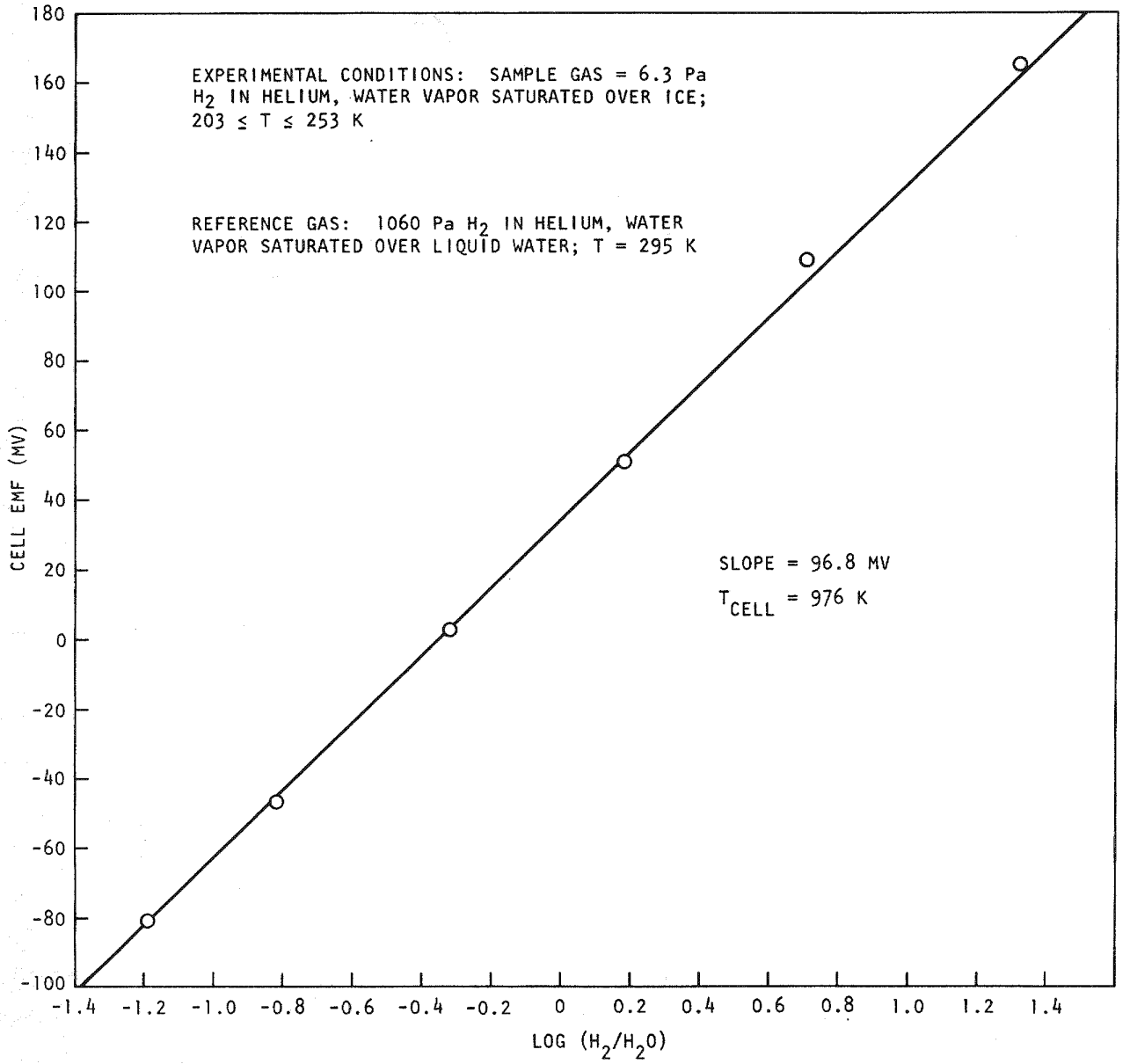

Fig. 3-9. Calibration plot of log (H_2/H_2O) vs cell emf

used to validate or improve the SLIDER code, a one-dimensional model for fission gas diffusion transport (including radioactive decay). Surface transport and back diffusion data will be used to establish a model for predicting the importance of these mechanisms to contamination of the reactor coolant system.

As part of the design and performance analysis of irradiation capsule GB-9 (Ref. 3-4), a series of laboratory diffusion tests were conducted from 1969 to 1971 to provide information on the interdiffusion of fission product gases (krypton and xenon) through high-pressure helium and adsorption beds. At the same time, the SLIDER code, written to model the diffusion of fission products through the multiple layers of HTGR fuel particles, was modified and applied to GCFR gas diffusion conditions. Thus, the SLIDER code was verified, in general, and a model for diffusion through adsorption beds developed. However, it was necessary to make some simplifications and use empirical factors to compute blanket region performance.

The objectives of the current work are to (1) verify that a one-dimensional model and code are applicable to the blanket region diffusion transport, (2) verify that the adsorption model is correct for conditions different from those previously tested for capsule GB-9, (3) measure the coefficient of the gas temperature effect on the diffusion parameter (which is not available in the literature for GCFR conditions), and (4) verify that measurements with krypton can be correctly applied to xenon diffusion through helium in the GCFR fuel rods.

A sketch of the measurement apparatus, which was constructed from components used on a previous assembly (Ref. 3-4) modified to suit present requirements, is given in Fig. 3-10. The new apparatus has been pressure and leak tested and fitted with a series of calibrated thermocouples, which will enable checking of the temperature profile of the diffusion tube and source sections. The apparatus is currently undergoing checkout of the thermal control system with the objective of maintaining isothermal conditions with a mean temperature fluctuation of no more than ±2 K (at temperatures from 295 to 623 K) with a slight gradient of ∿1 to 3 K from the top of the diffusion tube (hotter) to the bottom of the source region.

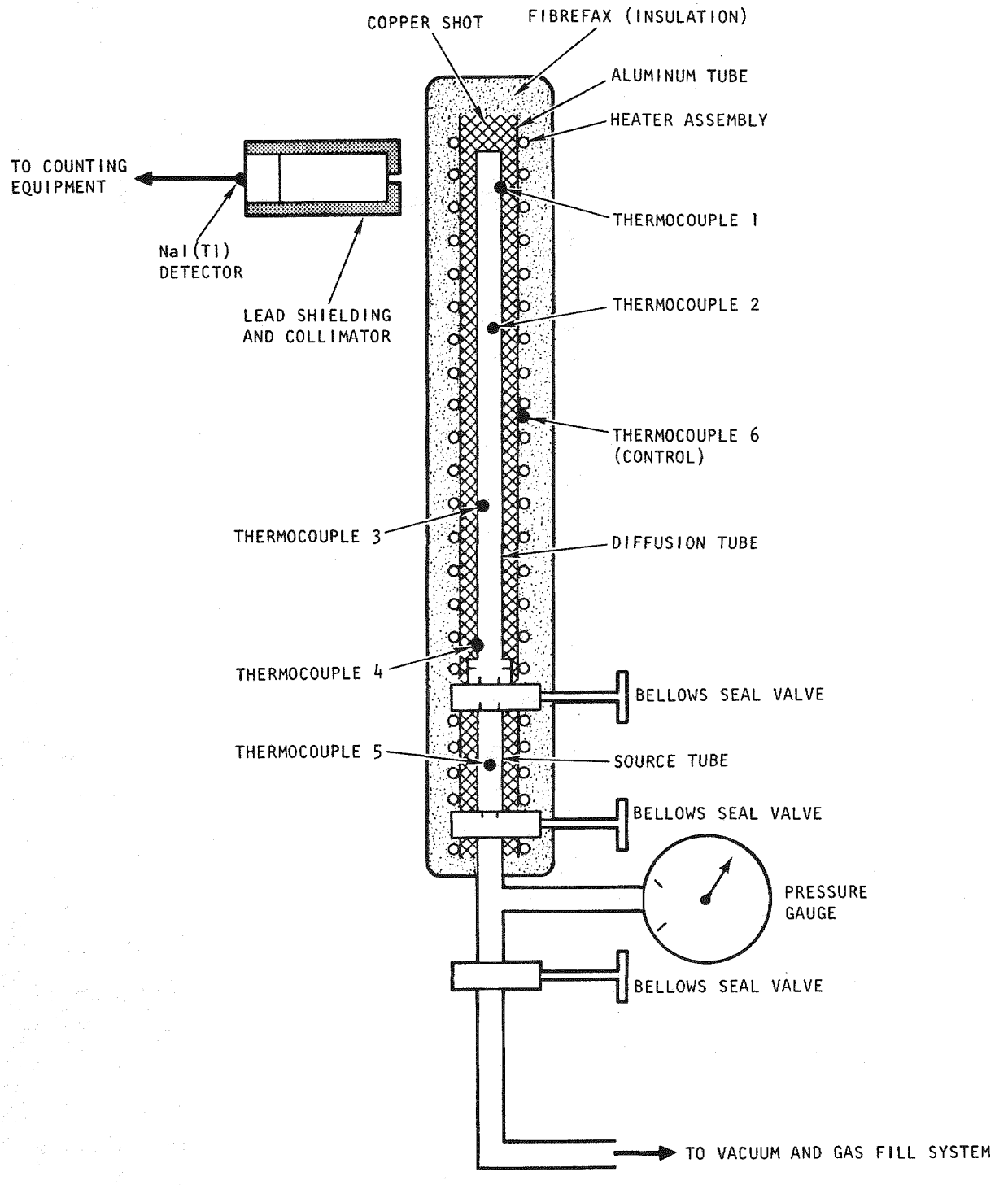

Fig. 3-10. Diffusion coefficient measurement apparatus

3.5. MONITOR STATION AND INSTRUMENTATION

For this subtask, a systems approach is initially being used to assure that all aspects are considered and will be capable of integration into the system at a later time. The major objectives of this subtask are to design, fabricate, and assemble a development model station radiation monitor. In order to establish the number, kind, and size of detectors and other equipment such as collimators, shielding, valving, mechanical drives, etc., the following variables are being evaluated: detector types; type and range of activity to be encountered; effects of changes with advent of first and subsequent leaks in one core assembly and first and subsequent core assemblies on a single monitor; transport times from fuel to detector; and PES gas dilution rates. Preliminary selection of instrument type will be made when the evaulation has been completed. The COUNT code will be used in this work.

3.5.1. System Functions and Criteria

The functions of the system are being defined, system criteria will be developed, and major components of the system are being identified and their location defined.

3.5.2. Electronic Processing

Indication of a core assembly leak, location of the leaking assembly, and monitoring of the leak rate over burnup and time will require processing of a number of signals from multiple detectors under various operating conditions [e.g., breathing (power cycling), multiple leaks per assembly, blanket versus core assemblies]. A preliminary review of the hardware and equipment likely to be required was made using hard-wired discrete instruments with set points to perform decision and alarm functions. In a comparison with the foregoing approach, it was clearly indicated that a committed minicomputer is vastly superior in its flexibility for providing decisions (is it breathing or a leak in all assemblies?) and actions (alarm indicating a new leak in one sextant of the core) and reducing the information to a usable form. This minicomputer is also probably less costly.

3.5.3. Radiation Detector Choices

An ion chamber coupled to a picoammeter with an automatic range changer was initially regarded as the preferred detector for identifying the occurrence of the first leak in a core subassembly where signal changes of 10^4 to 10^6 were expected. An NaI(Tl) scintillator was chosen as the preferred detector because of its high efficiency in indicating the occurrence of additional leaks in the same core subassembly and its photon energy resolution capability to monitor the leak rate.

Plastic scintillators were considered because of their rapid response and very wide operating range (10^8). They could also be used to replace the ion chamber and do not require range changing. However, the plastic scintillator cannot replace the NAI(Tl) scintillator because the plastic scintillator's low photon energy resolution capability is not sufficient for separating the photopeaks of the fission gases to be monitored. However, since the NaI(Tl) scintillator will require collimators, variable source-to-detector distance positioners, or both to maintain it in its operable range for subsequent leak detection, it can also perform the "first leak" detection function, thereby eliminating the need for either the ion chamber or plastic scintillator.

The Ge(Li) semiconductor detector was also considered. The high photon energy resolution capability of the Ge(Li) semiconductor is desirable but exceeds requirements and is very costly. The need for cryogenic cooling of the Ge(Li) semiconductor crystal is a disadvantage because of the added complexity and hardware and the loss of cooling which results in permanent damage to the expensive detector crystal. Thus, the Ge(Li) semiconductor is not preferable to the NaI(Tl) scintillator for monitor station service.

3.5.4. Equipment Selection

The radiation detection and electronic processing equipment needed to support and convert NaI(Tl) scintillator signals into useful output was identified, and preliminary costs were obtained. The major components include

1. NaI(Tl) detector assembly, including photomultiplier and preamplifier.

2. Nuclear instrumentation monitor and high-voltage supply.

3. Linear amplifier.

4. Single-channel analyzer and scaler.

5. Detector arm (TRIGA control rod drive assembly).

6. Collimator capstan.

7. Lead shield for detector assembly.

3.5.5. Monitor Station Layout

Work was initiated on the monitor station layout. Preliminary envelope dimensions for each well in the head of the PCRV were assumed to be a 1-m diameter and a 2.5-m length. Studies will be conducted to determine the best way to fit the equipment and the necessary internal shielding into the wells. High-pressure, bellows-sealed trim and diverter valves and remote operating or indicating flow meters are being selected from commercial vendor catalogs for sizing and arrangement studies.

3.6. PES PROGRAM PLANNING

No work was done on this task during this quarter.

REFERENCES

3-1. "Gas-Cooled Fast Breeder Reactor Quarterly Progress Report for the Period May 1, 1976 Through July 31, 1976," ERDA Report GA-A13975, General Atomic, August 31, 1975.

3-2. "Gas-Cooled Fast Breeder Reactor Quarterly Progress Report for the Period August 1, 1976 Through October 31, 1976," ERDA Report GA-A14112, General Atomic, November 1976.

3-3. "300-MW(e) Gas-Cooled Fast Breeder Reactor Demonstration Plant," General Atomic Report GA-A13045, July 15, 1974.

3-4. Lindgren, J. R., et al., "Planned Thermal Irradiation of Manifolded-Vented $(U,Pu)O_2$-Fueled Rod In ORR Capsule P-9," USAEC Report GA-9896, Gulf General Atomic, March 15, 1970, p. 71.

4. CORE FLOW TEST LOOP PROGRAM (189a No. 00582)

A series of out-of-pile simulation tests will be performed to (1) demonstrate the ability of the GCFR fuel, control, and blanket assembly designs to meet designs goals and (2) verify predictions of analytical models which describe design operation and accident behavior. The emphasis of the tests will be on obtaining thermal-structural data for steady-state, transient, and marginal conditions using electrically heated rod bundles in a dynamic helium loop. Testing will be performed in the range of cladding melting, and the consequences of local initiation of melting will be determined. The core flow test loop (CFTL) program plan (Ref. 4-1) describes the requirements for the test program to be conducted in the CFTL, which will be constructed and operated by Oak Ridge National Laboratory (ORNL). The principal work accomplished during this quarter was as follows:

1. A CFTL position description was presented to the GCFR (utility) Program Review Committee.

2. Detailed 37-rod bundle analysis was performed for comparison with previous predictions.

3. An alternate test bundle design was prepared to improve structural modeling of the inlet section.

4. Orientation sessions were held for new program personnel at ORNL, and written responses to their questions were prepared.

4.1. PROGRAM PLANNING

4.1.1. Program Plan

A draft revision to the CFTL program plan and the response to ORNL and ERDA review and comments on the revision were discussed in Refs. 4-2

and 4-3. Since the first issue of the program plan (Ref. 4-1) currently provides ORNL with sufficient guidance for CFTL loop design, the final issue of the first revision is awaiting approval of the core assembly interim configuration and review of the test program, particularly the fraction of testing related to accidents beyond the nominal design basis accident.

4.1.2. Position Description

The utility sponsors of the GCFR have urged ERDA to support an "earliest possible" date for operation of the demonstration plant, and representatives of ERDA have indicated that the CFTL was on the critical path and thus affected the program end date. The GCFR (Utility) Program Review Committee requested that GA prepare a position description on the CFTL and held CFTL program reviews at GA and ORNL. The GA position description is summarized below.

The CFTL program is sponsored by ERDA and is a joint program of GA and ORNL. The CFTL program is on the critical path for the development of the GCFR core assemblies, as shown in Fig. 4-1. Although the results of the test will provide significant information in support of the Final Safety Analysis Report (FSAR), the test itself is considered an engineering evaluation and is not directly required in support of the construction permit and subsequent GCFR licensing.

The GCFR core assembly development program is based on utilization of the extensive body of fuel data being developed under the LMFBR program and is supplemented by an incremental test program which evaluates the operational and environmental effects specific to the design of a 300-MW(e) demonstration plant core. The use of roughened rods to enhance heat transfer was studied by the British and applied to the advanced gas-cooled reactor (AGR). An extensive analytical and experimental heat transfer and fluid flow program on GCFR fuel rods with heat transfer enhancement has been under way for many years at the German Nuclear Center at Karlsruhe and the Swiss Federal Institute for Reactor Research. This work has been performed on

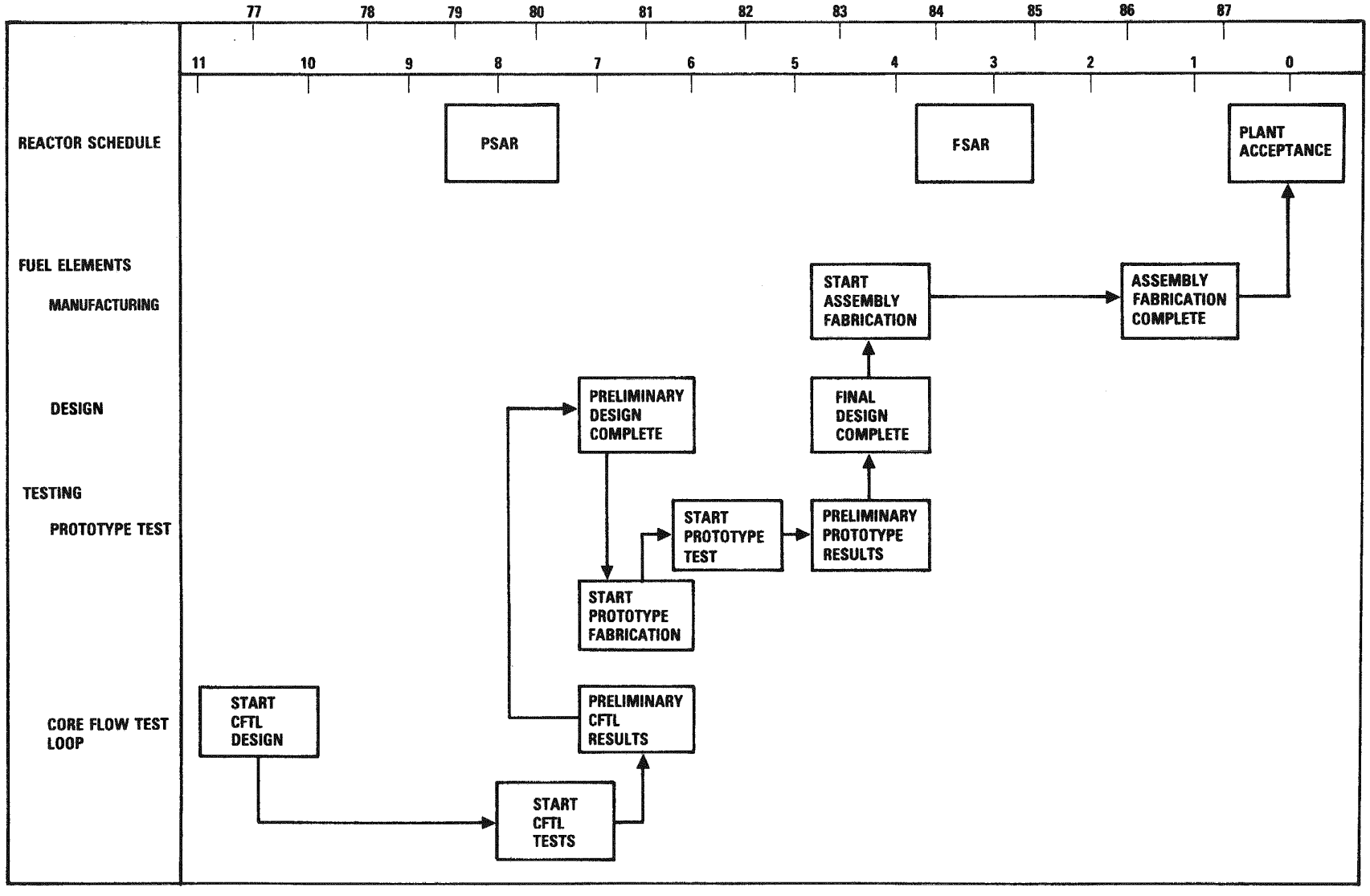

Fig. 4-1. Fuel assembly critical path

single, electrically heated rods and bundles of 12 to 37 electrically heated rods and is continuing.

A significant part of the core development program is conducted in the CFTL, a major test facility which provides flow testing of bundles of electrically heated rods and integral testing of core assembly models to demonstrate satisfactory design performance under nominal operating conditions and transients, verify analytical methods, and demonstrate assembly design margins. The results of these tests will provide an engineering evaluation of the core assembly preliminary design and establish the basis for the final design of the core assembly prior to release for fabrication.

It is the technical opinion of the GCFR Program that the CFTL is necessary for the orderly development of the core assemblies for a demonstration plant since no other facility is available for adequately testing the assemblies under simulated operating conditions. Utilization of the CFTL provides a basis for assurance of assembly operation to a burnup on the order of 50 MWd/kg, at which time fast neutron fluence effects become significant. Subsequent operational evaluation of the core provides a method for determining correctable failure conditions or life limiting conditions with a minimum impact on core cost (≈2/3 of a core at $25 M). If data from the CFTL are not available, the risk of an early life failure due to bundle effects is greater. This could result in a significant cost (≈1-1/3 of a core at $50 M) and demonstration plant shutdown for up to 3 yr.

4.2. TEST ANALYSIS AND PREDICTION

4.2.1. Prediction Code TSPEC

The computer code TSPEC was developed to provide a relatively simple, approximate analysis for predicting the performance of GCFR model core assemblies in the CFTL. The principal simplification of the code involves

neglecting of cross flow within the bundle. The test specifications will list the steady-state and transient input parameters, including the time functions of power and flow for each test run, and TSPEC will predict the resultant test parameters. The code performs four types of calculations:

1. Geometric bundle data.

2. Geometric bundle data and prediction of N steady-state runs.

3. Geometric bundle data and prediction of a series of steady-state runs with linear interpolation between the first and last input values.

4. Geometric bundle data and N transient runs.

A report (Ref. 4-4) has been issued which explains the structure of the code and provides the following user information: input instructions, sample calculations, code listing, and index of code variables.

4.2.2. Hot Spot Factors for the CFTL

Hot spot factors were determined for the CFTL at the 2σ confidence level for 100% power and steady-state conditions. As with the GCFR analysis (see Section 2), the uncertainties involved were classified as statistical or cumulative. Statistical uncertainties include tolerances of manufacturing, assembling, thermal bowing, bowing due to electromotive forces, and material properties; cumulative uncertainties are errors in measurements and calculations.

The effect of each uncertainty on temperature drops ΔT_i in the subchannel, film, or cladding were determined using a subchannel analysis code which includes mixing. The subfactors f_i, which define $\Delta T_i/\Delta T_{nom}$,

were added together to obtain the overall hot spot factors. The statistical subfactors were added together according to the equation

$$f_s = \sqrt{\sum_i (f_i - 1)^2} + 1 \quad ,$$

and the cumulative subfactors were directly added:

$$f_c = \Pi f_i \quad .$$

The overall hot spot factor is given by

$$F = f_s \cdot f_c \quad .$$

Table 4-1 lists the statistical and cumulative uncertainties with their effects on the temperatures in the core.

4.2.3. Thermal Performance of Bundle C

The performance of the CFTL 37-rod assembly was analyzed using the subchannel analysis code COBRA; the model used is shown in Fig. 4-2. The purpose of the analysis was to predict coolant and rod temperatures. Hot spot factors were used to determine the range of uncertainty for these temperatures at the 2σ confidence level. Two operating conditions were considered: 100% flow and power and 10% flow and power.

The Reynolds numbers for the 100% flow and power case are in the range 10^5, where the full effect of rod roughening will be felt. However, for the 10% flow and power case, the Reynolds numbers are in the range 10^4 or lower, and there will be no effect of roughening. Some subchannels in the 10% case are in the laminar range and some are in the range of transition from laminar to turbulent flow. Figures 4-3 and 4-4 show the expected temperatures for the maximum and minimum temperature subchannels and rods; Figs. 4-5 and 4-6 give the temperature uncertainty range for these temperatures.

TABLE 4-1
HOT SPOT FACTORS FOR CFTL 37-ROD ASSEMBLY[a]

	Uncertainty 2σ (%)	Channel Factor F_c	Film Factor F_f	Cladding Factor F_{cl}
Statistical factors				
Tolerances				
Rod pitch	0.44	1.010	1.003	1.000
Spacer standoffs	0.35	1.000	1.000	1.000
Bowing	1.0	1.000	1.000	1.000
EMF forces	Negligible	1.000	1.000	1.000
Cladding o.d.	0.28	1.003	1.000	1.000
Cladding o.d. } cladding Cladding i.d. } thickness	0.28 0.31	1.000	1.000	1.028
Cladding o.d. to i.d. eccentricity	5.22	1.000	1.000	1.029
Rib height	7.7	1.002	1.000	1.000
Correlations and properties				
Specific heat of coolant	0.5	1.000	1.002	1.000
Density of coolant	0.5	1.000	1.002	1.000
Viscosity of coolant	3.0	1.000	1.021	1.000
Conductivity of coolant	4.8	1.000	1.029	1.000
Conductivity of cladding	6.7	1.000	1.000	1.067
Film coefficient	6.7	1.000	1.067	1.000
Friction factor	6.7	1.005	1.019	1.000
Mixing	40.0	1.000	1.000	1.000
Total		1.012	1.078	1.078
Cumulative factors	Error (%)			
Thermohydraulic analysis	2	1.020	1.020	1.020
Inlet flow maldistribution	0 at location of hot spot	1.000	1.000	1.000
Inlet temperature measurement[b]	3°C	1.000	1.000	1.000
Flow measurement	2	1.020	1.016	1.000
Power measurement and system dead band	Measured = 1, power split = 2, local = 2	1.008	1.030	1.030
Axial heat transfer coefficient variation	-70	1.000	1.067	1.000
Cladding thermocouple error[b]	14°C	1.000	1.000	1.000
Total		1.049	1.139	1.051
Overall factors		1.062	1.228	1.133

[a] At 100% power and steady state.

[b] The inlet temperature deviation raises the temperature of all the components, and the thermocouples in the cladding may read the temperatures 14°C lower.

PITCH = 11.288 MM

d_{ROOT} = 7.26 MM

d_{ROUGH} = 7.52 MM

$d_{HANGER\ ROD}$ = 11.20 MM

ROUGHENING STARTS = 918 MM

HEATING STARTS = 645 MM

ROUGH LENGTH = 868 MM

HEATED LENGTH = 1140 MM

TOTAL LENGTH = 2240 MM

AXIAL POWER PROFILE = $\cos\left[1.049\left(\frac{2x}{\ell} - 1\right)\right]$

$\frac{x}{\ell}$ = 0 TO 1.0

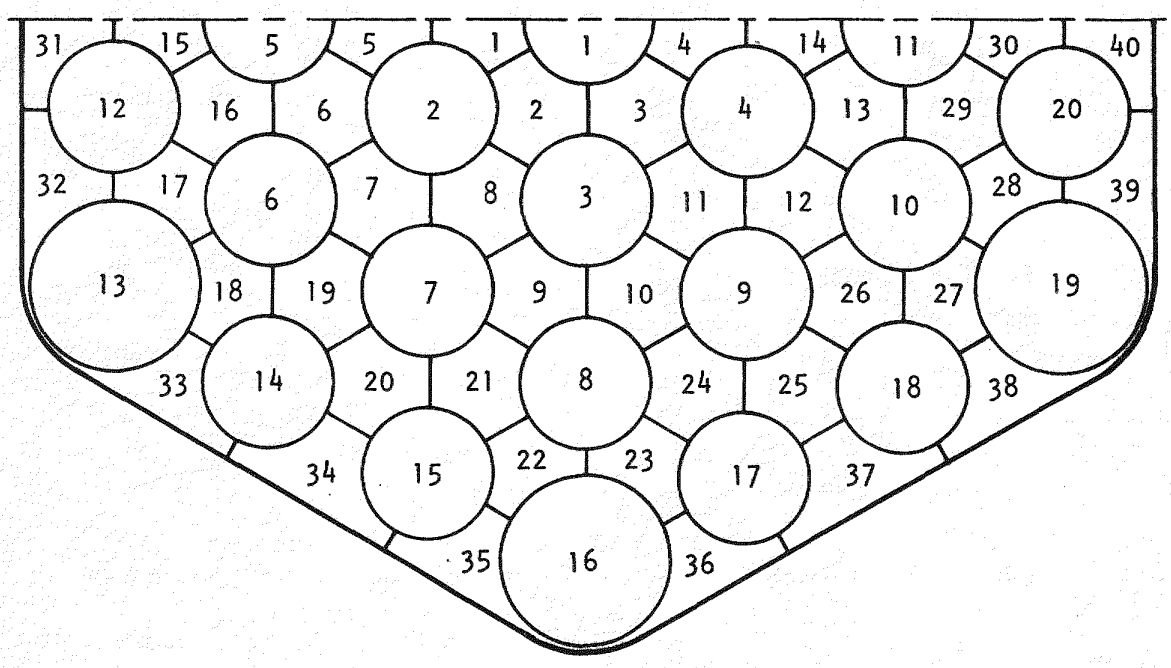

Fig. 4-2. COBRA model of CFTL 37-rod assembly

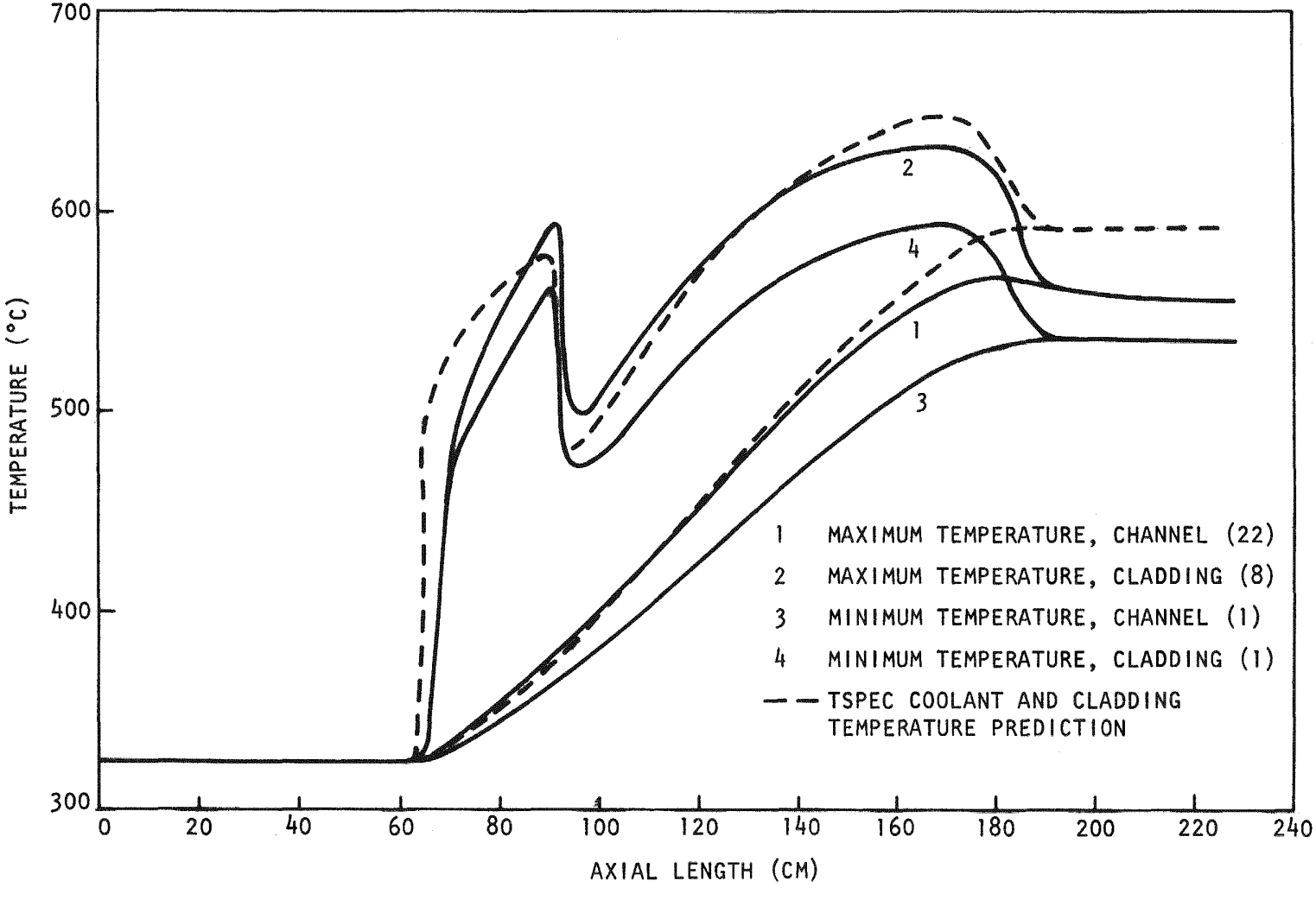

Fig. 4-3. Coolant and cladding temperatures, 100% power and flow

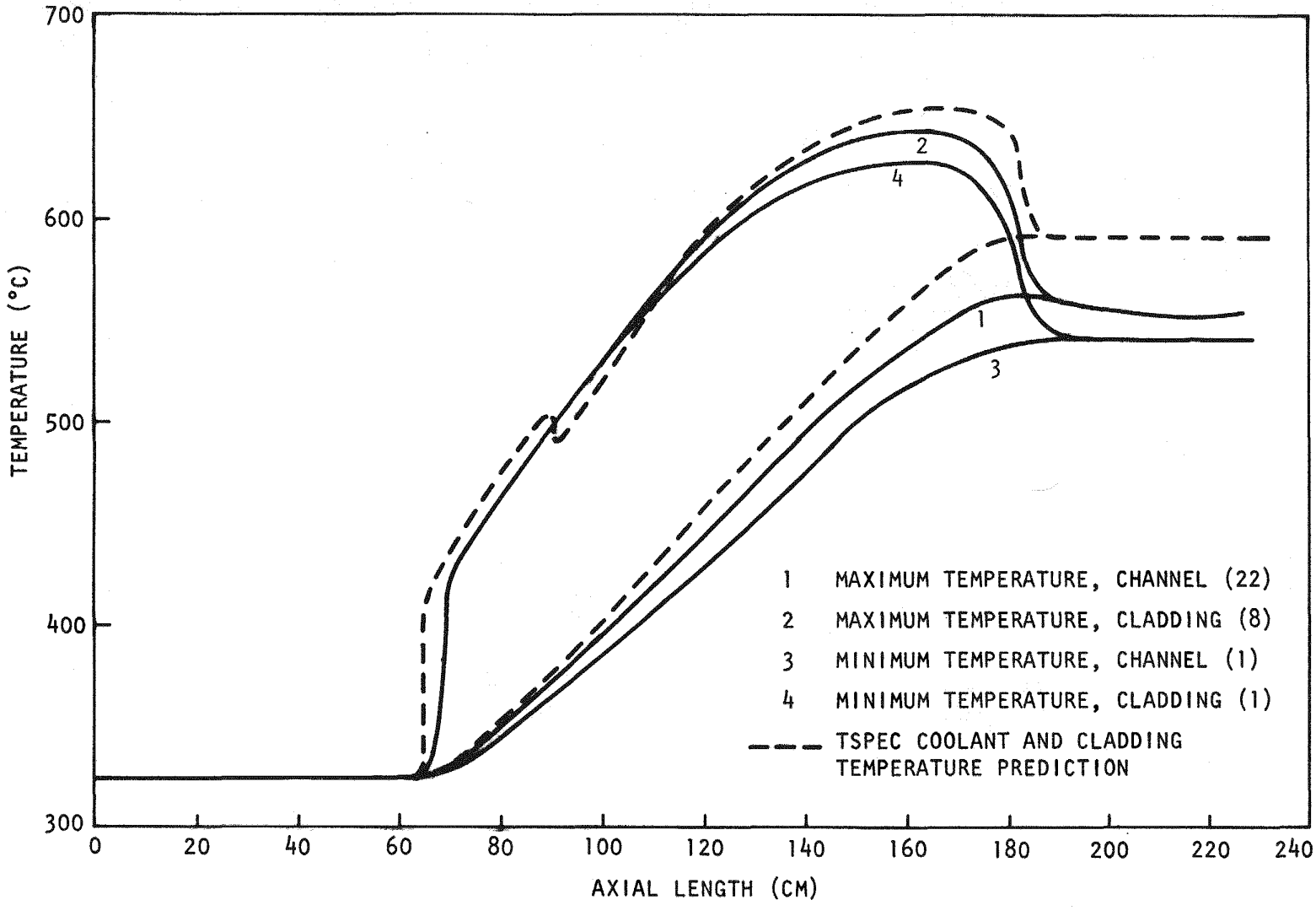

Fig. 4-4. Coolant and cladding temperatures, 10% power and flow

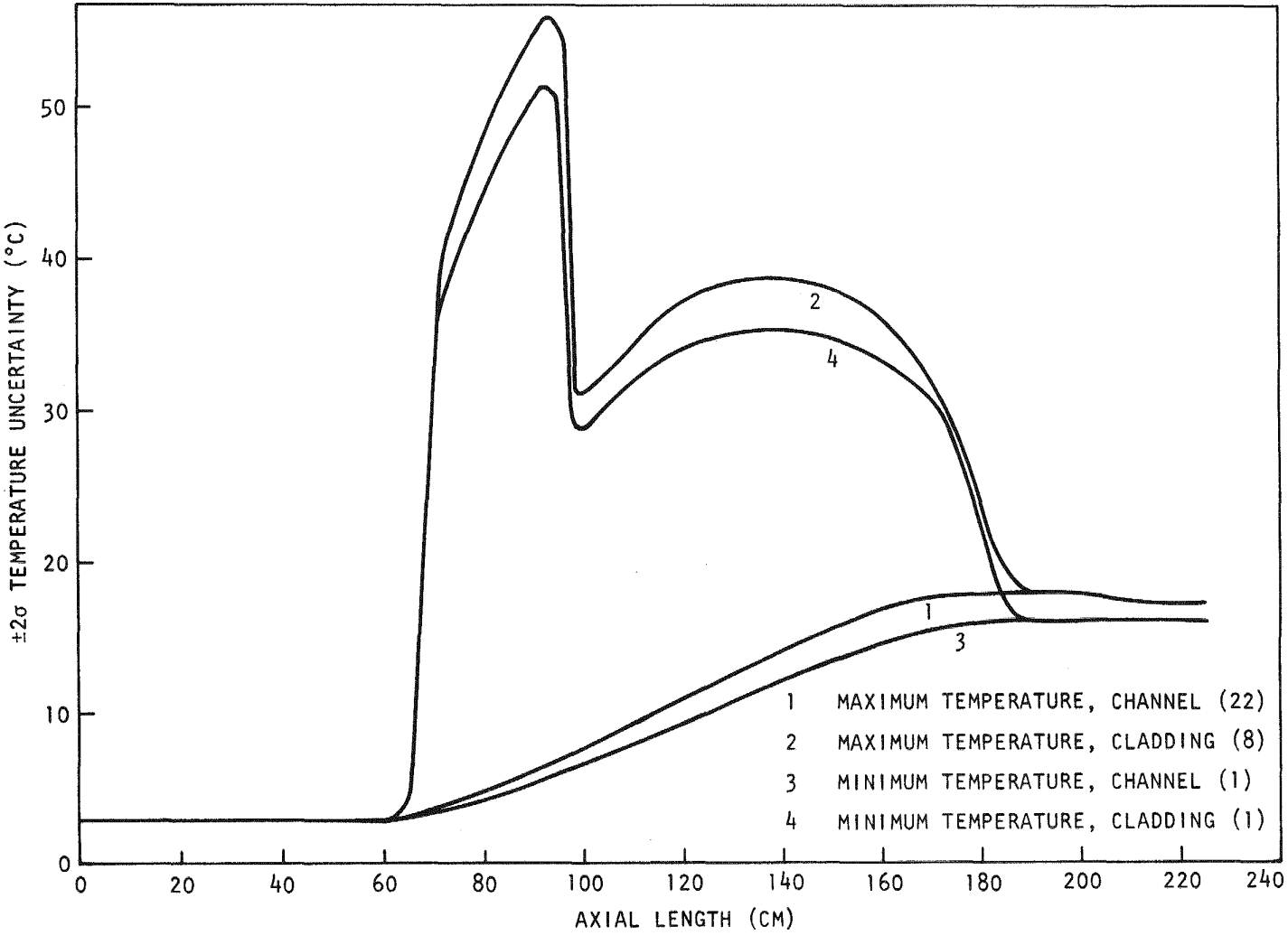

Fig. 4-5. Temperature uncertainty, 100% power and flow

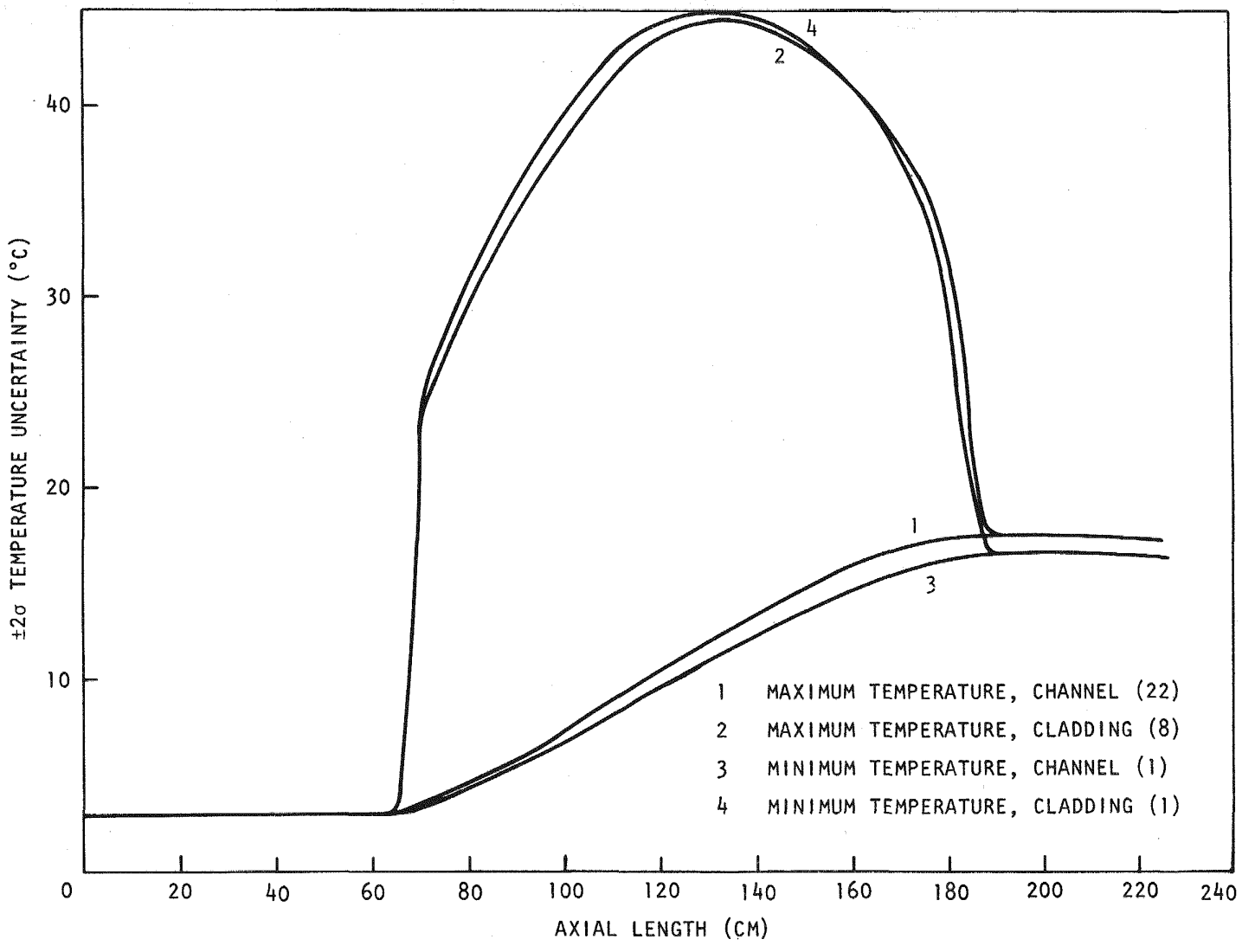

Fig. 4-6. Temperature uncertainty, 10% power and flow

The TSPEC code was used for comparing the results of the 37-rod assembly with the COBRA results. It was found that TSPEC predicted average temperatures which are higher than the maximum temperature of the COBRA analysis. This is because TSPEC does not consider mixing of the coolant from the internal subchannels with the coolant from the peripheral subchannels which are overcooled. This comparison is shown in Figs. 4-3 and 4-4.

4.3. TEST SPECIFICATION

The decision to retain the maximum test conditions given in the program plan (Ref. 4-1) was based on the justification that (1) current CFTL design and operating conditions are adequate to accommodate uncertainties in the GCFR, and (2) retention of the conditions will not perturb ongoing loop design and development activities at ORNL. The minimum operating conditions, in particular those associated with undercooling in the beyond design basis accident conditions, have not been resolved. Uncertainties include the reference GCFR conditions to be simulated and the practical capabilities which can be built into the CFTL.

4.4. TEST BUNDLE DESIGN AND FABRICATION

Consideration of the fuel rod simulator overall length disclosed the need for added stiffness in the length above the test bundle inlet grid to minimize the effect on the part of the rod simulator which is within the test section, in particular the heated part of the rod simulator. Figure 4-7 shows the change suggested by GA for the conceptual design of the inlet plenum area to accomplish increased rod simulator stiffness. The distance from the bottom of the inlet grid to the top of the upper closure, or tube sheet, to which the rod simulator will be attached has been reduced from 1170 to 405 mm. Since stiffness of a beam is defined as the inverse of deflection and deflection varies as the cube of the length, a reduction in length by a factor of $\sim$2.9 results in a 24-fold increase in rod simulator stiffness in the length above the inlet grid.

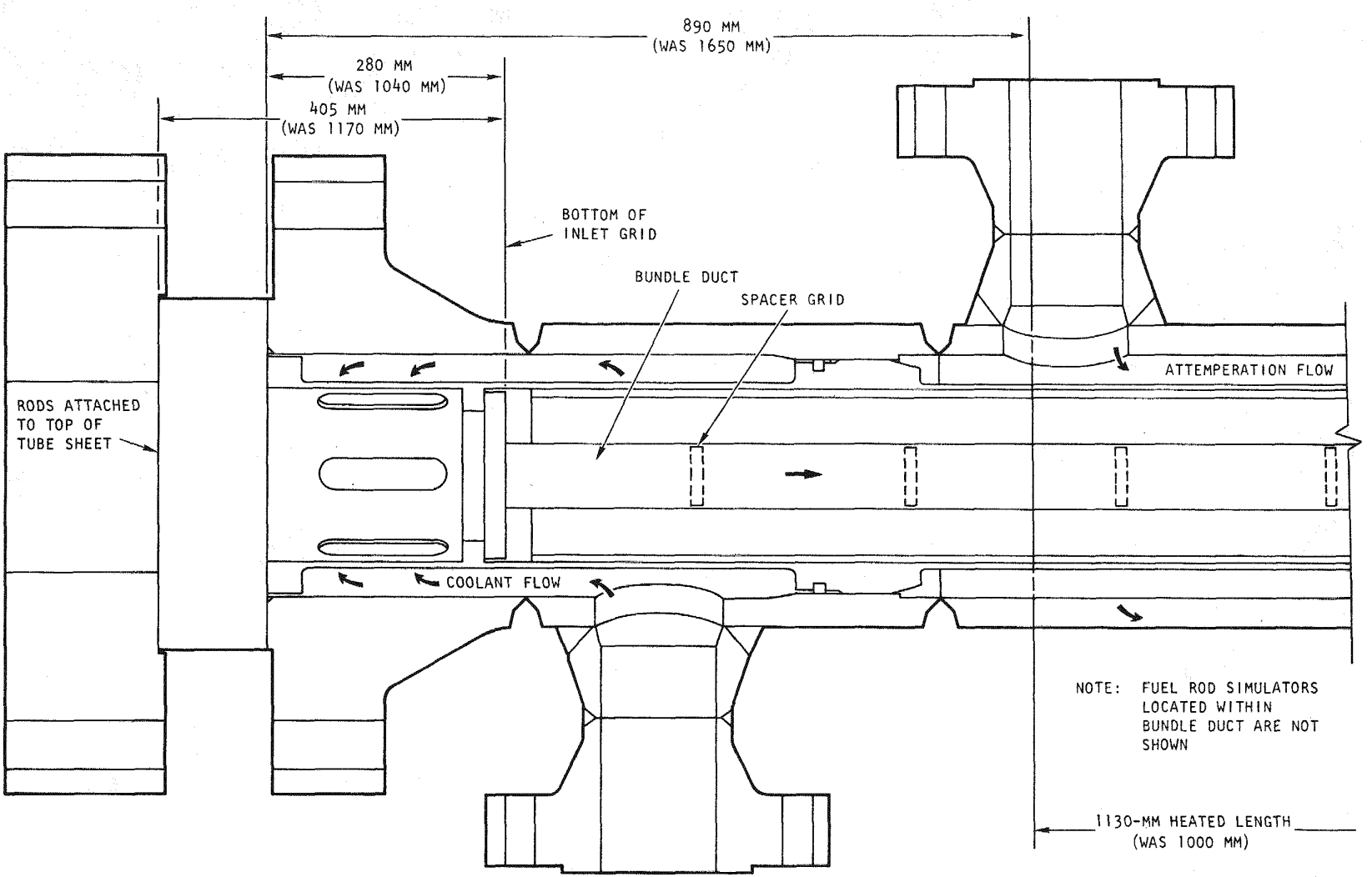

Fig. 4-7. Modified conceptual design of the coolant inlet end of the test vessel

To assist CFTL program participants in planning and design activities, the dimensions and power requirements listed in Table 4-2 for fuel rod simulators and blanket rod simulators were provided.

4.5. LIAISON WITH ORNL

ORNL substantially increased its conceptual design and analysis activities at the start of FY-77, and two coordinating meetings with new personnel were held at ORNL early in November to review the CFTL program plan (Ref. 4-1). The first meeting dealt with the design of the 37-rod bundle which models the fuel assembly in the preliminary tests and associated bundle fabrication planning and organizational responsibilities. The second meeting was concerned with program objectives, implementation, and scheduling. A detailed discussion of the analytical requirements was held to determine the ORNL and GA work scopes and interfaces.

On November 10, 1976, ORNL presented an in-depth CFTL review for the GCFR (Utility) Program Review Committee as a follow-on review to a CFTL review at GA in October.

On November 19-20, 1976, a GCFR Loop Experimenter's meeting was held in Washington with representatives from the U.S. and European GCFR test programs. The principal objective of this exchange of information was to enhance program coordination on the development of the GCFR, and several things were accomplished: (1) experimenters who are planning loops and tests benefited from the experience of those who are currently involved in testing; (2) presentation of the overall GCFR plans and status provided insight for completion of present tests and planning of future tests; (3) representatives of ERDA and the Nuclear Regulatory Commission (NRC) met with the individuals who are building the data base and planning the verification of the GCFR design.

TABLE 4-2
CFTL FUEL ROD SIMULATOR AND BLANKET ROD SIMULATOR
DIMENSIONS[a] AND POWER REQUIREMENTS

Fuel rod simulator (cladding material = 20% cold-worked 316 stainless steel	
Length (bottom of inlet grid to bottom of rod, cold) (mm)	220.0
Heated length (cold) (mm)	1130.0
Roughened length (cold) (mm)	860.0
Outside diameter, roughened (cold) (mm)	7.46
Outside diameter, smooth (cold) (mm)	7.20
Inside diameter (cold) (mm)	6.44
Lower axial blanket length (cold) (mm)	450.0
Power	
Maximum per rod (kW)	38
Maximum per test bundle (91-rod bundle, 85 fuel rod simulators) (MW)	3.23
Axial distribution	Chopped cosine
Maximum/average	1.21
Local/maximum	$\cos[1.049(2\frac{x}{L} - 1)]$, $L = 1130$, $x(\text{range}) = 0 \text{ to } 1130$
Blanket rod simulator (cladding material = 20% cold-worked 316 stainless steel	
Length (bottom of inlet grid to bottom of rod, cold) (mm)	2220.0
Outside diameter (cold) (mm)	21.6
Inside diameter (cold) (mm)	20.6
Wire-wrap spacer diameter (mm)	1.4
Wire-wrap pitch (mm)	300.0
Power	
Maximum per rod (kW)	45
Maximum per test bundle (61-rod bundle, 60 blanket rod simulators) (MW)	1.7
Axial distribution	Cosine
Maximum average	1.72
Local/maximum	$0.52 + 0.48[\cos 1.57(\frac{2z}{h} - 1.86)]$, $h = 1091.4$, $z(\text{range}) = 0 \text{ to } 2030$

[a] Dimensions are identical to those for GCFR fuel and blanket rods.

4.6. GCFR PROTOTYPE CORE ASSEMBLY TEST PLANNING

Program planning for testing of the full-size prototype core assemblies is continuing, and a summary of comments which were received with the outline plan (Ref. 4-5) was completed and issued to ERDA. The prototype core assembly tests will be conducted on full-size core assemblies to ensure that the core assemblies meet design qualification requirements prior to fabrication of the GCFR demonstration plant initial core. The prototype assemblies will duplicate the GCFR demonstration plant core assemblies except that PuO_2-UO_2 fuel in the rods will be simulated by depleted UO_2. The objective of the prototype test program is to evaluate the preliminary design of the full-size GCFR core assemblies by subjecting the assemblies to maximum GCFR helium flow conditions in a close simulation of the reactor core environment, but without radiation. One assembly of each type (fuel, control, and blanket) will be subjected to the equivalent of approximately 1 yr of reactor operation in a hot helium test loop.

Review of the test loop facility options for the prototype tests has continued. As noted in Ref. 4-2, the option of using the HHV loop in Julich was removed from active consideration because the operating capabilities of the HHV loop do not simulate closely enough the required GCFR core operating conditions. Several other loop siting options for prototype testing are being evaluated, including the EBOR facility at Idaho Nuclear Engineering Laboratory (INEL), the CARMEN-2 loop at Saclay, France, and a new facility (sited either in Europe or the U.S.) which would be especially designed for prototype testing. The CARMEN-2 loop circulator performance curves are being reviewed, and there may be a problem obtaining sufficient flow for concurrently testing all three types of core assemblies.

A technical meeting was held at INEL to discuss the EG&G proposal to conduct the prototype tests at INEL. The tests would be conducted in the old EBOR facility following conversion of the facility to a hot helium flow loop. The discussion centered around the feasibility of converting EBOR and the cost advantages of easing one of the prototype test requirements, i.e., changing the maximum temperature/flow requirement of 550°C at

full flow to 450°C at full flow and 550°C at half flow. This change would result in a significant reduction in helium heater size and heater power requirement with a concomitant reduction in facility and operating costs.

Reports (Refs. 4-6 through 4-8) covering the EBOR main helium blower problems which arose in 1966 were obtained and sent to INEL. These reports describe the failure and recommended blower modifications and operating instructions for the blower. Early determination of the adequacy of the EBOR blower is needed to permit a meaningful evaluation of the EBOR facility option.

REFERENCES

4-1. Hopkins, H. C., Jr., "Program Plan for GCFR Core Flow Test Loop," USAEC Report GA-A13080, General Atomic, August 9, 1974.

4-2. "Gas-Cooled Fast Breeder Reactor Quarterly Progress Report for the Period August 1, 1976 Through October 31, 1976," ERDA Report GA-A14112, General Atomic, November 1976.

4-3. "Gas-Cooled Fast Breeder Reactor Quarterly Progress Report for the Period May 1, 1976 Through July 31, 1976," ERDA Report GA-A13975, General Atomic, August 31, 1976.

4-4. Hopkins, H. C., Jr., "TSPEC - A Computer Program to Predict Approximate Model Performance in the Core Flow Test Loop," ERDA Report GA-A14057, General Atomic, November 1976.

4-5. Strong, W. R., "Outline Plan for GCFR Prototype Core-Element Test Program," General Atomic, unpublished data.

4-6. "Recommended Modifications to the Main Helium Blower," Chemet Engineers, September 19, 1966.

4-7. "Mechanical Seal Failure," Chemet Engineers, August 26, 1966.

4-8. "Main Helium Blower Operating Manual," Chemet Engineers, September 19, 1966.

5. FUELS AND MATERIAL ENGINEERING (189a No. 00583)

5.1. OXIDE FUEL, BLANKET, AND GRID PLATE SHIELDING MATERIALS TECHNOLOGY

This subtask is concerned with oxide fuel technology and blanket technology. As a result of the decision to replace ThO_2 as a candidate radial blanket material with UO_2, differentiation of the axial and radial blanket material has been suspended.

During this quarter, GA representatives participated in an exchange of information meeting with the committee on fuel-cladding chemical interaction (FCCI), and several conclusions were reached regarding temperatures in near-commercial liquid metal fast breeder reactor (LMFBR) designs, correlations for FCCI, and advanced alloys. Based on the limited information available, the group concurred on an order of preference for materials used for controls:

1. For location in the fuel or fuel-cladding interface,

    a. Vanadium.
    b. Niobium.
    c. Titanium.
    d. Chromium.
    e. Zirconium.

2. For location at the fuel-blanket interface,

    a. Titanium.
    b. Vanadium.

c. Niobium.

d. Zirconium.

GA agreed to submit GCFR fuel rod irradiation data to the committee.

5.2. CLADDING TECHNOLOGY

During this quarter, a master test matrix for the entire cladding technology program was formulated. This test matrix will be reviewed by ANL and Pacific Northwest Laboratory (PNL) personnel prior to finalization. The test program is shown in Fig. 5-1, and a brief description of the planned tests is given below.

1. Biaxial creep rupture tests on unirradiated ribbed and smooth cladding with a hoop to axial tensile stress ratio of 2. These tests have already been initiated in quasistatic helium at ANL and in recirculating helium at PNL. Comparison of the ANL and PNL tests is expected to demonstrate the effects of mass transfer.

2. Biaxial creep rupture tests on unirradiated ribbed and smooth cladding with a hoop to axial tensile stress ratio of unity. These tests are in support of tests on irradiated cladding. The test specimens will be aged at the irradiation temperature such that comparison of the results on unirradiated and irradiated specimens will indicate the effects of irradiation.

3. Tensile tests on unirradiated ribbed and smooth cladding. These tests are in support of the irradiated cladding tests. Aged specimens will be tested to determine the effects of irradiation.

4. Biaxial creep rupture tests on irradiated ribbed and smooth cladding with a hoop to axial tensile stress ratio of unity. The only cladding loading in the GCFR fuel rods will be due to fuel-cladding mechanical interaction which leads to the 1:1 stress state.

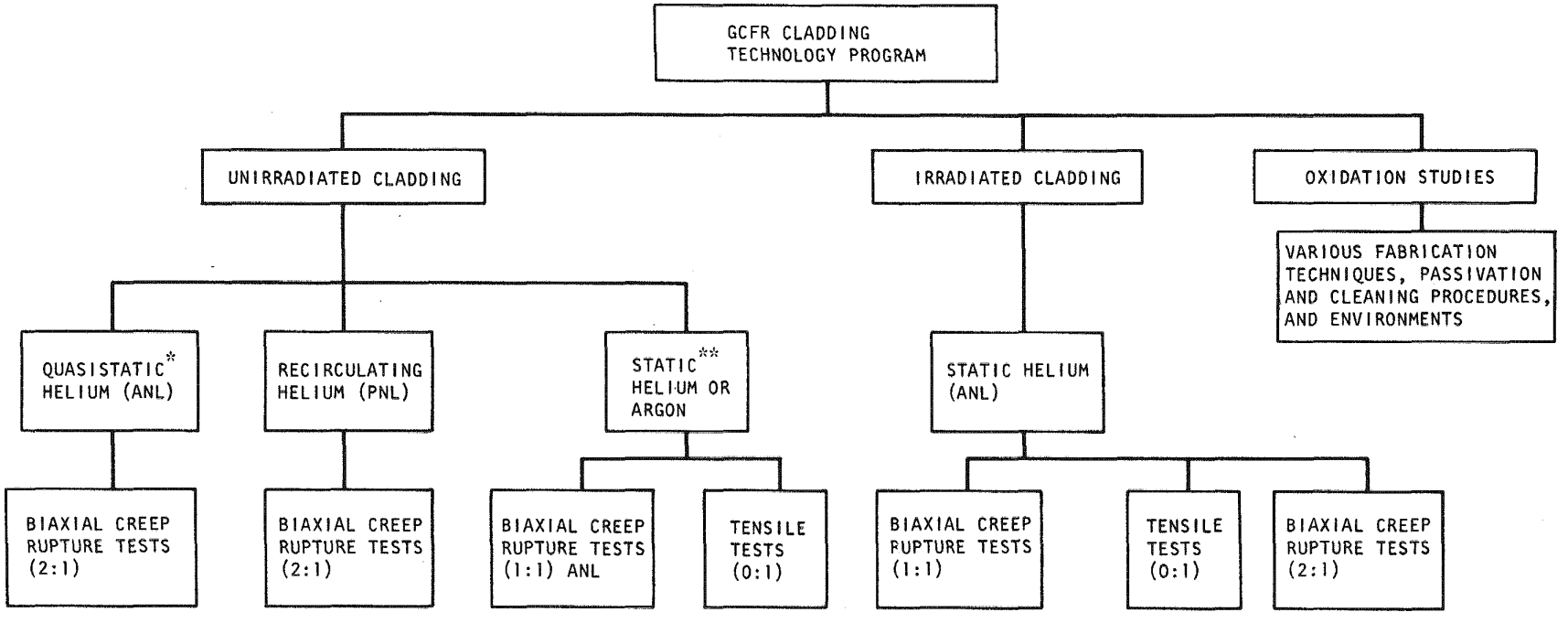

*QUASISTATIC MEANS FLOW THROUGH HELIUM SYSTEM.

**STATIC MEANS NO GAS FLOW.

Fig. 5-1. Cladding technology test program

Comparison of the results from this test with those of test 2 above will indicate the effects of irradiation.

5. Tensile tests on irradiated cladding. These tests will determine the effect of ribs on flow stress.

The detailed test matrix has been formulated and will be reviewed by GA, ANL, and PNL before finalization.

5.2.1. Mechanical Testing Program at Argonne National Laboratory

The purpose of this program is to determine the effects of the following factors on the behavior and mechanical properties of GCFR cladding:

1. Ribs, rib geometry, and fabrication technique.
2. Helium impurity and levels typical of the GCFR environment.

The first biaxial creep rupture test (ANL test 1) was conducted to determine the effect of the end cap design and the length of the specimen. In accordance with the second test matrix, ANL test 2 was completed. Both tests were performed at 650°C at a hoop stress of ∿238 MPa in a purified helium atmosphere. Ribbed and smooth claddings were tested.

During this quarter, draft copies of the test reports on the first and second tests at ANL were reviewed. The third test at ANL has been initiated. This test will be performed in a helium environment consisting of 300 MPa of hydrogen and 30 MPa of H_2O at 650°C. Under these test conditions, only chromium can oxidize owing to thermodynamic considerations.

Ribbed cladding fabricated by mechanical grinding at Kraftwerk Union and WMC Corporation have been received. These claddings will be used in future tests.

5.2.2. Helium Loop Test Program at Pacific Northwest Laboratory

The primary objective of this test program is to compare the mechanical properties determined in recirculating helium at PNL with those determined in quasistatic helium at ANL. The work scope has been defined, and the loop has been modified for unattended operation. An impurity monitoring system has been installed, and the first test was initiated. The first 100 hr of testing indicated many significant control problems, and efforts to solve them are under way.

To obtain better control of the test conditions, the following efforts were made during this quarter:

1. A calibration procedure for the Thermox meter has been formulated and will be forwarded to PNL.

2. A cleaning procedure for core components has been obtained from Hanford Engineering Development Laboratory (HEDL) and will be adopted for use at ANL and PNL.

3. An EG&G dew point hygrometer has been purchased for use at PNL.

5.3. F-1 FAST FLUX IRRADIATION EXPERIMENT

Postirradiation examination of the encapsulated seven-fuel-rod F-1 (X094) experiment, which received a maximum burnup exposure of ∿121 MWd/kg (see Table 5-1), is continuing at Argonne National Laboratory East (ANL-E). The final remaining F-1 capsule G-12 has been neutron radiographed at Argonne National Laboratory West (ANL-W) and received at ANL-E, where it will be examined. Six of the seven fuel rods in the final F-1 assembly have been de-encapsulated, and all are in excellent condition. The remaining fuel rod capsule, G-12 was received at Argonne National Laboratory Material Science Division (ANL-MSD) and will be de-encapsulated as soon as hot cell manipulator problems are overcome.

TABLE 5-1
SUMMARY OF OPERATING CONDITIONS AND PARAMETERS FOR THE F-1 (XO94) EXPERIMENT FUEL RODS

Capsule	Type of Pellet[a]	Test Condition: Cladding I.D. Maximum Temperature (°C)	Test Condition: Peak Linear Heat Generation Rating (W/cm)	Fuel O/M	Burnup (MWd/kg)	Type of Trap[b]	Purpose (Status)
					25 50 75 100 125		
G-1	A	760	456	1.992	→ →	S	Temperature effect, post-irradiation examination completed
G-2	A	725	439	1.971	→ →	S	Temperature effect, post-irradiation examination completed
G-3	A	695	439	1.987	→	S	Temperature calibration, post-irradiation examination completed
G-4	A	680	456	1.983	→ → → → →	A	Burnup effect
G-5	A	640	405	1.990	→ →	S	Temperature effect, post-irradiation examination completed
G-6	A	685	408	1.972	→ →	A	Reference/fast flux - thermal flux comparison, postirradiation examination completed
G-7	A	570	390	1.984	→ →	A	Overlap with LMFBR/temperature effect, postirradiation examination partially completed
G-8	A	672	451	1.985	→ → → →	S	Burnup effect
G-9[c]	A	702	445	1.968	→ → →	A	Surface roughening effect
G-10	A	712	469	1.968	→ → →	A	Surface roughening effect reproducibility
G-11[d]	A	712	494	1.947	→ → →	A	Low fuel oxygen-to-metal effect
G-12	S	690	445	1.976	→ → →	A	Solid pellet effect at reference cladding temperature
G-13	S	770	494	1.973	→ → →	A	Solid pellet effect at high cladding temperature

[a] A = annular, S = solid.

[b] A = active, S = sealed.

[c] This fuel rod was in capsule G-11.

[d] This fuel rod was in capsule G-9.

Profilometry showed that the maximum diametral increase of 0.05 mm, or 0.7%, occurred in rod G-4 at 121 MWd/kg exposure. For the rods which achieved 75 MWd/kg exposure, no difference was found between the strain in the ribbed and the smooth rods.

During de-encapsulation, it was discovered that capsule G-9, which was supposed to contain a ribbed rod, contained a smooth rod, G-11, instead. Capsule G-11 contained the ribbed rod G-9. The switch caused no appreciable change in operating conditions since the enrichment and the thermal barrier thickness was the same in the two capsules. The difference in capsule position in the experimental subassembly caused only a minor difference in operating temperature ($\sim$10°C).

Another surprising observation was that the dosimeter tubes made of SA 304 stainless steel experienced a growth in length of up to 100 mm (capsule G-4 at 121 MWd/kg, 8×10^{22} n/cm^2) more than the thermal barrier made of the same material. The dosimeters operated at a lower average temperature than the thermal barriers, and this temperature difference may have resulted in the occurrence of a very large difference in irradiation swelling.

A TAC-2D thermal analysis was performed on an F-1 experiment silicon carbide temperature monitor. Three runs were made to vary the thermal contact between the monitor and the molybdenum capsule and between the molybdenum capsule and the stainless steel capsule. The monitor temperature was found to vary from 402° ± 2°C for the case with the lowest contact resistance to 407° ± 2°C for the highest resistance. Since the silicon carbide monitors indicated local capsule temperatures which were 50°C higher than design, this result appears to indicate that the actual temperatures on the F-1 fuel rod capsules were higher than calculated. The uncertainty in the silicon carbide temperature determinations is of the order ±25°C.

Gamma scanning of F-1 rods G-4 (121 MWd/kg, O/M = 1.98) and (77 MWd/kg, O/M = 1.95) was completed, and the gamma scans were reviewed at GA to determine the location of sections to be cut from the rod for study of cesium

transport effects. Comparison of the distribution of Cs-137 in fuel rod G-4 at 52 and 121 MWd/kg and G-9 at 77 MWd/kg is shown in Table 5-2.

Fuel rod G-4 exhibits a normal distribution profile when compared with the earlier distribution analyses, and G-9 shows a greater depletion of Cs-137 in the fuel region; the cesium was predominantly shifted toward the upper blanket region. This shift may be due to either the higher rod temperature and/or the lower fuel O/M ratio. Lower O/M fuels are known to enhance cesium migration, and the G-9 data are in rough agreement with the observed O/M dependence. These rods thus represent an excellent opportunity to assess the cesium transport effects.

In the GA hot cells, the charcoal from the upper and lower charcoal traps of rod G-7 has been removed for fission product content and distribution analysis. This analysis of a rod removed from experiment F-1 at the 50 MWd/kg burnup interim was delayed by the limited funding of the post-irradiation task. The radiation-induced shrinkage of fission product trap charcoal from rods G-1 through G-13 was determined from preirradiation and postirradiation radiographs. The amount of charcoal shrinkage varied over the range 30% to 60% and was directly proportional to the fast neutron fluence.

Previously reported ternary fast fission yields for Th-232 and U-238 have been reviewed and corrected for fractional contributions of the bred isotopes U-233 and Pu-239, respectively. Calculations show that the fissile species account for 40% to 80% of the fission in the fuel particles. Based on the relative fission cross sections and the average concentrations of the fissile and fertile species averaged over the reactor residence time, the current yield values of the isotopic species in the experimental breeder reactor II (EBR-II) spectrum are

TABLE 5-2
DISTRIBUTION OF Cs-137 IN FUEL RODS G-4 AND G-9

Region	Cs-137 Distribution (%)		
	G-4[a]		G-9[b]
	Burnup = 52 MWd/kg	Burnup = 121 MWd/kg	Burnup = 77 MWd/kg
Upper trap	--	0.7	1.3
Upper blanket	13.1	4.2	36.5
Fuel region	77.2	87.0	52.0
Lower blanket	9.1	8.0	8.5
Lower trap	--	<0.1	1.9

[a] Surface cladding i.d. temperature = 680°C; fuel O/M = 1.98.

[b] Surface cladding i.d. temperature = 729°C; fuel O/M = 1.95.

	Tritons per fission ($\times 10^4$)
U-238	9
Pu-239	20
Th-232	6
U-233	15

These yields are higher than yield values of U-235 by factors of 4.5 to 10. This increased tritium yield may have a significant impact on all plutonium-fueled reactors, notably fast breeders.

Discussions with LMFBR personnel have focused on (1) confirmation of GA experimental data and (2) determination of an alternate irradiation vehicle for the dosimeters containing PuO_2 and $U\text{-}233O_2$ microspheres which were to have been irradiated in G-3 rods G-25 and G-26.

5.4. F-3 FAST FLUX IRRADIATION EXPERIMENT

The F-3 experiment was irradiated in location 4B3 in EBR-II to an exposure of ($\sim$46 MWd/kg); the burnup goal was 100 MWd/kg. These capsules shared a type J19A subassembly (X206) with the ANL group-08 high-temperature chemistry experiment, as reported in Ref. 5-1. The experiment reached an exposure of 46 MWd/kg on February 11, 1976, at which time it was removed from the core for a planned interim examination. It was discovered that nine of the ten rods had failed, apparently owing to inadequate capsule sodium bonds. Therefore, final examination at ANL-MSD and GA is under way.

At ANL, the capsule tubing of intact fuel rod G-18 was longitudinally slit at three locations 120-deg apart. The three sections of tubing were then peeled off the sodium and fuel rod. Extensive areas were found in which sodium was not present. Shrinkage voids are expected when the capsules are cooled from the top down during removal from EBR-II and until the subassembly duct is removed in the hot fuel examination facility (HFEF), at

which time the sodium is frozen. At present, no determination has been made as to whether the areas of the capsule or the fuel cladding where sodium was not actually visually present were wet with sodium during irradiation. Unfortunately, when the capsule tube was slit, the cladding was also inadvertently slit, and much of the fuel fell out while the capsule tube was removed. Some fuel remained at the ends of the rod and was potted with epoxy, and sections for metallographic examination were cut from the fuel-blanket interface. A "bulge" in the G-18 fuel cladding just above the reactor midplane was photographed and appears to extend at least 180-deg around the circumference and to have the point of greatest diametral increase at the location of a rib.

Shield material capsules and upper dosimeters from the F-3 rods were received at GA. The shield materials were removed from their subcapsules and are generally in good shape. The materials from G-19 were examined under a low-power stereomicroscope. The beryllium metal sample was in excellent condition, with some marks on it owing to removal and handling, and the small-diameter (1.2 mm) BeO rods were chipped on the ends. The two ZrH_x pellets were in good shape except for the $ZrH_{1.75}$ pellet, which had an axial crack. The dosimeters are currently being removed from their containment tubes.

5.5. F-5 PROTOTYPE IRRADIATION EXPERIMENT

Design work and ordering of materials continued for the F-5 prototype design fuel rod experiment. As previously reported (Ref. 5-2), the F-5 experiment for the study of the performance of fuel rods irradiated under simulated GCFR conditions to high burnups will (1) determine the reliability of the GCFR fuel rod design, (2) discover the failure modes which may exist, and (3) study the effect of a step power increase which simulates the 180-deg rotation of a subassembly at the core-blanket interface in the proposed GCFR demonstration plant. The F-5 experiment will consist of two 19-rod subassemblies, one of which will be irradiated starting January 1978 and continuing until EBR-II is shut down (currently planned for December 1980). A total of 43 rods will be irradiated.

During this quarter, two changes were made in the specification for the F-5 fuel: (1) the plutonium content was raised from 17% to 25% of total heavy metal, and (2) it was decided that solid instead of annular pellets will be employed. The smear density will remain at 85.5 ± 2%.

Calculations at GA for F-5 fuel U-235 enrichment gave 30.3 wt% for position 4B2, run 85A, for the fuel (recommended by the EBR-II project as being representative of the F-5 experiment when installed). The calculations have been documented, and it was recommended to ANL that 30.3 wt % enrichment value be used in the F-5 fuel specifications.

An integral F-5 fuel rod bottom end fitting and trap design was prepared by GA and accepted by the EBR-II project. This integral design incorporates a trap which is gun-drilled from bar stock and is similar to the design of the trap in the current GCFR demonstration plant fuel rod design. This bottom end fitting also incorporates a centering pin to ensure central location of the fuel rod in the subassembly shroud tube.

The EBR-II project has accepted a GA proposal to place a capsule containing candidate GCFR grid plate neutron shield materials in the inlet nozzle of the F-5 subassemblies.

ANL-MSD reports that the delivery date for the F-5 cladding is now estimated to be between February 24 and March 3, 1977.

The laser plenum puncturing and sealing equipment needed for the F-5 experiment at EBR-II has been given a lower priority and may not be available in June 1979, when depressurization of the F-5 fuel rods will be required during the interim examination. ANL-MSD will have to develop a backup method for plenum puncturing and sealing. Although this development is not needed immediately, it must be completed in a timely manner.

A proposed plan for sectioning and examining the high-priority rods G-4 [high burnup (121 MWd/kg)] and G-11 [low O/M = 1.947 (75 MWd/kg)]

from the F-1 experiment and a vented rod from GB-10 has been sent to ANL-MSD. The results of the examinations of these rods are expected to provide very useful information on cesium transport and behavior in the GCFR and data to be used in the design of the special blanket pellets to be employed at the fuel-blanket interface regions in some of the F-5 rods.

Studies being made at ANL Chemical Engineering Division (ANL-CED) on cesium transport and reaction with UO_2 pellets will also provide necessary design information. The above information combined with analytical work at GA is expected to result in a final design for the F-5 special blanket pellets by March 1, 1977. The special blanket pellets will be fabricated by GA.

Materials received at GA for the trap and dosimeters for the F-5 experiment are undergoing chemical analysis overchecks and metallographic characterization.

5.6. GB-10 VENTED FUEL ROD EXPERIMENT

During this quarter, nondestructive examination of the GA-21 vented fuel rod from the GB-10 experiment continued at ANL. A detailed gamma scan of the fuel rod was completed.

A distribution analysis of Cs-137 in the GB-10 fuel rod is shown in Table 5-3. Comparison of the GB-10 (vented rod) Cs-137 profile with fuel rods of similar composition (rod G-8 at 97 MWd/kg and rod G-4 at 121 MWd/kg) from the F-1 experiment (sealed rods) indicates a marked profile similarity. A parallel similarity is shown by the profiles of vented thermal flux rod GB-9 and sealed fast flux rod G-4 at 52 MWd/kg. The fuel loadings are essentially identical, the blanket lengths and fuel stoichiometry are similar, and therefore the fuel fission product chemical activity is also similar. The effects of the radial thermal flux profile and sweep gas flow through the rod during operation on the Cs-137 distribution in the fuel region are minimal, but they do appear to affect the cesium content of the trap.

TABLE 5-3
DISTRIBUTION AND COMPARISON OF Cs-137 IN GB-9,
GB-10, AND F-1 FUEL RODS

Region	Cs-137 Distribution (%)				
		F-1 Fuel Rods			
	GB-9[a]	G-4[b]		G-8[c]	GB-10[d]
Upper trap	ND[e,f]	--	0.7	ND	4.4
Upper blanket	25	13.1	4.2	6.6	10.9
Fuel region	64.5	77.2	87.0	85.9	74.9
Lower blanket	10.1	9.1	8.0	7.5	10.1
Lower trap	--	--	<0.1	ND	NA[g]

[a] Fuel O/M = 1.98; burnup = 56 MWd/kg.

[b] Surface cladding i.d. temperature = 680°C; fuel O/M = 1.98; burnup = 52 and 121 MWd/kg.

[c] Surface cladding i.d. temperature = 670°C; fuel O/M = 1.98; burnup = 97 MWd/kg.

[d] Surface cladding i.d. temperature = 750°C; fuel O/M = 1.985; burnup = 100 MWd/kg.

[e] ND = not detected.

[f] Chemical analysis of the GB-9 charcoal trap showed a 4×10^{-5} fraction of Cs-137 to be present in the trap, but none was detected by gamma spectrometry.

[g] NA = not applicable.

The Cs-137 loading on the GB-10 trap is significantly higher (4.4%) than the ∿1% for G-4 at 121 MWd and the 1.3% loading for the G-9 rod trap (as determined from recent scan analyses). The distribution pattern (profile) appears to change with burnup. Initially, a greater fraction of Cs-137 is found in the blanket regions. As burnup increases (>25 MWd/kg), the mobility of Cs-137 diminishes, which may be a result of the decreasing diffusion potential as the cesium concentration gradient diminishes throughout the sealed rods. Detailed postirradiation examination of the various capsule components will be helpful in further assessing the cesium transport effects.

A distribution analysis of Cs-137 in the F-3 fuel rods indicates a substantial amount of Cs-137 in the active and sealed traps (G-16). The distribution values are itemized in Table 5-4. The presence of sodium within the rod probably provides an efficient transport vehicle for the cesium. However, the presence of Cs-137 within the charcoal trap of rod G-16, purportedly a sealed trap, is anomalous.

The gamma scan profiles for the active trap G-16 and the sealed trap are essentially identical and indicate that this trap may indeed have been operating as an active trap. Sodium intrusion into the fuel rod would profoundly affect the distribution profile; i.e., it would tend to "smear" the Cs-137 activity over a larger area. Perhaps an examination of the cesium loading on the charcoal trap of the fuel rods may help ascertain when the failure in the F-3 fuel rods occurred.

5.7. HEDL CLADDING IRRADIATIONS

The objectives of the GCFR cladding irradiation and postirradiation test program are as follows:

1. To determine if the mechanical behavior, in terms of load-carrying ability, of irradiated GCFR ribbed cladding is different from that of irradiated smooth cladding under biaxial loading conditions. The stress state, but not the absolute level of stresses expected in the GCFR, will be simulated.

TABLE 5-4
DISTRIBUTION OF Cs-137 IN F-3 FUEL RODS

Fuel Rod	Cs-137 Distribution (%)	
	Fuel Region	Charcoal Trap
G-14	69	31
G-15	68	32
G-16	68	32 (sealed trap)
G-17	60	40
G-18	100	-- (sealed trap)
G-19	58	42
G-20	62	38
G-21	42	58
G-22	64	36
G-23	33	67

2. To determine if mechanical properties such as rupture life and creep ductility measured under the expected GCFR stress state (i.e., hoop to axial tensile stress ratio of unity) are equal to or significantly different from those determined under internal pressure loading conditions (hoop to axial tensile stress ratio of 2).

3. Using a statistically meaningful test program, to determine the quantitative effects of ribs and stress state on the creep rupture behavior of irradiated GCFR cladding.

Some ribbed and smooth GCFR cladding specimens have already been irradiated (Table 5-5), and arrangements have been made to ship the specimens to ANL-MSD for postirradiation testing. Some specimens are continuing to be irradiated as part of the HEDL cladding irradiation test capsules. Additional irradiation is considered necessary because the limited number of specimens in the initial test matrix does not cover the temperature range or the fluence levels typical of the GCFR. For these reasons, a preliminary second irradiation test matrix was formulated (Ref. 5-2) and is in the process of being finalized. A provision for irradiation of specimens to be tested in uniaxial tension is currently being added.

REFERENCES

5-1. "Gas-Cooled Fast Breeder Quarterly Progress Report for the Period February 1, 1976 Through April 30, 1976," ERDA Report GA-A13868, General Atomic, May 31, 1976.

5-2. "Gas-Cooled Fast Breeder Quarterly Progress Report for the Period August 1, 1976 Through October 31, 1976," ERDA Report GA-A14112, General Atomic, November 1976.

TABLE 5-5
GCFR CLADDING SPECIMENS WHICH HAVE COMPLETED IRRADIATION

Irradiation Temperature (°C)	Fluence (n/cm^2)	Type of Specimen	Date of Removal from EBR-II	Postirradiation Tests	
				Environment Temperature (°C)	Stress,[a] Root of Rib (MPa)
700	2.6 to 3.6 x 10^{22}	5 smooth, 5 ribbed by etching	9/75	700 (1.013 x 10^5 Pa static helium)	138
700	4.2 to 6 x 10^{22}	2 smooth, 3 ribbed by etching	3/76	700 (1.013 x 10^5 Pa static helium)	138

[a] The hoop stress to axial stress ratio is equal to one.

6. FUEL ROD ENGINEERING (189a No. 00583)

The objective of this task is to evaluate the steady-state and transient performance of the fuel, blanket, and control rods to determine performance characteristics, operating limits, and design criteria. To this end, analytical tools (such as the LIFE-III code) are being adapted and/or developed and applied to the analysis of GCFR prototypical and experimental rods. In addition, continuous surveillance of the LMFBR fuels and materials development program and technology is maintained to maximize the use of the technology and material properties. Support is also given to planning and designing of irradiation experiments.

6.1. FUEL, BLANKET, AND CONTROL ROD ANALYTICAL METHODS

6.1.1. Fuel Rod Analytical Method

The second draft of the LIFE-III user's manual (Ref. 6-1) was received from ANL and reviewed, and certain assumptions and mathematical derivations which are not clear or seem unreasonable were identified; contact has been made with the LIFE Working Group members.

6.1.2. Blanket Rod Analytical Method

The modeling theory and computer program structure of the LIFE code and its adaptation to blanket rod analysis continued to be studied. A report on a computer code for predicting the thermomechanical performance of light water reactor (LWR) fuel rods (Ref. 6-2) was obtained from ANL and reviewed. The LIFE-LWR code was developed by modifying the materials properties in the LIFE code. Of particular interest is the incorporation of UO_2 material properties into LIFE-LWR, because the GCFR radial blanket rod uses UO_2 as pellet material. In addition, the fuel anisotropic swelling model, which

uses a great deal of computer core memories, has been removed from LIFE in the generation of LIFE-LWR. Therefore, the fuel swelling model was brought back to the original isotropic swelling model, and the gas release constants were modified. It is believed that the suppression of anisotropic fuel swelling is applicable to the blanket rod analysis because the temperatures in the blanket fuel will be low, so that the anisotropic fuel swelling resulting from the migration of fission gas bubbles is not significant.

A problem which may arise from adapting LIFE to the blanket rod analysis involves the constant parameters built into the code. The LIFE code was developed from theoretical and experimental approaches; i.e., the fundamental equations used in the models were derived from applicable physical principles, but some parameters (constants) in the equations had to be determined by fitting the analytical results to the irradiated fuel rod data. Because these parameters in the current LIFE version were derived from irradiated fuel rods with high linear power ratings, they may not be valid for low-power blanket rod analysis. Thus, these constants may have to be recalibrated according to available data from fuel rods irradiated at a low power level. Since ANL has also received funds to work on GCFR fuel assembly modeling during the current fiscal year, it is expected that GA will work closely with ANL to develop the GCFR blanket rod analysis code from LIFE.

6.1.3. Control Rod Analytical Method

Representatives of GA went to ORNL on September 15-17, 1976 for discussions on Eu_2O_3 control material and the control rod analysis code ABSORB. Eu_2O_3, currently a backup GCFR control material, possesses several advantageous characteristics, such as a high melting point (>2300°C), a low burnup rate, and a lack of a gas-producing mechanism. However, it has low thermal conductivity, which places upper limits on the size of pellets which can be utilized. If the thermal conductivity could be increased without sacrificing nuclear worth (total absorption cross section), larger pellets could be used, thus reducing absorber assembly fabrication costs. ORNL has been examining Eu_2O_3 metal cermets in which thermal conductivity

is increased by forming a continuous metal matrix around the isolated europium phase. It has been found that a Eu_2O_3 - 15% tungsten cermet has a thermal conductivity about five times greater than that of Eu_2O_3. This is a very significant improvement and permits much larger absorber pellets to be considered in the design. The control rod analysis code ABSORB was evolved from the fuel rod analysis code FMODEL, but it has not been updated along with the current technology because the development program was cancelled and work is being performed on HTGR fuel modeling. However, the computer program tape was obtained and will be examined.

On September 29-30, 1976, GA representatives visited HEDL to discuss B_4C control material and control rod modeling techniques. HEDL has been examining the irradiation performance of the sealed and vented control rods, and there is a series of vented control rods being designed and irradiated for optimal study of design parameters for the LMFBR. This is of particular interest to GA because the GCFR control rod reference design will be vented. The control rod modeling technique was discussed, and the control assembly analysis code CONROD and control rod analysis code SIEXB were obtained and will be adopted for GCFR control rod design analysis.

6.2. ANALYSIS OF IRRADIATION TESTS

6.2.1. F-5 Experiment: Fuel-Interfaced Blanket Pellet Thermal Analysis

6.2.1.1. Introduction. It has been shown (Ref. 6-3) that to accommodate the swelling due to the formation of cesium uranate (Cs_2UO_4) resulting from the migration of cesium to the blanket region, an additional 14% void should be provided at the fuel-interfaced blanket pellet in the F-5 experimental fuel rod. There are many ways to incorporate this void into the region, but it is believed that the method chosen should at least be subject to thermal analysis to ensure that melting will not access at the fuel-interfaced blanket pellet. Two methods were investigated: a lower pellet density approach and a small pellet diameter approach. It was found that the maximum temperatures at the fuel-interfaced blanket pellet were 1200°

and 1300°C for low pellet density and small pellet diameter, respectively. These values are well below the UO_2 melting temperature (∿2800°C). However, it is recommended that the low pellet density of 0.8 theoretical density be taken for the F-5 fuel-interfaced blanket pellet design because the small pellet diameter approach may provide a large pellet-cladding gap for cesium to pass through and may cause a serious pellet eccentricity problem inside the rod.

6.2.1.2. Method of Analysis. Thermal analysis of the F-5 experimental fuel rod was carried out using the computer code GCFR*TAC-2D. In the current version, UO_2 thermal conductivity is a function of temperature only. To reflect the dependence of thermal conductivity on pellet porosity, the current equation was replaced by the following equation, taken from (Refs. 6-4 and 6-5):

$$K_{UO_2} = \frac{41.26(1 - P)}{1 + 0.5}\left[\frac{1}{129.4 + T_K} + 1.60173 \times 10^{-14}\right]T_K^3 \text{ W/cm-°C} \quad ,$$

where P is fractional porosity.

6.2.1.3. GCFR*TAC-2D Model. The F-5 experimental fuel rod was modeled according to GCFR*TAC-2D, as shown in Fig. 6-1. The fuel rod was divided into four blocks: lower blanket, fuel, upper blanket, and cladding. In addition, a gap was provided between the cladding and the fuel and blanket regions. The fuel material is $(Pu,U)O_2$ which has a density 89.34% of theoretical density, and the lower and upper blanket materials use UO_2. The two approaches for incorporating the 14% additional void were (1) low pellet density (0.8 theoretical density) and (2) small pellet diameter (0.584 cm). Although reduction of the pellet density or diameter was required only at the fuel-interfaced blanket pellet, the change was assumed to be throughout the blanket region. The effect of this assumption is believed to be small because the axial heat flow is small compared with the radial heat flow. Furthermore, this assumption is conservative with regard to the higher

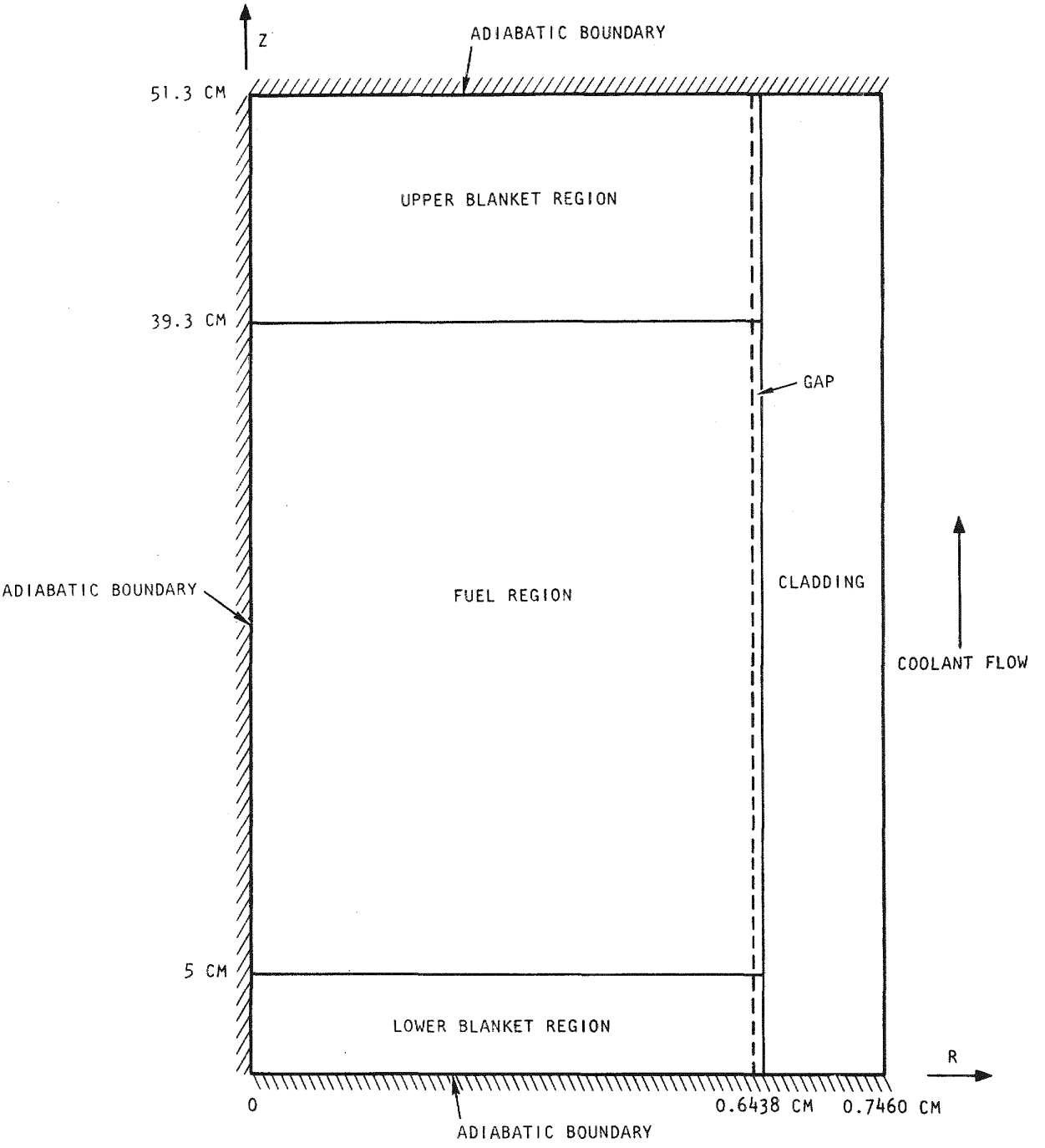

Fig. 6-1. TAC-2D model of the F-5 fuel rod

temperatures at the blanket region because the temperature gradient and the thermal conductivity in the axial direction are lower for the small pellet diameter and low pellet density, respectively. The coolant outside the cladding flows in the positive Z direction with an inlet temperature of 371°C and a flow rate of 109 kg/hr (Ref. 6-6). For the purpose of determining the temperature at the fuel-interfaced blanket pellet, it is assumed that the two axial boundaries (Z = 0, 51.31 cm) were adiabatic, which may cause some effect at both ends. The heat flow across the rod centerline (r = 0) is zero owing to symmetry.

6.2.1.4. Rod Axial Linear Power Profile. Since the F-5 test assembly will be in the same location (4C3) in EBR-II as in the F-3 experiment, the F-3 experiment axial linear power as shown in Fig. 6-2 is applicable to F-5 rod thermal analyses (Ref. 6-7). The axial linear power distribution was taken to be uniformly conservative at the maximum power generated at the end of life in the blanket region. The maximum linear power in Fig. 6-2 corresponds to 393 W/cm.

6.2.1.5. Results and Discussion. The results of the temperature distribution output from GCFR*TAC-2D are shown in Fig. 6-3. The maximum fuel-interfaced blanket pellet temperatures are ∿1200° and ∿1300°C for the low-pellet density and the small pellet diameter, respectively. Therefore, degradation of heat flow is more pronounced because of the increase in gap size rather than the increase in pellet porosity. Note that for the upper blanket region, the temperature at the upper end is higher than the temperature at the lower end, which is contrary to reality. This phenomenon can be explained by the uniform power input in the blanket region and the adiabatic boundary condition at the upper end, which are conservative assumptions (i.e., they result in higher temperature values).

6.2.1.6. Recommendations. From the preceding analysis, it is concluded that the maximum temperature at the fuel-interfaced blanket pellet is far below the UO_2 melting temperature (∿2800°C) for the low pellet density and small pellet diameter approaches. Both approaches are acceptable from the viewpoint of temperature distribution, but it is felt that the small

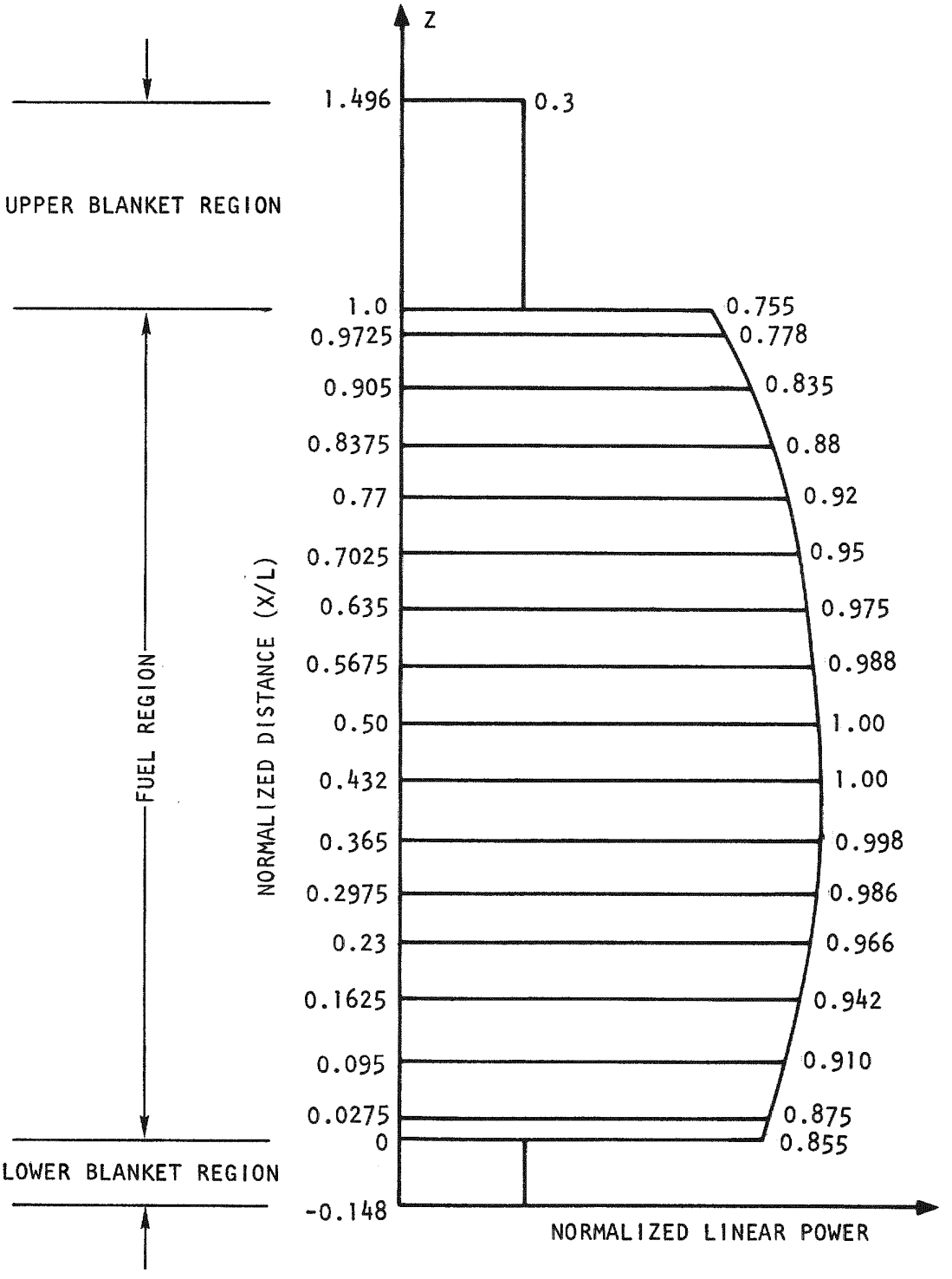

Fig. 6-2. Rod axial linear power profile

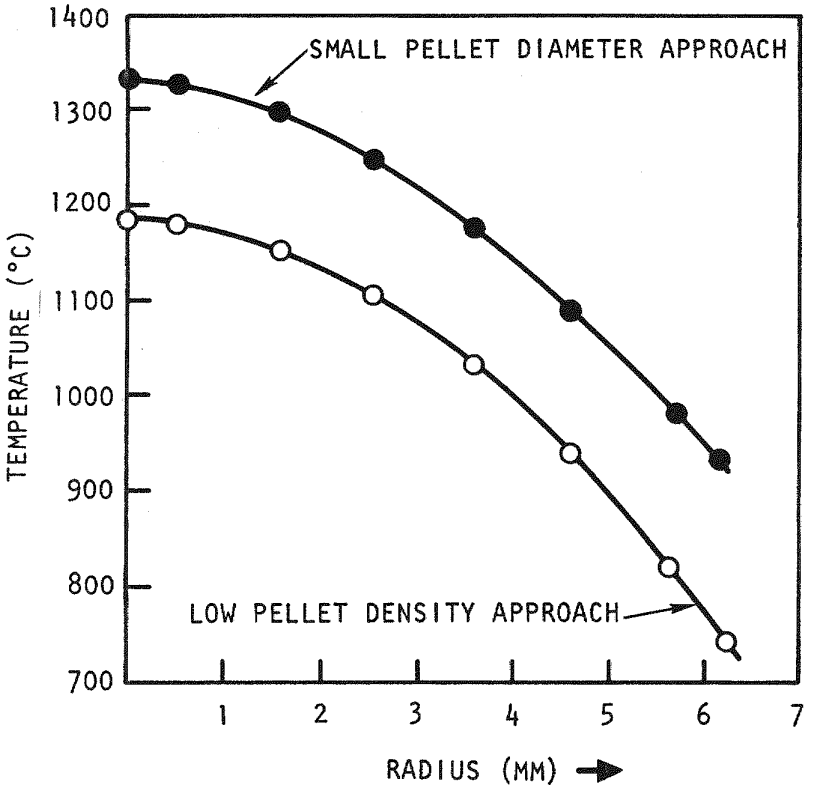

Fig. 6-3. Temperature profile of fuel-interfaced blanket pellet

pellet diameter approach may provide a larger pellet-cladding gap for cesium to pass through the first blanket pellet. Moreover, it would be easier for the small-diameter pellet to reside away from the center of the cladding, which may cause unfavorable heat transfer. As a result, it is recommended that the low-density approach (0.8 theoretical density) be taken for the F-5 experiment fuel-interfaced blanket pellet design.

6.2.2. Irradiation Performance Analysis Data File

A performance analysis data file for irradiation experiments F-5, F-1, GB-10, and F-3 (in that order of priority) has been established and maintained to allow convenient retrieval for analysis and interpretation of experimental results. The original documents will be placed in this file, and summaries will be prepared for the user's convenience. Hence, a controlled central file will be set up in accordance with the following guidelines:

1. Name: GCFR Experimental Fuel Rod Performance Analysis Data File.

2. Storage: five-drawer steel file cabinet.

3. Accessibility: documents can be checked out by interested persons by registration of name and date.

4. Organization: documents and data will be organized according to the following classifications:

    a. Performance analysis input.

        (1) Dimensional data.

            Content: as-built dimensional data and geometrical configurations of components such as the fuel rod, pellet, and test capsule.

            Form: drawings or tables.

(2) Material composition and property data.

Content: materials used for the construction of components; initial filling gas. For pellets, density, O/M ratio, composition, and enrichment will be specified. Sources of data such as thermal conductivity will be documented by photocopy or original document.

Form: charts.

(3) Power history.

Content: actual run-by-run reactor power history, core fission rate map, and gamma heat rates. Location and map of test assembly.

Form: original reports issued by EBR-II project.

(4) Coolant flow history.

Content: run-by-run reactor coolant history, including inlet temperatures and mass flow rate for the test assembly channel.

Form: original reports issued by EBR-II project.

b. Postirradiation examination.

Content: gamma scanning, neutron radiographs, profilometry, and destructive examination results, including fission gas pressure.

Form: charts, graphs, photographs.

c. Performance analysis.

(1) Nuclear analysis.

Content: rod axial power profile and power history obtained via the LAMDA code and gamma scan results for Zr-95.

Form: charts or graphs and computer output.

(2) Cladding temperature analysis.

Content: cladding temperature history obtained via the TAC-2D code.

Form: computer output and charts.

(3) Rod irradiation performance analysis.

Content: LIFE code analysis of irradiated fuel rod according to input power and cladding temperature histories.

Form: computer output and charts.

d. Computer code.

Content: Computer programs such as LAMDA, TAC-2D, and LIFE.

Form: Computer program user's manual.

The development of the central file will begin by collection of already existing documents and the data described above.

6.3. ROD ANALYSIS AND PERFORMANCE

For some time, there has been an ongoing effort to develop a MARC structural model to study the mechanical interactions between fuel and cladding resulting from operational transients. Now that a new version of the MARC code has been received at GA, this model has been made operational. Several test cases have been run to exercise various features of the code and to check the code's operation. At the present time, the general operation of the code appears satisfactory. To illustrate the current status and operation of the code, a typical test problem is given below.

A thin slice of a GCFR fuel rod (containing annular pellet fuel) was modeled using axisymmetric plane strain assemblies to model the fuel and cladding and beam assemblies (with the MARC 'GAP' option set) to model the fuel-cladding gap. The mesh for this model is shown in Figs. 6-4 and 6-5. Temperature-dependent material properties were used for $(U\text{-}Pu)O_2$ and 316 stainless steel. Creep and plasticity effects were not considered, but the plasticity-temperature limit (TPL) of the fuel was simulated by dropping the elastic modulus of the fuel three orders of magnitude when the transition temperature (taken to be 1500°C) was reached.

Starting with the rod at room temperature, the fuel was taken to a temperature of 521°C, which very nearly closed the fuel-cladding gap. The fuel was then taken to 577°C, and the gap closed. Next, the fuel was taken to 1132°C, which caused it to expand and strain the cladding outward (Fig. 6-6); the displaced mesh is shown as solid lines and the original mesh is shown as dashed lines. The displacements are shown to scale. The fuel temperature was then taken to 1688°C, which is above the TPL transition temperature, and the fuel relaxed inward, relieving the stress on the cladding (Fig. 6-7). Finally, all temperatures were reduced back to room temperature, whereupon the gap reopened, and the fuel and cladding returned to their original states.

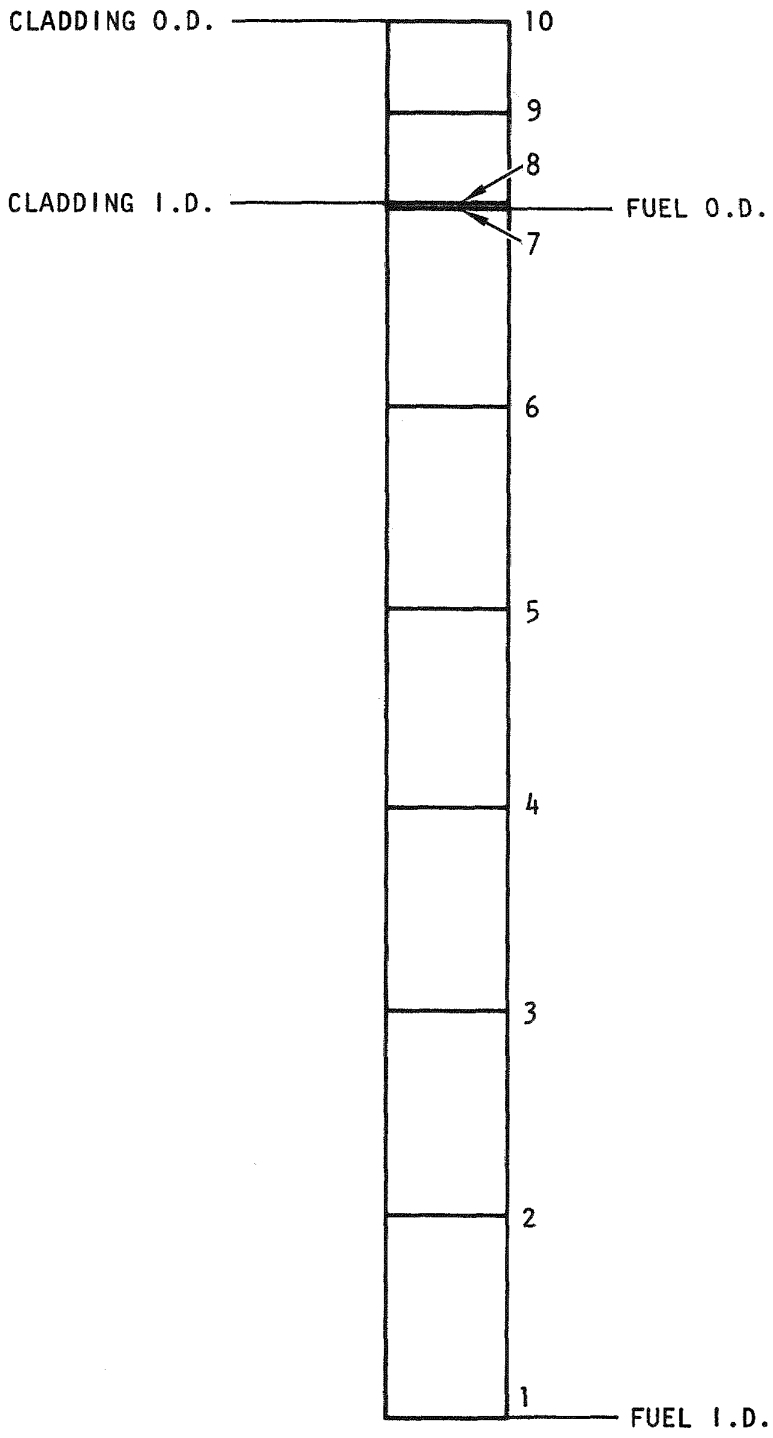

Fig. 6-4. Test model input mesh

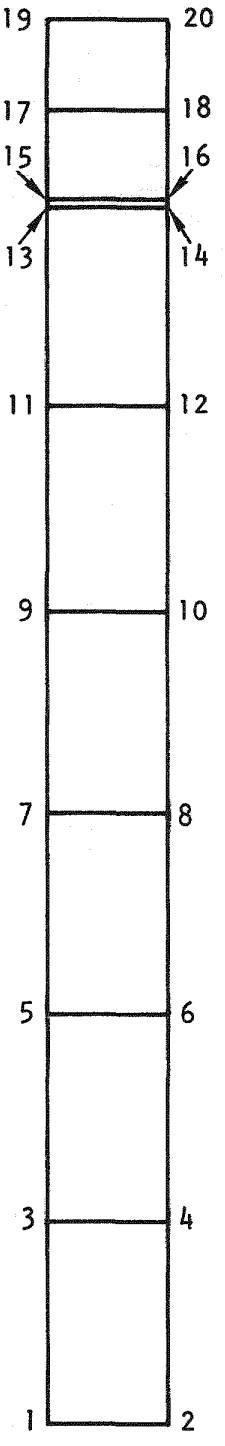

Fig. 6-5. Test model input mesh

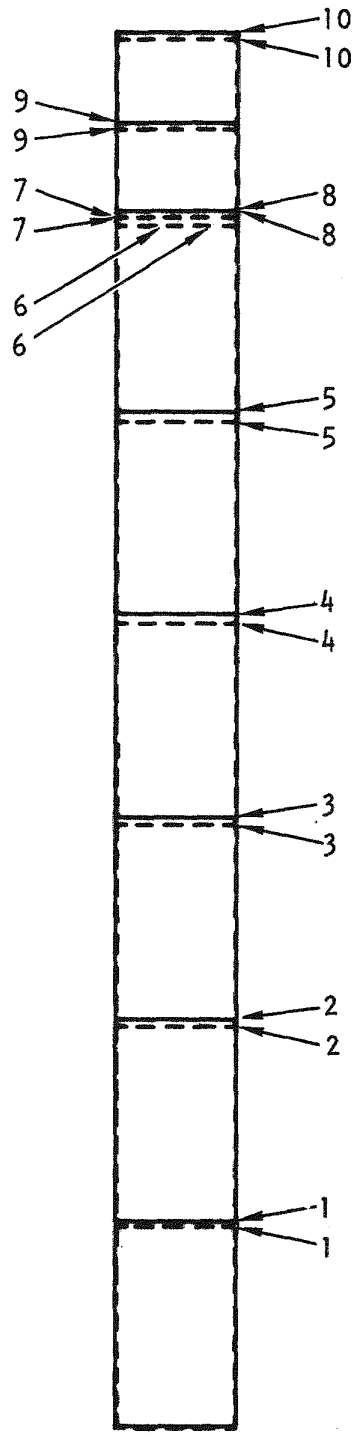

Fig. 6-6. Test model with fuel at 1132°C

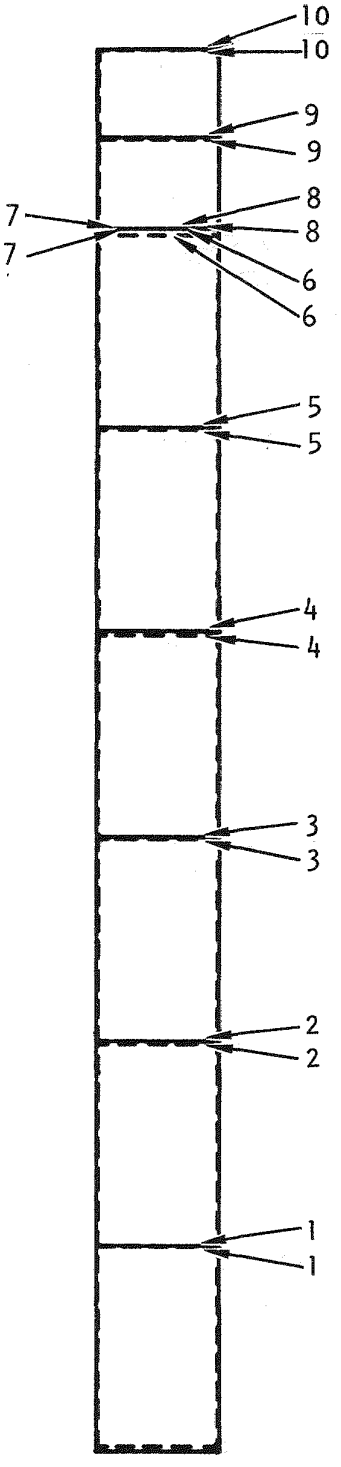

Fig. 6-7. Test model with fuel at 1688°C

The above problem was run to illustrate the operation of the code. Additional, more realistic cases have also been run. An example of one of these cases is a preliminary study of the effect of power increases on fuel rod cladding stresses. Under the constraints and assumptions of this preliminary analysis, it was found that some plastic deformation of the cladding would occur if the rod was rapidly brought to full power from an initial power level of 89% or below.

Again, a thin slice of a GCFR fuel rod containing annular fuel was modeled. The input mesh for this model was the same as before except that the gap assemblies were removed. The fuel and cladding were assumed to be stress free and in contact at the initial power level of interest. (The fuel was presumed to have swelled out to the cladding to just close the fuel-cladding gap, and creep was assumed to have relaxed all residual thermal stresses.)

To determine the fuel and cladding temperatures during power increases, thermal analyses were done using the TAC-2D code in an axial location where the local coolant temperature was 524°C; a local rod linear power (at 100% power) of 35.1 kW/m was chosen. It was assumed that the coolant temperature was held constant during the power change (i.e., coolant flow rate was matched to power level). The steady-state temperature distributions for various power levels are given in Table 6-1.

Figure 6-8 illustrates what happens if the rod is rapidly brought from 75% power to 100% power. The displaced mesh is shown as solid lines, superimposed over a dotted line representation of the original mesh. Displacements have been magnified by a factor of 25 for ease of viewing. Results of this preliminary analysis are shown in Fig. 6-9, which gives the maximum cladding hoop stress resulting from various power increases. The horizontal line represents the monotonic yield strength of unirradiated SA 304 stainless steel. This is taken to be a conservative estimate of the cyclic yield strength of irradiated 20% CW 316 stainless steel, since this information

TABLE 6-1
NODAL TEMPERATURES AT VARIOUS POWER LEVELS

	Temperature (°C)							
	Node 1	Node 2	Node 3	Node 4	Node 5	Node 6	Node 7	Node 8
100% power	1560	1489	1366	1202	1010	805	626	612
90% power	1431	1369	1262	1121	954	776	616	603
85% power	1368	1311	1212	1081	927	761	611	599
80% power	1307	1253	1163	1042	901	746	606	594
75% power	1246	1197	1114	1004	874	732	601	590

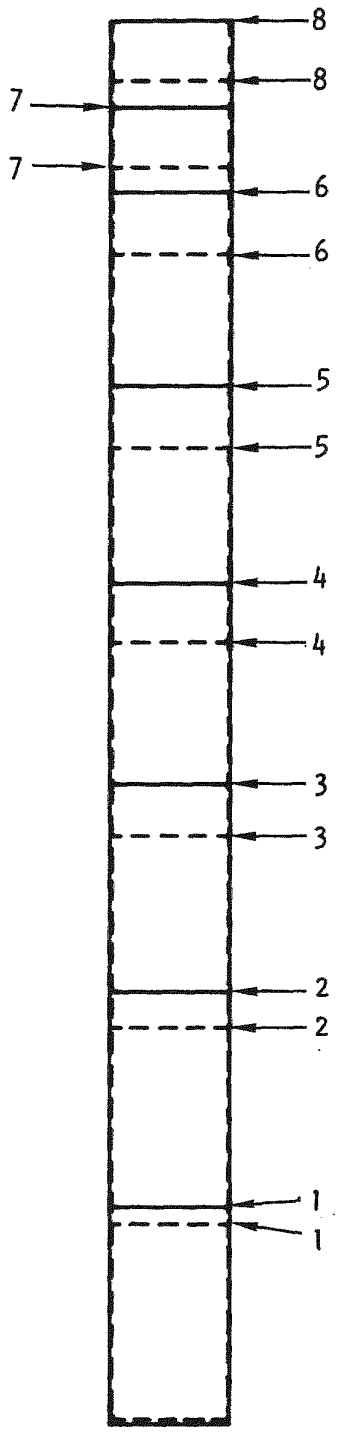

Fig. 6-8. Effect of power rise from 75% to 100%

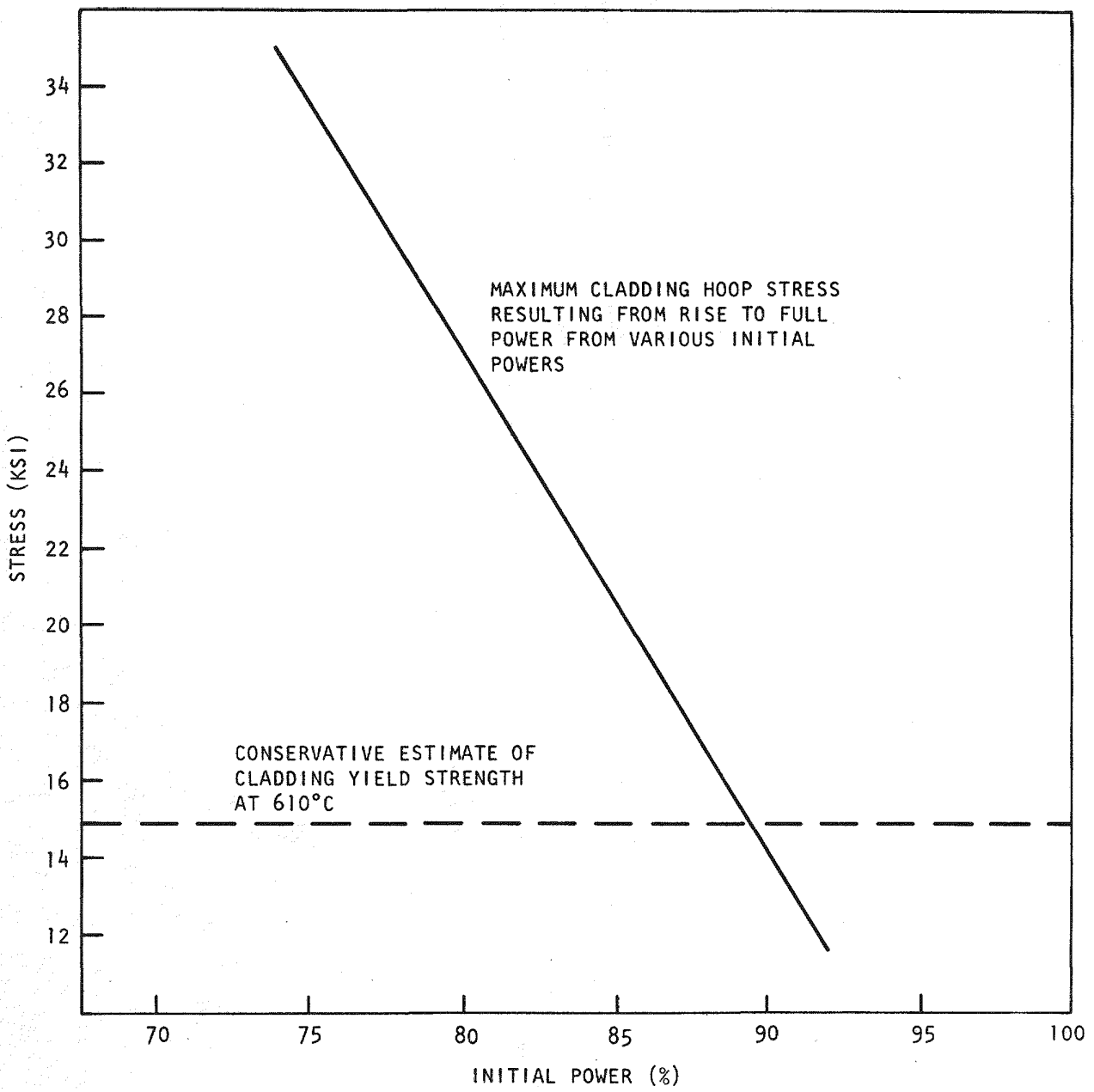

Fig. 6-9. Results of preliminary analysis

is unavailable. This is quite a conservative estimate since irradiation is expected to harden CW 316 considerably.

It can be seen that a rapid rise to full power from an initial power level of about 89% or less will result in plastic strain in the cladding. Cladding at this temperature and under this loading is allowed up to approximately 0.5% total plastic strain according to a preliminary estimate using the GCFR core consumables design criteria. Determination of the amount of plastic strain present in the cladding was beyond the scope of this analysis but will be the focus of future work.

6.4. ROD MECHANICAL TESTING

Because of the higher priority of other efforts, this subtask has been delayed. It is planned to do limited mechanical testing of the fuel rod during FY-77 to determine the effect of the machined ribbing on the unirradiated cladding properties.

REFERENCES

6-1. Billone, M. C., et al., "The LIFE-III Fuel-Element Performance Code User's Manual," Argonne National Laboratory Revised Draft, September 1976.

6-2. Billone, M. C., "Status Report on LIFE-LWR: A Computer Code to Predict the Thermal and Mechanical Performance of Light-Water-Reactor Fuel Rods," Argonne National Laboratory, unpublished data.

6-3. Chang, K. H., "The Effect of Cesium Migration on the F-5 Rod Blanket Pellet Design," General Atomic, unpublished data.

6-4. Ogawa, S. G., E. A. Lees, and M. F. Lyons, Power Reactor High Performance UO_2 Program, General Electric Report GEAP-5591, 1968.

6-5. Hann, C. R., et al., "GAPCON-THERMAL-1, A Computer Program for Calculation of Gap Conductance in Oxide Fuel Pins," Battelle Northwest Laboratory Report BNWL-1778, 1973.

6-6. Flynn, P. W., General Atomic, private communication.

6-7. Rucker, R., General Atomic, private communication.

7. NUCLEAR ANALYSIS AND REACTOR PHYSICS (189a No. 00584)

The scope of activities planned under this subtask encompasses the validation and verification of the nuclear design methods which will be applied to the GCFR core design. This will primarily be done by evaluating the methods using a critical assembly experimental program specifically directed toward GCFR development. Program planning and coordination activities, critical assembly design and analysis, and the necessary methods development will be carried out during the course of this program.

The major effort during the previous quarter was concerned with post-analysis of the experiments conducted in the phase II assembly. A major portion of this effort involved refining the steam flooding calculation in the dry and the poisoned core configurations. Preliminary analyses of Doppler worth in the dry and the steam-filled core are in reasonable agreement with experimental results. The calculations of boron control worths were also in good agreement with the experimental results.

During this quarter, the major effort continued to be concentrated on postanalysis of the phase II assembly experiments. Kinetics parameters were generated, and the effect of the reflector and steam entry upon central reactivity worths was investigated. Selected configurations were recalculated for the steam entry experiment using the new methodology for shielding of resonance cross sections; this methodology was compared with earlier methods.

7.1. PHASE II GCFR CRITICAL ASSEMBLY ANALYSIS

7.1.1. Analysis of Kinetics Parameters

The analyses of the phase II experiments using the as-built specifications from ANL have been carried out with cross sections generated without

the recently upgraded capability for shielding resonance cross sections. Table 7-1 summarizes the results of the beta-effective calculations carried out using PERT and the fluxes derived from 2DB calculations on the three assembly configurations from the phase II GCFR critical experiments. A study was made on the effects of the prescription for assigning decay parameters for the delayed-neutron precursor groups. ENDF/B-4 provides decay data for six basic precursor groupings for each of the five principal fissionable isotopes. A series of beta calculations was carried out using the resulting tabulations of the 30 decay group parameters. Another series of calculations used parameter tables for only six decay groups in which the groupwise data were averages of the corresponding decay group data for the five fissionable species (with a fission fraction weighting). Comparison of the results in Table 7-1 for the $6\lambda_i$ and $30\lambda_i$ cases reveals excellent agreement and substantiates the adequacy of using only six precursor groups with appropriate weighted-average decay parameters.

The energy structure for the cross sections and fluxes was found to have a larger effect on the beta calculations. Table 7-1 also compares the PERT results from 10- and 28-group cross section sets and the corresponding 2DB-generated 10- and 28-group real and adjoint flux data. As shown, the 28-group results provide about 1% lower effective beta values and correspondingly higher conversion factors.

7.1.2. Central Worth Comparisons

Table 7-2 compares the 28-group perturbation calculations for material worths at the center of the phase II assembly with and without the steel reflector around the blanket and with simulated steam flooding of the core and blankets. The reflector addition only slightly changes the calculated values for the major materials but the calculation/experimental comparison (C/E) is improved a few percent. The significant spectral shift due to polyethylene flooding does not significantly alter the C/E values for the fuel and structure worths, but the boron and CH_2 worth calculations are markedly different.

TABLE 7-1
SUMMARY OF KINETICS PARAMETERS CALCULATED FOR
AS-BUILT PHASE II CONFIGURATIONS

Parameter	Phase II Configuration		
	No Reflector	Reflector Around Blankets	Reflected and 0.0175 g/cm^3 CH_2 in Void Channels
β-effective (% Δk/k)			
28-group fluxes			
$6\lambda_i$	--	0.3424	0.3441
$30\lambda_i$	0.3427	--	0.3441
10-group fluxes			
$6\lambda_i$	0.3465	0.3463	0.3473
$30\lambda_i$	0.3464	0.3461	0.3472
Conversion factor (Ih/%)			
28-group fluxes			
$6\lambda_i$	--	942.0	936.9
$30\lambda_i$	939.2	--	934.8
10-group fluxes			
$6\lambda_i$	934.1	936.0	931.7
$30\lambda_i$	932.4	934.2	929.7
Neutron lifetime (10^{-8} s)			
28-group fluxes	36.57	37.79	54.34
10-group fluxes	35.96	36.61	50.13

TABLE 7-2
SUMMARY OF CENTRAL WORTH CALCULATIONS FOR PHASE II
AS-BUILT CONFIGURATIONS

Material	Core-Center Reactivity Coefficients Calculated Using Fluxes from 28-Group 2DB Cases					
	No Reflector		Reflector Around Blankets		Reflected and 0.0175 g/cm^3 CH_2 in Void Channels	
	Calculated Worth (Ih/kg)	C/E	Calculated Worth (Ih/kg)	C/E	Calculated Worth (Ih/kg)	C/E
He	-189.3		-188.6	--	-148.4	--
B-10	-3738	1.090	-3765	1.103	-5794	1.347
C	-35.26	1.661	-35.05	--	-16.58	--
304 stainless steel	-9.245	1.234	-9.279	1.214	-8.626	1.180
Mo	-27.86	1.330	-27.97	--	-39.73	--
U-235	203.5	1.211	204.1	1.198	206.3	1.258
U-238	-13.67	1.195	-13.06	1.160	-14.80	1.147
Pu-239	276.4	1.194	277.1	1.164	265.6	1.155
Pu-240	51.86	1.229	52.00	--	35.34	--
CH_2 foam	-10.91	-0.07	2.35	0.01	323.1	0.982

7.1.3. Phase II Recalculations with Improved Methods

A selected number of calculations performed in the postanalysis of phase II were recomputed using the improved methodology now available in the GFE4 and GGC-5 spectrum codes for shielding resonance cross sections of iron, nickel, chromium, oxygen, and U-238. The three basic configurations of the phase II program were studied in order to directly compare them with the earlier results and to evaluate the effects of the improvements on eigenvalue, neutron balance, and other parameters.

Energy shielding and Benoist bidirectional diffusion modifiers were calculated using the DTFX and PLADIF codes for phase II in 10 and 28 groups. DTFX incorporated a uniform absorber to simulate core leakage as calculated from a previous 2DB diffusion calculation. For the 10-group shielding factors, a full-width model of the three matrix unit cells were used. For the 28-group shielding factors, an approximate half-width model was used owing to computer storage limitations. Shielding factors were not calculated for the radial and axial blankets because their spectra are primarily determined by inleakage from the core, which results in significant calculational difficulties.

The PLADIF code was utilized to calculate the directional diffusion modifiers for the core and both blankets for 10 and 28 groups for the dry and 0.0175 CH_2 cases. Cross sections were generated for a phase II "average" reflector by using the inleakage into the reflector (as calculated by PERT on a previously run 2DB diffusion calculation) as a fission spectrum input into GGC-5. (Prior methods had simply taken structural cross sections from blanket spectrum calculations to be representative of the reflector.) This fission spectrum had positive and negative groups, and yet the GGC-5 code still calculated a fundamental mode spectrum which was very close to the spectrum calculated by 2DB (Table 7-3). A small amount of U-238 was added to the reflector composition as the fission neutron source, and these cross sections were used for the radial and axial reflectors and the matrix material.

TABLE 7-3
FLUX COMPARISON FOR PHASE II REFLECTOR

Group	Normalized Fission Spectra	28-Group 2DB Diffusion Calculation	28-Group Collapse of 99-Group GGC-5 Spectrum
1	0.00092	0.000017	0.000017
2	0.0124	0.00022	0.00022
3	0.0405	0.00078	0.00076
4	0.1122	0.00323	0.00309
5	0.1047	0.00628	0.00601
6	0.0952	0.0131	0.0140
7	0.2830	0.0508	0.0482
8	-0.0501	0.0620	0.0611
9	0.3321	0.0624	0.0648
10	0.0892	0.0953	0.0884
11	0.0842	0.1028	0.0813
12	0.2571	0.0817	0.0833
13	0.2487	0.0468	0.0572
14	0.0150	0.0826	0.1162
15	-0.0395	0.0743	0.0701
16	0.0439	0.0377	0.0324
17	-0.0157	0.0407	0.0376
18	-0.0141	0.0336	0.0345
19	-0.1144	0.0451	0.0418
20	-0.0631	0.0321	0.0312
21	-0.0649	0.0270	0.0288
22	-0.00126	0.0109	0.0137
23	-0.1471	0.0407	0.0353
24	-0.0934	0.0248	0.0238
25	-0.0665	0.0140	0.0142
26	-0.0413	0.00905	0.00723
27	-0.00457	0.00118	0.00330
28	-0.00319	0.00071	0.00145
	1.000	1.00	1.00

Diffusion calculations were subsequently carried out using the 2DB code. Table 7-4 lists eigenvalues and leakages given by the old and new methods for 10- and 28-group calculations with the old as-built models for the basic, unreflected phase II configuration and the configuration with a steel reflector surrounding the blankets. As expected, shielding of structural uranium and oxygen scattering reduces capture and increases leakage, and there is more of an effect on k for the bare case than there is for the reflected case. Table 7-4 also shows a preliminary evaluation of the steam worth given by the new 10-group analysis. A significant improvement in the steam worth is apparent: the reactivity worth C/E for the steam entry is now typical of other light scatterers. A more refined, extended steam worth study will be carried out as soon as better experimental details and assembly modeling are available from ANL.

Table 7-5 compares the core neutron balance parameters given by the new cross sections with earlier GA and ANL results (Refs. 7-1, 7-2). Besides using the core and blanket cross sections from the new GGC-5 cases, the revised GA analyses utilize a just-critical core radius, the previously described shielded scattering in the reflector specific to the structural isotope densities, and better modeling of the matrix and ZPR structure around the reflectors. The change in shielding of the scattering cross sections significantly increased the leakage, but at the same time appreciably reduced the relative capture rates owing to hardening of the average core spectrum. The new eigenvalues, near 0.993, for GA analyses are now comparable to the typical results found for fast benchmarks in the Cross Section Evaluation Working Group data testing program with ENDF/B-4 (Ref. 7-3).

7.2. METHODS DEVELOPMENT

7.2.1. Diffusion Codes

The investigation of the burnup algorithms in 2DB was completed. After minor modifications, the 2DB algorithms could be used to the same

TABLE 7-4
SUMMARY OF 2DB CALCULATIONS FOR EVALUATION OF IMPROVED
CROSS SECTION GENERATION PROCEDURES

	10-Group Analyses			28-Group Analyses		
	Earlier GGC Cross Sections	Revised GGC Cross Sections	Change (%)	Earlier GGC Cross Sections	Revised GGC Cross Sections	Change (%)
Unreflected phase II configuration						
Eigenvalue	0.99789	0.99242	-0.55	0.99803	0.99257	-0.55
Net leakage	0.15963	0.18095	13	0.16358	0.18238	12
Reflected phase II configuration[a] (dry, R_{core} = 56.88 cm)						
Eigenvalue	0.99675	0.99345	-0.33	0.99798	0.99358	-0.44
Net leakage	0.07493	0.10247	38	0.07788	0.10292	32
Reflected phase II configuration[a] (R_{core} = 56.10 cm)						
Dry	0.99159	0.98808	-0.36	0.99266	--	--
Wet	1.00214	0.99469	-0.75	1.00468	--	--
$\delta\rho$ for CH_2	1.062% k	0.672% k	-36	1.205% k	--	--
Steam worth C/E	2.03	1.29	-36	2.30	--	--

[a]Models with as-built core radii. Blanket cross sections for iron, chromium, nickel, and manganese used in reflector; no matrix or structure around reflector zones.

TABLE 7-5
COMPARISON OF NEUTRON BALANCE DATA FOR PHASE II DERIVED USING REVISED CROSS SECTION PREPARATION PROCEDURES WITH PREVIOUS ANL AND GA EVALUATIONS

	Core	Radial Blanket	Axial Blanket	Radial Reflector	Axial Reflector	Matrix[a] Table + Knees	Reactor Total
Neutron production ($\nu\Sigma_f\phi$)							
ANL	95.43	3.39	1.18	--	--	--	100.00
GA	95.36	3.57	1.07	--	--	--	100.00
GA revised	95.34	3.48	1.18	--	--	--	100.00
Fission							
ANL	32.53	1.26	0.44	--	--	--	34.23
GA	32.55	1.33	0.40	--	--	--	34.28
GA revised	32.53	1.30	0.44	--	--	--	34.26
Absorption							
ANL	60.37	19.53	6.15	2.48	0.47	0.06	89.06
GA	61.39	20.90	5.99	3.21	0.62	0.79	92.90
GA revised	60.53	20.33	6.31	2.69	0.44	1.13	91.42
Capture							
ANL	27.84	18.27	5.71	2.48	0.47	0.06	54.83
GA	28.84	19.56	5.60	3.21	0.62	0.79	58.62
GA revised	28.21	19.06	5.89	2.69	0.44	1.13	57.38
Effective leakage[b]							
ANL, k = 0.9994	35.12	-16.14	-4.97	-2.48	-0.47	-0.06	11.00
GA, k = 0.99767	34.19	-17.32	-4.92	-3.21	-0.62	-0.79	7.33
GA revised, k = 0.99278	35.50	-16.82	-5.12	-2.69	-0.44	-1.13	9.30

[a] Different models in all three cases.

[b] To provide leakage + absorption = production/k.

maximum burnup time step sizes (on the order of 250 days) as the GA algorithms used in FEVER, GAUGE, and BUG. The 2DB algorithms are more general in that the burnup chains need not be restricted to a lower triangular form. However, the 2DB algorithms would not be suitable for thermal reactor calculations because collapse to one energy group in the 2DB algorithms implies no neutron spectrum change during burnup. There is still a need to provide a more general input format for the treatment of burnup in 2DB to take advantage of the generality of the basic 2DB algorithms. It is planned to modify 2DB so it can use the same burnup chain input description as the GA codes GAUGE and BUG.

7.2.2. Nuclear Data Adjustment Studies

To determine the sensitivity of calculated GCFR parameters to potential alterations in nuclear data for prime core materials, ENDF/B-4 data for U-238 was modified to incorporate the total inelastic scattering cross section recommended by Ref. 7-4. The U-238 total cross section was kept the same, while changes in inelastic scattering were accommodated by changing the elastic scattering. The Code Evaluation Working Group GGC-5 calculation was rerun with the modified U-238 data set, and the following results were obtained:

k_∞: 0.99% increase

k_{eff}: 0.67% increase

σ_c^{238}: 0.94% decrease

σ_f^{238}: 2.78% increase

$\sigma_c^{238}/\sigma_a^{239}$: 0.57% decrease

Further evaluations are being considered.

REFERENCES

7-1. "Gas-Cooled Fast Breeder Reactor Quarterly Progress Report for the Period May 1, 1976 Through July 31, 1976," ERDA Report GA-A13975, General Atomic, August 31, 1976.

7-2. Bohn, E. M., et al., "The GCFR Critical Experiments Program," Nucl. Eng. Design 40 (1977).

7-3. "Cross Section Evaluation Working Group Benchmark Specifications (ENDF-202)," Brookhaven National Laboratory Report BNL 19302, November 1974.

7-4. Pieroni, N., "Method to Investigate Neutron Inelastic Cross Section Data by Analyzing Fast Nanosecond Decaying Spectra," Kernforschungszentrum Karlsruhe Report KFK 1968, May 1974.

8. SHIELDING REQUIREMENTS (189a No. 00584)

The purposes of the shielding task are to verify the adequacy of the methods and data (physics and engineering) for the design of GCFR shields and to evaluate the effectiveness of various shield configurations. This task also coordinates and provides liaison with the analytical and experimental GCFR shielding activities at ORNL.

During the last quarter, a topical report summarizing the physics design of the revised grid plate shielding conducted during FY-76 was prepared (Ref. 8-1). A Monte Carlo calculation of the revised grid plate shielding, including the fuel rod lattice, was initiated to assess the effect of rod streaming on neutron-induced damage to the grid plate. The DOT-III two-dimensional calculations of the revised lower shield and wraparound shield performed by ORNL were received, and the first set of DOT-II two-dimensional calculations of the revised upper axial shield were completed.

During this quarter, a topical report summarizing the GCFR shielding benchmark calculations performed by GA and ORNL was completed (Ref. 8-2). New shielding cross section sets were generated which included self-shielding and new weighting function techniques.

8.1. SHIELDING BENCHMARK CALCULATIONS

During this quarter, the GA/ORNL benchmark calculations discussed in Refs. 8-3 and 8-4 were updated using self-shielded scattering cross sections for iron. The 1976 GA benchmark results are significantly different from the 1975 results and are in much better agreement with the ORNL results. The 1976 benchmark calculations were performed in the same manner as the 1975 benchmark calculations (Refs. 8-3, 8-4) except for the updated self-shielded iron neutron cross sections. The flow diagram for the generation

of the neutron-coupled gamma ray cross sections at GA and their use in the 1DFX code is shown in Fig. 8-1. A more detailed discussion of the computer programs is given in Ref. 8-6. Note that GGC-5 processes the neutron transport cross sections (Refs. 8-6, 8-7); LAPHANO couples the N multigroup neutron cross sections to the production of G multigroup gamma ray cross sections (Ref. 8-8); DINT generates the gamma ray transport cross sections (Ref. 8-9); and RCOUPL prepares the final neutron-coupled gamma ray sections for use in 1DFX (Ref. 8-10).

The method used to modify the iron scattering cross sections is outlined in Ref. 8-4 and discussed in more detail in Ref. 8-2. The improvement in the results from the GA iron cross sections is illustrated in Figs. 8-2 and 8-3. Figure 8-2 compares the unself-shielded GA broad-group iron total cross sections with the ORNL fine-group cross sections. After the GA fine-group cross sections were modified with a $1/[\sigma_t(E) + \sigma_o]$ within-fine-group weighting spectrum, the results, were in excellent agreement with the results from the ORNL cross sections (Fig. 8-3). The only significant difference was in the neutron group having an energy level between approximately 19.5 and 25 KeV.

In the new iron neutron-coupled gamma ray cross section set, the self-shielding correction was applied to only the iron neutron cross sections generated in the GGC-5 program; the same gamma production cross sections prepared by the LAPHANO code were used in RCOUPL for the 1975 and 1976 benchmark calculations. Therefore, the effect of self-shielding on the 24-broad-group gamma production cross sections was not included in the new coupled set. (The self-shielding option available in LAPHANO has not been tested or used at GA. The use of this option and its relative importance are under investigation.)

8.1.1. Results and Discussion

The results of the 1975 GCFR shielding benchmark calculations are discussed in Ref. 8-4. Figures 8-4 through 8-9 present the updated GA benchmark calculations along with the 1975 calculations. As can be seen

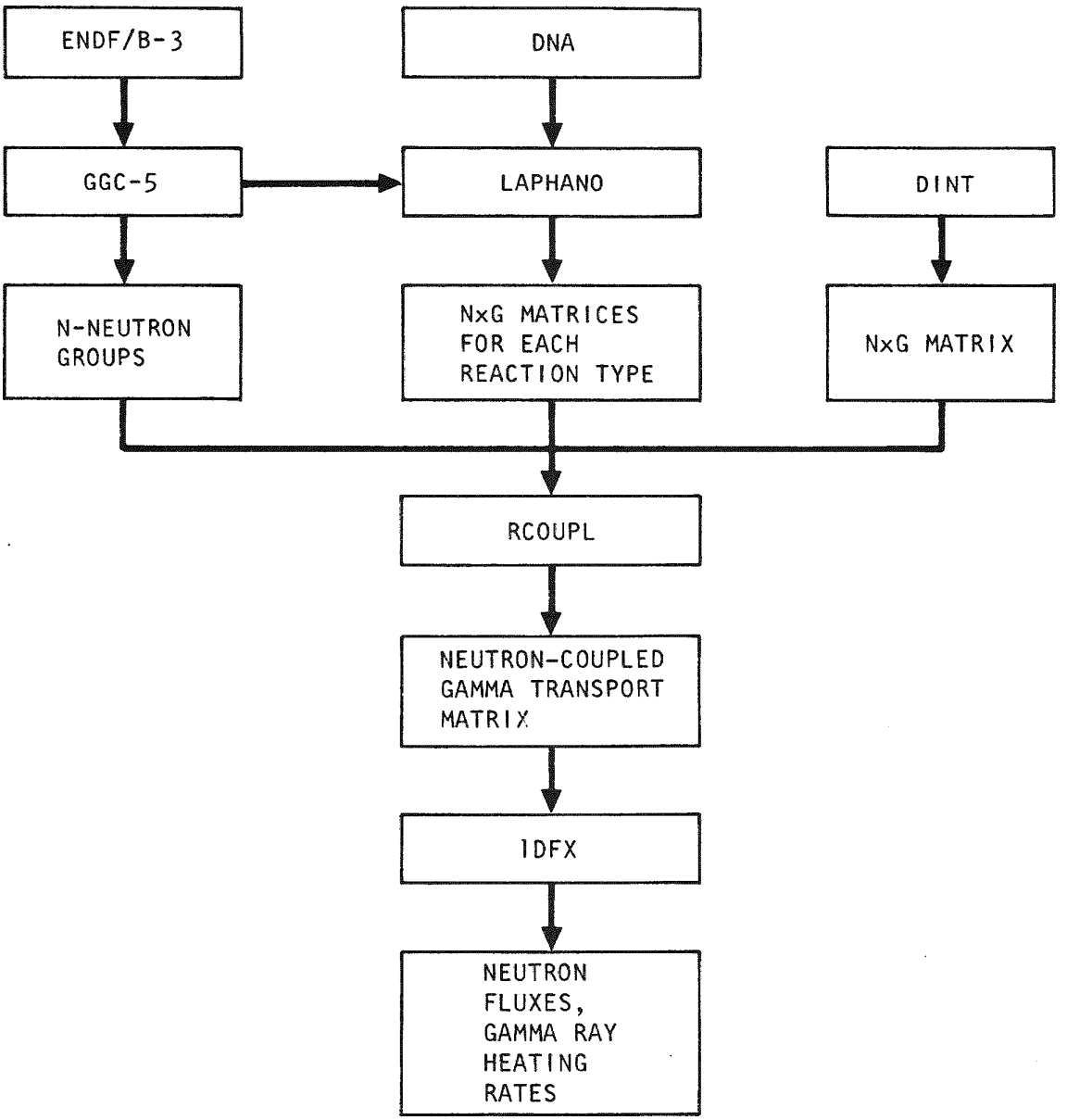

Fig. 8-1. Flow diagram for generation of neutron-coupled gamma ray transport matrices and their use in the 1DFX transport code

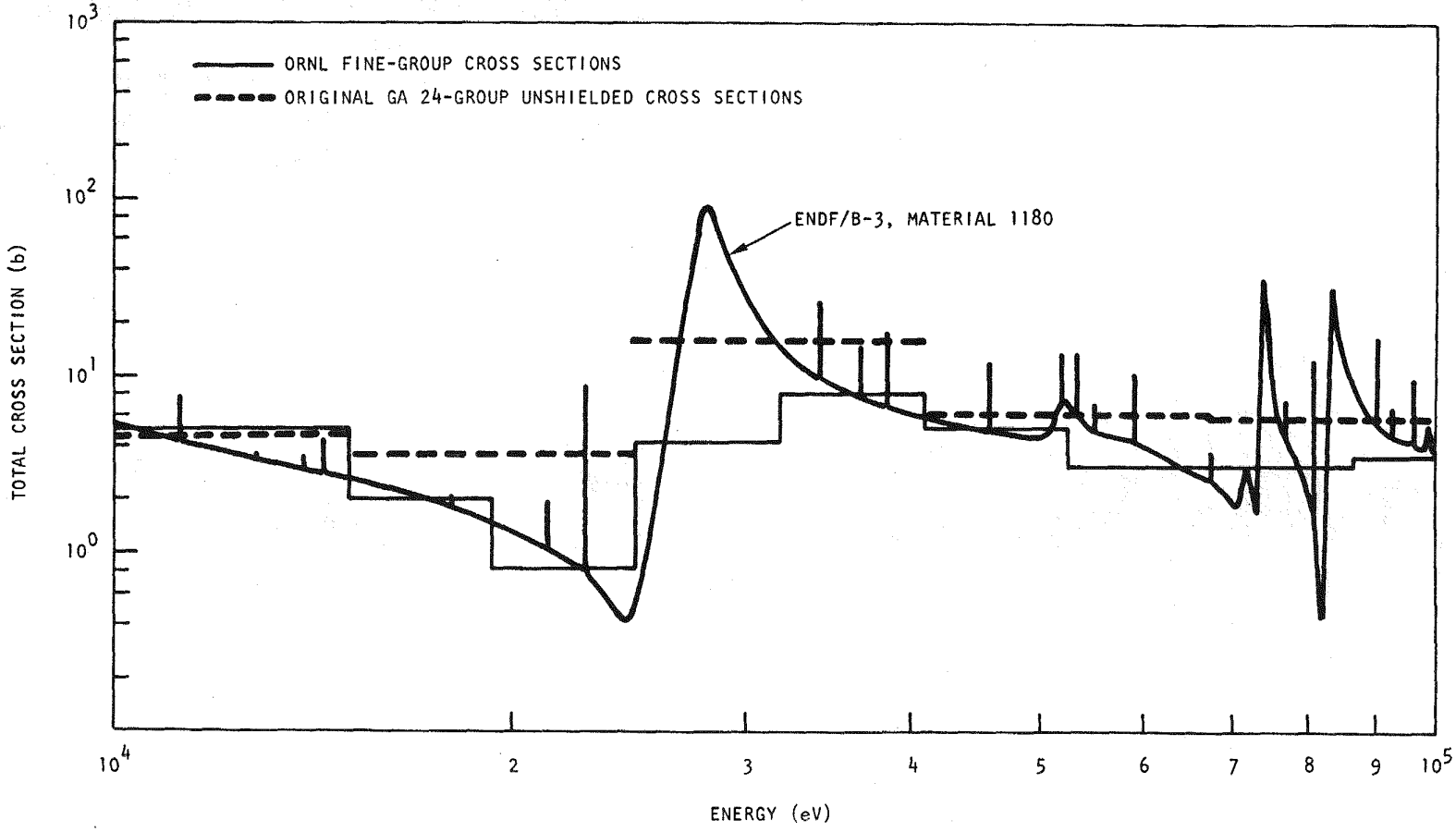

Fig. 8-2. Total cross sections for pure iron vs energy

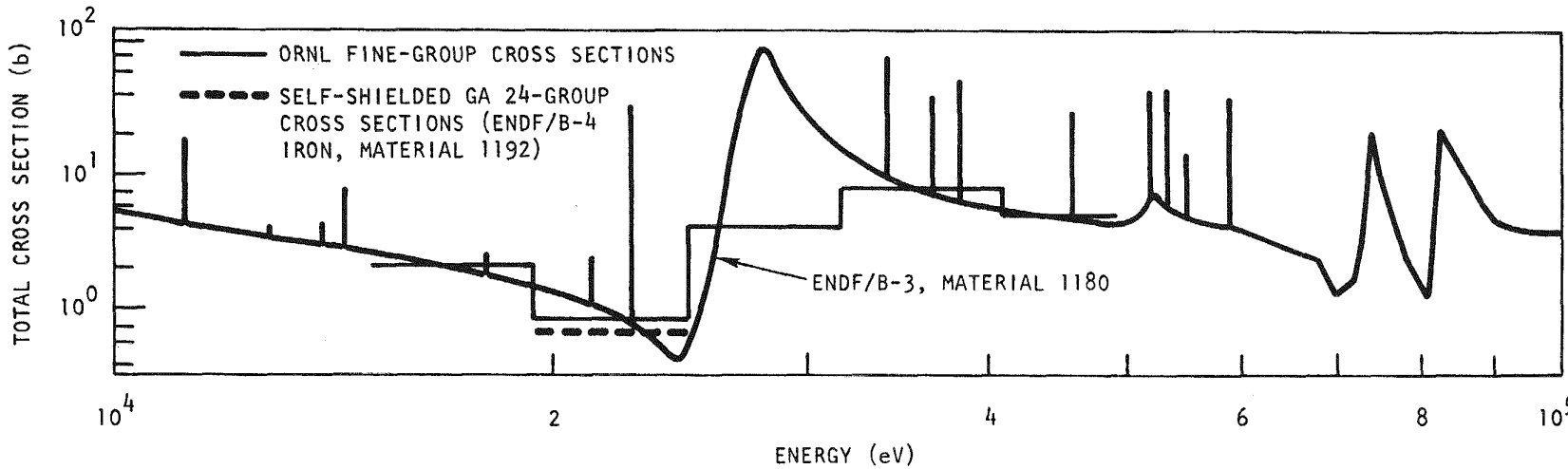

Fig. 8-3. Total cross sections for pure iron vs energy

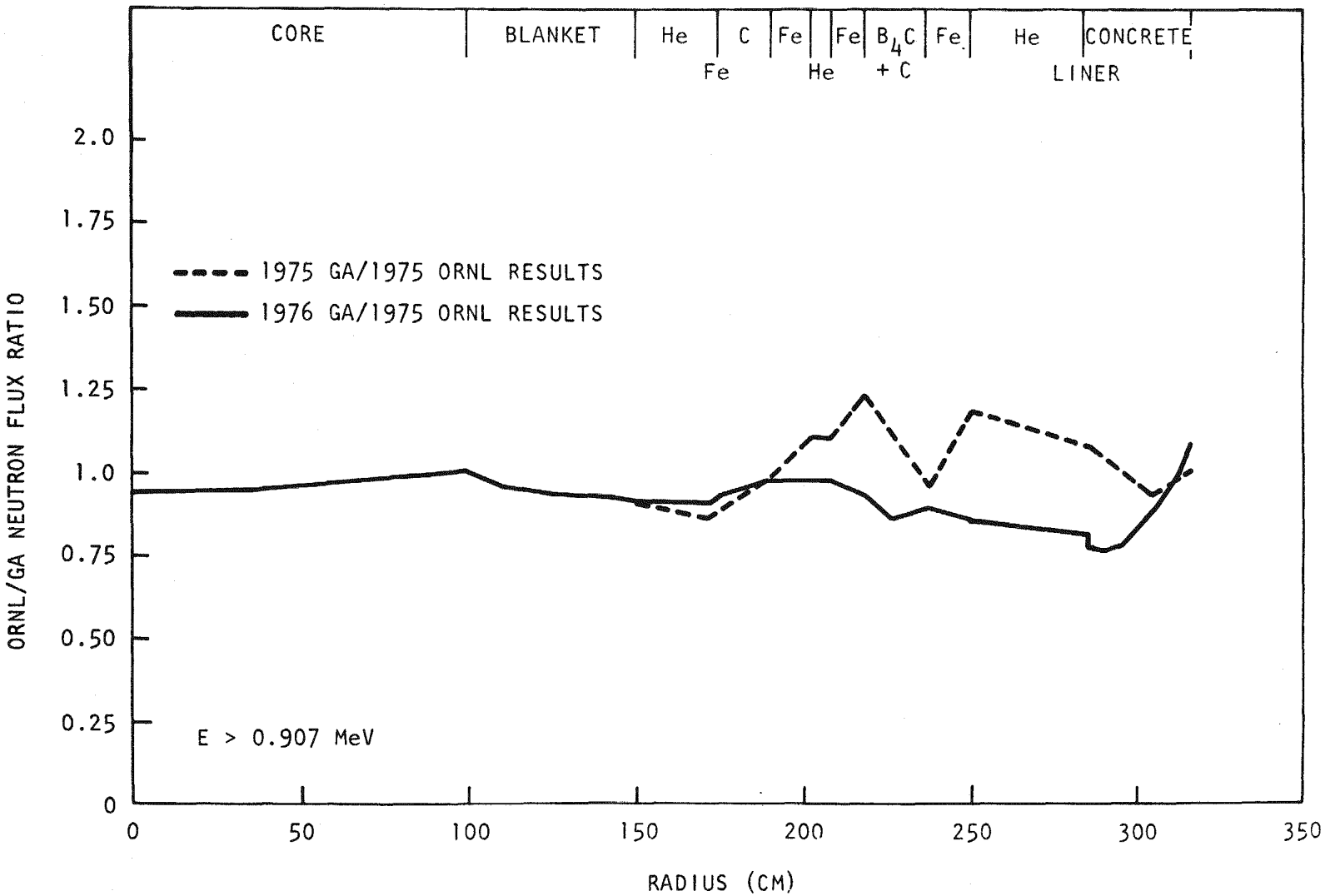

Fig. 8-4. ORNL/GA neutron flux ratio vs radius

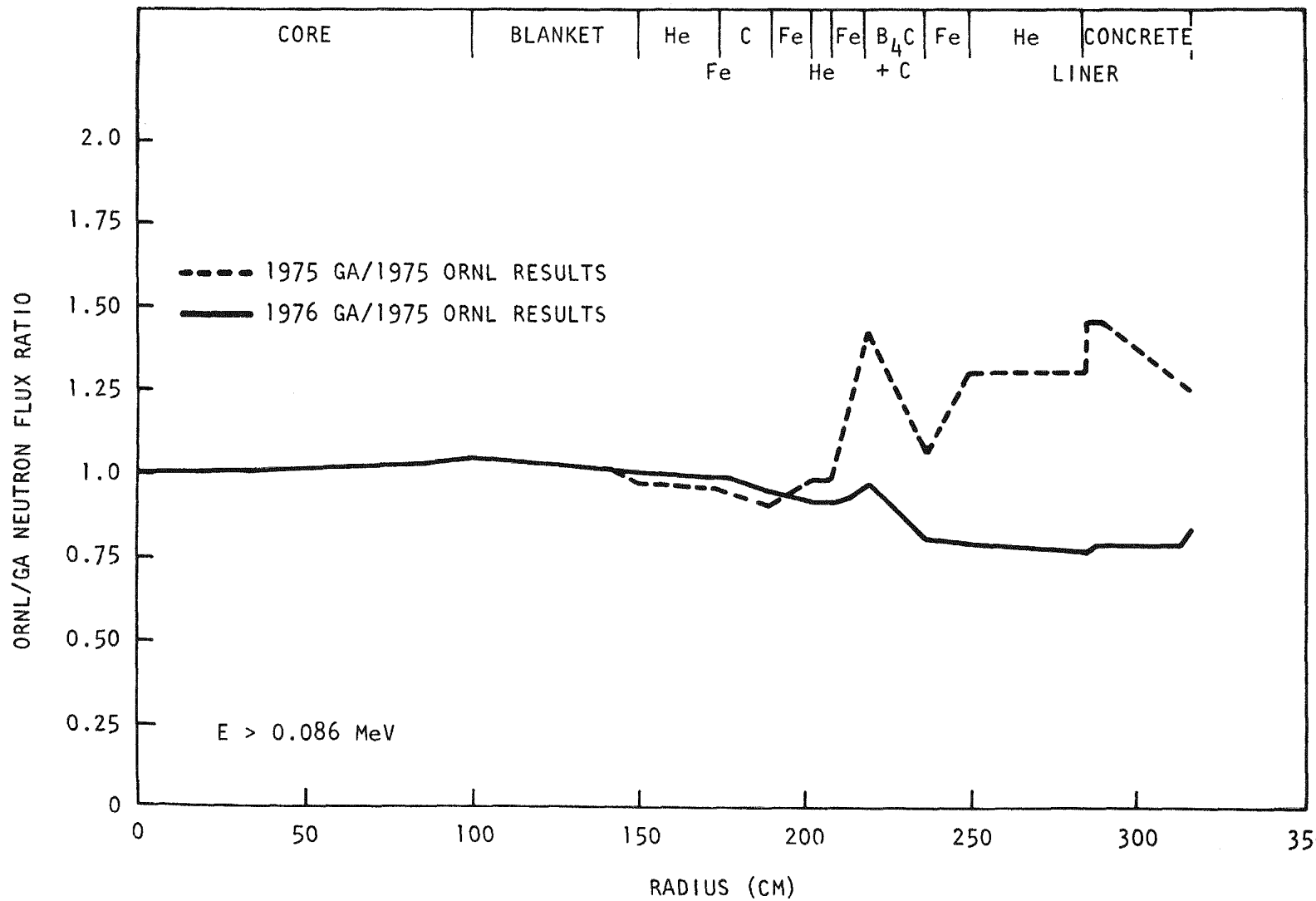

Fig. 8-5. ORNL/GA neutron flux ratio vs radius

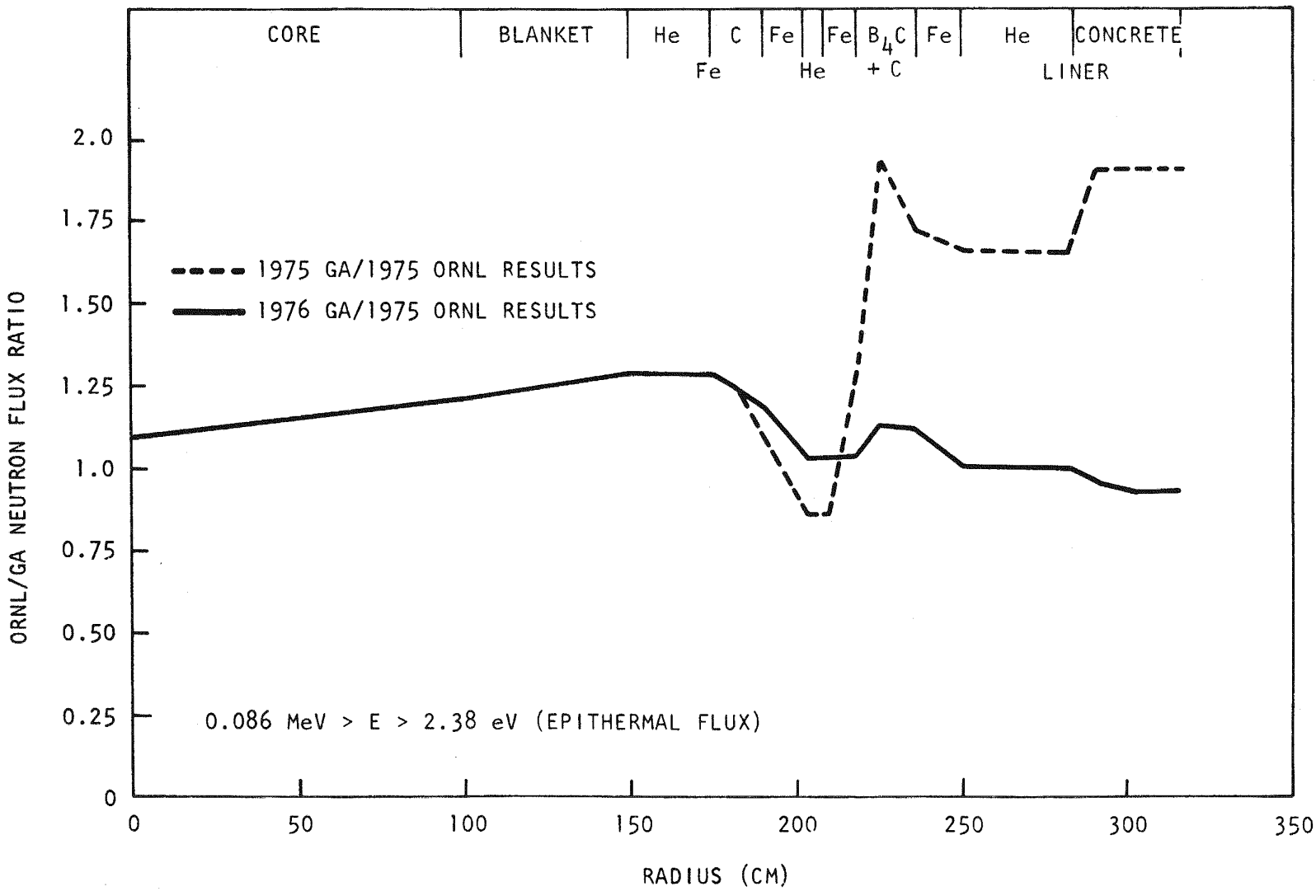

Fig. 8-6. ORNL/GA neutron flux ratio vs radius

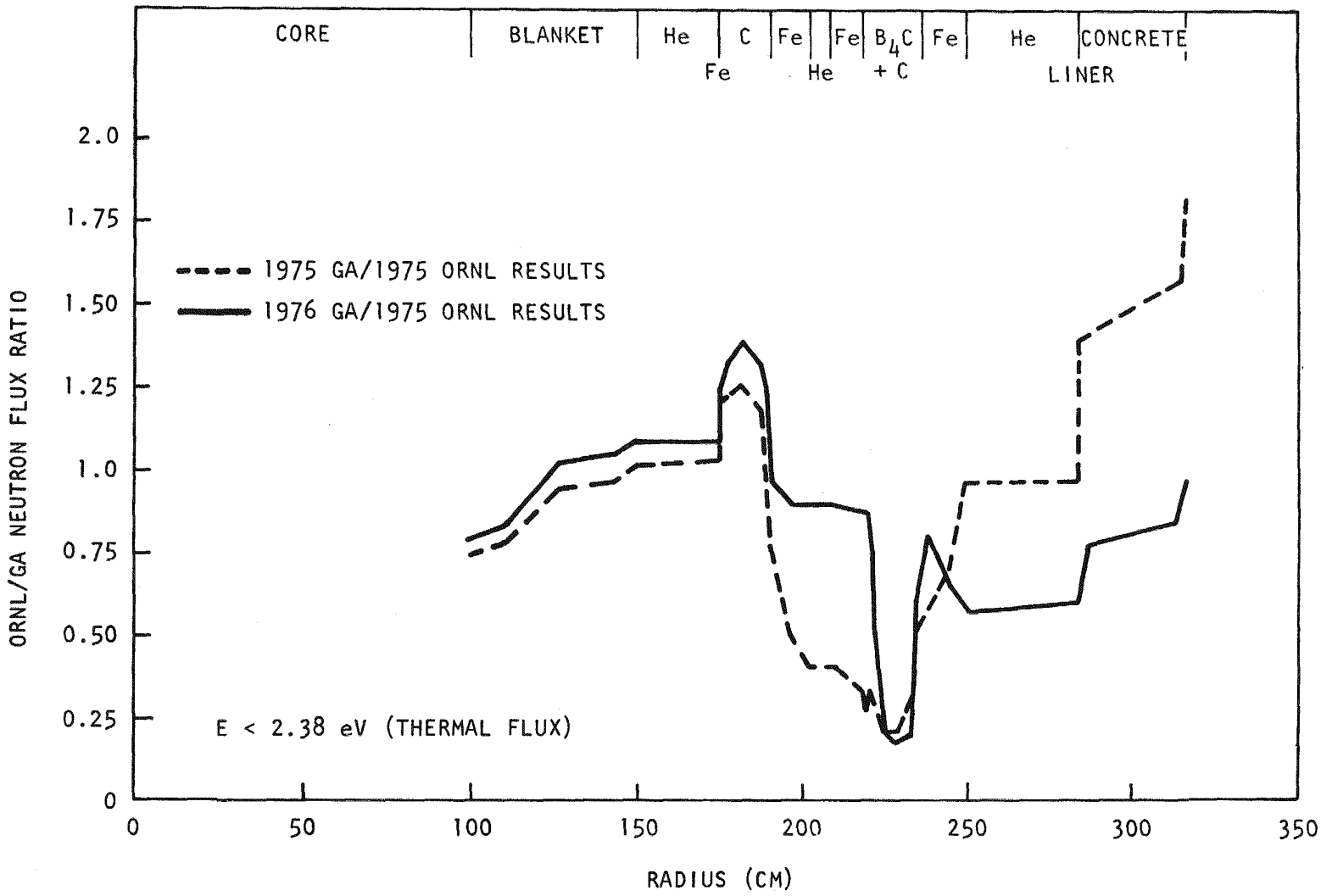

Fig. 8-7. ORNL/GA neutron flux ratio vs radius

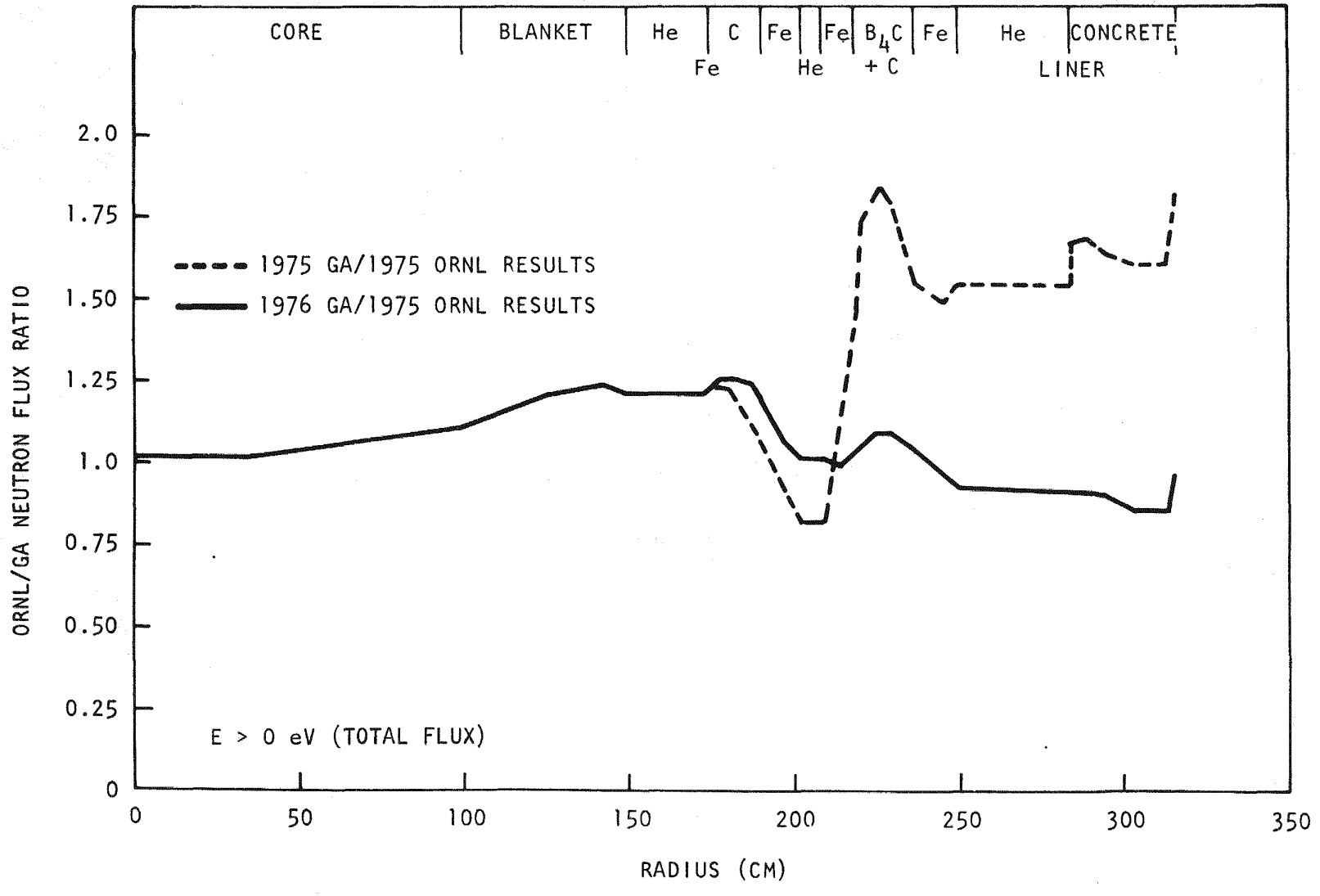

Fig. 8-8. ORNL/GA total neutron flux ratio vs radius

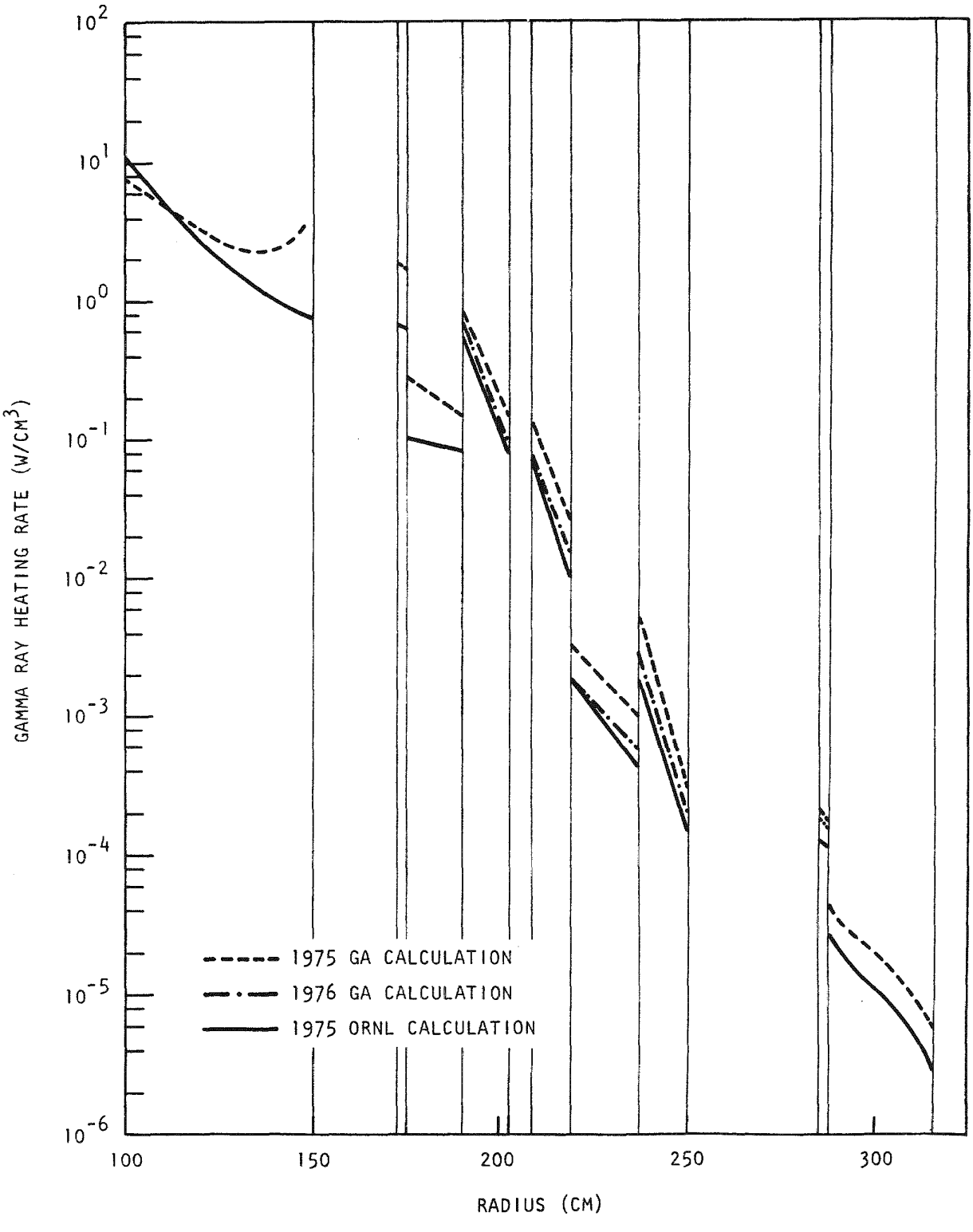

Fig. 8-9. Gamma ray heating rate vs radius

from these figures, the ORNL results remained unchanged. Hence, the differences in the 1975 and present neutron flux ratios and gamma heating rates reflect the improvement in the GA calculations resulting from the self-shielded iron scattering cross sections. Figure 8-4 indicates that the present agreement between ORNL and GA neutron fluxes with E > 0.907 MeV is significantly improved over that obtained in 1975; this is also true for the results given in Fig. 8-5 for neutron fluxes with E > 0.086 MeV. In Fig. 8-6, the current GA calculated epithermal neutron flux is vastly improved beyond a radius of r $\sim$ 200 cm, and Fig. 8-7 shows that the GA thermal flux is very significantly improved in the first two layers of iron and in the concrete. However, previous differences in the B_4C region persist, suggesting the need for further study of thermal flux calculations in boronated regions. For the final neutron flux results, the improvement in the total flux (Fig. 8-8) dramatically illustrates the general effect of the new self-shielded iron cross sections from the iron of the inner shield through the concrete, in which the new GA results and ORNL results differ by about 10% or less. This is a significant improvement over the 1975 results, in which the differences were as large as 80%.

Figure 8-9 shows the improvement in the agreement of the calculated gamma heating rates in the iron regions. The smaller improvement in the outer iron layer in the outer radial shield is probably due to the small net change in the GA calculated thermal flux in this region, as shown in Fig. 8-7. The resulting GA calculated gamma production would produce essentially the same gamma heating in this layer as well as in the concrete and the adjacent boronated graphite and iron regions.

The net concrete gamma heating was essentially unchanged in the 1976 GA results. This was probably due to two causes: (1) gamma production in the outer iron layer of the outer radial shield (which also heats the concrete) did not decrease because the net thermal flux did not change in the GA calculations; (2) the thermal flux in the concrete as calculated in the improved GA benchmark problem nearly doubled, increasing the neutron source for gamma production in the concrete. Gamma heating in the concrete will be investigated in the future.

8.1.2. Summary and Conclusions

The benchmark problem examined by GA and ORNL was defined based upon a modification of the GCFR reference radial shield at the core midplane, but with a region of B_4C and graphite in the outer radial shield. Two sets of calculations were performed at GA, the first set in 1975 and the second in 1976. Both sets were compared with the ORNL calculations performed in 1975; neutron fluxes and gamma heating rates were also compared. From these comparisons, it was deduced that the GFE code used in the GGC-5 code at GA for fine-group cross section library preparation required self-shielding in the scattering cross sections in the resonance energy range for iron as well as chromium and nickel. The new self-shielded iron cross sections were used in the second GA benchmark calculations, and better agreement with ORNL results for neutron fluxes and gamma heating rates was obtained.

The results of the GCFR benchmark calculations performed at GA and ORNL have led to the following major conclusions:

1. Differences of 10% or less in the fast neutron fluxes throughout practically the entire core, blanket, shield, liner, and concrete demonstrate that the methods and cross sections used by both laboratories were compatible and consistent.

2. Earlier differences in calculated epithermal and thermal neutron fluxes in the iron of the shield were correlated with differences in shielding treatment of the iron cross sections in the resonance range, in which GA used higher values than ORNL. This resulted in an important improvement to the GFE code used at GA, in which scattering cross sections were accurately modified by self-shielding.

3. Allowing for the effects of conclusion 2 and the improvements discussed above, the gamma production and gamma transport calculations performed at both laboratories are basically in agreement.

4. The good agreement between the GA and ORNL neutron-coupled gamma ray transport calculation indicates that the use of 24 neutron energy groups and 15 gamma energy groups by GA is adequate when compared with the use of 51 neutron energy groups and 25 gamma energy groups by ORNL.

8.2. GENERATION OF SHIELDING CROSS SECTIONS

New shielding cross section sets were generated utilizing improved weighting function techniques. The most recent production version of the GGC-5 code was employed, which enables the use of broad-group-dependent buckling and a mixed fission spectrum (Ref. 8-11). New self-shielded GAM data sets for chromium, nickel, and iron were used. The GFE-4 code, which produced the GAM data, was modified to include a $[E(\sigma_t + \sigma_o)]^{-1}$ weighting option in order to prepare self-shielded (composition-dependent) fine-group cross sections for GGC-5 (Ref. 8-12). The necessity for accurately treating resonance self-shielding became apparent during the GA/ORNL radial shield benchmark calculations and the criticals program. As discussed in the preceding section, the radial shield benchmark calculation revealed that the lack of self-shielding of iron scattering resonances results in overprediction of down-scatter into the thermal range and therefore overprediction of heating due to capture gamma rays.

New broad-group energy boundaries which conform to those used for core design calculations were chosen. The compatible group structures will enable core design and shielding to use the same cross sections for the core and blankets; or will also allow distributed fission sources for shielding calculations to be obtained from core design and burnup calculations. New cross section sets were generated for 28, 22, and 10 broad energy groups in the fast range above 2.38 eV and for 9, 4, 2, and 1 groups in the thermal range below 2.38 eV.

REFERENCES

8-1. Perkins, R. G., and R. J. Cerbone, "Physics Design of the 300-MW(e) Gas-Cooled Fast Breeder Reactor Demonstration Plant Grid Plate Shielding," ERDA Report GA-A14124, General Atomic, September 1976.

8-2. Rouse, C. A., D. R. Mathews, and P. K. Koch, "Gas-Cooled Fast Breeder Reactor Shielding Benchmark Calculations," General Atomic, unpublished data.

8-3. "Gas-Cooled Fast Breeder Reactor Quarterly Progress Report for the Period August 1, 1975 Through October 31, 1975," ERDA Report GA-A13766, General Atomic, January 5, 1976.

8-4. "Gas-Cooled Fast Breeder Reactor Quarterly Progress Report for the Period November 1, 1975 Through January 31, 1976," ERDA Report GA-A13815, General Atomic, March 22, 1976.

8-5. Cerbone, R. J., et al., "Shielding Analysis of the 300-MW(e) GCFR, A Topical Report Summarizing the Shielding Physics Analysis Performed During Fiscal Year 1975," ERDA Report GA-A13558, General Atomic, August 12, 1975.

8-6. Archibald, R. J., and D. R. Mathews, "The GAF/GAR/GAND Fast Reactor Cross Section Preparation System, v. II: GAND2 and GFE2 - Computer Programs for Preparing Input Data for the GAFGAR, GGC and MICROX Codes From an ENDF/B Format Data File," USAEC Report GA-7542 (Vol. II), Gulf General Atomic, March 1973.

8-7. Mathews, D. R., et al., "GGC-5, A Computer Program for Calculating Neutron Spectra and Group Constants," Gulf General Atomic Report GA-8871, September 27, 1971.

8-8. Dudziak, D. J., et al., "LAPHANO: A P_0 Multigroup Photon-Production Matrix and Source Code for ENDF," USAEC Report LA-4750-MS, Los Alamos Scientific Laboratory, September 21, 1973.

8-9. Adams, K. G., et al., "DINT: A Computer Program Which Prepares Multigroup Coherent-Incoherent Cross Sections for Photon Transport Calculations," Sandia Laboratory Report SC-RR-720684, August 14, 1973.

8-10. Nagel, M., and R. J. Cerbone, "Neutron-Coupled Gamma-Ray Cross Section Requirements for Gas-Cooled Fast Breeder Reactors," USAEC Report GA-A13329, General Atomic, March 12, 1975.

8-11. "Gas-Cooled Fast Breeder Reactor Quarterly Progress Report for the Period August 1, 1976 Through October 31, 1976," ERDA Report GA-A14112, General Atomic, November 1976.

8-12. "Gas-Cooled Fast Breeder Reactor Quarterly Progress Report for the Period May 1, 1976 Through July 31, 1976," ERDA Report GA-A13975, General Atomic, August 31, 1976.

9. SYSTEMS ENGINEERING (189a No. 00585)

The scope of the systems engineering task is to implement systems integration and coordinate interface requirements between all plant systems, i.e., the NSSS, the nuclear island, and rest of the BOP. An important part of this task is the development and implementation of effective documentation management, and additional work includes the development of methods for the assessment of core thermal-hydraulic performance as well as the selection and analysis of major thermal-hydraulic system parameters.

9.1. CORE THERMAL-HYDRAULIC PERFORMANCE

Activities for this subtask are devoted to the development of accurate computer models for the evaluation of core thermal-hydraulic performance. The requirements for and methods of core temperature monitoring are also being investigated.

9.1.1. GACOOL/Nuclear Analysis Interface

The core power distribution data have been analyzed, and the acceptability and accuracy of using the chopped cosine function to describe power distribution within the active core region has been confirmed. This results in considerable simplification in data handling and storage for GACOOL. In this respect, the peak-to-average power distribution and the extrapolated length are adequate to define the core power distribution within the active core region. A parabolic power distribution and a nonsymmetric cosine function are being used to describe power distribution within the axial and radial blankets, respectively. The original capability of GACOOL for accepting generalized power distribution data is maintained and could be exploited later, when refined numerical power distribution data become available.

9.1.2. GACOOL Development

The draft of the GACOOL Manual has been updated to reflect some of the major changes in the computer program, including a review and documentation of the basic assumptions, methods, and equations and a description of the new input/output specification.

The GACOOL pressure drop and heat transfer routines have been reviewed and checked for consistency with the methods used in other GCFR design and analysis computer programs at GA. Calculations of the exit pressure losses and the viscous drag within the fuel assembly were found to be inconsistent and were modified. Inlet and exit pressure loss coefficients and spacer pressure drop are now based on more current data.

The new version of GACOOL has the capability of running multiple cases and is designed to perform core orifice grouping and interchanging studies. In this new version, the core power distribution and fuel assembly design data are transferred within the computer program, resulting in more efficient operation of GACOOL. This was a basic step in modifying the computer program to perform multicase operation and orifice grouping/interchanging studies.

Several subprograms have been evolved, including a subprogram for calculating the core mean average outlet temperature under various combinations of orifice grouping arrangements for the fuel and blanket assemblies. As an alternative to the present capability of the program to accept arbitrary power distribution data, a subprogram has been developed to internally generate power distribution data. This subprogram is based on chopped cosine power distribution data for the active core region, parabolic power distribution for the axial blankets, and non-symmetric cosine power distribution data for radial blankets. Incremental thermal power generation for differential assemblies along the fuel and blanket assemblies is found by other subprograms. By introducing the integrated closed-form equations, calculation of the differential thermal

power output along the fuel and blanket assemblies is highly accurate and independent of the number and size of assemblies considered. This ensures accurate calculation of the maximum midwall hot spot cladding temperature and results in an accurate estimation of the core outlet temperature.

9.1.3. Core Orificing Studies

Orifice grouping studies were performed using GACOOL, and several alternative arrangements were considered. A seven-set grouping was found to be most favorable. This grouping consists of four orifice sets for the core and three for the radial blanket region. The core outlet temperature for this arrangement is 538.3°C (1001°F) compared with a maximum of 541.1°C (1006°F) for the "ideal" orifice size. The draft of the core orificing report has been updated to include the results of this study.

Orifice interchanging studies were performed to investigate the effects of orifice misfitting on the assembly outlet temperature and the consequent maximum midwall cladding hot spot temperature. The results indicate that temperatures in excess of 700°C (1292°F) can occur when a blanket orifice is fitted on a fuel assembly. The consequences of misfitting a fuel assembly with a wrong orifice set were found to be less severe within the core region. The analysis provides some data on the use of the outlet temperature difference between identical assemblies as a means of detecting possible orifice misfit.

9.1.4. Core Temperature Monitoring

The feasibility of measuring the average coolant outlet temperature from each fuel assembly by infrared imaging of the reactor core has been the subject of work reported in the previous quarter (Ref. 9-1). The conclusions of this study are presently being reviewed by a consultant from the University of California at San Diego for accuracy, completeness, and the existence of any problem areas which were not previously identified. The result of this review will probably lead to the selection of a reference design concept and identification of the scope of tests in a nonradioactive environment

to confirm the proposed infrared core temperature monitoring system. The impact of the change from thermocouples to an infrared system on cost and design requirement changes was also assessed.

9.2. SYSTEMS INTEGRATION

This subtask is concerned with the development of methods for the control of NSSS physical interfaces and NSSS and NSSS/BOP functional interfaces. This work requires the review of all change notices and coordination of the changes with the overall plant design.

Systems integration activities were initiated during this quarter. The first goal of this subtask is the establishment of a methodology which can be applied to the systems integration of the GCFR demonstration plant. Another important item within this subtask is the definition and establishment of the functional and physical interfaces for all plant systems.

Efforts are currently under way to outline and collect pertinent information for a draft of a plan for GCFR systems integration which will be issued toward the end of this fiscal year.

9.3. DOCUMENTATION MANAGEMENT

This subtask is concerned with the development and implementation of the necessary methods for effective documentation management. General design descriptions of the NSSS and the overall GCFR demonstration plant will be prepared and collected in a design book.

This subtask was begun during this quarter. As a preliminary step in the development of the design book, the following two studies were made:

1. Document planning: the engineering documents to be produced during the first year of the program definition and licensing phase (PDLP) were analyzed. The results of this analysis are presented in Fig. 9-1.

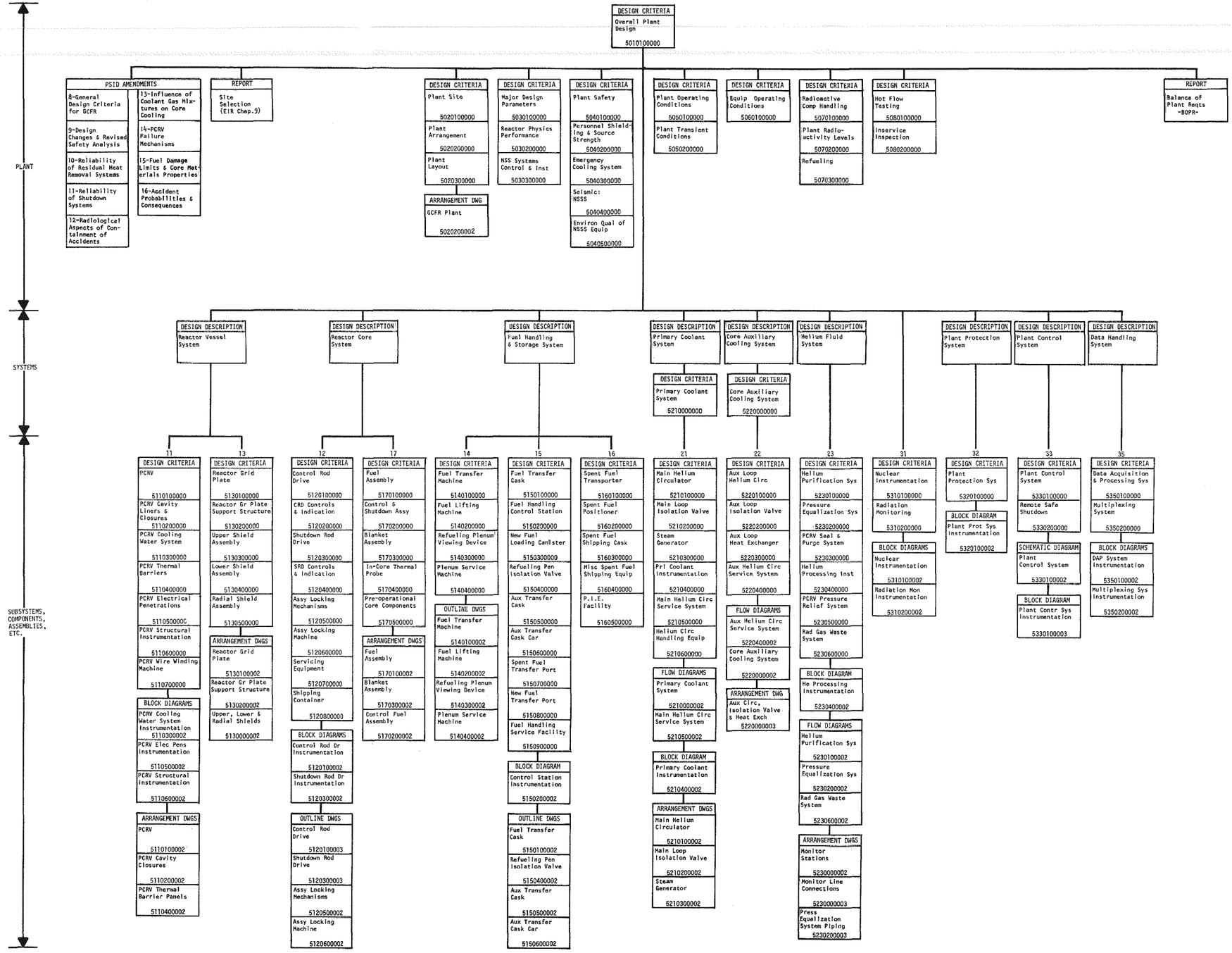

Fig. 9-1. Engineering document tree for the program definition and licensing phase

2. Document formats: internal (HTGR) and external (CRBR) procedures were reviewed for potential application to the GCFR demonstration plant.

As a result of these studies and other considerations, two decisions have been made about the design book:

1. Insofar as is practicable, engineering documents produced during the PDLP will serve a dual purpose; i.e., they will be used as input to the design book and support for the PSID (Ref. 9-2) and Preliminary Safety Analysis Report (PSAR).

2. The design book will be divided into the following major sections:

Reactor vessel system
Reactor core system
Fuel handling and storage system
Primary coolant system
Core auxiliary cooling system
Helium fluid system
Plant protection system
Plant control system
Data handling system

REFERENCES

9-1. "Gas-Cooled Fast Breeder Reactor Quarterly Progress Report for the Period August 1, 1976 Through October 31, 1976," ERDA Report GA-A14112, General Atomic, November 1976, p. 9-8.

9-2. "Gas-Cooled Fast Breeder Reactor Preliminary Safety Information Document," Gulf General Atomic Report GA-10298, February 15. 1971.

10. COMPONENT DEVELOPMENT (189a No. 00586)

10.1. REACTOR VESSEL

The scope of this subtask is to assure that the design of the PCRV and related components which contribute to the integrity of the pressure boundary is satisfactory and to test critical component configurations to make certain that they attain the design objectives. This subtask will demonstrate by analyses and tests that the PCRV and its penetrations and closures meet the design criteria. It will also provide assurance that (1) the design of the thermal barrier satisfactorily protects the liner and PCRV from the effects of high temperatures, and (2) the flow restrictors for the large penetrations can be developed to limit the flow of helium from the primary coolant systems to acceptable levels in the event of structural failure of a penetration or closure component.

During the previous quarter, drawings showing two alternate PCRV configurations for the low pressure drop around the primary coolant loop were prepared. The first configuration had the steam generator and helium circulator in the same cavity, which resulted in six radial cavities for three steam generators and three auxiliary circulators. The PCRV was sized by the concrete ligaments between the reactor core cavity and the steam generator cavity and between the steam generator cavity and the circumferential wire-winding channels. This configuration, entitled A-1, is shown in Fig. 10-1. The second configuration, entitled B-1 and shown in Fig. 10-2, has the steam generators and helium circulators in separate cavities, resulting in nine radial cavities for three steam generators, three helium circulators, and three auxiliary circulators. The ligament between these nine radial cavities determines the size of the PCRV design.

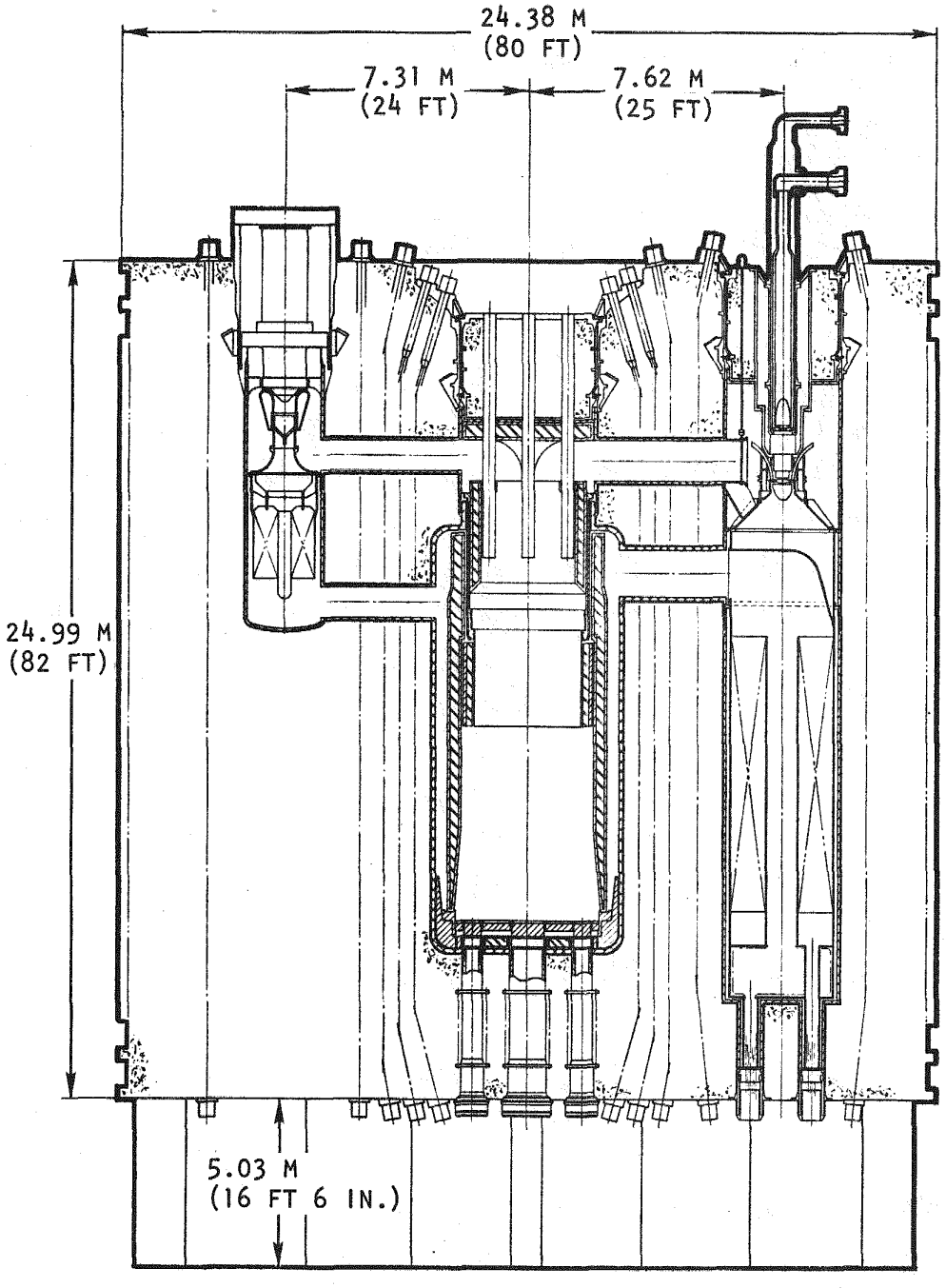

Fig. 10-1. Configuration A-1: nonreverse-flow helium circulator and nonresuperheat steam generator in same cavity

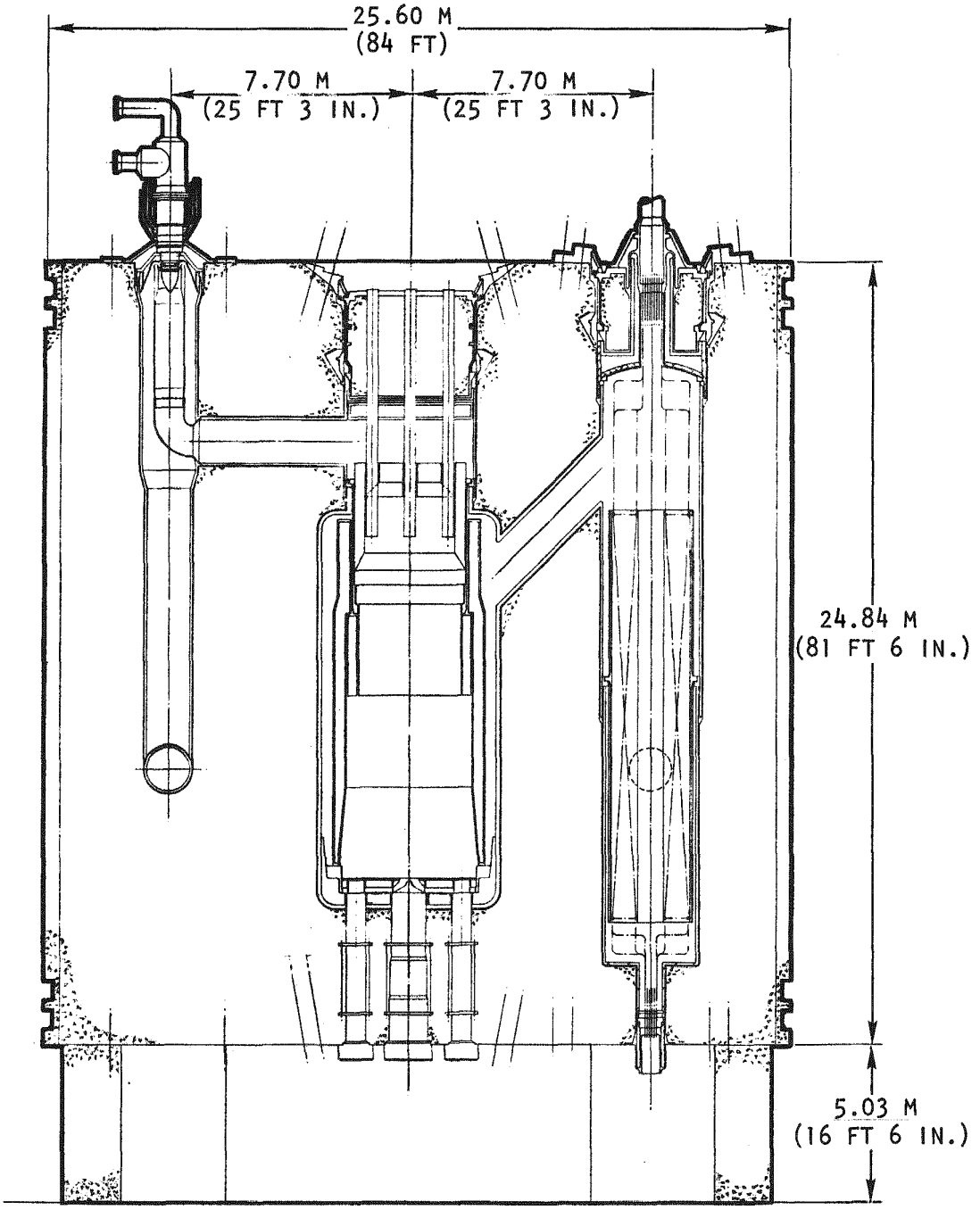

Fig. 10-2. Configuration B-1: reverse-flow helium circulator and nonresuperheat steam generator (straight-through) in separate cavities

The drawings of the two configurations show the reactor internals, the cavity closures, and the placement of the tendons. Structural analyses performed with the three-dimensional finite-element computer code for the thermal conditions for the PCRV have established that the peripheral tendons are not required; therefore, the drawings for the two configurations are being prepared without the peripheral tendons.

Coordination discussions concerning the PCRV model closure tests being conducted by ORNL for GA were held. These discussions pertained to the materials and material specifications for the configuration of the 1/15-scale model of the reactor cavity closure. (The prototype configuration of the reactor core cavity closure is shown in Fig. 10-3.) The ORNL machine shops have established that fabrication of the model is feasible, so they are proceeding with detailing the design of the model. The fixture for the 1/15-scale model testing program was successfully pressurized to 193 MPa (28,000 psi) with no leakage. There was a minor problem with the test fixture closure thread seizing, but this problem was resolved by reworking the fixture.

During this quarter, layout drawings for the PCRV configurations for the low pressure drop in the primary coolant loop were completed. Two configurations (A-1 and B-1) containing the nuclear core and radiation shielding, the helium circulators, and the steam generators were prepared; these are the nonresuperheat designs. The first PCRV configuration (A-1) has a steam generator and a helium circulator in the same cavity. The second configuration (B-1) has the straight-through steam generators and reverse-flow helium circulators in separate cavities. This arrangement allows these components to be removed independent of each other for maintenance or replacement. Configuration A-1 was preliminarily sized for the vertical cross section by calculating the concrete ligament between the reactor core cavity and the steam generator cavity and the ligament between the steam generator cavity and wire-winding channels, resulting in a diameter of 24.38 m (80 ft) and a height of 25.00 m (82 ft). The B-1 configuration has a total of nine radial cavities around the reactor core cavity: three steam generator cavities, three helium circulator cavities,

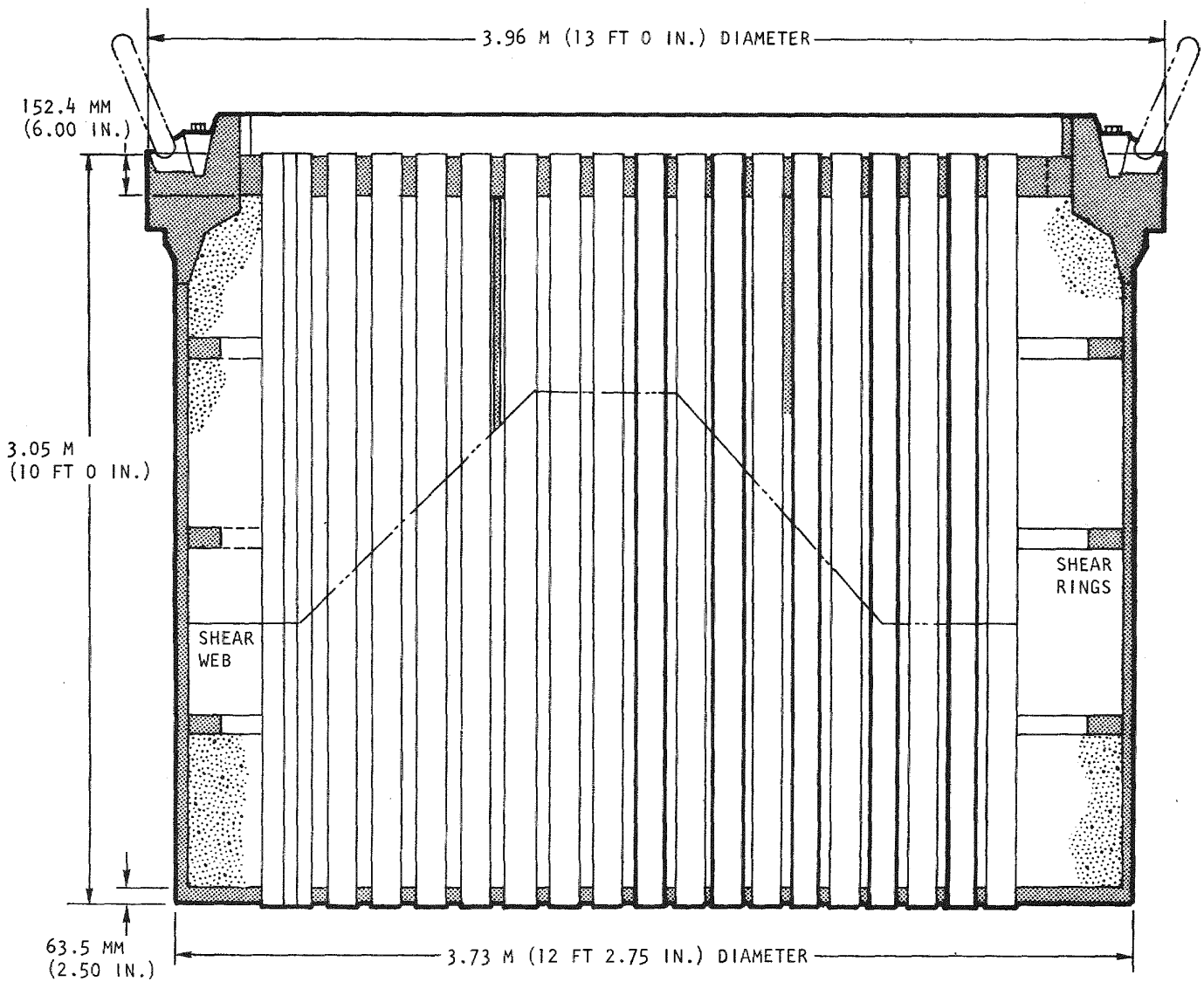

Fig. 10-3. Prototype configuration of reactor cavity closure

and three auxiliary circulator cavities. This configuration was sized by providing sufficient concrete for the circumferential ligaments between the nine radial cavities, resulting in a diameter of 25.29 m (83 ft) and a height of 24.77 m (81 ft, 3 in.).

A technical review meeting was held with interfacing design groups to discuss the configurations. It was decided to suspend work on configuration B-1 because of the congested top head which resulted in a larger-diameter PCRV and a correspondingly increased cost. It was recommended that configuration A-1 be revised to incorporate the reverse-flow helium circulator. Therefore, two PCRV configurations, A-2 and C-1 (Figs. 10-4, 10-5), were prepared to show the incorporation of the current reverse-flow helium circulator; both designs have the helium circulators and the center-supported steam generators in the same cavity. Configuration A-2 has the helium coolant flowing down over the steam generator coils and then up a central duct through the steam generator to the inlet plenum of the reverse-flow helium circulator. In configuration C-1, the helium coolant exits at the bottom of the steam generator and enters a separate duct which passes through the reactor vessel parallel to the steam generator cavity. This duct enters at the side of the inlet plenum of the helium circulator. These PCRV configurations have a diameter of 25.60 m (84 ft) and a height of 24.38 m (80 ft). It was decided to use configuration C-1, which has a bypass duct, as a basis for studying new PCRV configurations without resuperheat and one which has a steam generator with resuperheat.

A study was conducted on the feasibility of fabricating and constructing the reactor cavity closure (the prototype configuration is shown in Fig. 10-3) in accordance with current ASME Boiler and Pressure Vessel Code requirements. The closure is considered to be governed by the rules of the ASME Code, Section III, Division 2. However, for portions of the closure which are unbacked by concrete, the rules of the ASME Code, Section III, Division 1, Subsections NB-2000 through 5000, are applied. For this study, the penetration tubes and stiffened top plate were considered

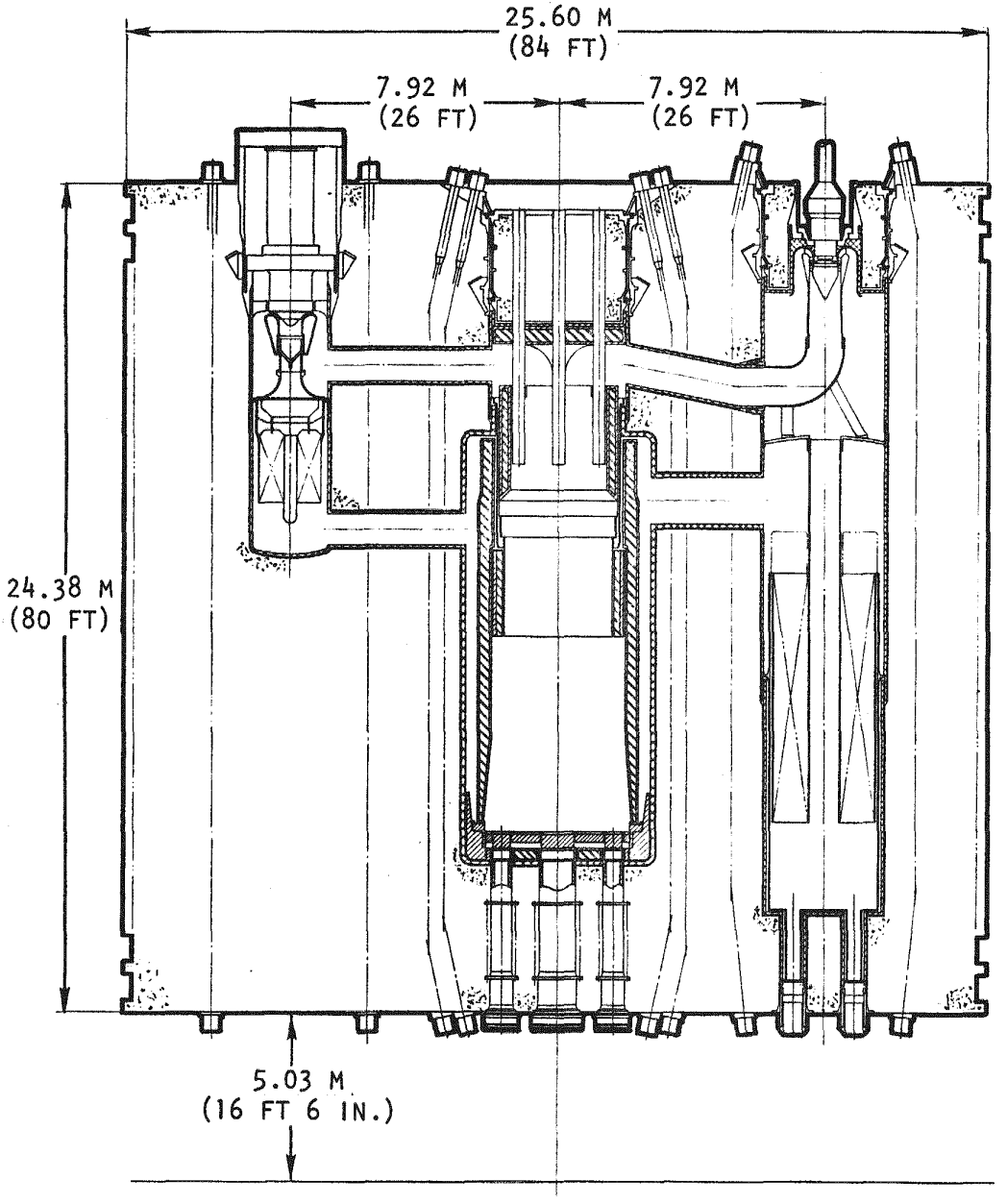

Fig. 10-4. Configuration A-2: reverse-flow helium circulator and nonresuperheat steam generator (center duct) in same cavity

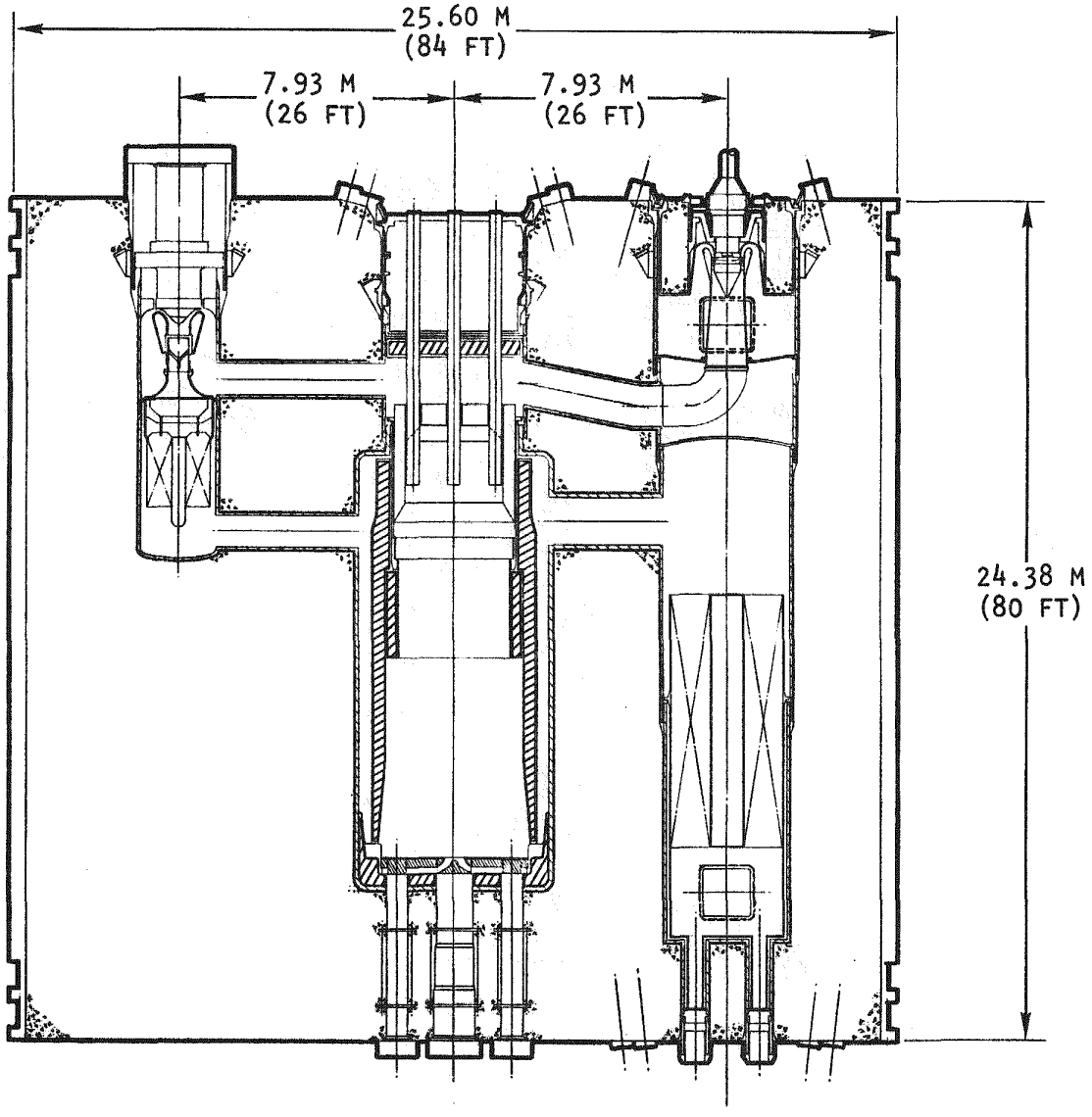

Fig. 10-5. Configuration C-1: reverse-flow helium circulator and nonresuperheat steam generator (bypass duct) in same cavity

to be unbacked by concrete for load-carrying purposes. A possible fabrication and concreting procedure was evaluated, and it was concluded that it is feasible to fabricate and construct the design in accordance with the ASME Code requirements.

Members of the ORNL Pressure Vessel Test Group met with GA on November 3, 1976 to coordinate the closure model testing program. A set of the assembly and detail drawings for the 1/15-scale model of the reactor cavity closure was received from ORNL for review and approval; the prototype model of the reactor cavity closure is shown in Fig. 10-3. The program for the 1/4-scale model testing of closures was discussed. There are two alternatives for the testing fixture: a steel forging for the testing vessel or a prestressed concrete testing vessel. Agreement was reached between GA and ORNL on the following items:

1. During January 1977, GA will provide information on the types of tests to be conducted using the 1/4-scale test fixture.

2. During March 1977, GA will supply the steam generator cavity and reactor core cavity closure holddown system design.

3. GA will comment on the ORNL design of the 1/15-scale model of the reactor core cavity closure.

4. ORNL will provide drawings of the instrumentation structure for the 1/15-scale model testing of the reactor core cavity closure.

Information on item 1 is being prepared for transmittal to ORNL, and for item 2, GA has commented on the design of the 1/15-scale model of the reactor core cavity closure, all questions have been resolved, and GA has approved the design. Regarding item 3, GA has received the ORNL drawings of the instrumentation structure for the 1/15-scale model of the reactor core cavity closure and has reviewed these drawings in preparation for giving approval.

ORNL has indicated that the concrete has been cast in the 1/15-scale model for the steam generator closure; this model is shown in Fig. 10-6 with the steel shell and internal reinforcing bar and the structural instrumentation before the concrete was cast. As soon as the concrete is cured, the testing program will be started.

During this quarter, analysis of a proposed PCRV reactor cavity closure cooling method was performed. The reactor cavity closure is cooled at all surfaces except the penetrations for control and shutdown rods and for fuel and blanket assemblies by a liner cooling coil system. Installation of cooling coils around these penetrations would be very difficult and costly. A possible alternative method of maintaining the liner and concrete temperatures near these penetrations below the limit of 339 K (150°F) for steady-state normal operating conditions would be to utilize the purge helium from the HPS, some of which is bypassed through the annuli between the assembly extension tubes and the penetrations. A preliminary analysis was performed to determine the purge flow conditions necessary to prevent the natural convection currents (due to buoyancy effects) from the upper reactor plenum from flowing upward through the annuli. The maximum potential pressure due to buoyancy effects was conservatively calculated to be 242.7 Pa (0.0352 psi) based on a helium purge temperature of 314 K (105°F) taken from Ref. 10-1. A parametric study was performed to determine the required purge flow rates through the annuli for various assumed clearances between the assembly extension tubes and the penetrations; the calculated mass flow rates are presented in Table 10-1. From these results, it can be concluded that it is desirable to minimize the clearances between the assembly extension tubes and the penetrations so that large purge flow rates are not imposed on the HPS and large purge flow rates of cold helium are not mixed with the primary coolant.

During this quarter, a logic diagram, a work breakdown structure, and a schedule for thermal barrier activities were drafted. Engineering activities such as development test work, design, thermal analysis, and drafting were also performed. In addition, thermal barrier design efforts continued

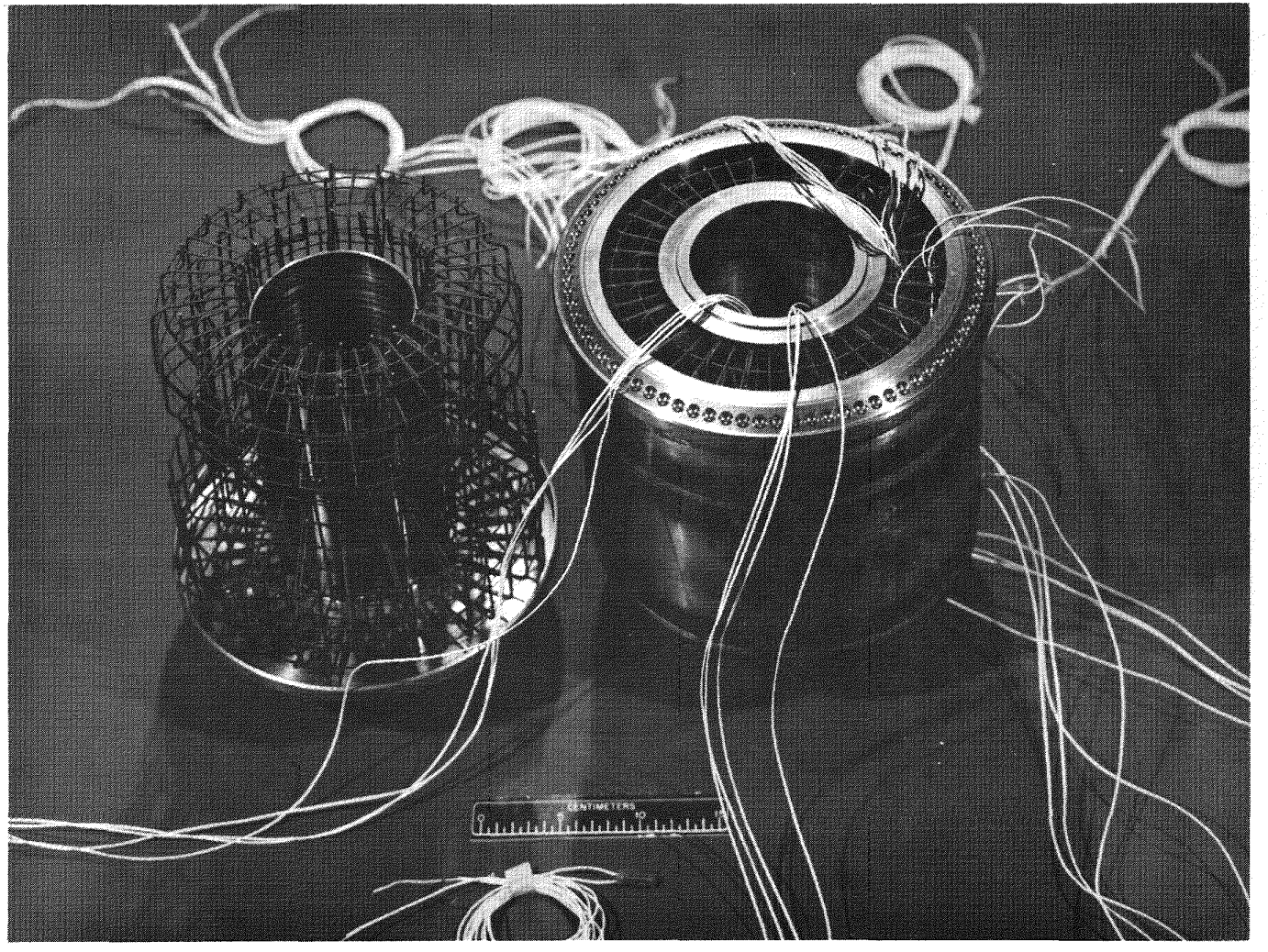

Fig. 10-6. 1/15-scale fabricated model of steam generator

TABLE 10-1
PURGE FLOW RATES THROUGH ANNULI BETWEEN ASSEMBLY EXTENSION TUBES AND REACTOR CAVITY CLOSURE PENETRATIONS

Clearance[(a)] [mm (in.)]	Purge Mass Flow Rates for Each Annulus [kg/s (lbm/hr)]	
	Fuel and Blanket Assembly Extension Tubes	Control and Shutdown Rod Extension Tubes
1.270 (0.05)	0.00213 (16.9)	0.00243 (19.3)
1.588 (0.0625)	0.00417 (33.1)	0.00476 (37.8)
1.905 (0.075)	0.00684 (54.3)	0.00780 (61.9)
2.223 (0.0875)	0.00895 (71.0)	0.01019 (80.9)
2.540 (0.1)	0.01084 (85.9)	0.01233 (97.9)
3.175 (0.125)	0.01596 (126.7)	0.01817 (144.2)

(a) Clearance = radius of the penetration minus radius of the tube.

in support of PCRV configuration studies, and a draft of the design criteria was completed and submitted for review. Design layout studies are in progress in an effort to integrate the thermal barrier design with a proposed shielding and support structure design in the lower main reactor cavity region.

10.2. CONTROL AND LOCKING MECHANISMS

The scope of this task covers design studies and comparative evaluation of alternate control rod drive and core assembly locking mechanism concepts. The conceptual work will be carried to the point of identifying ancillary and support equipment required for operating, servicing, handling, storing, and shipping new and replaceable components. Only by using a total system approach will it be possible to arrive at a meaningful evaluation whereby features and trade-offs can be identified and weighted against basic functional criteria, interface impact, and economic considerations.

During this quarter, work was initiated on an alternate mechanism concept for supporting and locking a core assembly to the grid plate. The original reference concept for this function requires supporting and locking tubular members for each core assembly to extend upward in the upper plenum cavity and through the PCRV closure plug. The actuating mechanism for each lock is contained in its own pressure housing, extending above the top of the closure plug. There are 184 such mechanisms for supporting the fuel and blanket assemblies and 27 similar mechanisms incorporated into the primary and secondary control rod drives for supporting the control assemblies.

This study phase is directed toward determination of core assembly support and locking methods which will minimize

1. Coolant flow interference.
2. Penetration structural complexity of PCRV closure plug.
3. Missile vulnerability above PCRV closure plug.

4. Number of primary coolant barrier seals.

5. Access congestion above PCRV closure plug.

It takes only a cursory observation of the current reference design concept to realize that by eliminating the upward-extending lock mechanisms in the coolant flow path through and above the PCRV closure plug, all five objectives can be satisfied. In addition, by eliminating the lock mechanism penetrations through the upper PCRV closure, additional cavity space within the concrete plug may be available to completely contain primary and secondary control rod drive mechanisms; this would satisfy the third and fifth objectives for these components.

Thus far, concepts of locking a core assembly using mechanisms localized in or at the top of the grid plate have been investigated. A lock-actuating machine will be required to disengage and engage the core assemblies during fueling operations. As presently envisaged, this machine would be introduced into the upper plenum cavity through access penetrations or existing rod drive penetrations in the PCRV closure plug.

The viability of a support and locking concept such as that described above is highly dependent on accommodation of the requirement for measuring the outlet gas temperature of each core assembly. The original reference concept, which has the lock-actuating members extending through the PCRV closure plug, provides convenient straight-line access paths for centrally leading steel-sheathed thermocouple assemblies to the gas outlet region of each fuel assembly. Alternate means for satisfying this requirement will also be studied.

Figure 10-7 provides a cross section view through the PCRV illustrating the current reference design arrangement of core assembly lock and rod drive mechanisms extending up through the top of the PCRV closure plug. Figure 10-8 shows a cross section view through the upper region of the PCRV, which is representative of one of the alternate approaches discussed. This figure illustrates how the upper reactor region would appear with the fuel assembly

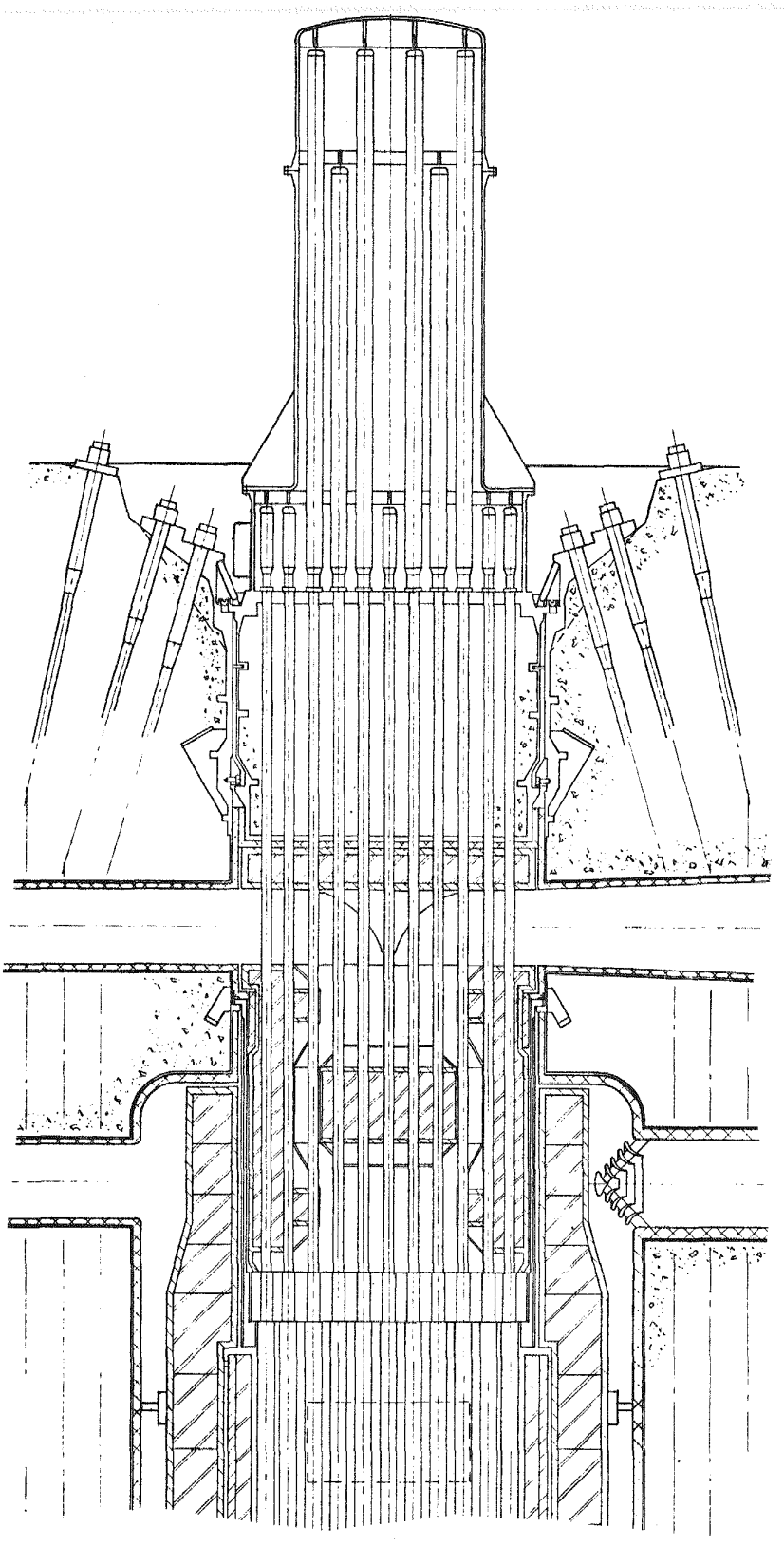

Fig. 10-7. Cross section view through PCRV

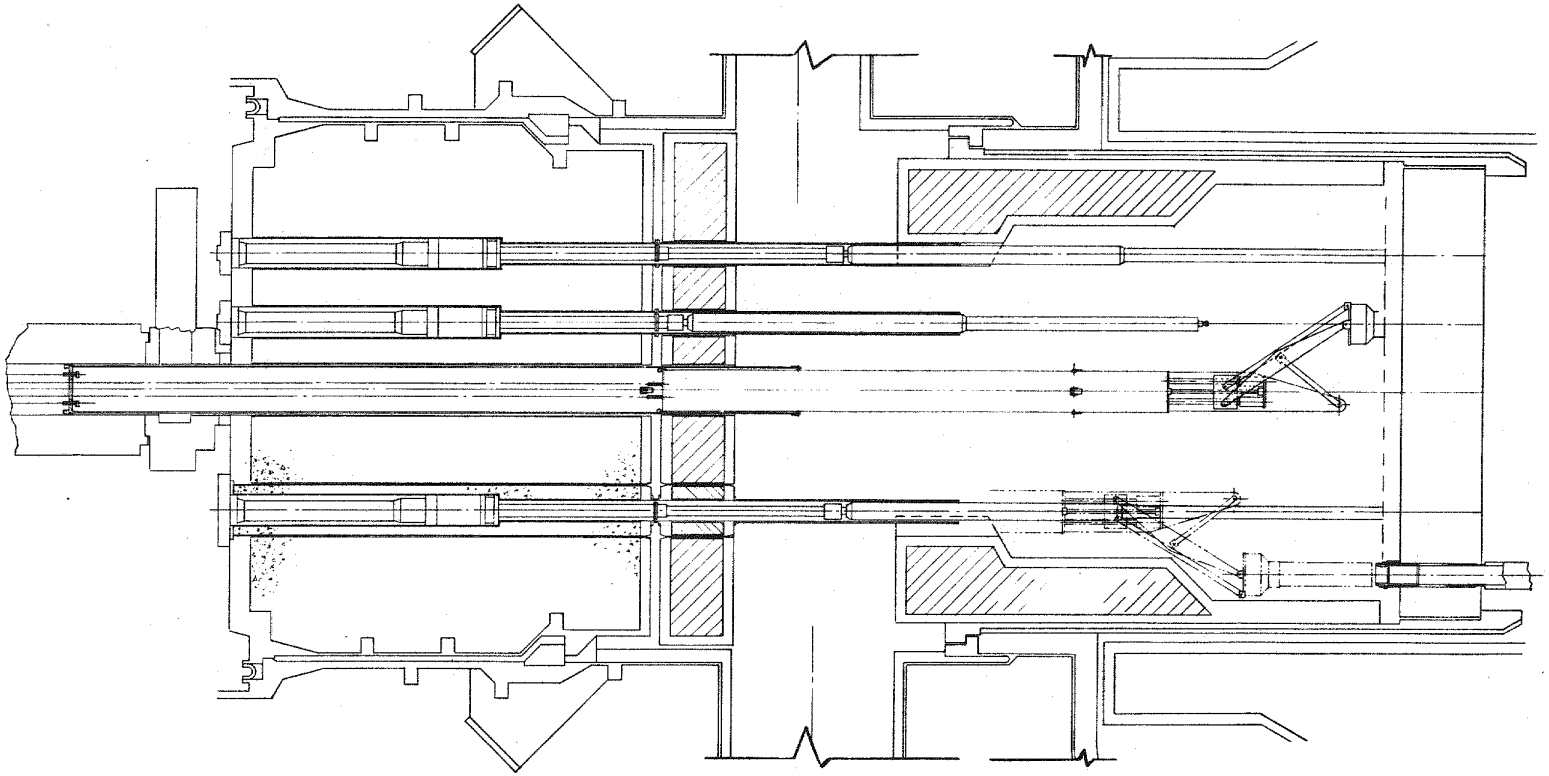

Fig. 10-8. Cross section view through upper region of the PCRV

lock mechanisms located within the grid plate and containment of the control rod drive mechanisms within the upper closure plug. A lock-actuating machine occupies a vacated control rod drive penetration in the upper closure plug.

10.3. FUEL HANDLING DEVELOPMENT

The fuel handling component conceptual design studies initiated during the latter part of FY-76 will continue through FY-77. Because the in-vessel machines are so complex, they are believed to require the most development time and thus received the most effort during this quarter.

Certain ex-vessel components were identified for further conceptual design study commencing during the early part of 1977. For example, the fuel transfer cask (FTC) was subjected to preliminary layout studies during FY-76, and some concepts were investigated, resulting in a preliminary FTC configuration consisting of an internal, multicavity rotating chamber. At present, a three-cavity magazine is contemplated, with a maximum of two fuel assemblies carried at any time, leaving one space empty. This arrangement enables the FTC to remain in position below the PCRV while exchanging new fuel in the FTC for spent fuel in the reactor, allowing only one vacant space in the core at any time. Future studies will verify the maximum quantity of fuel assemblies which can safely be transferred and accommodated when considering such things as maximum cask size, auxiliary system requirements, and the general effect of capacity on plant refueling time. Another ex-vessel equipment item which will be studied during the FY-77 conceptual design phase is the new fuel loading canister.

The in-vessel fuel transfer machine (FTM) and the fuel lifting machine (FLM) concept layout studies continued during this quarter. The FTM bar linkage system was revised to improve stability when the telescoped machine is operated near its geometric center location. Studies and modifications of the grapple head mechanisms and the fuel assembly carriage were made to facilitate the handling and hand-over operations to the FLM. In addition, layouts and studies were made on the interface and interchangeability aspects of removable subassemblies (i.e., fuel assembly carriage,

manipulator machine) utilizing a support saddle and remotely fastened hardware for a different proposed plenum service machine (PSM) concept. A preliminary shielding calculation indicates that a small shielding sleeve would be adequate for the lower transition portion of the FLM; this was incorporated in the layout studies of the design concept.

During this quarter, the major conceptual design layout study effort concentrated on the PSM. The contemplated functional requirements of the PSM can be satisfied with only a large mechanism, resulting in a very large machine package and corresponding radial PCRV refueling penetration diameter. Such large radial penetrations are not practical and may not be acceptable because of PCRV bottom head stress limitations. Reducing the penetration diameter to the size required by the FLM is desired and could be accomplished by deleting the dropped fuel assembly recovery requirement from the PSM functional requirements and adding it to the functional requirements for the FTM. The proposed design concept would utilize the FTM for dropped fuel assembly recovery. A large interchangeable manipulator can be attached to the FTM in place of the lifting mechanism. This operation must be remotely done in the fuel handling service facility, outside the plenum. A significant conceptual design effort concerning the remote disconnection mechanism is presently under way.

The PSM design concept is greatly simplified by assigning the task of fuel assembly recovery to the FTM. The remaining functional requirements of servicing, inspection, and repair related to the entire refueling plenum can be satisfied by a relatively small manipulator and a small, adjustable television camera. The manipulator would reach most of the plenum, and if it were lightweight, its supporting mechanism would be small, resulting in a radial penetration size not greater than that needed for the FLM. Since the television camera would be attached to the supporting mechanism of the PSM manipulator, it could be remotely positioned, providing good viewing capability. The PSM is readily available for inspection during normal refueling operations and can satisfy any viewing requirement during the time repair work is performed by the PSM; therefore, it was

suggested that the plenum viewing device be considered for deletion from the present in-vessel fuel handling equipment list.

10.4. CORE SUPPORT STRUCTURE

The purposes of this subtask are to assure the availability of the structural analysis methods and to determine the materials mechanical behavior required for assessing structural integrity of the GCFR core support structure under all anticipated operational and safety-related loading conditions.

During this quarter, the core support structure design criteria were drafted. An important consideration of the design criteria is the maximum allowable reactivity change of the core due to the deformation of the core and the core support structure. One proposed criterion requires that the maximum reactivity change due to loss of the pressure in the core shall be limited to $0.10. In the event of a safe shutdown earthquake, the equivalent of a $0.10 step reactivity insertion or an oscillating reactivity change with an amplitude of $0.60 shall be permitted. This amplitude is the combined effect of the movement of the grid plate and the core components.

A draft copy of Ref. 10-2 has been sent to ERDA. The Westinghouse Electric Advanced Reactors Division was contacted about a possible meeting on CRBR core support design information, and a copy of the CRBR equipment specification on the core support structure (Ref. 10-3) was received. A summary report (Ref. 10-4) was submitted to the chairman of the Fourth International SMIRT Conference.

10.4.1. Structural Analysis of the Thermal Stress in the Grid Plate

Analytical expressions for the deflection and moment in the grid plate under thermal or radiation swelling loads have been derived. The derivation, which assumes that the loads are linear through the thickness, is an arbitrary

axisymmetric function of the radius with a simply supported edge condition. The expressions for axial displacement and radial moment can be derived as

$$w = -\frac{6(1-\nu)}{hR^2} F(R)(r^2 - R^2) + \frac{1+\nu}{h}\left[\int_0^R \frac{1}{r} F(r)dr - \int_0^r \frac{1}{r} F(r)dr\right] ,$$

$$M_r = -\frac{(1-\nu^2)D}{h}\left[\frac{F(R)}{R^2} - \frac{F(r)}{r^2}\right] ,$$

where $F(r) = \int_0^r \alpha \Delta T r dr$,

$$D = \frac{Eh^3}{12(1-\nu^2)} ,$$

R = radius of grid plate,

r = radius at any point on grid plate,

h = thickness of plate,

E = Young's modulus of plate material,

ν = Poisson's ratio of plate material,

α = coefficient of thermal expansion,

ΔT = difference in temperature of the top and bottom surfaces.

Therefore, if the radial temperature distribution is known and the difference in the temperatures of the top and bottom surfaces of the grid plate is given, the axial displacement as well as the radial moment of the grid plate can be determined. The radial stress of the grid plate can be obtained from the known moment.

During the last quarter (Ref. 10-5), the first term of Eq. 10-5 was given as

$$Q\left[\frac{2}{D\sqrt{h^2 + t^2}} + \ldots\right] \quad .$$

The first term of Eq. 10-5 should be

$$Q\left[\frac{4}{D\sqrt{h^2 + t^2}} + \ldots\right] \quad .$$

This correction affects the calculation of the clamping effect; i.e., the value should be 48.34% instead of 25.58%. With this corrected clamping effect, the analytical and finite-element models and the test are in close agreement using the effective modulus E^* given by the ASME Code.

10.5. REACTOR SHIELDING ASSEMBLIES

The purpose of this subtask is to develop analytical methods and experimental programs for evaluating the reference design of the reactor shields. This evaluation considers heating and cooling of the shields, materials evaluation, seismic effects, the need for flow tests, structural analysis, and alternate shield configurations necessary for developing a satisfactory design.

During the previous quarter, an intermediate report (Ref. 10-6) was issued on the analytical methods used for the shield assembly. This report covers the structural, heat transfer, and hydrodynamic methods for shield analysis, the results of the shield heat transfer and hydrodynamic analysis, and a discussion of a shield flow test. Configuration studies are currently in progress to determine the method of support for the outer radial, wrap-around, preshield, and lower shield assemblies. These assemblies will require a support penetrating the thermal barrier and resting on the PCRV

liner of the bottom head. The pressure drop characteristics of the proposed outer radial shield support and the wraparound shield configurations are being evaluated.

10.6. MAIN CIRCULATOR, VALVE AND SERVICE SYSTEM

The purpose of this subtask is to develop the helium circulator, its service system, and the main loop isolation valve to demonstrate performance and reliability by testing under anticipated operating conditions. The overall objective for FY-77 is to initiate predesign and performance analysis of the circulator configuration, service system, and loop isolation valve. Requirements for the circulator subcomponents will be established and preliminary design layouts made. Service system requirements and system diagrams will be prepared, and a conceptual design of the main loop isolation valve will be completed. Work has been initiated on the conceptual and preliminary design of the helium circulator and service system.

10.6.1. Circulator Design and Performance Analysis

Late in FY-76, under private funding, conceptual design and analysis was initiated for the bearings, shaft, bearing housing, steam piping, and circulator support structures for an updated (no resuperheater cycle) GCFR main helium circulator. Preliminary sizing analysis of the circulator steam piping indicates that the best mechanical arrangement for the main circulator is for the steam to enter the center pipe of the two concentric pipes leading into and out of the circulator drive turbine. In order to obtain minimum thrust loads with this steam pipe arrangement, the helium flow through the circulator compressor is reversed; i.e., helium must enter the circulator from an annulus around the circulator and exit downward through a center duct. In order to obtain reasonable blade and disk stress levels and in order for the steam flow passages to clear the bearing housing, it is necessary to use large-diameter disks with short blades. The large

bearing housing results from the large shaft diameter [approximately 22.9 cm (9 in.)] required to obtain first-order critical speeds above 130% of design speed.

Even with the short blade design, the stress levels in the circulator and turbine blades tend to be high owing to the ΔP and Δh requirements and resulting high tip speeds. However, with further optimization of the design parameters, it is possible to obtain acceptable stress levels and still maintain good efficiencies and overall performance of the circulator and turbine. Short blades with low aspect ratios on large-diameter disks result in acceptable stress levels and frequency characteristics. In addition, the resulting lower rotating speeds of the shaft and bearings make it easier to satisfy the critical speed requirements.

The progress of circulator design work during this quarter was inhibited by the need to establish the primary system parameters for the updated reference design, including the system pressure drop and mass flow conditions for the circulator. Consideration is being given in the proposed reference design to establishing a design point at 107% power to account for 5% overpower for the "valve wide open" condition plus a 2% overpower to account for measurement uncertainties. These requirements result in a circulator pressure drop requirement of approximately 345 kPa (50 psi) and a helium flow rate of about 317 kg/s (709 lb/s), which together with the overall system design parameters specified in the GA design criteria, form the basis for a circulator conceptual design for the updated system.

The development plan for the GCFR main helium circulator (Ref. 10-7) will be reviewed, updated, and reissued during FY-77 to reflect any changes in scope or procedure due to design or test requirements.

10.6.2. Main Loop Isolation Valve

A topical report (Ref. 10-8) evaluating main loop isolation valve designs applicable to the GCFR has been prepared and is undergoing internal

review prior to issue. A partial draft of this report was submitted to ERDA last quarter for information and comment. In addition, design criteria for the GCFR main loop isolation valve have been prepared under private funding. Several types of valves suitable for gas-cooled reactors have been evaluated in Ref. 10-8 with respect to the GCFR design criteria, including the split butterfly valve similar to that used in the Fort St. Vrain HTGR, the ring valve used in the large HTGR, and the louver valve previously proposed for the GCFR demonstration plant reference design. None of these valves appear to adequately meet the present GCFR design criteria. Reference 10-8 also describes in detail the preliminary design work in progress on a flow-actuated butterfly valve with a mechanical override actuator. This valve (shown in Fig. 10-9) is mounted at the circulator compressor outlet center body. The valve is normally flow and pressure actuated in a manner similar to that of a conventional check valve, but additional torque may be applied by an electrically driven mechanical actuator. The valve override actuator shaft also actuates the valve position indicator switches.

10.6.3. Main Circulator Service System

Conceptual design work has begun on the main circulator service system. Preliminary sizing of system components is in progress but is being delayed because of changes in the circulator requirements resulting from revised primary coolant system and circulator design parameters. A comprehensive review of HTGR service system problems has been completed, and design improvements will be incorporated into the GCFR service system.

10.7. STEAM GENERATOR

The purpose of this subtask is to design and develop a steam generator which meets the operational, performance, and safety requirements of the GCFR. For this fiscal year, the scope of work includes development of a conceptual design for a first-of-a-kind steam generator. This will be accomplished by performing work in the following areas: (1) optimization of tube

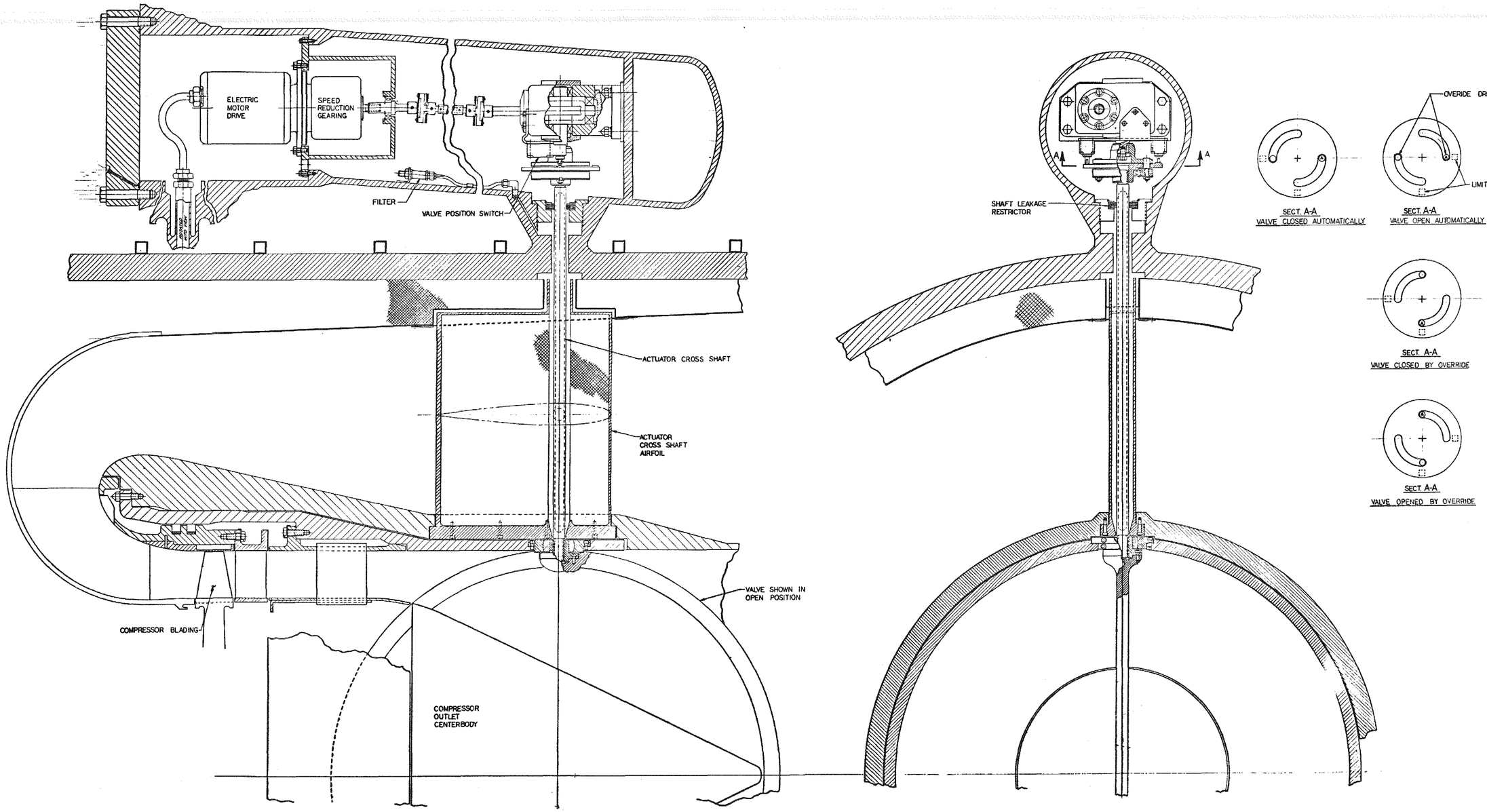

Fig. 10-9. The main circulator isolation valve

geometry for performance, cost, and boiling stability; (2) structural and stress analysis of tubing, tube sheets, and tube supports (thermal growth studies will be initiated); and (3) preliminary vibration analysis for the chosen tube geometry and support system.

During this quarter, as part of the GCFR steam cycle design and cost optimization study [for the 0.27-MPa (40-psi) primary system pressure loop design], steam generators using 2-1/4 Cr-1 Mo steel were sized with and without a resuperheater. Compared with previous steam generator sizing studies, the present study utilized an increased inside tube surface roughness, a single (rather than dual) value for longitudinal tube spacing for ease of fabrication, and increased tube wall thicknessess for the economizer and evaporator. These changes resulted in moderate increases in the number of tubes and bundle length.

In order to (1) provide the required cross sectional area for the four steam generator penetrations (resuperheater unit) in the bottom of the steam generator cavity in the PCRV, (2) provide for the above described changes, and (3) permit in-service inspection, steam generators were sized for bundle frontal areas greater than the 6.63 m^2 (71.4 ft^2) previously considered. Table 10-2 gives the characteristics of steam generators with and without a resuperheater.

In terms of bundle geometry, the smallest frontal area corresponds to a 3.0-m (10 ft) o.d. and 0.9-m (3-ft) i.d., and the largest area corresponds to a 4.0-m (13-ft) o.d. and 1.5-m and (5-ft) i.d. For a steam generator with a frontal area of 6.63 m^2 (71.4 ft^2), the active bundle length and surface area for a unit with a resuperheater are almost identical to those for a unit without a resuperheater. For steam generators with frontal areas greater than 6.63 m^2 (71.4 ft^2) (with a resuperheater), it is not possible for the bundle to utilize the allotted helium pressure drop [0.043 MPa (6.3 psi)] because the transverse tube spacing is held constant at a selected minimum value of 3.5 cm (1.375 in.). For frontal areas less than

TABLE 10-2
STEAM GENERATOR DESIGNS

Frontal Area [m^2 (ft^2)]	Surface Area [m^2 (ft^2)]	Total Bundle Length[a] [m (ft)]	No. of Tubes, Resuperheater/ Main Bundle	Bundle Helium ΔP [MPa (psi)]	Type
10.5 (113.0)	3,176 (34,166)	5.76 (18.9)	360/230	0.016 (2.3)	With resuperheater[b]
8.6 (92.0)	2,926 (31,485)	6.52 (21.4)	360/225	0.026 (3.8)	
6.6 (71.4)	2,685 (28,885)	7.92 (26.0)	360/222	0.043 (6.3)	
6.6 (71.4)	2,707 (29,128)	8.10 (26.6)	295	0.045 (6.6)	Without resuperheater[c]

(a) Does not include space between resuperheater and main bundle.

(b) With resuperheater: helium temperature in = 544°C (1011°F), out = 342°C (648°F); water temperature in = 208°C (406°F), out = 496°C/468°C (925°F/875°F); helium flow rate = 0.96 x 10^6 kg/hr (2.12 x 10^6 lb/hr); water flow rate = 3.9 x 10^5 kg/hr (8.53 x 10^5 lb/hr); water pressure drop = 1.79 MPa (260 psi).

(c) Without resuperheater: helium temperature in = 544°C (1011°F), out = 344°C (651°F); water temperature in = 208°C (406°F), out = 513°C (955°F); helium flow rate = 0.98 x 10^6 kg/hr (2.17 x 10^6 lb/hr); water flow rate = 4.3 x 10^5 kg/hr (9.46 x 10^5 lb/hr); water pressure drop = 1.79 MPa (260 psi).

6.63 m^2 (71.4 ft^2), it is possible to achieve full helium-side pressure drop with transverse tube spacings greater than 3.5 cm (1.375 in.). It can be seen from Table 10-2 that increasing the frontal area from 6.63 m^2 (7.14 ft^2) to 10.5 m^2 (113.0 ft^2) increases the required surface area by 18%, decreases the active bundle length by 27%, and decreases the bundle helium pressure drop by 63%. This relatively favorable trade-off between surface area increase and pressure drop decrease is balanced by the increased cost of larger PCRV dimensions. This study is continuing and is establishing an improved definition of the size, geometry, and design performance of the demonstration plant steam generator.

As part of the study to assess the implications of reduced steam pressure at reduced load, a preliminary study was made of the steam generator static boiling stability characteristics. The results show that approximately 1.38 MPa (200 psi) of additional inlet pressure drop at 100% load are required to achieve the same boiling stability index at 12.4 MPa (1800 psia) compared with 20 MPa (2900 psia) at 25% load.

Preliminary analysis of the stresses encountered in the steam generator tubes during normal and emergency operations has been performed. The purpose of this analysis was to support the geometries chosen for the performance sizing study. The stresses under consideration were those imposed on the tubes within the tube bundles and in the lead tubes in the bundle entrance and exit sections. They arise from internal and external pressure, thermal gradients, thermal expansions, and support loads.

Minimum (not necessarily nominal) tube wall thicknesses for all tubes considered for the resuperheater and the nonresuperheater cases are shown in Table 10-3. These thicknesses are based on a nominal o.d. and the worst of the three following operating conditions: (1) normal operation at 100% power, (2) emergency operation with full pressure inside and atmospheric containment equalization preesure outside the tubes, and (3) emergency operation with full helium pressure outside and containment equalization pressure inside the tubes. In addition, the basic wall thicknesses were increased by 6% to compensate for curvature in accordance with the ASME Boiler and

TABLE 10-3
RECOMMENDED GCFR STEAM GENERATOR MINIMUM TUBE WALL THICKNESSES

	Resuperheater		Nonresuperheater	
	Nominal o.d. [mm (in.)]	Wall [mm (in.)]	Nominal o.d. [mm (in.)]	Wall [mm (in.)]
Heat transfer tubes				
Resuperheater	25.4 (1.0)	3.20 (0.126)	-- N/A[(a)]	-- N/A
Superheater	25.4 (1.0)	3.30 (0.130)	25.4 (1.0)	4.37 (0.172)
Evaporator	25.4 (1.0)	2.74 (0.108)	25.4 (1.0)	2.74 (0.108)
Economizer	19.05 (0.75)	2.21 (0.087)	19.05 (0.75)	2.21 (0.087)
Lead tubes				
Resuperheater exit	38.1 (1.5)	4.32 (0.170)	-- N/A	-- N/A
Resuperheater inlet	38.1 (1.5)	3.66 (0.144)	-- N/A	-- N/A
Superheater	31.75 (1.25)	3.81 (0.15)	31.75 (1.25)	5.33 (0.210)
Feedwater	19.05 (0.75)	2.21 (0.087)	19.05 (0.75)	2.21 (0.087)

[(a)] N/A = not applicable.

Pressure Vessel Code, Section III, and also by 0.76 mm (0.030 in.) for corrosion allowance. The material chosen for all tubes was 2-1/4 Cr-1 Mo, specification SA-213/Grade T-22.

A preliminary analysis of the lead tube flexibility requirements indicates that thermal growth of the tubes and the tube bundle structural supports will produce effective lead tube end displacements above the tube support plate of approximately 7.62 mm (0.3 in.) in the resuperheater tubes and 4.06 mm (0.16 in.) in the superheater tubes. The end displacements in the lead tubes between the tube support plate (the tube bundle in the case of the feedwater tubes) and the various PCRV penetration tube sheets range between 17.78 mm (0.7 in.) (feedwater tubes) and 48.18 mm (1.7 in.) (resuperheater inlet tubes). These displacements are due to the thermal growth of the various support members and reflect the midplane location of the steam generator main support flange, which is a feature of the steam generator design configurations under study. Tentative expansion loops have been specified to accommodate these thermal displacements. As the design progresses, the geometry and sizing of the expansion loops will be further refined.

Preliminary sizing of the tube sheets for the steam generator PCRV penetrations was performed using modified equivalent solid plate methods, as described in the ASME Boiler and Pressure Vessel Code, Section III. Normal and emergency (helium side at atmospheric pressure) operations were considered for tube sheets with the tube pitch-to-diameter ratio set at 1.4. The thicknesses required ranged from 0.250 mm (9.88 in.) for the feedwater tube sheet in the resuperheated steam generator during emergency operations to 0.250 mm (17.25 in.) for the superheater discharge tube sheet in the nonresuperheater steam generator during normal operation.

A draft of a report on the evaluation of steam generator designs applied to the 300-MW(e) GCFR demonstration plant (Ref. 10-11) was submitted to ERDA for review and comment. The report is currently in final review.

10.8. AUXILIARY CIRCULATOR, VALVE AND SERVICE SYSTEM

The general objectives of this subtask are (1) to prepare and issue a core auxiliary cooling system (CACS) component development plan document, (2) to develop components for the CACS which meet reliability and safety criteria, and (3) to demonstrate the performance and reliability of critical components by testing under anticipated operating conditions.

The work scheduled in FY-76 included the preparation of the CACS component development plan (Ref. 10-10) under ERDA funding. The design criteria for the principal components such as auxiliary circulator, electric motor drive and control, core auxiliary heat exchanger, and auxiliary loop isolation valve have been completed under private funding.

Since the last quarter, the CACS development plan has been substantially revised to include an expanded definition of the safety-related qualification and design verification programs. It has also been updated to include the latest HTGR experience, including data on the auxiliary circulator bearing and seal test and the steam generator tube vibration and corrosion-erosion tests. In general, the CACS development plan for the GCFR is based on the HTGR development program with a provision for additional development testing to meet the specialized GCFR requirements. The development plan document is presently in review.

The first phase of the work for FY-77, which consists of an evaluation of alternative conceptual designs for the CACS, including design optimization between the CACS equipment of the NSSS and core auxiliary cooling water system equipment of the BOP program, has been delayed owing to the need for completion of safety design criteria. It is anticipated that an increased effort can be made during the next quarter without an adverse effect on the schedule.

REFERENCES

10-1. "300-MW(e) Gas-Cooled Fast Breeder Reactor Demonstration Plant," General Atomic Report GA-A13045, July 15, 1974.

10-2. Chang, K. H., A. S. Chuang, and C. E. Washington, "A Structural Analysis of the GCFR Core Support," General Atomic, unpublished data.

10-3. "Clinch River Breeder Reactor Plant Equipment Specification, Core Support Structure," 4th rev., Westinghouse Advanced Reactor Division Specification E953023, April 23, 1976.

10-4. Chuang, A. S., K. H. Chang, and C. E. Washington, "Comparison Study on GCFR Core Support Grid Plate Displacements Among Experimental, Analytical, and Finite-Element Models," General Atomic unpublished data.

10-5. "Gas-Cooled Fast Breeder Quarterly Progress Report for the Period August 1, 1976 Through October 31, 1976," ERDA Report GA-A14112, General Atomic, November 1976, p. 10-13.

10-6. Penzes, L., S. K. Bhat, and V. Jovanovic, "Mechanical Aspects of the Thermal Shielding for the Gas-Cooled Fast Breeder Reactor," ERDA Report GA-A14045, General Atomic, October 18, 1976.

10-7. Mouritzen, G., "Development Plan for the GCFR Helium Circulators," USAEC Report GA-A13207, General Atomic, December 6, 1974.

10-8. Johnson, E. R., "Main Loop Isolation Valve Evaluation," General Atomic, to be published.

10-9. Baroczy, C. J., "Evaluation of Steam Generator Designs for Application to the 300-MW(e) Gas-Cooled Fast Breeder Reactor," General Atomic, to be published.

10-10. Khoe, J. H. F., "Core Auxiliary Cooling System Component Development Plan," General Atomic, to be published.

11. PLANT DYNAMICS (189a No. 00638)

11.1. CONTROL SYSTEMS

Development of the component mathematical models has been completed, and a summary description of each model is given below. These are the initial models for GCFR application, and it is expected that modifications will be made in the future as more information is obtained about the components and their effects on system simulation. Integration of these models into the system simulation is nearing completion. The steam-side components (steam generator, helium circulator, and resuperheater) have been coupled, and this coupled system is being checked. The reactor model will be added following verification of the steam-side simulation.

The nonlinear component models have been developed in accordance with the following general guidelines:

1. Models developed from fundamental conservation equations (energy, mass, and momentum) as applied to appropriately determined control volumes (lumped parameter modeling).

2. Models suitable for use in an overall system model with an integration step size of 0.1 s.

3. Modeling emphasis on accurate prediction of basic plant measurement variables such as controller inputs and component inlet and outlet fluid flows, temperatures, and pressures.

Linear component models are obtained from these nonlinear models using a digital computer algorithm based on the theory of small perturbations. Each integration variable in the nonlinear model becomes a state variable

in the linear model, and the state variable influence coefficient matrix is determined by perturbing each of the nonlinear model integration variables.

11.1.1. Core Model

The core model consists of two models, the reactor power model and the core thermal model, coupled through the average fuel temperatures and normalized reactor power. The reactor power model is based upon the point kinetics equations with six delayed neutron groups in the prompt jump approximation (prompt neutron effects have too high a frequency to be of interest in this simulation) and the assumption that the power level is proportional to the neutron density except during a reactor scram, when decay heating must be treated separately. Using the point kinetics formulation, the normalized fission power level is determined as a function of reactivity which is calculated as the sum of rod- and temperature-induced reactivities. The rod-induced reactivity is determined as a function of the position of a single representative control rod, and the temperature-induced feedback is a function of the average rod fuel and blanket temperatures predicted by the core thermal model. The inputs to the reactor power model are the average temperatures from the core thermal model and the control rod position from the control rod controller and drive model. The model provides normalized power output.

The core thermal model is based on a typical fuel rod and adjacent coolant channel within the active region of the core. Heat generated in the circumferential blanket assemblies is considered as a percentage of the total core thermal power. The helium flow which does not pass through the active core region is determined as a percentage of total reactor helium flow. The typical fuel rod is divided into six regions, as shown in Fig. 11-1. The choice of these regions is based on rod construction and power gradients. Each region contains five thermal nodes, as shown in Fig. 11-2. The major modeling assumptions are

1. Primary coolant mass storage and thermal storage effects are of a high frequency relative to the range of interest for the plant

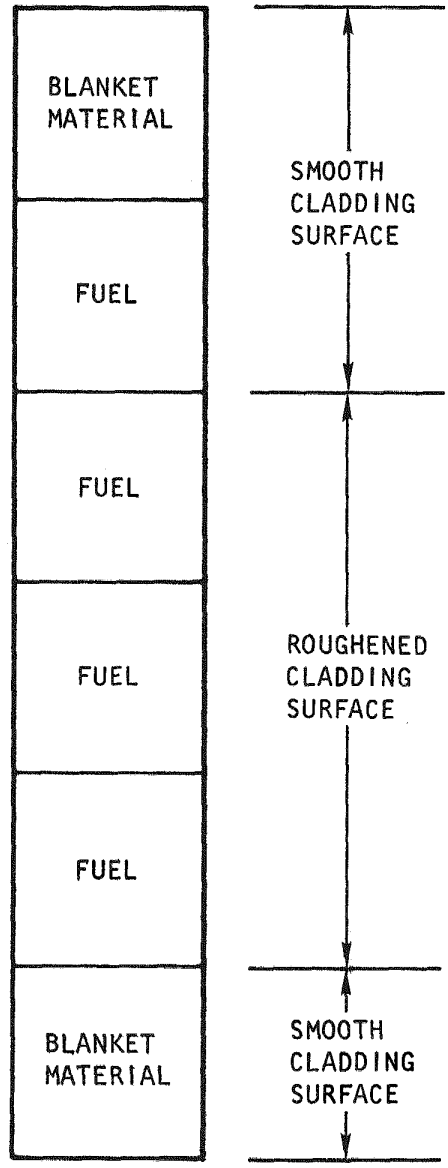

Fig. 11-1. Fuel rod regions

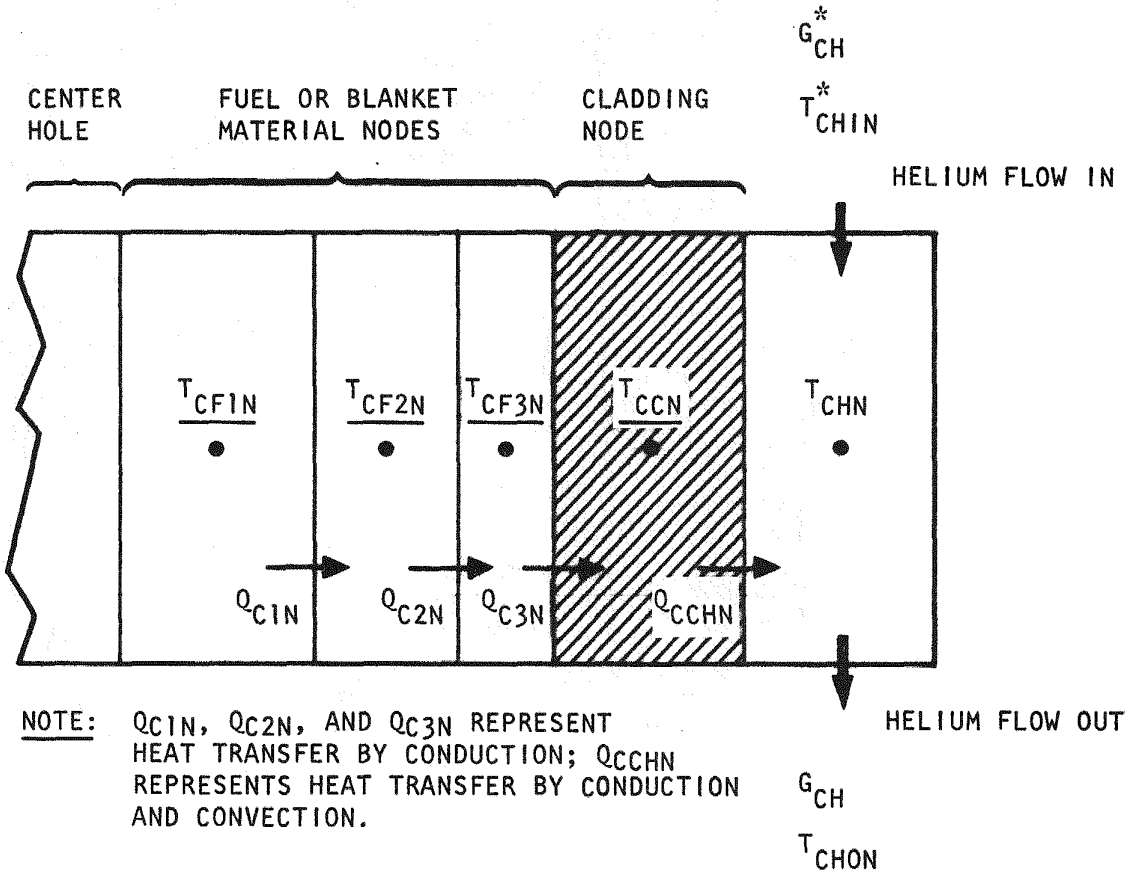

NOTE: Q_{C1N}, Q_{C2N}, AND Q_{C3N} REPRESENT HEAT TRANSFER BY CONDUCTION; Q_{CCHN} REPRESENTS HEAT TRANSFER BY CONDUCTION AND CONVECTION.

F = STEAM MASS FLOW
G = HELIUM MASS FLOW
H = ENTHALPY
L = LENGTH
P = PRESSURE
Q = HEAT FLUX
R = DENSITY
T = TEMPERATURE
W = WATER MASS FLOW
* = MODEL INPUTS
___ = INTEGRATION VARIABLES (STATE VARIABLES)

Fig. 11-2. Thermal model schematic for a typical region of a fuel rod

system simulation (all thermal storage is lumped into the core inlet and outlet plenums).

2. The dynamics of the active core region can be predicted from a typical fuel rod with average power and average helium flow properties.

3. Heat transfer between nodes by conduction in the axial direction is negligible.

4. Heat generation takes place only in the blanket and fuel nodes.

5. The axial power distribution is a function of long-term effects and does not appreciably vary over the load range of interest (i.e., 25% to 100%).

6. The coolant is always in equilibrium with the cladding surface (i.e., instantaneous changes in helium temperature are allowed).

7. Helium flow is uniform along the entire length of the fuel rod.

The inputs to the core thermal model are upper plenum helium temperature, helium flow rates, and fractional power level. The outputs are average fuel and blanket node temperatures for the reactor power model and core exit helium temperatures.

The overall core model contains thirty-three integration variables: twelve fuel node temperatures; six blanket node temperatures; six cladding node temperatures; one node temperature each for the grid plate, core box structure, (to include the thermal capacitance represented by these large core structures), and outlet helium temperature (mixed mean) in the core inlet plenum; and six normalized delayed neutron precursor concentrations.

Since this core model was developed to accurately predict conditions during a scram condition, it is reasonable to anticipate that the number of integration variables (representative of model fineness) can be reduced for on-line control system studies. This reduction will be made (to reduce model complexity and simulation usage costs) if simulation system checks verify this supposition.

11.1.2. Steam Generator Model

The steam generator is a once-through, helium-heated subcritical generator. It consists of two bundles of small-diameter tubes coiled in the form of a helix. Water and steam flow through the tubes, and hot helium which has passed through the reactor core flows over the tubes to form a countercurrent heat exchanger. The smaller tube bundle is called the resuperheater and this section is modeled separately (see Section 11.1.3).

For the main tube bundle, the three regions (subcooled water, two-phase steam-water mixture, and dry steam) which exist on the water/steam secondary side are referred to as the economizer, evaporator, and superheater, respectively. The boundaries of these regions are set by thermodynamic properties (0% and 100% quality) and are free to move with respect to the ends of the steam generator. The location of these boundaries at any instant in time is a function of several quantities, such as feedwater flow rate and temperature, helium flow rate and temperature, and steam generator back pressure.

The actual physical processes associated with heat transfer and fluid flow in a multiphase heat exchanger such as the steam generator are quite complex. In order to represent these processes with a low-order mathematical model, a number of assumptions must be made to simplify the problem. The basic assumptions made in conjunction with the development of the model are

1. One steam generator coil can be represented by a single average tube whose properties (area, length, steam-water inventory, heat

transfer coefficients, feedwater and helium flow, and tube metal mass) represent the properties of the entire coil.

2. Fluid flow and heat transfer in the steam generator are adequately represented if the model consists of three nodes. For convenience, these nodes are the economizer (contains subcooled water and extends from the steam generator inlet to the 0% quality boundary), evaporator (two-phase region from 0% to 100% quality boundaries), and superheater (dry steam, extends from 100% quality line to steam generator outlet).

3. The mass, momentum, and energy storage in each node can be characterized by the rate of change of the appropriate average property.

The model schematic is shown in Fig. 11-3. Note that the model contains eight integration variables (state variables). A ninth integration variable is used to provide a single-order lag on the input water enthalpy. This lag is used to approximate the thermal transport lag in the economizer section. Unlike the other two sections, perfect mixing cannot be assumed in the economizer section, and the water transport time in this section is approximately 80% (at full-flow conditions) of the total steam generator transport time. Other model variables are determined from these integration variables and the input parameters using thermodynamic state equations (steam property functions and tables and the gas equation), weighted averages, and algebraic flow - pressure drop relationships.

11.1.3. Reheater Model

The reheater (or resuperheater) is the smaller tube bundle in the steam generator module. It has essentially the same basic construction characteristics as the larger main bundle. Steam from the helium circulator turbine flows through the tubes, and hot helium flows over the tubes to form a countercurrent heat exchanger. The difference between the basic assumptions made for this model and those made for the steam generator model relates to the number of nodes used. Based on the small mass storage

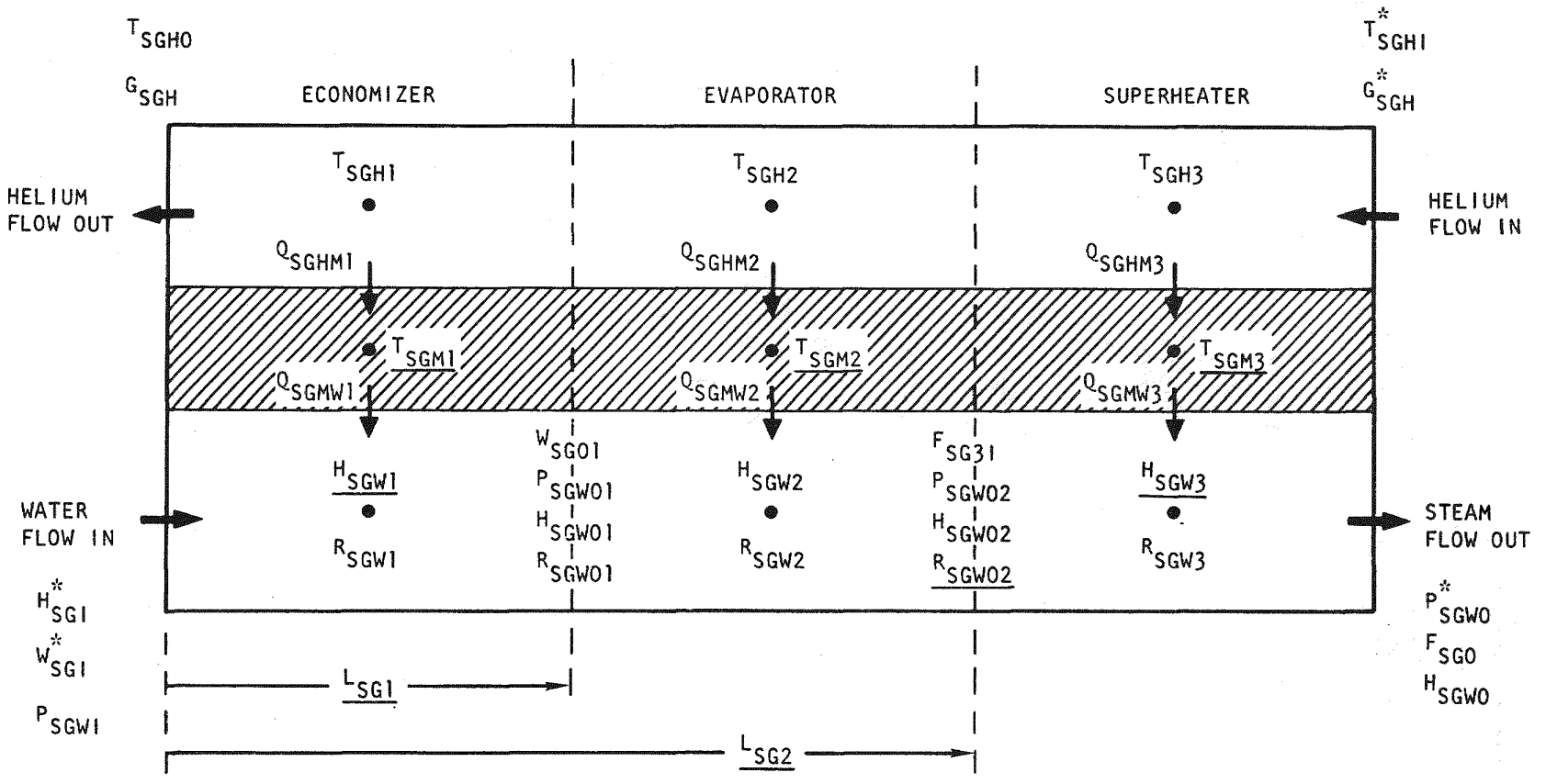

F = STEAM MASS FLOW
G = HELIUM MASS FLOW
H = ENTHALPY
L = LENGTH
P = PRESSURE
Q = HEAT FLUX
R = DENSITY
T = TEMPERATURE
W = WATER MASS FLOW
* = MODEL INPUTS
__ = INTEGRATION VARIABLES (STATE VARIABLES)

Fig. 11-3. Steam generator model

and energy exchange in the reheater relative to other components such as the steam generator, fluid flow and heat transfer in the reheater are adequately represented by a one-node model. The model, which is essentially a fixed-boundary version of one steam generator node (as described in Section 11.1.2), is shown in Fig. 11-4. The major difference between the two models is in consideration of steam mass flow. Owing to the small mass inventory and low pressure drop in the reheater, the steam mass flow through the reheater is assumed to be constant. This flow is determined from the algebraic flow pressure drop relationship between the helium circulator turbine outlet pressure and the pressure in the main turbine hot reheat header.

11.1.4. Helium Circulator Model

The helium circulator model consists of the helium circulator, helium flow and pressure loss calculations, a steam-side mass (volume) node upstream and downstream of the circulator turbine, and three control valves which can be used to adjust the steam flow through and around the circulator turbine. This model is shown in Fig. 11-5. The helium flow and pressure loss calculations and the circulator turbine control valves are included with the circulator for modeling convenience.

This model contains five integration variables, two each for the steam properties (density and enthalpy) at the two mass nodes and one for the rotation rate (speed) of the circulator compressor-turbine shaft. On the steam side, the mass node pressures are determined from the two integration variables and steam property tables. Steam flows through the valves are calculated by means of the algebraic flow - pressure drop relationship.

The helium circulator comprises an axial flow compressor driven by a steam turbine. These two items are mounted on a single shaft and bearing assembly.

The circulator turbine is driven by the superheated steam from the steam generator module. Turbine performance characteristics are expressed

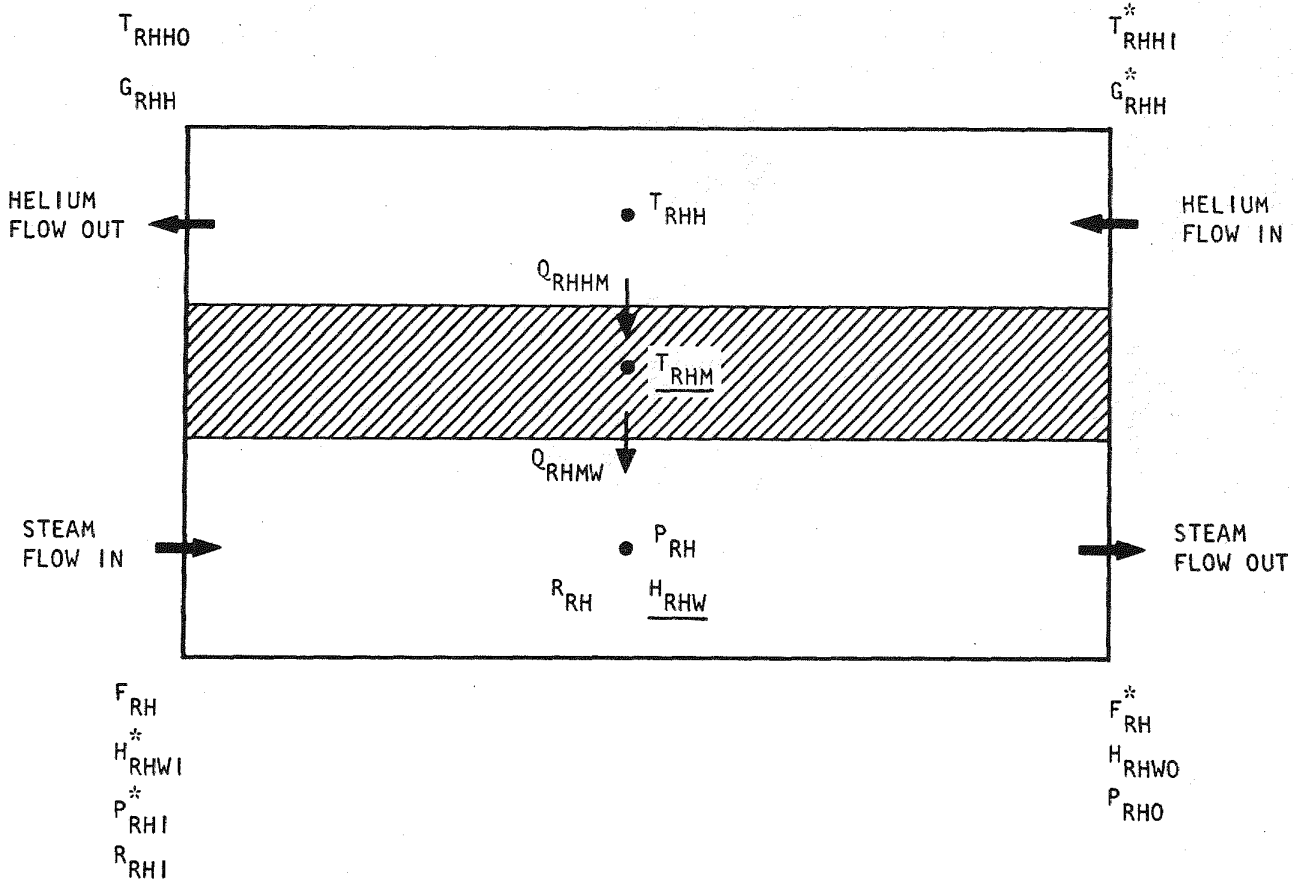

Fig. 11-4. Reheater model

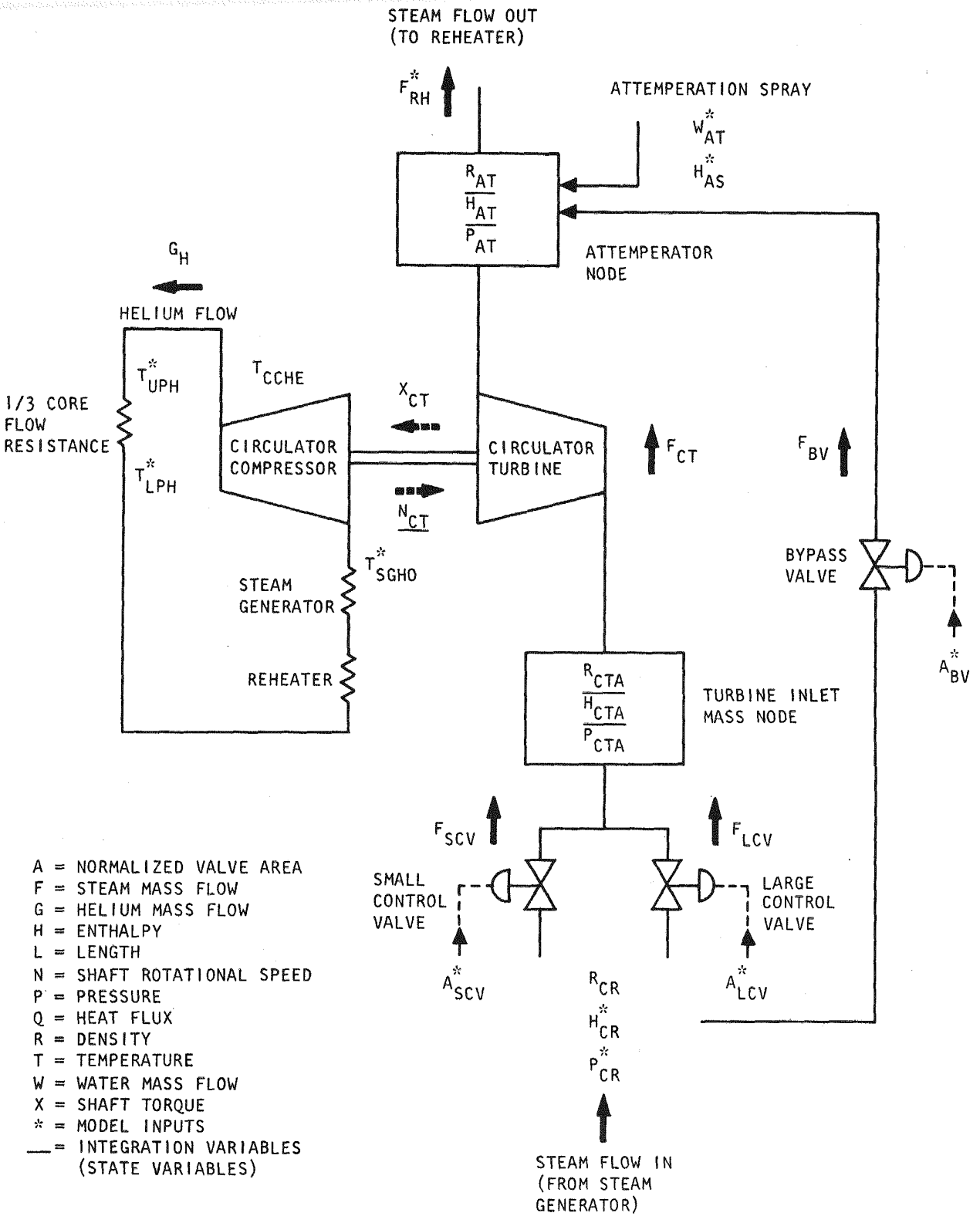

Fig. 11-5. Helium circulator model

as functions which give turbine nozzle pressure ratio versus overall pressure ratio for various speeds (blade Mach numbers). The steam flow rates are computed from the nozzle pressure ratio and total inlet pressure and enthalpy using gas thermodynamic relationships for the expansion process. The performance characteristics also include correlations of overall efficiency versus velocity ratio (blade speed to nozzle exit velocity) and blade Mach number. Using the pressure ratio, flow rate, and efficiency, the turbine power, and hence the torque, are computed for a known speed. The net torque acting on the circulator at any instant is found by subtracting the compressor torque from the turbine torque and also subtracting the estimated bearing torque losses. This net torque is then divided by the polar moment of inertia of the rotating assembly to obtain the speed derivative (shaft acceleration).

The compressor model is coupled to a simplified model of the primary cooling loop, which gives the loop flow and pressure loss characteristics. Helium flow rate and compressor pressure rise and torque are determined by use of an iterative procedure. Compressor performance characteristics are expressed in normalized form as algebraic functions of torque versus helium flow rate and pressure rise versus helium flow rate.

11.2. SEISMIC ENGINEERING

A topical report (Ref. 11-1) on the first phase of the dynamic test of the grid plate - core assembly and the analytical and SAPIV finite-element simulation of the test results was completed. The results of these tests show the existence of system resonant frequencies which are approximately half the frequencies of the single core assembly owing to the rotational effect of the grid plate. The most important result of these tests is that shear deformation in the grid plate is significant, especially for horizontal excitations, and must be included in the design analysis. Details of the test results are discussed in Ref. 11-2; only the analytical results and the SAPIV finite-element simulation are presented in this section.

The analytical technique used the Rayleigh-Ritz method (Ref. 11-3) to determine the unknown frequencies and mode shapes of the single-model fuel and blanket assemblies. A polynomial approximation of the mode shape was substituted in the expression of the total energy, and the unknown frequencies were calculated. Double pin supports were assumed for the boundary condition. The same boundary condition was applied in the SAPIV finite-element simulation (Ref. 11-4). Table 11-1 shows the results of the computation with corresponding test frequencies and the differences between them. This table also presents the range of damping factors as a percentage of critical damping.

Figure 11-6 illustrates the mode shape at a frequency of 1498 Hz. Based on this measurement, the effective elastic modulus of the grid plate was determined by the thin and the thick plate theories (Ref. 11-5). The analytical method using thin plate theory applies the energy method utilizing the measured frequency and mode shape in the energy expression, and the unknown effective elastic modulus is obtained. In this derivation, the measured mode shape is approximated by a fourth-order polynomial.

An iterative method was employed in the SAPIV finite-element simulation, and the effective elastic modulus of the grid plate was estimated until the measured frequency was matched. Table 11-2 shows the results of the computation using the analytical and SAPIV methods and the ASME Code value using thin plate theory. The effective elastic modulus determined using the analytical and SAPIV methods is about 35% higher than the corresponding ASME Code value.

The frequency and mode shape shown in Fig. 11-7 were also determined using SAPIV and thin plate theory. The calculated frequency was 4587 Hz, which corresponds to a difference of 3% compared with the test results. When Mindlin's thick plate theory (Refs. 11-5, 11-6) was applied to the data in Fig. 11-6, and the value of the effective elastic modulus obtained was lower compared with the corresponding value of the ASME Code (Table 11-2).

TABLE 11-1
COMPARISON OF EXPERIMENTAL AND ANALYTICAL FREQUENCIES
FOR SINGLE CORE ASSEMBLIES

	Test (Hz)	SAPIV Frequency (Hz)	Analytical Frequency (Hz)	Damping Factor (%)
Fuel	54	55.8 (3.3%)[a]	55.8 (3.3%)	0.2 to 0.35
Blanket	38.5	38.7 (0.5%)	42 (9%)	0.5 to 0.65

[a]Number in parentheses is difference in percentage.

TABLE 11-2
EFFECTIVE ELASTIC MODULI OF DIFFERENT THEORIES

Theory	Analytical Value (Pa)	SAPIV Value (Pa)	ASME Value (Pa)
Thin plate	1.861×10^9	1.829×10^9	1.378×10^9
Thick plate	1.086×10^9	--	--

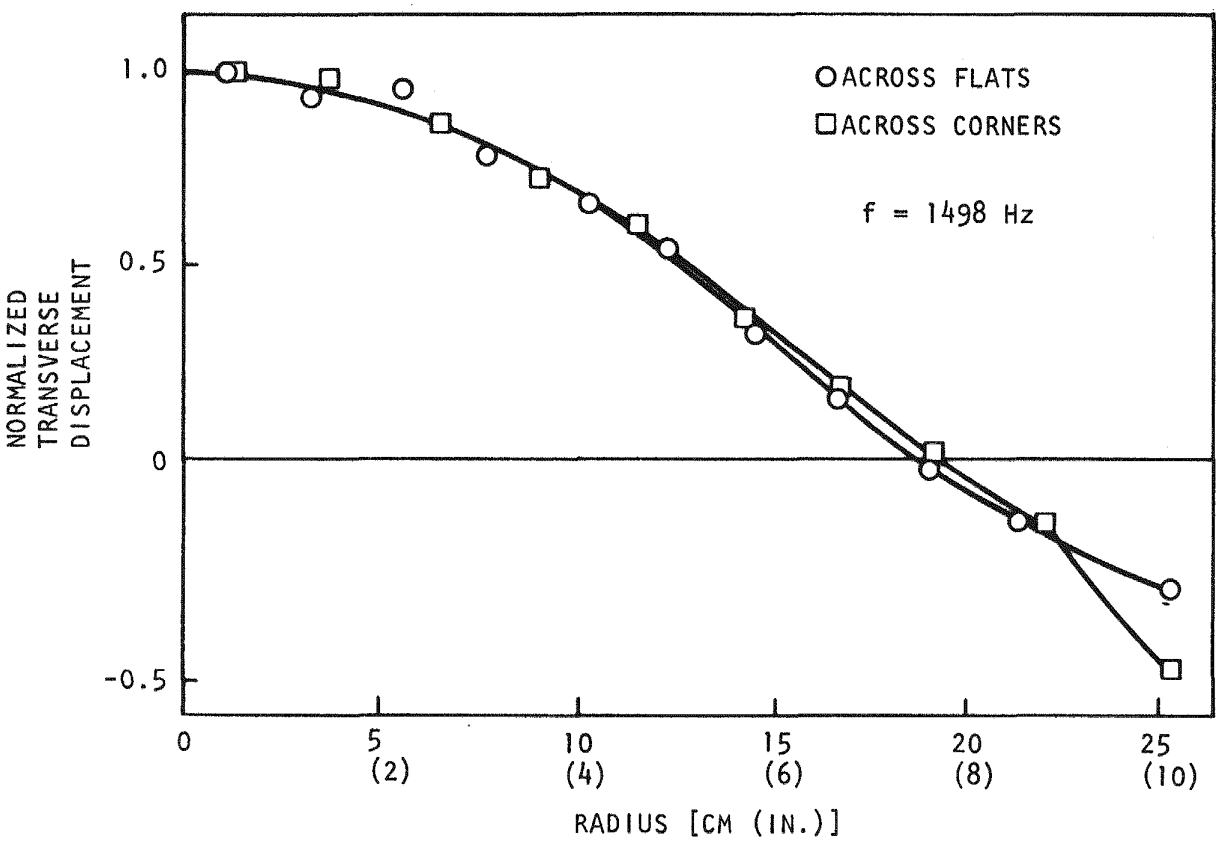

Fig. 11-6. Grid plate mode shape at fundamental frequency

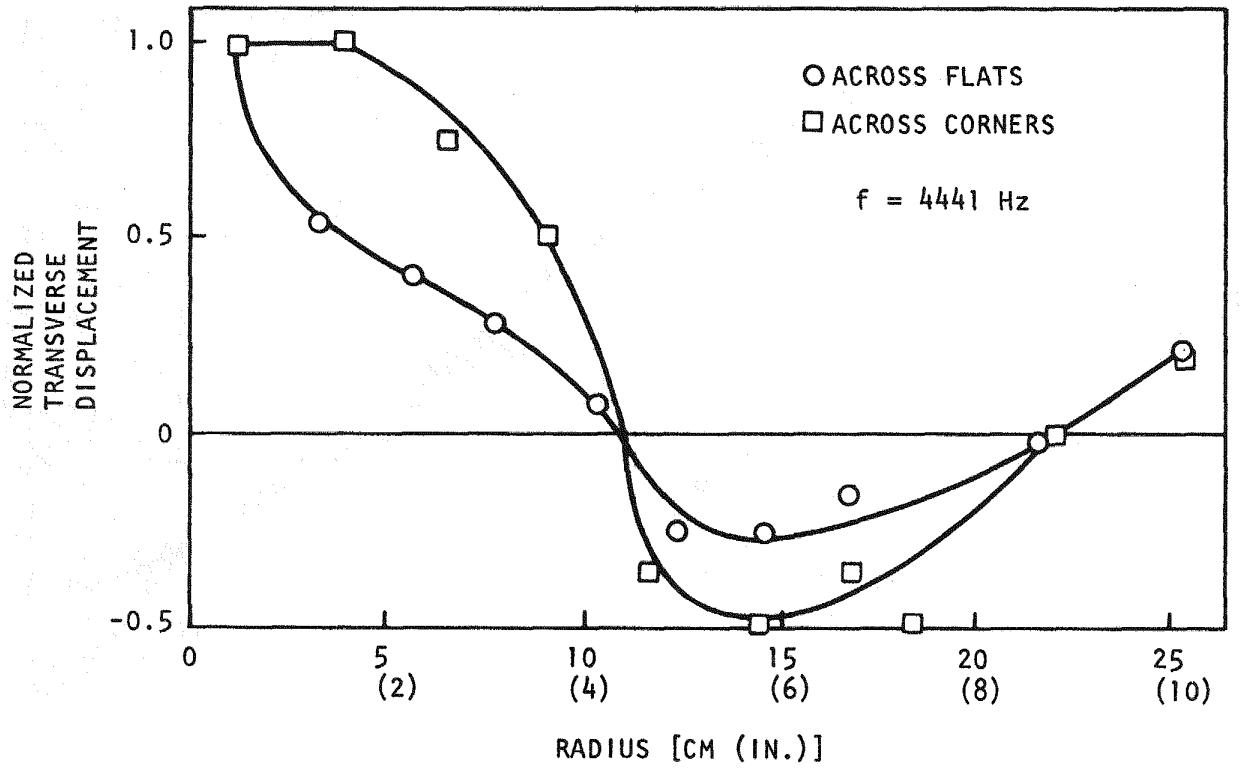

Fig. 11-7. Grid plate mode shape at second bending frequency

The lowest system frequencies for the grid plate - core assembly were also calculated by the analytical technique and the SAPIV finite-element method. For the analytical method, thick plate theory was applied, and a type of shear mode was determined at a frequency of 20.5 Hz; the lowest symmetric mode was found at a frequency of 21.6 Hz. The computer model of the SAPIV code using thin plate theory predicts a frequency of 21.2 Hz (drum mode), which is about 8% lower than the test frequency. However, the SAPIV analysis does not include the fundamental frequency of 21 Hz. The results of the computation are compared with the test data in Table 11-3.

The analytical solution of the combined grid plate - core assembly is discussed in Ref. 11-6, in which Mindlin's theory, including the thickness-shear and flexural effects of a thick plate, is applied.

Figure 11-8 illustrates the different effects on the free vibration of the grid plate - core assembly for the vertical and horizontal vibration modes. For case 1, the plate is considered fixed at radius a (Fig. 11-8) without the ring. The frequency was computed using the general formula (Ref. 11-7) for a thin plate for the lowest axisymmetric (drum mode) and asymmetric modes. The mass of the plate and the core were also determined, but the effect of rotary inertia was not obtained. The effect of rotary inertia was added to the computation for case 2, and for case 3, the terms of transverse shear were added. In case 3, the frequency of the transverse shear mode (asymmetric mode) becomes the lowest value in comparison with that of the drum mode (axisymmetric mode). For case 4, the simply supported ring was added to the perforated plate; for case 5, the rigidity of the core assemblies was replaced by the elastic properties, and the system frequencies were reduced to their fixed values. Thus, Fig. 11-8 illustrates that the effect of rotary inertia of the core was the greatest reducing factor on system frequencies when the frequencies were calculated based on the customary plate formula. The effects of transverse shear, flexibility of the core assemblies, and the ring further significantly reduce the system frequencies; none of these effects can be ignored when trying to obtain values comparable to those of the test data.

TABLE 11-3
FREQUENCIES OF GRID PLATE CORE ASSEMBLIES

Test (Hz)	SAPIV (Hz)[a]	Analytical (Hz)
21	---	20.5 (2%)[a]
23	21.2 (8%)	21.6 (6%)

[a]Number in parentheses is difference in percentage (comparison with test).

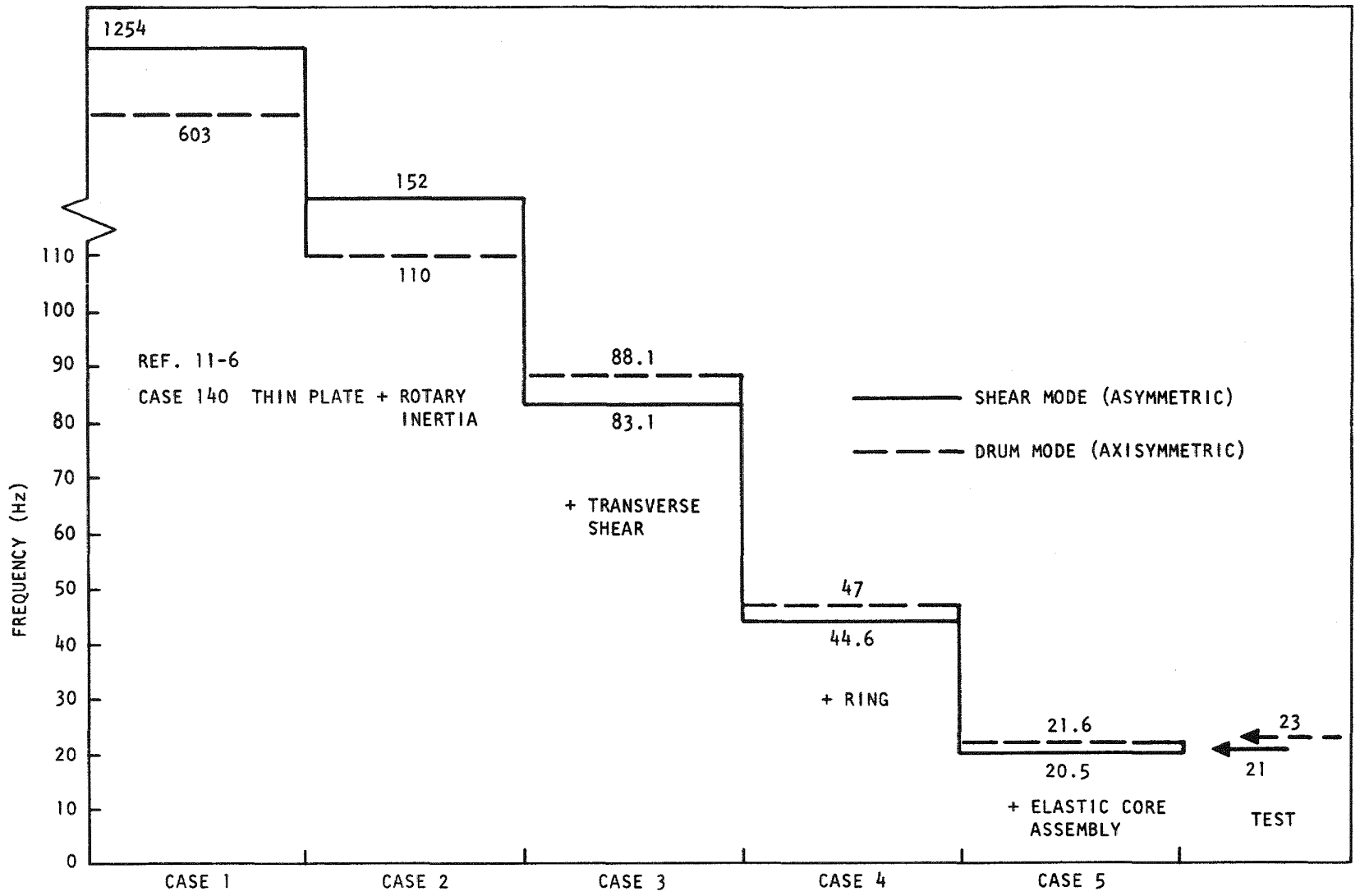

Fig. 11-8. Effects on the frequency of the grid plate - core assembly

11.3. FLOW AND ACOUSTIC VIBRATIONS

Flow-induced and acoustically induced vibrations are important dynamic loads for reactor components during plant operation. In order to ensure unimpaired operation of at least those structures, systems, and components whose structural integrity in service is essential for safe reactor operation and shutdown, a study has been initiated to determine the expected vibration loads in the GCFR system. The objective of this study is to confirm the adequacy of GCFR reactor internal components for flow-induced and acoustically induced vibrations.

During this quarter, efforts were devoted to an investigation of flow-induced and acoustically induced vibrations during the operation of gas-cooled reactors and to the formulation of design criteria for the GCFR thermal barrier cover plates.

A summary report (Ref. 11-8) presents an overview of the vibration problem encountered in the past with CO_2-cooled reactors. No such problems have been reported so far for helium-cooled reactors. This study indicated that the failures of the components were to a large extent due to poor knowledge of the environment in which they had to work. The environmental parameters of temperature, gas flow, noise, etc., proved to be more destructive than anticipated. The problems could be solved, however, although sometimes at high costs.

This report also assesses the significance of solving these problems for GCFR design and development. It was concluded that it would be prudent to evaluate the potential of the GCFR system for flow-induced and acoustically induced vibration phenomena and to develop conservative design criteria.

The following design criterion has been proposed for the PCRV thermal barrier cover plates: the design shall be capable of withstanding an acoustic environment with the characteristics listed below.

Center Frequency f (Hz)	Band Width Δf (Hz)	Space-Time Root Mean Square Pressure p (Pa)
5 to 500	5	224
500 to 5,000	0.01f	$10f^{1/2}$
5,000 to 15,000	0.01f	707

Figure 11-9 shows these maximum design loads in 1/10 octave bands.

REFERENCES

11-1. Penzes, L. E., "Core Support Structural Dynamic Model Test," General Atomic, to be published.

11-2. Gas-Cooled Fast Breeder Reactor Quarterly Progress Report for the Period August 1, 1976 Through October 31, 1976, ERDA Report GA-A14112, General Atomic, November 1976.

11-3. Timoshenko, S., and D. H. Young, Vibration Problems in Engineering, 3rd ed., Van Nostrand, New York, 1954.

11-4. Bathe, K., E. L. Wilson, and F. E. Peterson, "SAPIV, A Structural Analysis Program for Static and Dynamic Response of Linear Systems," University of California, Berkeley, Report EERC73-11, June 1973.

11-5. Mindlin, R. D., and H. Deresiewicz, "Thickness-Shear and Flexural Vibration of a Circular Disk," J. Appl. Phys. 25, 1329-1332 (1954).

11-6. Penzes, L. E., "Seismic Model of the Core Support Structure for the Gas-Cooled Fast Breeder Reactor," ERDA Report GA-A13542, General Atomic, September 12, 1975.

11-7. Szilard, R., Theory and Analysis of Plates, Prentice-Hall, Englewood Cliffs, New Jersey, 1974.

11-8. Halvers, L. J., "Flow-Induced and Acoustically Induced Vibration Experience in Operating Gas-Cooled Reactors," General Atomic, to be published.

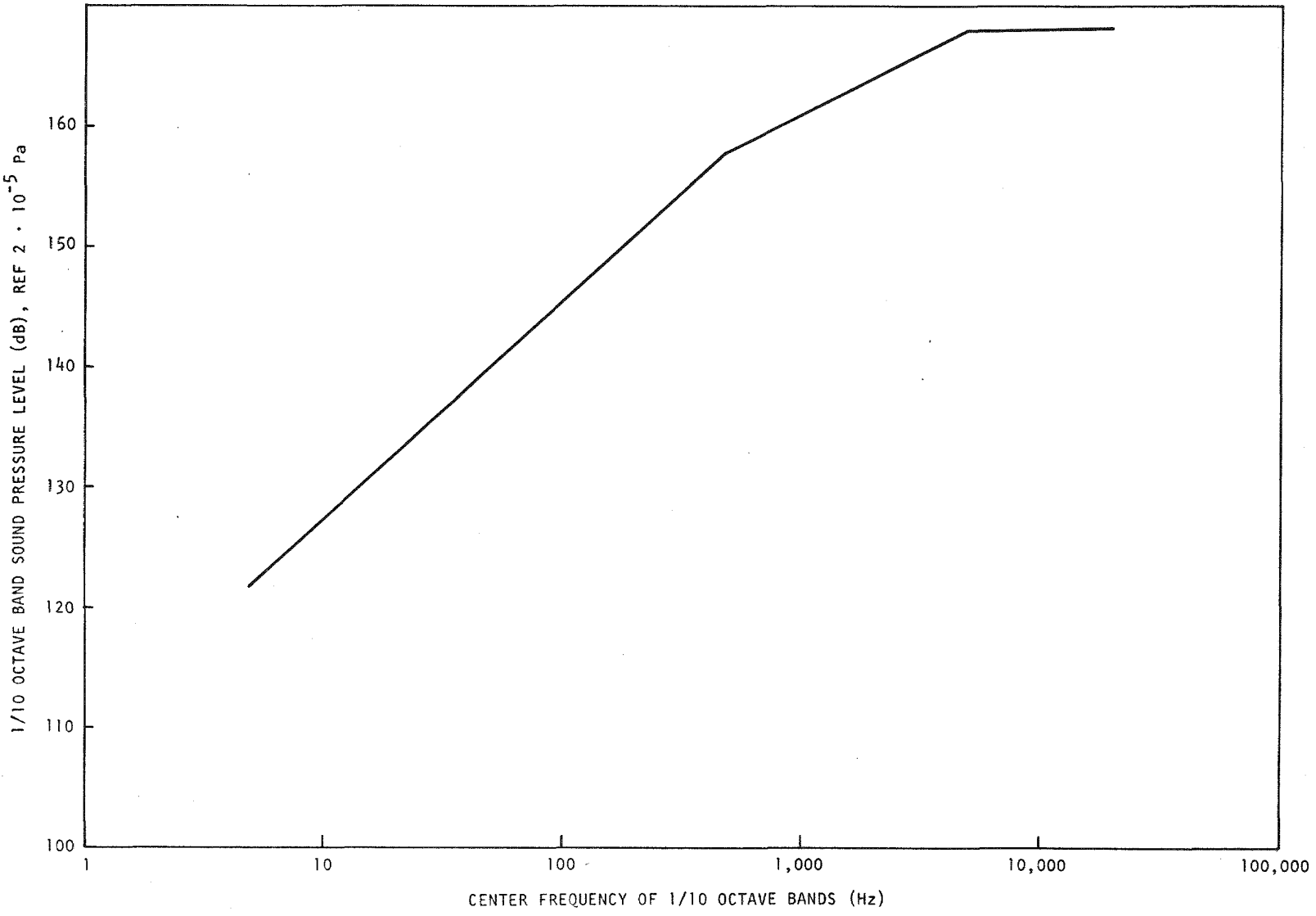

Fig. 11-9. Proposed maximum allowable 1/10 octave band acoustic design loads

12. REACTOR SAFETY, ENVIRONMENT, AND RISK ANALYSIS (189a No. 00589)

The purpose of this task is to investigate the safety characteristics of the GCFR. A liaison and coordination subtask integrates the ERDA-sponsored GCFR safety work at GA and the national laboratories into a national GCFR safety program which is responsive to the need for GCFR safety research. Safety research at GA includes probabilistic accident analysis, accident consequence analysis, radiological and environmental analyses, and postaccident fuel containment (PAFC) analyses.

Logical probabilistic methods are employed to determine the probabilities associated with various accident initiation and progression sequences and to identify potential design modifications which would help reduce risks. The thermal behavior of the fuel assembly duct walls under conditions of loss of shutdown heat removal is being analyzed to determine the time of duct wall melting relative to fuel melting, because duct wall melting has been identified as an important phenomenon influencing the accident sequence. PAFC analyses are being performed to assess the capability of the current design and to identify potential modifications which could improve the molten fuel containment capability. A new analytical program has been initiated during this quarter to analyze the behavior of fuel aerosols in the PCRV and the containment. The initial objective is to define the level of detail which is required or desirable for analysis aerosol behavior following low-probability accidents leading to core damage.

12.1. REACTOR SAFETY PROGRAM COORDINATION

Coordination of the safety analysis programs at GA, ANL, and EG&G, Idaho, was continued and provides the means by which a cooperative safety

analysis effort which serves GCFR program needs is maintained. A report on core disruptive accidents (Ref. 12-1) which documents the first two years of GCFR accident analysis work at ANL was received and is being reviewed.

A new subtask was initiated during this quarter in response to an ERDA request to investigate analytical methods for predicting the reliability of new components and/or systems. The purpose of this subtask is to determine if such procedures can reduce the uncertainty that nonconventional components will meet assigned reliability targets. The approach proposed by GA was reviewed and agreed upon at a meeting at ERDA headquarters on November 17, 1976. GA proposed to develop the necessary methodology and apply it to a trial component over a 2-yr period. This effort will be the basis for an in-depth evaluation of the usefulness of statistical design methods in the GCFR program.

The GCFR reliability analysis task at EG&G was reviewed with the aim of identifying areas in the GCFR reliability analysis program in which EG&G could participate. It was agreed that EG&G would review past and current engineering reliability programs to establish the current state of the art and to develop recommendations for a GCFR engineering reliability effort. In addition, work areas have been identified for the expanded FY-78 effort.

12.2. PROBABILISTIC ACCIDENT AND RISK ANALYSES

12.2.1. Introduction

Accident initiation and progression analysis (AIPA) techniques developed in FY-74 (Ref. 12-2) are being applied to the probabilistic analysis of potential accident sequences leading to low-probability, high-consequence outcomes. The consequences of these sequences are also under study at ANL and at GA under other subtasks. The objective of this work is to assess the risks of these accident chains in the GCFR.

During FY-77, the analysis effort is concentrating on two areas which have been shown by previous work to be significant in affecting GCFR risks.

The first area involves the development of a more detailed probabilistic analysis of GCFR residual heat removal (RHR) systems. The second area involves the development and assessment of containment event trees for the GCFR.

12.2.2. Residual Heat Removal Reliability Analysis

During FY-77, a more detailed probabilistic analysis of GCFR RHR systems is being performed to further identify the level of achievement of the current design and to consider potential design improvements. Forced-convection shutdown cooling is achieved in the GCFR by using two separate RHR systems, each of which has multiple loops for redundancy. The normal operational RHR system utilizes steam-driven main circulators, main cooling loops, and portions of the normal steam power conversion system components. A diverse backup safety RHR system is provided by the CACS which utilizes electric-motor-driven circulators and pressurized water loops which exhaust heat to the atmosphere. Electrical power for the continued operation of these RHR systems is provided from either off-site or redundant on-site emergency diesel supplies. Reliability models are being developed to qualitatively represent and quantify GCFR main loop, CACS, and electrical power system operation as necessary to provide RHR.

Three key initiating events have been considered to enable a greater level of detail to be achieved in the RHR analysis effort. These events, their anticipated frequencies of occurrence, and the rationale for their selection are shown in Table 12-1. The selection of these particular events as significant (with regard to the likelihood of RHR failure and the potential consequences of such failure) was aided by previous less detailed studies of the RHR systems (Ref. 12-3).

Because of the number of main loop cooling subsystems required to perform at different times following shutdown, main loop cooling system reliability modeling task has been broken into three distinct phases of operation, as depicted in Figs. 12-1 through 12-3. The first phase of main loop cooling, illustrated in Fig. 12-1, employs the three main

TABLE 12-1
INITIATING EVENTS SELECTED FOR RHR RELIABILITY ASSESSMENT

Initiating Event	Anticipated Frequency	Rationale for Selection
Transient (includes loss of off-site power, condenser vacuum, etc.)	10/yr	High frequency of residual heat removal demand; shown to be significant in previous work (Ref. 12-3)
Depressurization ($\leq$30 cm^2)	10^{-3}/yr	Relatively high frequency of long-term residual heat removal demands from a depressurized reactor; shown to be more significant than DBDA in previous work (Ref. 12-3)
Earthquake ($\geq$design basis earthquake)	10^{-5}/yr	Potential for common mode failure of RHR systems; not analyzed in depth in previous work (Ref. 12-3)

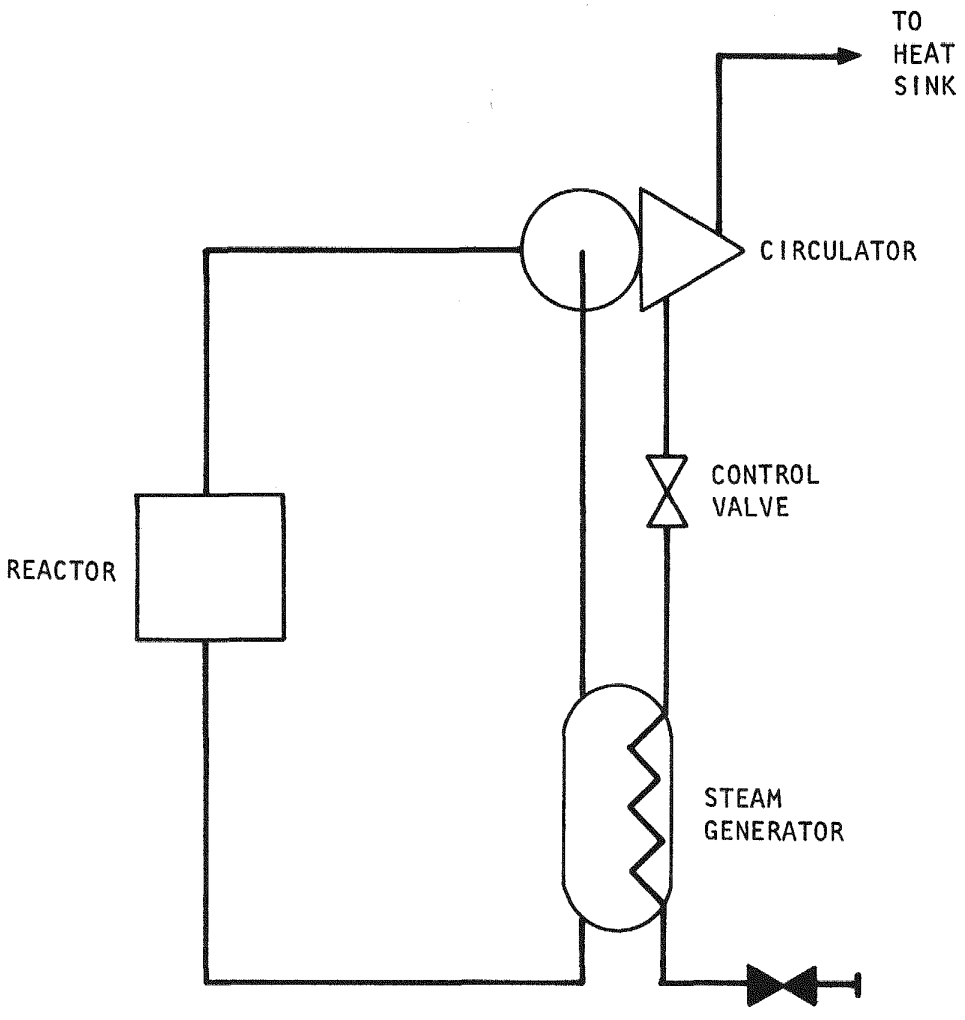

Fig. 12-1. Main loop residual heat removal, phase 1

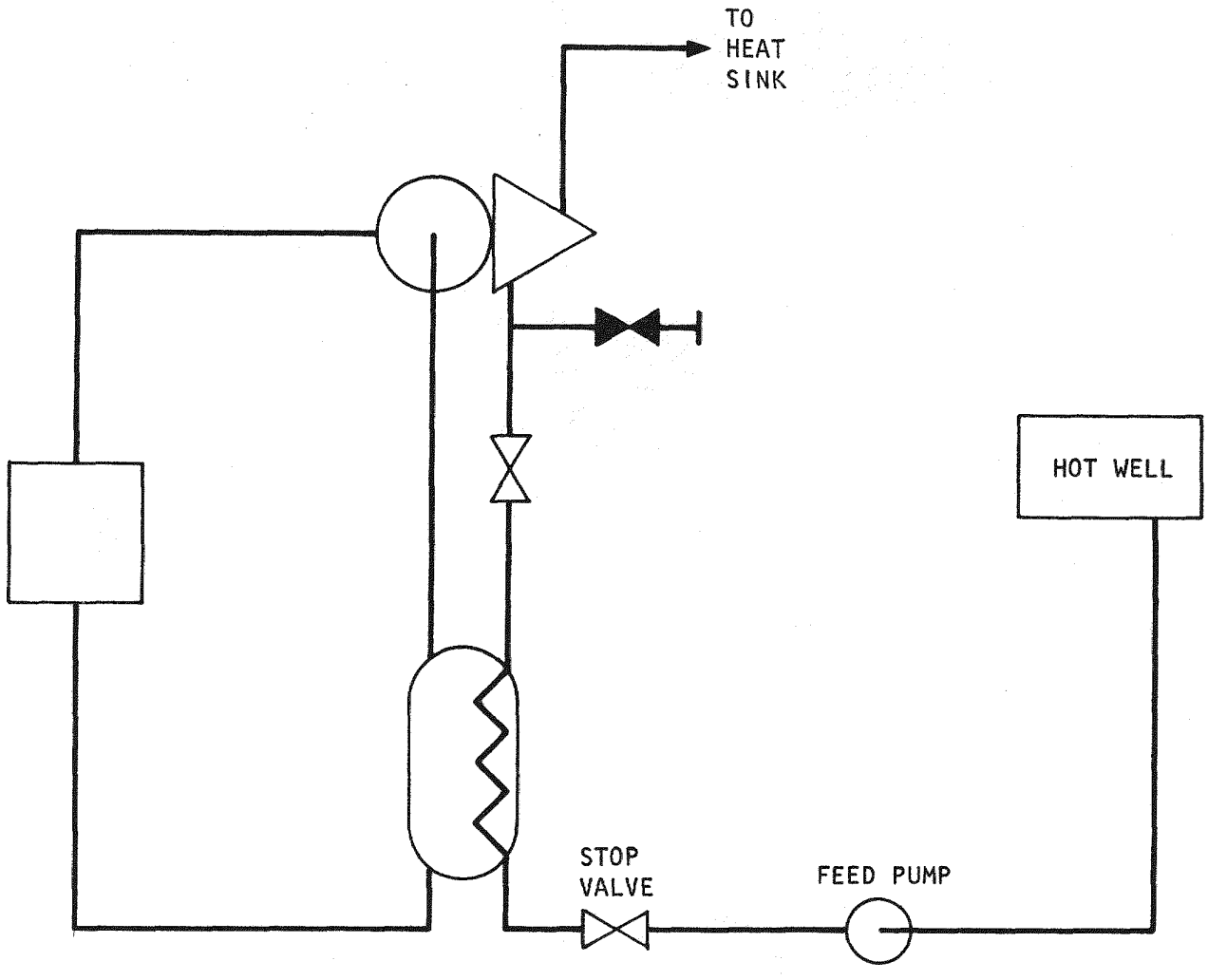

Fig. 12-2. Main loop residual heat removal, phase 2

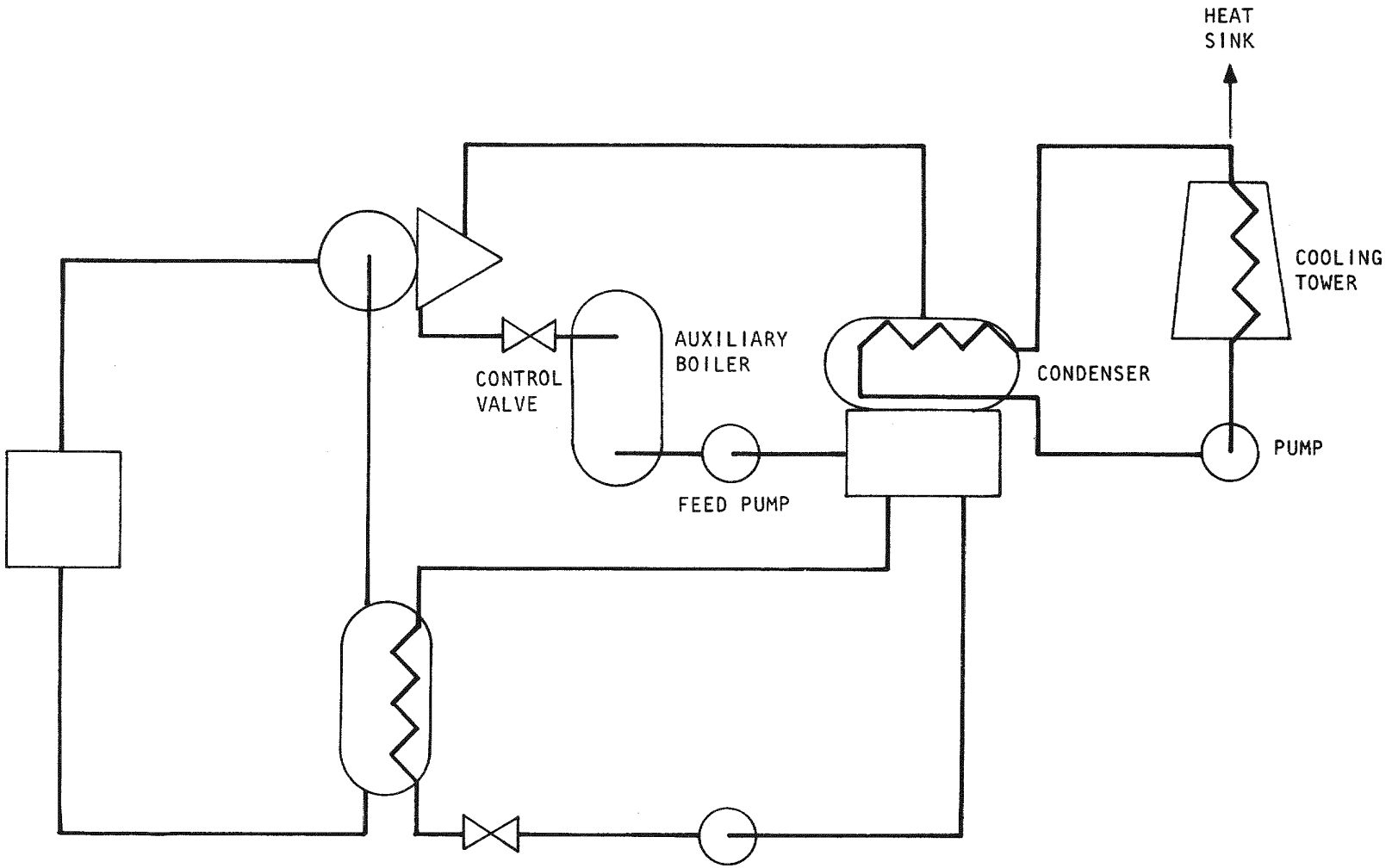

Fig. 12-3. Main loop residual heat removal, phase 3

helium circulating loops, with reactor residual heat providing the necessary circulator drive steam from the steam generators. Heat removal to the environment is accomplished by the steam generators using either normal power conversion system components or direct relief to the atmosphere. Cooling in this phase requires no on- or off-site ac power and can continue for more than 15 min (limited by steam generator inventory) using only safety class, Seismic Category I components.

The second phase of cooling, illustrated in Fig. 12-2, is an extension of phase 1 with the addition of a shutdown feedwater supply to maintain steam generator inventory. Electrical power (ac) is required to drive the shutdown feed pumps, and cooling can be maintained for 1 hr or more.

Phase 3, illustrated in Fig. 12-3, employs auxiliary boilers to provide circulator drive steam, with (1) the steam generators continuing to serve as heat dumps and (2) heat rejection by direct relief to the atmosphere for a limited time or through normal power conversion system components (condenser, circulating water system, etc.) for longer time periods.

During this quarter, qualitative reliability models representing the three phases of main loop cooling were completed. A failure mode and effects analysis of this system which considers the impact of single failures as well as common mode failures has also been completed. Data being identified under the data bank task (Section 15) will be employed to quantify this model during the next quarter.

12.2.3. Containment Event Tree Analysis

During FY-77, the accident sequence analysis work performed in previous years (Ref. 12-3) is being supplemented by the probabilistic analysis of sequences leading from a loss of coolable core geometry through containment release to the public.

During this quarter, the effects of various containment activity removal mechanisms (radioactive decay, gravity settling, containment cleanup system, etc.) on accident consequences were examined as a function of time of containment failure. The containment failure modes examined were melt-through, isolation failure, and shell rupture. The assumed radiological source term in the containment was based upon the WASH-1400 (Ref. 12-4) release fractions as applied to the 300-MW(e) GCFR demonstration plant core radionuclide inventories. Other WASH-1400 assumptions were used where applicable. The TDAC (Ref. 12-5) computer code was used for off-site dose calculations.

Table 12-2 gives the results of this parametric study by ranking the various containment failure modes in order of decreasing consequences. These consequences are normalized to the consequences resulting from the unfailed containment. The range of consequences is significant, covering approximately four and one-half orders of magnitude. The study has shown that with the containment cleanup system operating, even a small delay in the time of containment failure (i.e., failure delayed by more than 5 hr) significantly reduces the potential off-site dose consequences. Similarly, if containment shell failure can be avoided, the consequences are significantly reduced.

The results of the parametric study described above will serve to define the time intervals of interest for the probability determinations to be made in the next quarter. With relative probabilities of failure assigned to the failure modes described above, a comparison of relative risk can be made using the relative consequences given in Table 12-2.

12.3. ACCIDENT CONSEQUENCE ANALYSIS

12.3.1. Introduction

The consequences of low-probability accident sequences leading to core damage are investigated under this subtask to determine the expected behavior of the GCFR core and the performance of its activity barriers in

TABLE 12-2
CONTAINMENT FAILURE MODE RANKED BY CONSEQUENCE

	Failure Mode	Relative Consequence[a]
1.	Isolation failure without CCS[b]	30,000
2.	Rupture without CCS at $t < 10$ hr	$10{,}000 \leq C \leq 30{,}000$
3.	Isolation failure with CCS	10,000
4.	Rupture without CCS at $10 \leq t \leq 20$ hr	$3{,}000 \leq C \leq 10{,}000$
5a.	Rupture without CCS at $t > 20$ hr	$1{,}000 \leq C \leq 3{,}000$
5b.	Rupture with CCS at $t < 2$ hr	$1{,}000 \leq C \leq 3{,}000$
6.	Rupture with CCS at $2 < t < 3$ hr	$300 \leq C \leq 1{,}000$
7a.	Rupture with CCS at $3 < t < 5$ hr	$100 \leq C \leq 300$
7b.	Any melt-through at $t < 5$ hr	$100 \leq C \leq 300$
8a.	Any melt-through at $t > 5$ hr	$1 \leq C \leq 100$
8b.	Rupture with CCS at $t > 5$ hr	$1 \leq C \leq 100$
9.	Leakage only	1

[a] Normalized to consequences resulting from an unfailed containment with its design leakage rate.

[b] CCS = containment cleanup system operating.

mitigating the potential release of activity from the containment. During FY-76, analyses were performed to determine the assembly duct wall heat-up and melting sequence relative to fuel heat-up during a loss of decay heat removal accident. At present, analyses of thermal bowing of declad fuel rods and the effect of bowing on heat transfer to the duct wall and induced stress distributions are being performed. In addition, a study of reactivity insertion limits has been made to determine the magnitude and rate of reactivity insertion which leads to incipient fuel melting in the GCFR demonstration plant. A new analysis effort to determine the behavior of aerosols potentially generated during core disruptive accidents has been initiated.

12.3.2. Loss of Decay Heat Removal Accident Analysis

12.3.2.1. Introduction. Analysis to determine fuel rod bowing during a loss of decay heat removal accident has been continued. It was shown in previous analyses (Ref. 12-6) that rod-to-rod interference can occur following cladding melting during a loss of decay heat removal accident. Physical interference between two rods was indicated wherever their deflection shapes overlapped. Rod-to-rod interference introduces interactive contact forces to make the deflections physically compatible (i.e., without overlap) and induce additional stresses. Analyses of deflections not restrained by neighboring rods for the fixed-pinned boundary condition and deflections restrained by the duct wall or the unfueled corner rod at the free end but not by neighboring rods for the fixed-free boundary condition have been the starting point for subsequent analysis of rod-to-rod interference.

12.3.2.2. Conditions and Assumptions. The physically compatible deflection shapes of the fuel rods subject to (1) transverse and axial temperature distribution, (2) net interactive point contact forces near the core midplane or at the top of the core induced as a result of rod-to-rod interference, and (3) reactive forces at the free ends of the fuel rods resulting from deflection restraint induced by the duct wall or the unfueled corner support rod have been analyzed for rods located along a traverse to the duct midflat at the

time of 50% heat of fusion at the duct midflat and along a traverse to the duct corner at the time of 50% heat of fusion of the duct corner. These traverses are shown in Fig. 12-4.

The assumptions for the previous analyses (Ref. 12-6) are also valid for the current analysis. The cladding and grid spacers have melted over the core length such that the fuel rods are laterally unsupported over the core length. The assumptions are summarized as follows:

1. The fuel pellets fuse together and form a single rod.

2. The lateral transverse stresses in cross section planes are neglected.

3. The temperature T of the declad fuel rod is a linear function of the transverse coordinate y and a chopped cosine function of the axial coordinate z.

4. The axial thermal expansion is unrestrained owing to concurrent expansion of the duct.

5. Material properties such as modulus of elasticity and coefficient of expansion of the fuel are independent of temperature and are evaluated at the volumetric average temperature of the rod.

6. The interactive contact forces are assumed to be point contact.

12.3.2.3. Discussion of Results. Since rod-to-rod interference occurs solely in the cases of fixed-pinned and fixed-free end supports, only these cases have been considered. The lower end of the fuel rods is modeled as a fixed connection because refrozen cladding is assumed to prevent rotation. At the upper end, the boundary condition depends on the strength of pellet bonding at the cool inlet region and the stiffness of the remaining cladding in the upper axial blanket region.

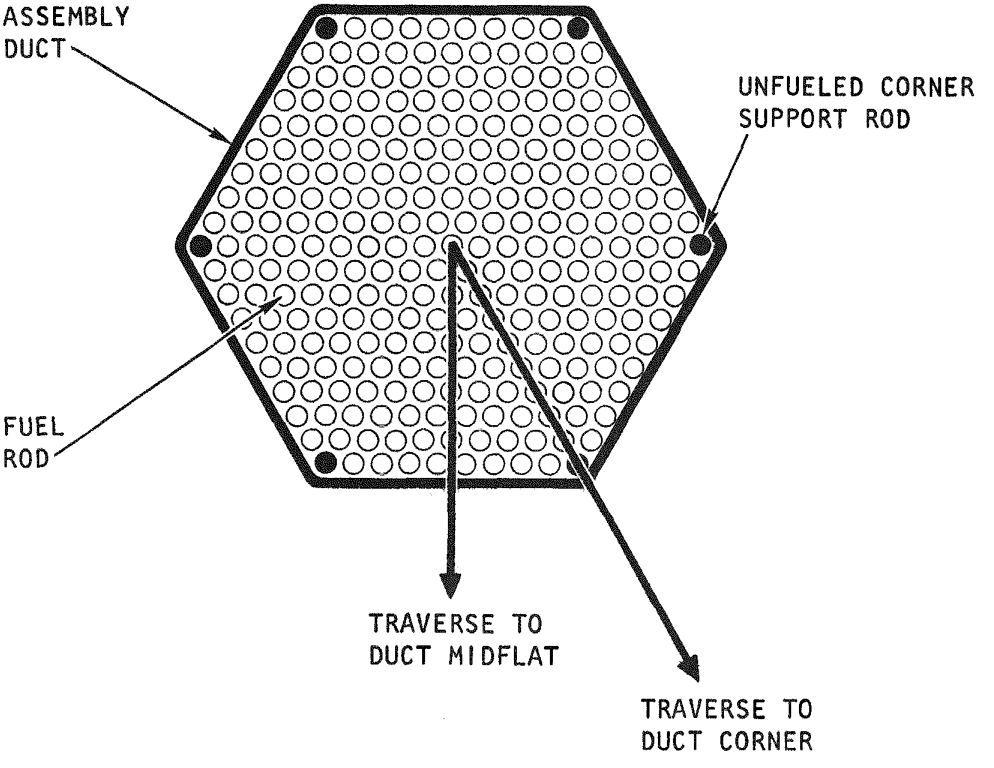

Fig. 12-4. Fuel assembly cross section

Analysis of physically compatible deflection (i.e., with no overlap) which takes into account interference between rods has been completed for all the cases shown in Figs. 12-5 through 12-11. As expected, a general "tightening up" of the rod bundle over a significant fraction of the core is observed. The final deflection shapes of the fuel rods are significantly influenced by choice of upper boundary condition, number of rows of rods which interfere, rod-to-rod spacing, and stiffness of individual rods under the temperature conditions in question. The final deflection of each rod has been determined by superposing the unrestrained thermal deflection of the rod on the deflections of that rod due to (1) net interactive point contact force acting near the core midplane or at the top of the core induced as a result of rod-to-rod interference and (2) reactive force at the free end of the fuel rod resulting from deflection restraint induced by the duct wall or the unfueled corner support rod. The distance S between rods is equal to the minimum allowable deflection without interference; the distance C is the clearance between the duct wall and the adjacent fuel rod or the clearance between the unfueled corner support rod and the adjacent fuel rod, depending upon the rod traverse in question. Since all rods deflect toward the assembly center, the gap between the outermost fuel rods and the duct wall is increased while the fuel rod pitch is decreased. The fuel rods are numbered from the duct toward the assembly center.

A weak restraining moment by the unmelted cladding in the upper axial blanket is simulated by a pinned support at the top (i.e., there is no restraining moment for rotation, there is only shear restraint). At the core - lower blanket interface, the fuel rod is modeled as a fixed support because refrozen cladding is assumed to prevent rotation. Figures 12-5 to 12-8 show the physically compatible deflections for this type of end support. The final deflection patterns are similar for the high- and low-ΔP core designs. Between four and six rods interfere in all cases. The exact number of rods which interfere in each case is determined by a process of eliminating the coupled equations which characterize the deflection with respect to a common reference line at the point of contact of the fuel rods and the interactive point contact forces induced near

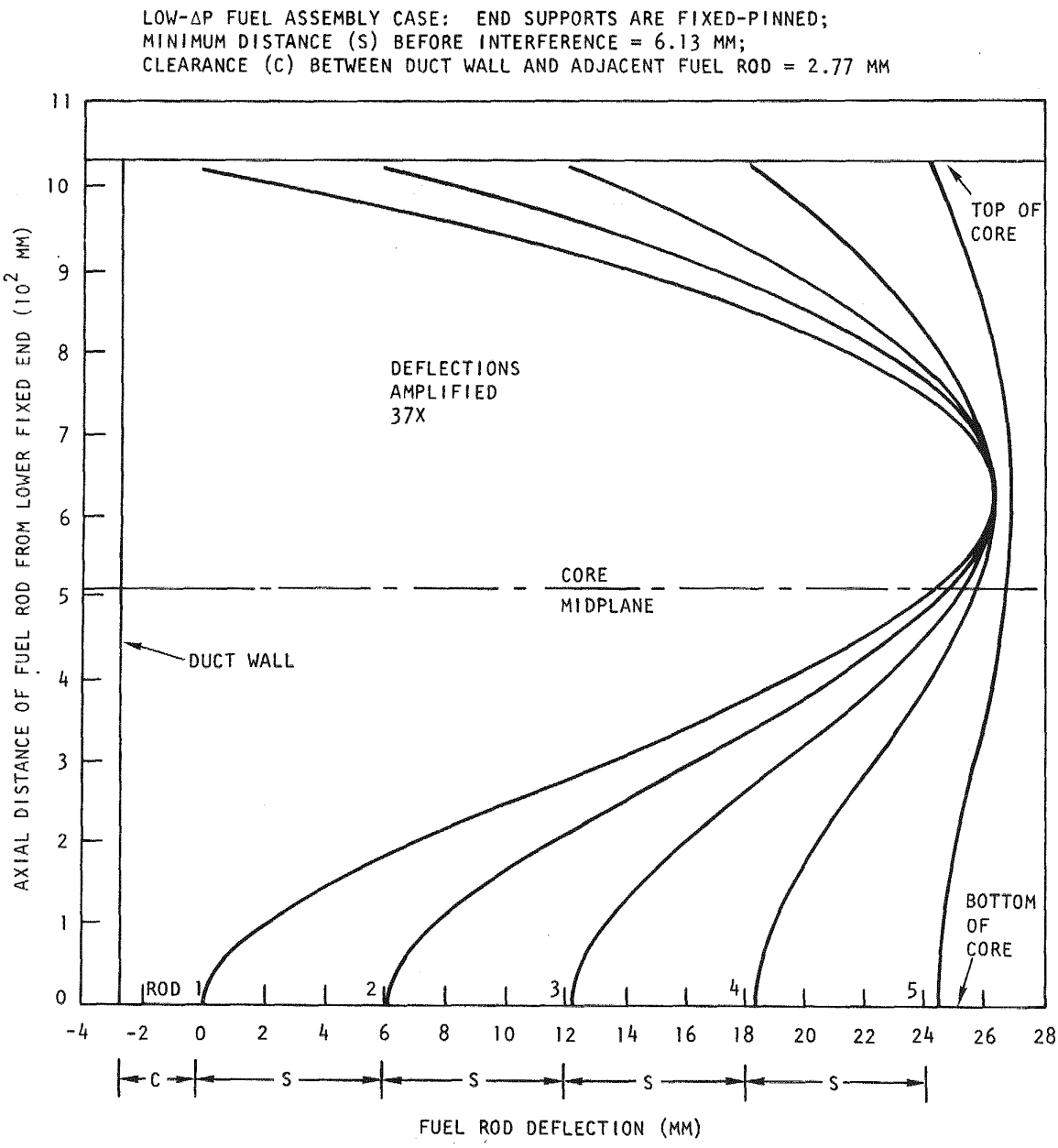

Fig. 12-5. Thermal deflection with respect to the centerline of the fuel rod along a traverse to the midflat at the time of 50% heat of fusion at the duct midflat

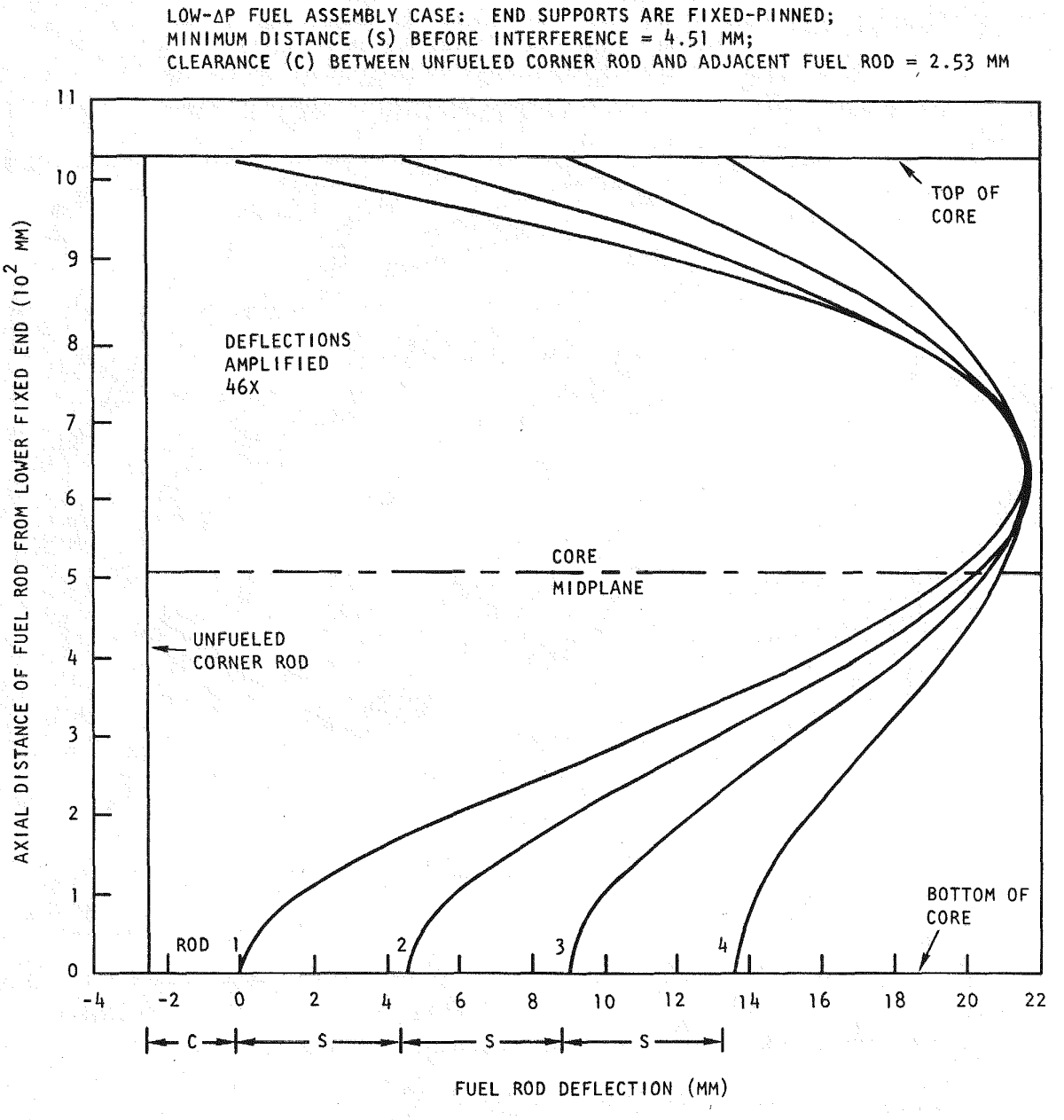

Fig. 12-6. Thermal deflection with respect to the centerline of the fuel rod along a traverse to the duct corner at the time of 50% heat of fusion at the duct corner with the unfueled corner rod melted

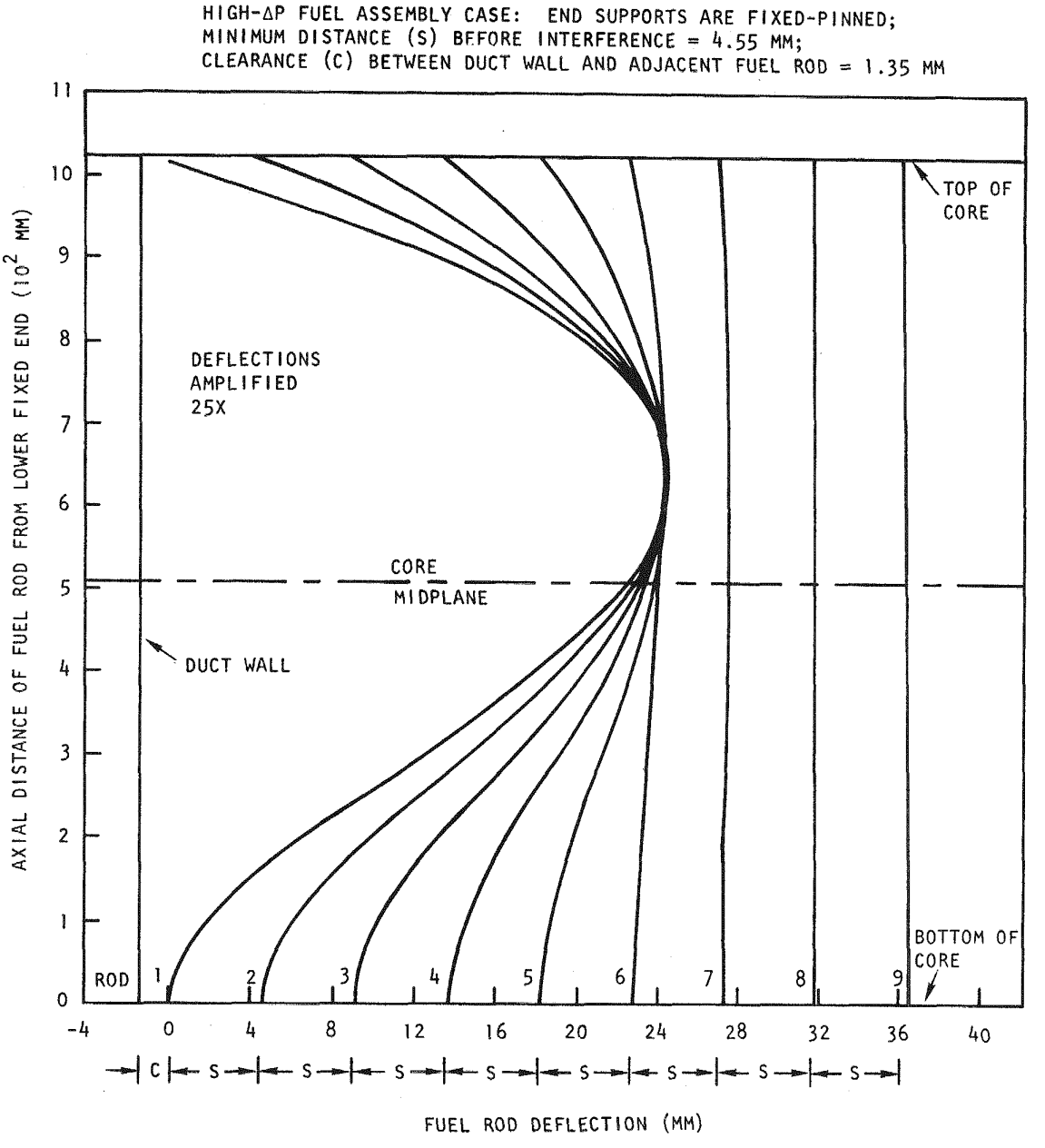

Fig. 12-7. Thermal deflection with respect to the centerline of the fuel rod along a traverse to the midflat at the time of 50% heat of fusion at the duct midflat

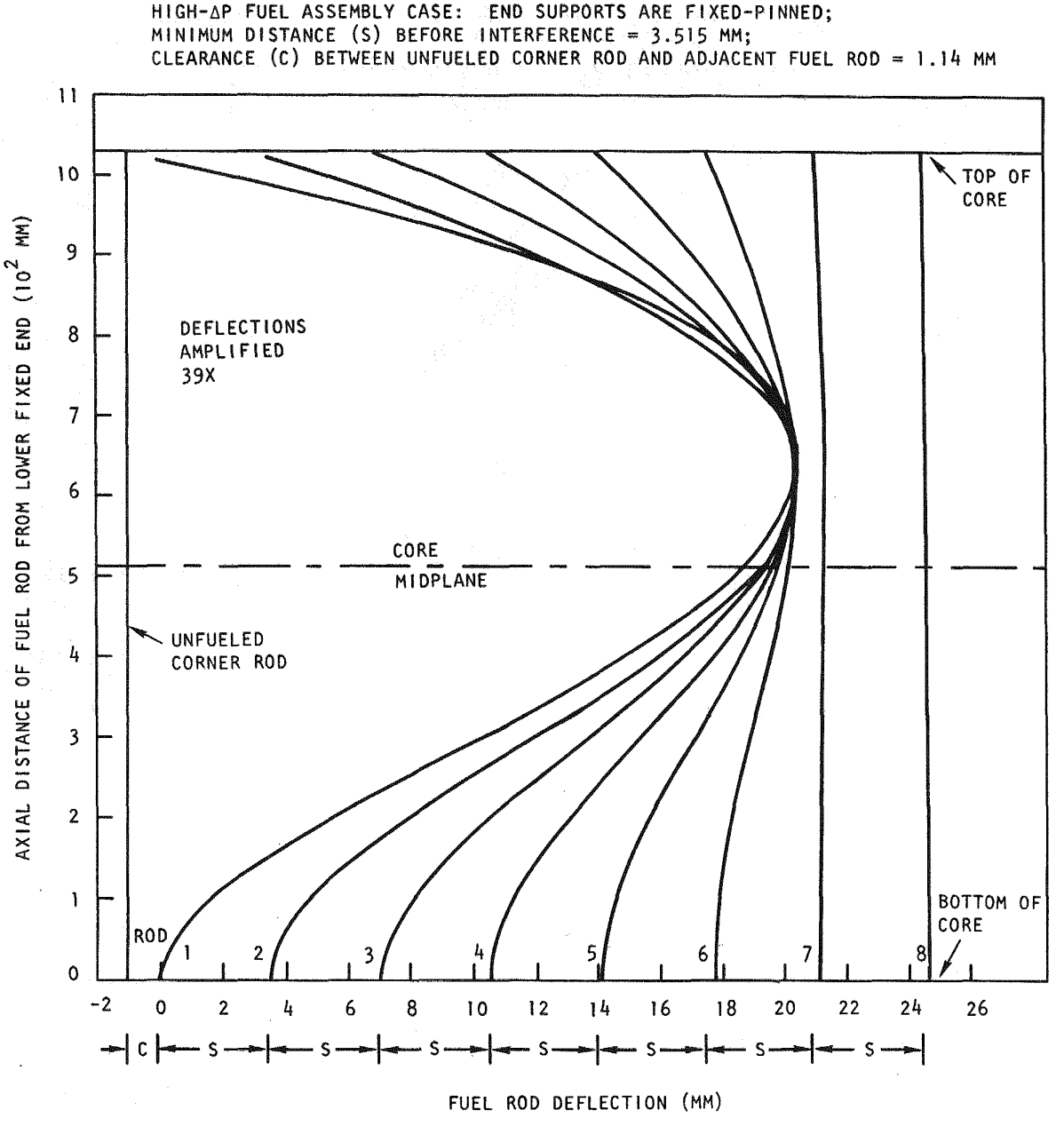

Fig. 12-8. Thermal deflection with respect to the centerline of the fuel rod along a traverse to the duct corner at the time of 50% heat of fusion at the duct corner with the unfueled corner rod melted

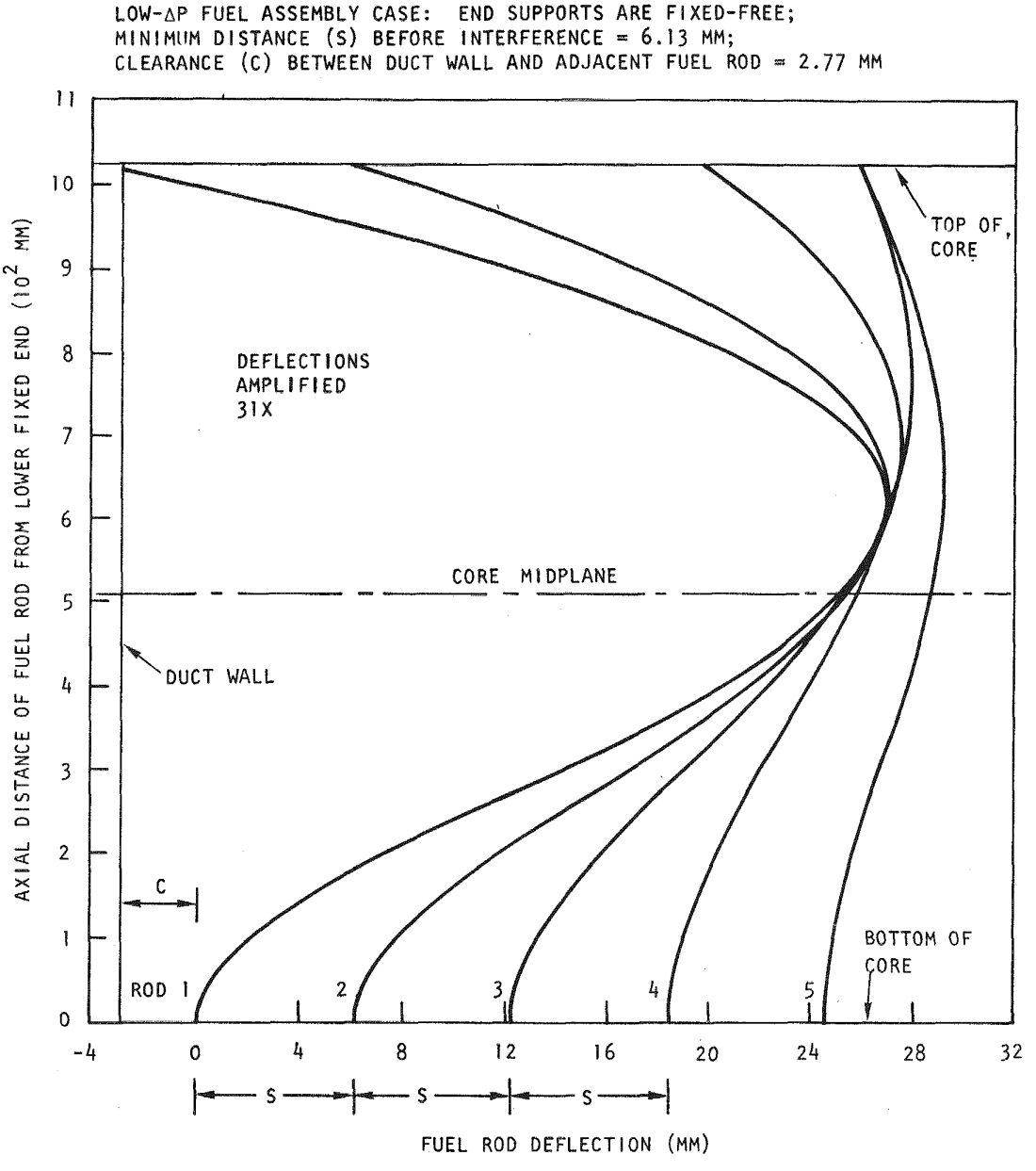

Fig. 12-9. Thermal deflection with respect to the centerline of the fuel rod along a traverse to the midflat at the time of 50% heat of fusion at the duct midflat

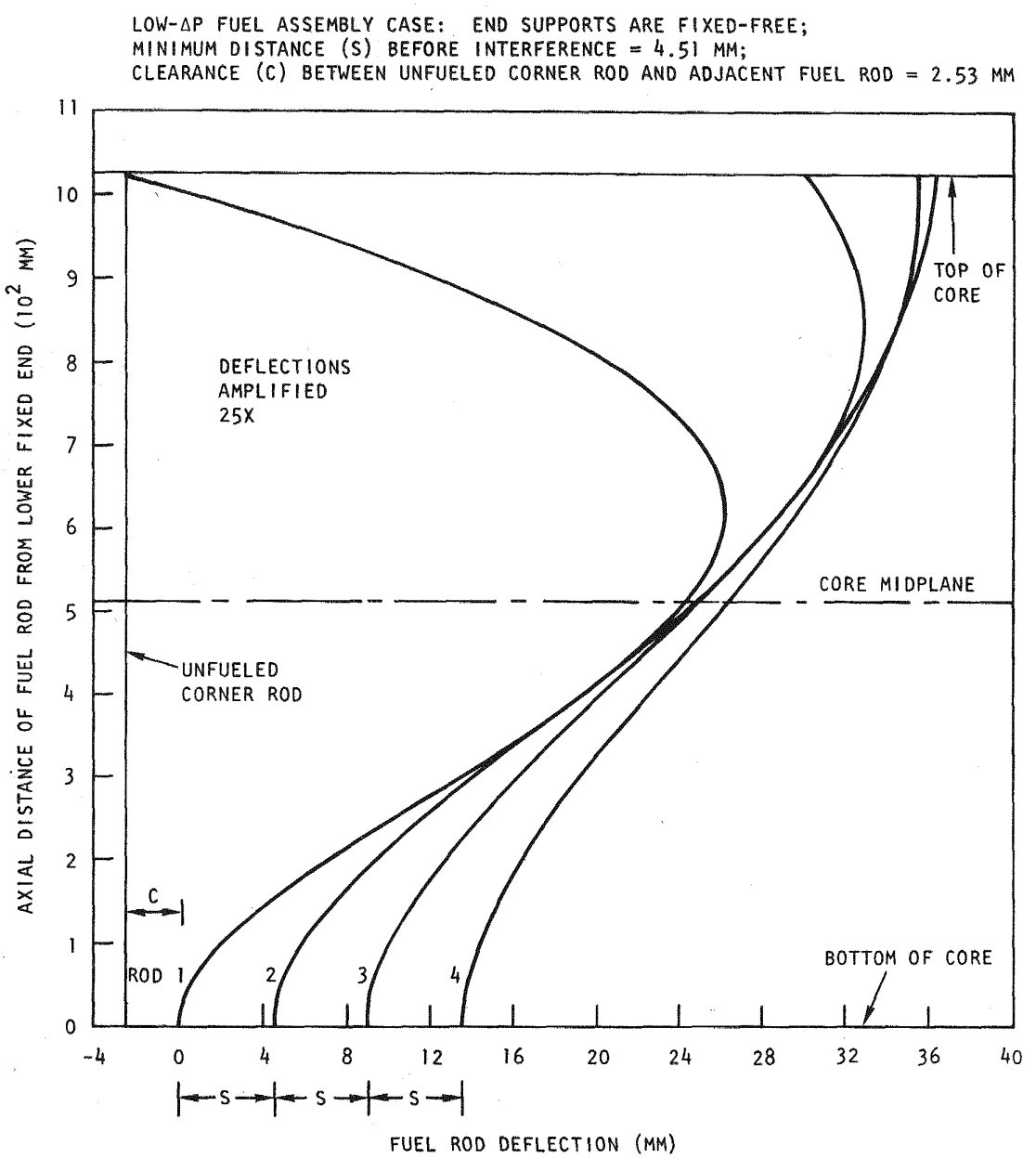

Fig. 12-10. Thermal deflection with respect to the centerline of the fuel rod along a traverse to the duct corner at the time of 50% heat of fusion at the duct corner with the unfueled corner rod melted

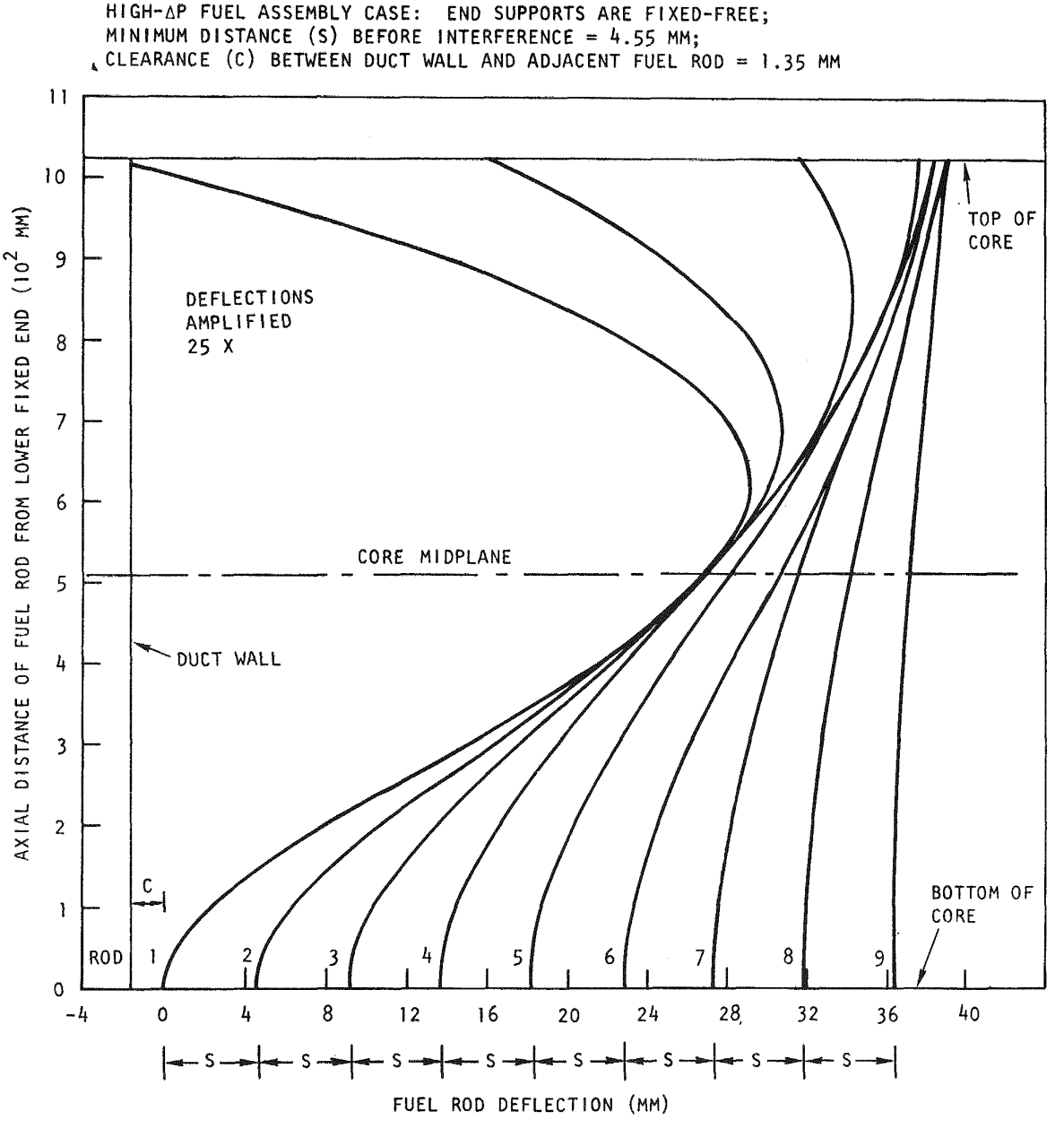

Fig. 12-11. Thermal deflection with respect to the centerline of the fuel rod along a traverse to the midflat at the time of 50% heat of fusion at the duct midflat

the core midplane as a result of interference between rods. The maximum deflections occur in the upper half of the core.

If bonding of fuel pellets is weak near the top of the core, the fuel rods could become detached at the core - upper blanket interface as a result of bowing-induced stresses. Such a condition is simulated by a free upper boundary condition, where neither moment restraint nor shear restraint is present. As described in Ref. 12-6, in this case, the fuel rods will initially tend to bow outward until interference with the duct wall or the unfueled corner support rod occurs. It is assumed that the fuel rods are free to deflect outward toward the duct wall, which prevents further outward deflection and thus forces the rods to deflect inward toward the assembly center. As a result, between four and eight rows of fuel rods, depending upon the rod traverse in question, experience interference over a significant fraction of the core length, thus introducing coupled interference forces in the upper half of the core length. Figures 12-9 through 12-11 show the physically compatible deflections for this fixed-free boundary condition. The high-ΔP core design results in the largest final deflections and the largest number of rods interfering because it combines the largest temperature gradients with the smallest rod-to-rod spacing. The final deflections of the fuel rods for the traverse to the duct midflat and the traverse to the duct corner are very similar.

Previous analyses (Ref. 12-6) revealed that rod-to-rod interference can occur following cladding melting during a loss of decay heat removal accident. The current analysis shows that rod interference leads to reactive contact forces owing to compatibility requirements (i.e., with no overlap), inducing more stresses (in addition to thermal stresses). At the same time, a general tightening up of the rod bundle toward the assembly center occurs primarily near the core midplane. The resulting bending stresses in the fuel rods have already been determined for cases without interference and are being calculated for cases with interference. Out-of-pile direct electric heating experiements at ANL are expected to yield information on the bending strength of bonded fuel pellet stacks.

This information will be vital in determining whether the fuel rods can break following cladding melting during a loss of decay heat removal accident.

Analyses are currently in progress to determine the influence of fuel rod bowing on heat transfer to the duct wall during this accident sequence. The BOXRAD code has been modified to include transient bowing of fuel rods based on (1) the deflection shapes determined in the bowing anlaysis and (2) the computed temperature gradient across the fuel rods. Preliminary results indicate that the influence of fuel rod bowing on the duct melting time is very small. The larger resistance for heat transfer from the outermost row of rods to the duct wall is compensated for by the reduced heat transfer resistance between the deflected rods. Furthermore, the tightening up of the fuel bundle is likely to reduce the duct corner melting delay.

12.3.3. Reactivity Insertion Analysis

The response of the core to generalized, subprompt critical reactivity insertion events was analyzed. The objective of the analysis was to determine the magnitude of reactivity insertion required to cause incipient fuel melting in the event of complete failure of the primary scram system as well as the backup shutdown system. The reactivity margin to fuel melting thus determined is related to the control rod reactivity worth. The independent parameters considered were (positive) reactivity insertion magnitude, reactivity insertion rate, plant protection system (PPS) response, and plant control system (PCS) response.

If the core inlet helium conditions are fixed at their design point values, the core adjusts to a reactivity insertion by an increase in core power. Without the automatic PPS and PCS response, the increased power heats the core until the overall core negative temperature coefficient of reactivity compensates for the original positive reactivity insertion. The peak fuel and/or cladding temperature are solely determined by the reactivity insertion magnitude; e.g., for subprompt critical excursions, the

insertion rate does not alter the monotonic nature of the temperature rise. Therefore, the maximum fuel temperature can be plotted against the insertion magnitude (Fig. 12-12) without consideration of the reactivity insertion rate. Reactivity insertions up to \$0.85, which is the worth of a fully inserted control rod, were considered at insertion rates up to \$8.5/s; i.e., full withdrawal is postulated to occur in 0.1 s. This reactivity insertion rate is 20 times faster than that resulting from ejection of a control rod due to a gross failure of its pressure housing above the PCRV closure plug and is considered a very conservative, nonmechanistic upper limit. Reactivity insertions up to \$0.55 do not lead to expected fuel temperatures in excess of the melting fuel temperature in the maximum-powered fuel rod as long as there is no significant increase in the coolant inlet temperature. Thus, the time available for protective action to mitigate reactivity insertion up to \$0.55 is determined by the helium loop feedback characteristics, which are discussed below.

The PPS automatically acts to limit the effects of reactivity insertions. It was found that each cent of reactivity insertion leads to an eventual steady-state increase in core power of about 1%. Fast insertions can result in very high power spikes which are sufficiently short, so that the engendered fuel temperature rise does not follow the spike, but instead follows a time profile similar to a decaying exponential rise. Even the fast insertions are easily detected by the several PPS flux detectors which initiate a reactor trip on insertions in excess of a few cents. Therefore, melting may be prevented by PPS action. Figure 12-13 shows an important reactivity insertion event characteristic. Successful initiation of either a PPS reactor trip (requiring $\sim$0.5 s for insertion of a fully withdrawn control rod) or a diverse PPS backup shutdown rod insertion (requiring $\sim$9 s for insertion of the fully withdrawn shutdown rods) terminates a subprompt critical reactivity insertion event prior to any reactor fuel reaching its solidus temperature.

Figures 12-12 and 12-13 are based on a fixed core inlet temperature. The core inlet temperatures cannot be held steady for an arbitrarily sized reactivity insertion. Since the NSSS is designed for no more than 107%

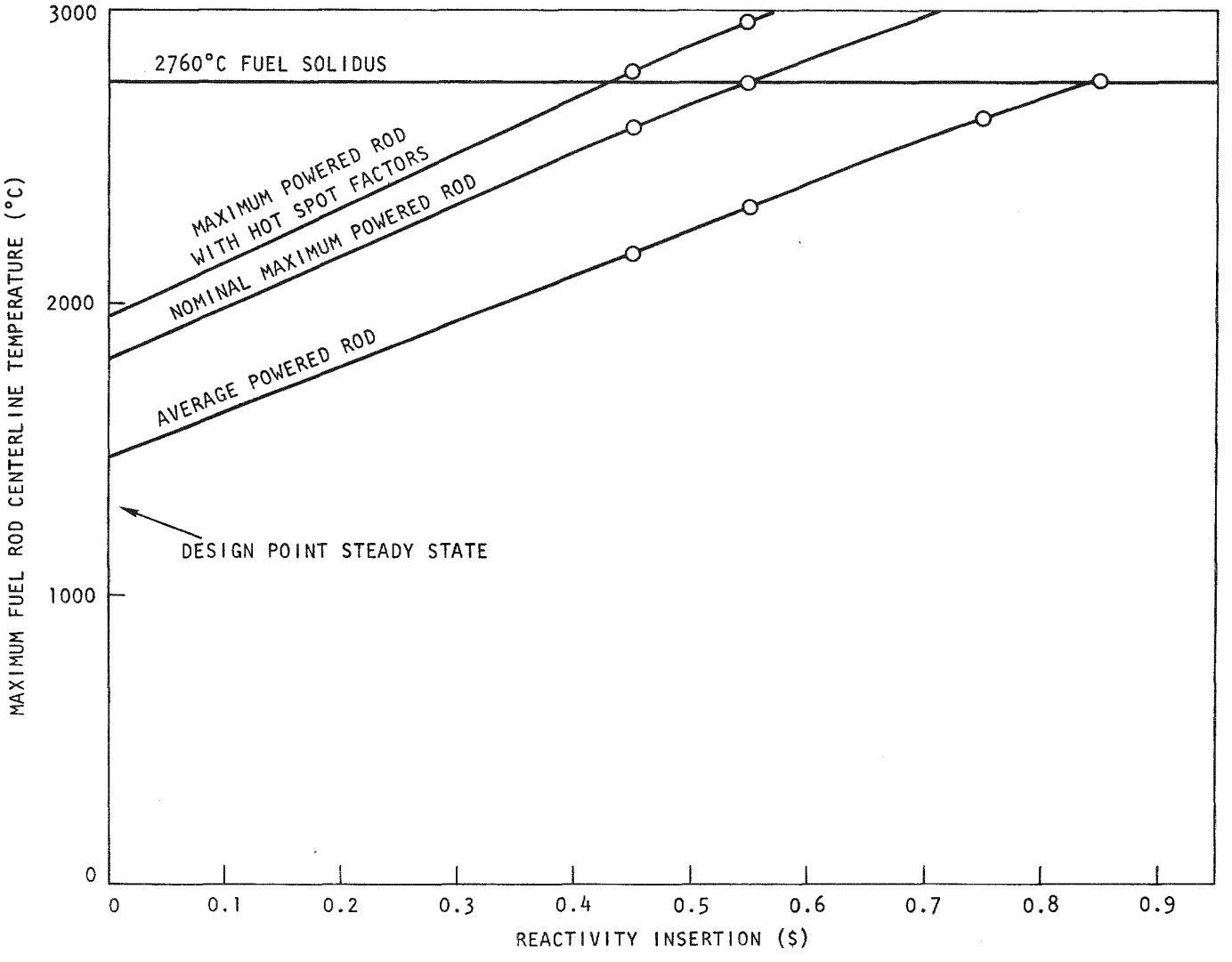

Fig. 12-12. Fuel centerline temperature vs reactivity insertion

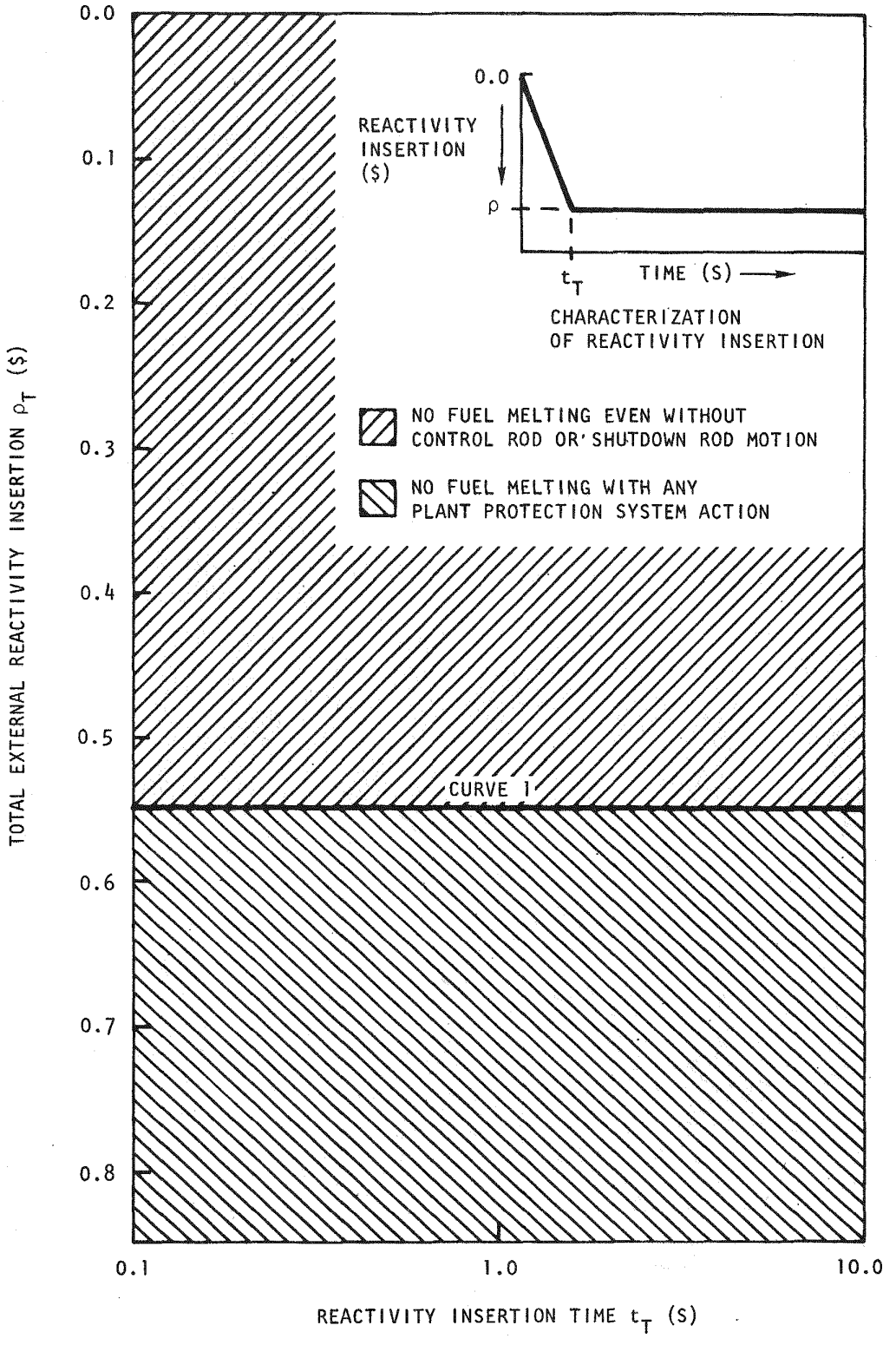

Fig. 12-13. Generalized overpower transient diagram

of the rated reactor power, it is impossible to maintain a constant core inlet temperature for insertions as small as $0.8. Thus, the favorable results in Fig. 12-13 are misleading if the core inlet temperature is allowed to rise. This inlet temperature feedback effect was studied by computer simulation of the largest possible fast insertion ($0.85), postulated to occur nonmechanistically in one-tenth of a second. The simulations, which are based on a conservatively acting PCS which reduces core helium and NSSS feedwater flow, show that the helium assumptions used are reasonble for at least 10 s after the insertion. Therefore, Fig. 12-13 demonstrates that even the relatively slow PPS backup shutdown rods can successfully terminate a reactivity insertion event before the onset of fuel melting.

12.3.4. Aerosol Behavior Analysis

During this quarter, a new work task was initiated to analyze the behavior of aerosols potentially created during core disruptive accidents. The initial objective of this task is to determine the level of effort required or desirable to demonstrate adequate safety margins for the GCFR demonstration plant. Aerosol behavior in the PCRV and the containment will be studied. Initial efforts have concentrated on a review of the LMFBR aerosol research program and a study of the HAARM-2 and PARDISEKO codes.

12.4. POSTACCIDENT FUEL CONTAINMENT

The study of upward heat removal by natural helium circulation under a partial core meltdown condition was reported in Ref. 12-6. During this quarter, further studies on downward heat removal which considered the chemical reactions between the graphite, core, and shielding materials were completed. As a conclusion of the preliminary phase of the PAFC study, a feasibility study of the current 300-MW(e) design has been prepared.

12.4.1. Homogeneous Solution of the Debris Mass

PAFC analyses under this subtask have been based on a stratified model of the molten fuel and the molten stainless steel. However, in the presence

of graphite, chemical reactions to form carbides start at about 1600°C, and the products form a homogeneous compound solution at about 2000°C. Small-scale experiments have been successfully performed by Peehs et al. (Ref. 12-7).

It is assumed that following a postulated full-core meltdown in the 300-MW(e) plant, chemical reactions between graphite and the oxide fuel and between graphite and stainless steel occur so that a solution of the mixed carbides is formed. Owing to the uncertainties in the chemical processes and the physical properties of the carbide products, a simple, but conservative, computational model was chosen for the analysis. Chemical reactions are assumed to be completed at the time of accident initiation. The homogeneous solution is initially assumed at its lowest melting point, and heat of fusion is neglected owing to the wide range of the melting temperatures of the constituents. The initial configuration, in which the homogeneous solution is contained in a crucible formed by the excess graphite in the lower shield, is shown in Fig. 12-14. The analysis was performed by using the Kulacki and Goldstein correlation (Ref. 12-8) for the internal convection in the homogeneous solution and the NUTAP computer code for the numerical solution.

Table 12-3 compares the results of the homogeneous solution model and the stratified model. Two lower melting point temperatures were chosen for the homogeneous solution. The time to reach the quasi-steady state is shorter for the homogeneous solution model because of the comparatively smaller solid thickness of the remaining lower axial shield, which permits more effective downward heat removal. It is surprising that the downward heat flow for the homogeneous solution model is even smaller than that for the stratified model. This is because the homogeneous solution has a lower melting point temperature. For a lower melting point, the heat balance requires thinner crusts at the upper and lower boundaries of the fluid layer, and hence a more violent fluid motion is permitted in the thicker fluid layer to transfer a larger fraction of heat upward.

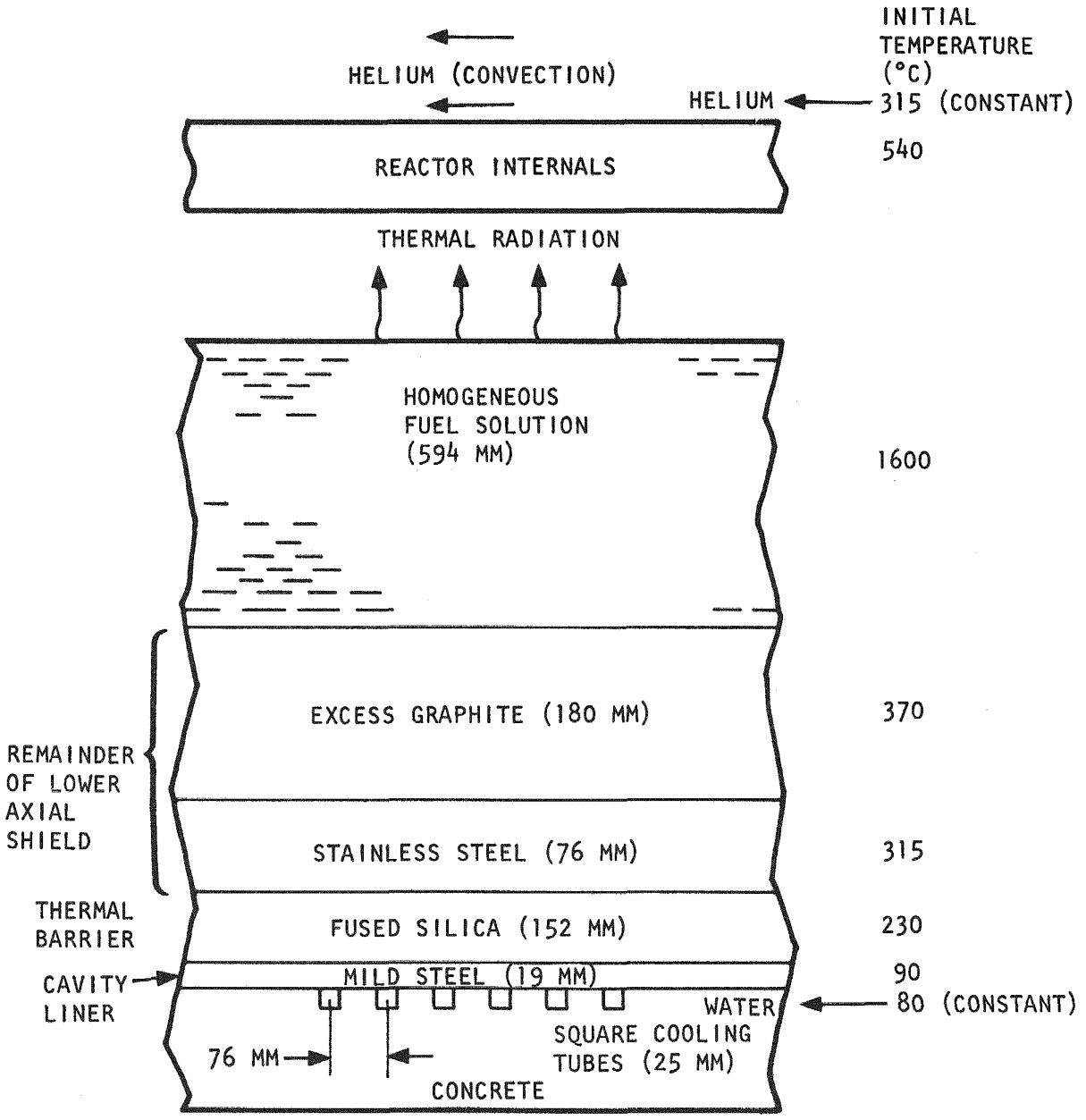

Fig. 12-14. Computational model for the analysis with the homogenous fuel solution

TABLE 12-3
COMPARISON OF ANALYTICAL RESULTS USING EITHER
THE HOMOGENEOUS SOLUTION MODEL OR
THE STRATIFIED MODEL

	Homogeneous Solution		Stratified Model
Melting point of fuel mixture (°C)	1600	2400	3100
Time to reach quasi-steady state (hr)	13	24	40
Maximum downward heat flow (MW)	0.74	1.2	1.4
Fraction of downward heat flow	0.14	0.25	0.33
Maximum cavity liner temperature (°C)	136	170	184
Bottom stainless steel casing of lower axial shield	Molten	Molten	Molten
Fused silica layer (152-mm thick)	Intact	25% molten	40% molten

Maximum cavity liner temperatures for the homogeneous solution model are even lower than those for the stratified model, indicating that at least the homogeneous carbide solution can be effectively contained in the reactor cavity without breaching the lower portion of the cavity liner. However, for both models, the bottom stainless steel casing of the lower axial shield is molten because of the thick, 152-mm fused silica thermal barrier. Therefore, mechanical means must be provided to prevent the graphite blocks from floating unless the thickness of the fused silicon thermal barrier can be reduced.

Because of the uncertainties in the physical properties of the homogeneous solution as well as in the thicknesses of the material layers involved in the analysis, a parametric study was made; the results are shown in Table 12-4. The base case has the same initial conditions as given in Fig. 12-14 except that the thermal barrier thickness is reduced to 50 mm to ensure that the bottom of the lower axial shield does not melt. The thermodynamic properties of the homogeneous solution, such as thermal conductivity and viscosity, are especially uncertain, and the thicknesses of the homogeneous solution, excess graphite, and fused silica thermal barrier can be varied. Results from the parametric study show that the temperatures at all points in the lower reactor cavity region are insensitive to the thermodynamic property variations in the homogeneous solution except that the fluid temperature itself is slightly influenced. The overall temperature and heat flux distributions seem to be more affected by changes in the material thicknesses in the lower shield and the fused silica thermal barrier.

12.4.2. Generation of Carbon Monoxide From Carbide Formation

During core meltdown, the oxide fuel, stainless steel, and fused silica can react with graphite in the lower shield to form different carbides. If these reactions proceed to completion, a great portion of the decay heat can be absorbed by the endothermic reactions, so that the cavity liner heat load can be reduced. However, significant quantities of the noncondensable CO gas can be released, causing containment pressure buildup and a combustion hazard.

TABLE 12-4
PARAMETRIC STUDY OF THE HOMOGENEOUS SOLUTION MODEL

	Maximum Homogeneous Solution Temperature (°C)	Graphite-Steel Interface Temperature (°C)	Cavity Liner Temperature (°C)	Downward Heat Flux ($W/m^2 \times 10^{-4}$)	Fraction of Downward Heat Flow
Base case[(a)]	1737	1256	179	5.64	0.25
Conductivity of homogeneous solution decreased 25%	1759	1254	179	5.68	0.25
Conductivity of homogeneous solution decreased 50%	1791	1250	178	5.64	0.29
Viscosity of homogeneous solution increased 100%	1754	1266	180	5.80	0.25
Viscosity of homogeneous solution decreased 50%	1722	1247	177	5.60	0.25
Homogeneous solution thickness increased 20%	1736	1250	178	5.64	0.25
Graphite thickness decreased 50%	1736	1383	199	6.80	0.29
Fused silica thickness increased 50%	1737	1351	163	4.75	0.20
Fused silica thickness increased 200%	1751	1501	136	3.17	0.14

[(a)]Conductivity of homogeneous solution = 16 W/m-°C; kinematic viscosity = 0.005 kg/s-m; fused silica thickness = 50 mm; homogeneous solution melting point = 1600°C.

If all the oxide fuel is converted to carbide, about 10,000 kg of CO gas is generated. The equilibrium pressure of the containment can increase from 0.18 to 0.42 MPa, with a partial pressure of CO equal to 0.05 MPa. In the melting process, half of the 152-mm-thick fused silica thermal barrier can melt. If the chemical reaction to form silicon carbide is also considered, the equilibrium containment pressure can reach as high as 0.62 MPa, which is very close to the containment failure pressure of 0.69 MPa.

The completeness of these chemical reactions depends on the interface temperature and the partial pressure of the CO gas. For interface temperatures above 2000°C, it is found that the UO_2-C reaction can reach its completion if the CO gas generated is released to the containment. However, less than 2% of the oxide fuel can be converted to carbide if the CO gas generated remains in the PCRV, even if the interface temperature is above the melting point of UC_2 (2260°C). The thermal barrier thickness was found to be a major factor affecting the fuel-graphite interface temperature. For the 50-mm thick thermal barrier, the interface would never reach the melting point of UC_2. Therefore, the chemical reaction is controlled by a diffusion process, and only 6% of the oxide fuel is converted to carbide. For the 152-mm thermal barrier, the reaction product is molten. The time required to convert all the oxide fuel to carbide is estimated to be in the range 45 to 65 hr after the accident.

The flammability of the CO in the containment was also estimated for several cases, i.e., with or without the inclusion of SiO_2 in the carbide-forming reactions and considering either a uniform gas mixture of air, CO, and helium or only the release of CO to the containment. For each case, the chemical reactions were assumed to reach completion. The results of the calculations showed that the flammability limit of the CO content would be exceeded in each of the above cases.

In conclusion, the chemical reactions to form carbides are generally not desired owing to the CO generated. It was found that the chemical reaction reaches only 2% of its completion if there is no leak to the containment or the system is still fully pressurized. If there is a leak to the containment,

these reactions can still be controlled by lowering the temperature in the reaction zone. One way of doing this is by reducing the thermal barrier and the lower shield thickness; the other way is to allow some low-melting-point sacrificial material to form a compound solution with the oxide fuel so that a low temperature pool can be obtained.

12.4.3. Feasibility of the PAFC for the Current Design

During this quarter, a PAFC feasibility study on the current 300-MW(e) design was completed. The PCRV with its thick concrete wall, steel liner, cooling system, and massive shielding inside the reactor cavity offers an excellent natural crucible for containing the molten core debris. Following a core meltdown accident, the lower shield plus the thermal barrier function as a multilayered barrier against melt-through. A moderately enhanced cavity liner cooling system removes the downward-flowing heat; the use of either forced helium convection with one CACS loop or natural circulation of helium removes the upward-flowing heat. Even if the cavity liner is breached, the massive PCRV still serves as a vast heat sink and can provide for an extended delay of melting through the concrete vessel, so that a less demanding approach to ex-vessel fuel containment can be considered.

It appears advantageous to choose an optimum quantity of the shielding material and an optimum thickness for the thermal barrier so that the lower shield can be kept sufficiently cool to prevent fuel boiling, generation of large amounts of CO gas, and flotation of the graphite blocks. With the optimum lower shield and thermal barrier, the advantages of storing the initial decay heat, reducing the heat flux and cavity liner temperature, and offering a sufficiently long grace period without cooling are still retained.

Owing to the opposing thermal barrier thickness requirements under normal operating conditions and PAFC conditions, the fused silica thermal barrier can be split into two parts, with the upper barrier located above the lower main shield. The thickness of the lower barrier can be determined by PAFC conditions, and the two parts combined can function as the original thick barrier for normal operating conditions.

A more uniform temperature in the cavity liner to prevent liner buckling can be obtained by reducing the tube spacing and choosing an optimum liner thickness. Lateral heat transfer in the liner can also be enhanced by cladding the inside of the cavity liner with a high-conductivity metal. Theoretically, CO gas generation can be controlled by reducing the lower shield and thermal barrier thicknesses; however, CO generation may still be caused by (1) local hot spots resulting from uncertain lower fuel crust conditions or (2) rapid transient effects. Therefore, a nongraphite shielding material, e.g., boron nitride, may have to be considered.

The wraparound section of the lower shield must be thick enough to protect the side portion of the reactor cavity liner from hot spots and to provide sufficient volume for containing the molten core debris without reducing the main helium path. Conduction heat transfer inside the radial shield can be enhanced by reducing its internal gaps. Convection heat transfer can also be enhanced, if necessary, by adding cooling fins in the axial direction.

In the current design, the lower end of the radial shield is the most critical location and would melt first owing to thermal radiation from the molten core pool. This condition can be improved by relocation of the radial shield. Melting of the lower steel tip of the radial shield can be allowed if more containing space is provided in the lower shield. However, the graphite blocks must be interlocked with each other to prevent mechanical failure of the radial shield.

Natural convection in helium cooling loops and water cooling loops can provide a completely passive means of cooling. Therefore, the reliability of the cooling systems can be greatly increased. A preliminary study has indicated that increasing the elevation difference between the core auxiliary heat exchangers and the auxiliary loop coolers would make heat removal entirely by natural convection.

Prevention of molten fuel flowing through the refueling penetration in the lower shield and the PCRV lower head can be accomplished by the engineering design of the lower reactor cavity. Some feasible methods of doing this are (1) employing stepped gaps to avoid any straight flow path; (2) using high-melting-point cover plates to protect the top portion of the refueling penetrations; and (3) using a low-melting-point., high-density metal such as lead to cover the gap so that these gaps can be filled by the melt of this material to avoid further penetration of the less dense molten fuel. A modified configuration of the lower reactor cavity based on the natural crucible concept for PAFC and the above discussion is shown in Fig. 12-15.

12.5. LICENSING SUPPORT AND INTEGRATION

As part of the licensing support activity, the CRBR licensing proceedings are being monitored in order to obtain guidance on Nuclear Regulatory Commission (NRC) positions with respect to core disruptive accidents in fast reactors. The CRBR plant safety margin licensing requirements and the types of analyses required to establish compliance with these requirements are being evaluated to provide a direction for the scope of the analyses required on beyond design basis accidents for the GCFR demonstration plant.

12.6. ENGINEERING RELIABILITY INTEGRATION

During FY-74, -75, and -76, efforts were directed toward the adoption and application of probabilistic techniques to the analysis of accident sequence risks for the GCFR (see Section 12.2). Quantification of these accident sequence probabilities was performed by assigning generic failure data to GCFR components and systems. For portions of the GCFR plant which employ conventional systems or components, these assignments can be made with reasonable confidence. For portions of the plant which employ new systems or components, those assignments are made with greater uncertainty. The objectives of the work performed under this subtask are to identify, develop, and apply the engineering and analytical methods necessary to help reduce the uncertainty of new design items.

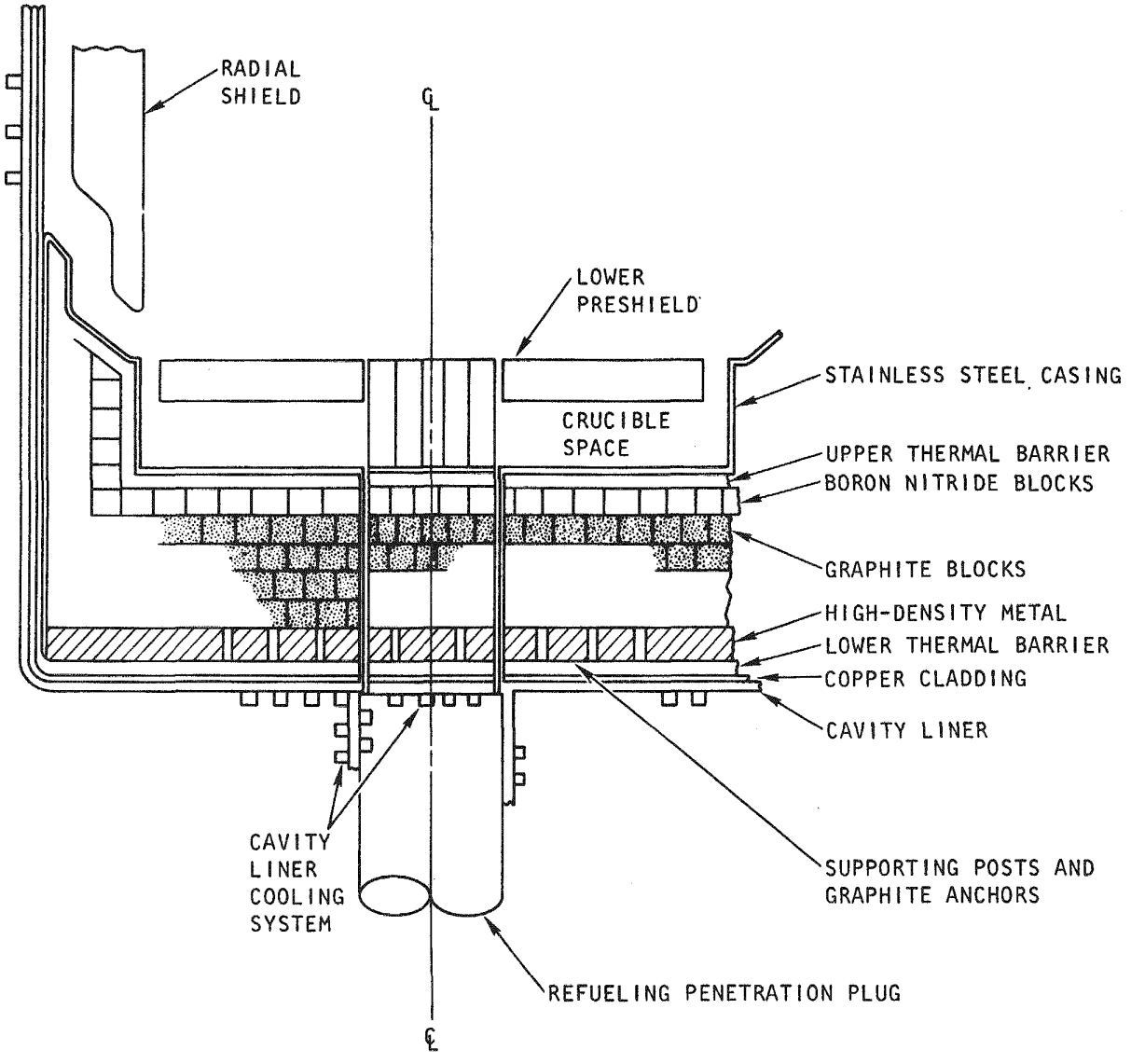

Fig. 12-15. Modified configuration of the low reactor cavity for postaccident fuel containment

This subtask was established late in the quarter, and initial efforts were directed at establishing the subtask work scope and objectives. Therefore, no technical progress is reported for this quarter.

REFERENCES

12-1. "Gas-Cooled Core Disruption Accidents," Argonne National Laboratory Report ANL/RAS/GCFR-76-1, November 1976.

12-2. "GCR Accident Initiation and Progression Analysis - Progress Report for the Period February 1 Through June 30, 1974," USAEC Report GA-A13094, General Atomic, October 8, 1974.

12-3. Kelley, A. P., Jr., "Gas-Cooled Fast Breeder Reactor Accident Initiation and Progression Analysis Progress Report for the Period July 1, 1975 Through June 30, 1976," General Atomic, to be published.

12-4. "Reactor Safety Study - An Assessment of Accident Risks in U.S. Commercial Nuclear Power Plants," NRC Report WASH-1400, October 1975 (NUREG-75/014).

12-5. Buckley, D. W., "TDAC - An Analytical Computer Program to Calculate the Time-Dependent Radiological Effects of Radionuclide Release," General Atomic, unpublished data.

12-6. "Gas-Cooled Fast Breeder Reactor Quarterly Progress Report for the Period August 1, 1976 Through October 31, 1976," ERDA Report GA-A14112, General Atomic, November 1976, Section 12.2.

12-7. Peehs, M., et al., "Experimental Investigations on the Compatibility of a SNR-Type Corium with Graphite," Paper Presented at the International Meeting on Fast Reactor Safety and Related Physics, Chicago, Illinois, October 1976.

12-8. Kulacki, F. A., and R. J. Goldstein, "Thermal Convection in a Horizontal Fluid Layer With Uniform Volumetric Energy Sources," J. Fluid Mech. 55, 271-287 (1972).

13. GCFR SAFETY TEST PROGRAM (189a No. 00588)

ERDA has placed the responsibility for coordination of the National GCFR Safety Test Program with GA. GA will review and direct the program so that it is responsive to the safety test needs and identifies new test needs for which test plans must be proposed and implemented on a time scale which is consistent with GCFR program needs.

13.1. GRIST-2 PROGRAM

The GRIST Program is being developed by ERDA, ANL, EG&G, and GA as a follow-on to analytical and experimental programs being conducted under the LMFBR and GCFR programs. The GRIST program has the objective of going beyond design basis accidents and, in particular, investigating the behavior of melted cladding and fuel. The GCFR Safety Program Review Committee has reached the consensus that GCFR fuel tests in a transient facility are needed to investigate fuel behavior during unprotected loss of flow and reactivity insertion transients. Acting on this recommendation, ERDA has directed that work commence on a transient GCFR test facility (to be known as GRIST-2). This program has a high priority and will replace work previously scheduled for the steady-state GCFR loop program in the engineering test reactor (ETR) (GRIST-1).

During this quarter, EG&G, Idaho, issued a conceptual design plan for the GRIST-2 facility (Ref. 13-1) based on preliminary test facility requirements submitted by ANL and GA. EG&G has proposed either a blowdown or a circulating loop facility to be installed at the TREAT upgrade reactor. The design will be developed to accommodate test bundle sizes of up to 37 fuel rods of prototypic length, including simulation of the axial blankets. Based on transient analysis performed at ANL, a maximum full-flow test time of 15 s has been proposed. For this condition, the blowdown facility is

estimated to have a 10% cost advantage compared with a circulating facility. GA has reviewed the GRIST-2 conceptual design plan and has listed its major concerns (Ref. 13-2) as described below.

13.1.1. Fuel Preconditioning Burst Concept

EG&G has proposed the use of a preconditioning power burst followed by a relaxation time to establish the initial temperature distribution in the test bundle. The phenomenological uncertainties for postulated reactor transients with failure to scram which form the primary justification for an in-pile test program relate to the transient phase where melting and relocation of fuel and cladding occur. The transient phase prior to cladding or fuel melting can be analytically predicted during an accident sequence as well as during a test. Therefore, it is justifiable to combine the premelting test phases in a way which suits the limitations imposed by current and near-term test reactors. However, such a nonprototypic preconditioning phase must establish the temperature distribution in the entire fuel bundle, including the axial blankets, at the time that fuel or cladding melting begins.

The preconditioning burst concept is capable of reproducing the radial temperature distribution in a fuel pin but may result in a rather symmetric axial temperature distribution over the length of the fuel and axial blankets. In the GCFR at full power, the lower axial blanket operates at a temperature which is approximately 250°C hotter than that for the upper axial blanket. During the accident phase prior to cladding or fuel melting, this temperature difference is increased. The preconditioning burst concept may not establish this nonsymmetric axial temperature distribution in the fuel bundle. During unprotected loss of flow accidents, the temperature difference between the upper and lower axial blanket may have an important influence on the motion of molten fuel and cladding in the blanket region.

Recent out-of-pile experiments and analyses at ANL have shown that the depth of penetration and the refreezing mode of molten fuel into

simulated blanket bundles is sensitive to the temperature of the bundle. In addition, the potential for cladding refreezing and the depth of molten cladding penetration prior to refreezing will be influenced by the higher temperature of the lower axial blanket. During reactivity insertion transients, the molten fuel is ejected from the pin and swept out of the bundle in the downward direction. This fuel sweep-out behavior may also be influenced by the higher temperature of the lower blanket region. Based on these considerations, it is concluded that the test preconditioning phase is important for establishing the temperatures calculated to exist in the upper and lower axial blanket regions at the time that cladding or fuel melting begins.

The LMFBR test program in TREAT (particularly the R test series) made extensive use of the "flat top" preconditioning concept. The power is initially raised to about twice the nominal power density and maintained for several seconds. Power is then reduced to about the nominal power density for an additional few seconds prior to reaching initial melting conditions. This mode of operation appears inherently better able to establish the higher temperature condition in the lower axial blanket prior to fuel or cladding melting.

An alternate mode of preconditioning consists of an extended low-power low-flow phase to establish the overall axial temperature distribution; this phase would be followed by a reduced preconditioning burst to establish the radial temperature profile within the rods. Operation at a small percentage of the nominal flow and power for about 1 min could suffice to establish the axial temperature profile.

It is recommended that these and possibly other preconditioning modes be considered with respect to their ability to establish the axial and radial temperature distribution which is predicted to exist in the fuel rods at the time of initial fuel or cladding melting.

13.1.2. Coolant Flow Requirements

The GRIST-2 conceptual design plan is based on coolant flow requirements derived from three transient calculations performed at ANL. The limiting flow capability is assumed to require a nominal full-power flow rate through a 37-rod bundle for 15.5 s. GA considers these transients to be among the most rapid transients of interest for testing in each of the accident categories. The probabilistic accident analyses performed at GA indicate that initiating events resulting in such rapid transients are of significantly lower probability than accident initiators which result in much slower transients.

13.1.3. Unprotected Loss of Flow Accidents

Loss of feedwater to the steam generators with failure to scram has been identified as a relatively high-probability initiator for an unprotected loss of flow accident. Preliminary analysis of an unprotected loss of feedwater accicent indicates a coolant flow history as shown in Fig. 13-1. Up to the time of cladding melting, the reactor power either remains at 100% or decreases somewhat, depending on the control system action. The positive reactivity effects associated with cladding relocation followed by fuel relocation may then introduce a power transient similar to those calculated by ANL for unprotected loss of flow accidents. Slower loss of flow accidents do not necessarily result in increased coolant flow requirements, since the preconditioning phase must establish only the temperature distribution in the fuel bundle at the time of initial cladding melting. However, the slower loss of flow transients need to be considered to assure that their requirements fall within the test capability.

13.1.4. Unprotected Depressurization Accidents

All depressurization accidents with failure to scram have been shown to be of significantly lower probability than the higher-probability loss of flow accident sequences in the pressurized reactor. Therefore, it is

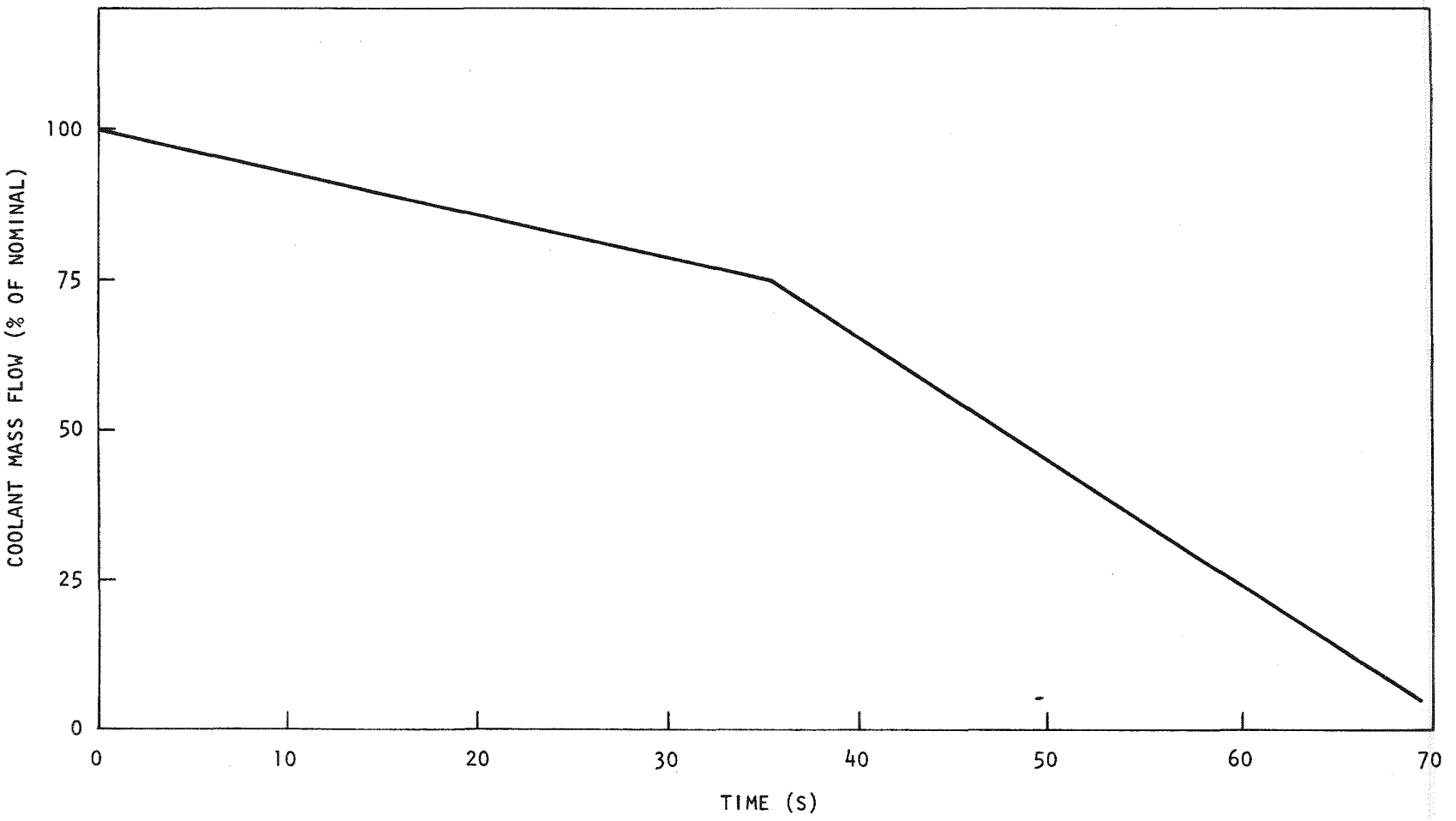

Fig. 13-1. Coolant mass flow rate during a common loss of all feedwater accident with failure to scram

anticipated that the emphasis on test requirements for depessurization accidents with failure to scram can be assigned a significantly reduced priority.

13.1.5. Reactivity Insertion Transients with Failure to Scram

In this category of accidents, inadvertent withdrawal of a control rod has been identified as the highest-probability accident initiator. The average reactivity insertion rate for this event is \$0.35/s, i.e., a factor of 30 lower than the transient upon which the conceptual test plan is based. Figure 13-2 shows fuel temperature, cladding temperature, and reactor power up to incipient fuel melting during an inadvertent control rod withdrawal accident. Accommodation of this transient will be very taxing for the GRIST-2 facility. It may again be possible to condense the premelting accident phase into a more efficient preconditioning test phase. However, for tests with preirradiated fuel, the slow gas release from the fuel and venting from the rods during the premelting phase may have a significant influence on fuel behavior following melting and may impose limitations on the test preconditioning phase. Furthermore, it will be important to provide test facility capability for such slow reactivity insertion rates during the accident phase extending from initial fuel melting to fuel rod failure which may extend over a relatively long period of time. For such slow reactivity ramp rates, internal fuel motion effects and continued slow gas release may influence fuel rod behavior in a manner which could be distinctly different from transients with more rapid reactivity insertion rates.

13.1.6. Conclusions

Loss of flow and reactivity insertion transients which are significantly slower than those used as the basis for the GRIST-2 conceptual design plan should be studied and accommodated by the GRIST-2 test capability. The need for a slow transient test capability is derived from probabilistic accident analyses which have shown that in the GCFR the most likely initiating events leading to core melting result in these slow transients. Such slower

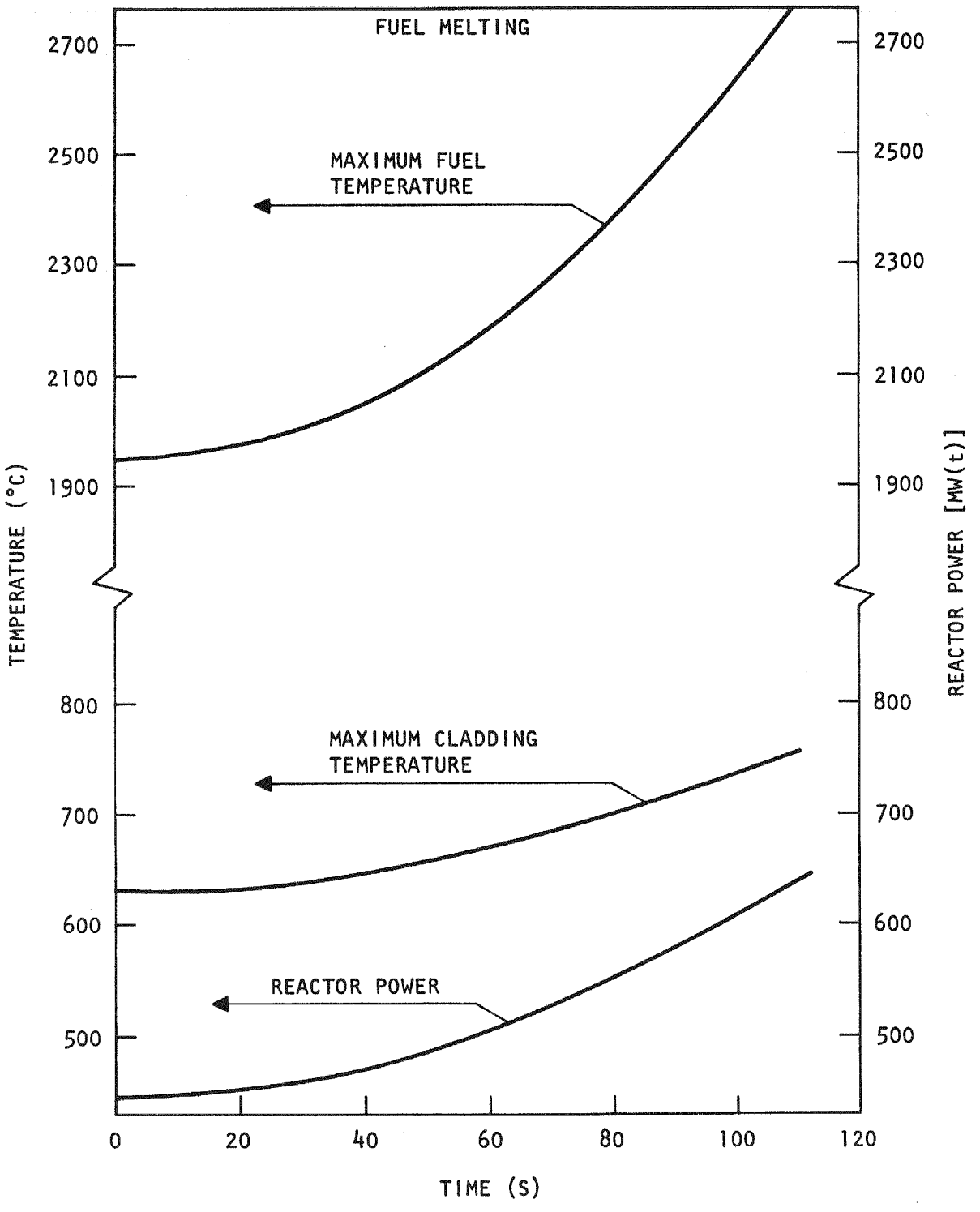

Fig. 13-2. Maximum fuel and cladding temperature and reactor power up to initial fuel melting during an inadvertent control rod withdrawal accident with failure to scram

transients may require a coolant flow capability up to ten times larger than that provided for in the GRIST-2 conceptual design plan. Such an increased flow capability may be more economically provided by a recirculating loop facility rather than a blowdown facility. The inability of the GRIST-2 facility to accommodate such slower transients would, in the opinion of GA, significantly reduce the useful contribution which this facility can make toward establishing the important fuel safety features of the GCFR design.

Resolution of these concerns was accomplished at a meeting at EG&G, Idaho, during January through review of the EG&G proposed GRIST-2 facility requirements (Ref. 13-3).

13.2. DUCT MELTING AND FALLAWAY TEST PROGRAM

An out-of-pile test program has been initiated at the Los Alamos Scientific Laboratory (LASL) to investigate assembly duct melting and fallaway phenomena during a loss of decay heat removal accident. GA is defining the test objectives, criteria, and requirements, and LASL will develop a test program plan. Development of objectives, criteria, and requirements for the duct melting and fallaway test (DMFT) program is nearing completion, and issuance is expected shortly.

Coolant flow capability is required to preheat the test bundle to the desired initial condition. It is thus desirable to maintain flow requirements at a minimum since for the actual tests, no flow is required. Various preheat procedures have been analyzed to determine the most efficient procedure. Based on a review of initiating events, a rapid loss of flow design basis event was selected for DMFT simulation, and a procedure was developed to preheat the DMFT test assembly to the initial temperature appropriate to the event.

The initiating event selected was a loss of forced circulation. All small circulator turbine control valves are postulated to be closed during

normal operation owing to a fault in administrative procedures. The event is initiated by a spurious reactor trip which automatically causes all large circulator turbine control valves to close. It is postulated that the small control valve cannot be opened. The large and small closed circulator turbine control valves cause the circulator turbine to coast down to a small percentage of design point rpm within tens of seconds. About 40 s after reactor trip, the forced-convection pressure drop in high-powered fuel assemblies decreases to a level comparable to the natural buoyancy forces; thus, the downward flow is conservatively assumed to end.

At the assumed time of flow stoppage (i.e., 40 s), the core axial temperature profile is not the nominal full-power steady-state distribution. It is desired to have the calculated core condition at 40 s be equal to the DMFT initial condition. A preheat procedure was developed for the DMFT which achieves this goal using a constant helium flow with variable fuel rod power. This procedure is expected to minimize DMFT costs since flow control is the simplest possible strategy (e.g., on then off, once). The power is already required to be variable in order to simulate the decay heat power generation transient.

Two reference preheat procedures were developed, one at a flow rate of 1.4% of the nominal full-power flow rate and the other at 0.7% flow. It was necessary to develop a power versus time relation for each flow rate which would result in an acceptable temperature distribution. The coolant temperature at the test bundle entrance is assumed to be 320°C. For the 1.2% flow case, the power is raised to 2% of nominal and held constant for 300 s. Then, the power is raised to 5.4%, and after 25 s, the axial temperature distribution shown by the solid lines in Fig. 13-3 is achieved in the test bundle . The dashed lines in the figure are the desired temperatures for the initial test condition. Note that the cladding temperature and the fuel temperature adjacent to the cladding are within about 20°C of the desired temperature. Also note the excellent correlation in helium temperatures. The MINGAF and GAFTRN-II computer codes used in this study do not explicitly model the duct walls, but the excellent

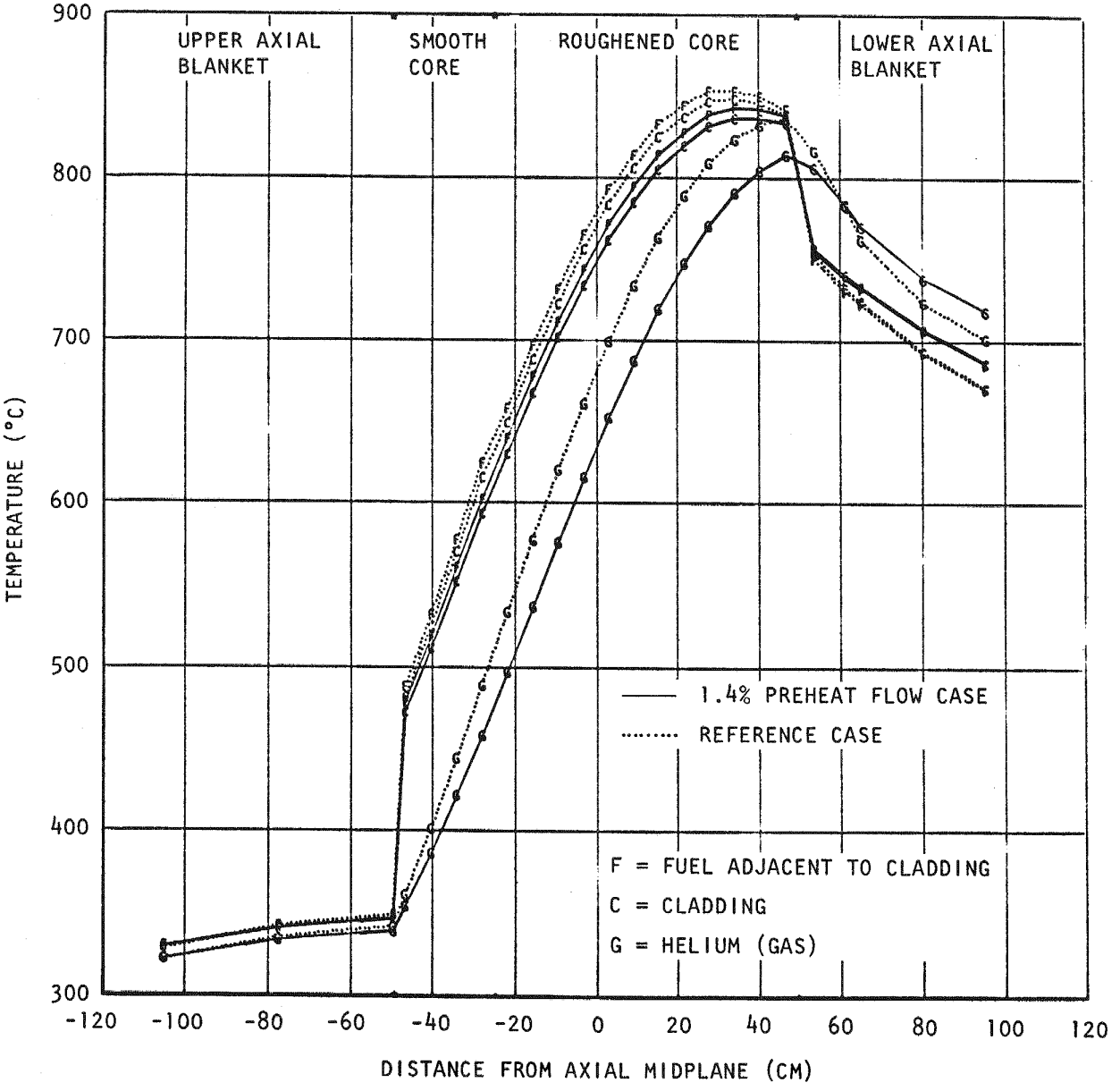

Fig. 13-3. Axial temperature distribution for the 1.4% flow preheat transient (at +25 s)

agreement of the fuel, cladding, and gas temperatures suggests that the duct wall correlation should also be acceptable.

The lower-flow preheat procedure was developed to test the sensitivity of the final temperature distribution to preheat flow rates. The power history is optimized at 0.7% for 400 s followed by 3.0% for 60 s. The resulting temperature distribution is shown as the solid lines of Fig. 13-4 and compared with the desired distribution, shown as the dashed lines.

It is concluded from this analysis that acceptable initial temperature distributions can be achieved in the DMFT by preconditioning procedures requiring less than 2% of the nominal full-power coolant flow rate.

REFERENCES

13-1. Arbtin, E., "Transmittal of the GRIST-2 Conceptual Design Plan and Supporting Documents - ARB-44-76, Rev 1," EG&G, Idaho, private communication.

13-2. Broido, J. H., "Review of GRIST-2 Conceptual Design Plan," General Atomic, private communication.

13-3. Arbtin, E., "GRIST-2 Facility Requirements, ARB-52-76," EG&G, Idaho, private communication.

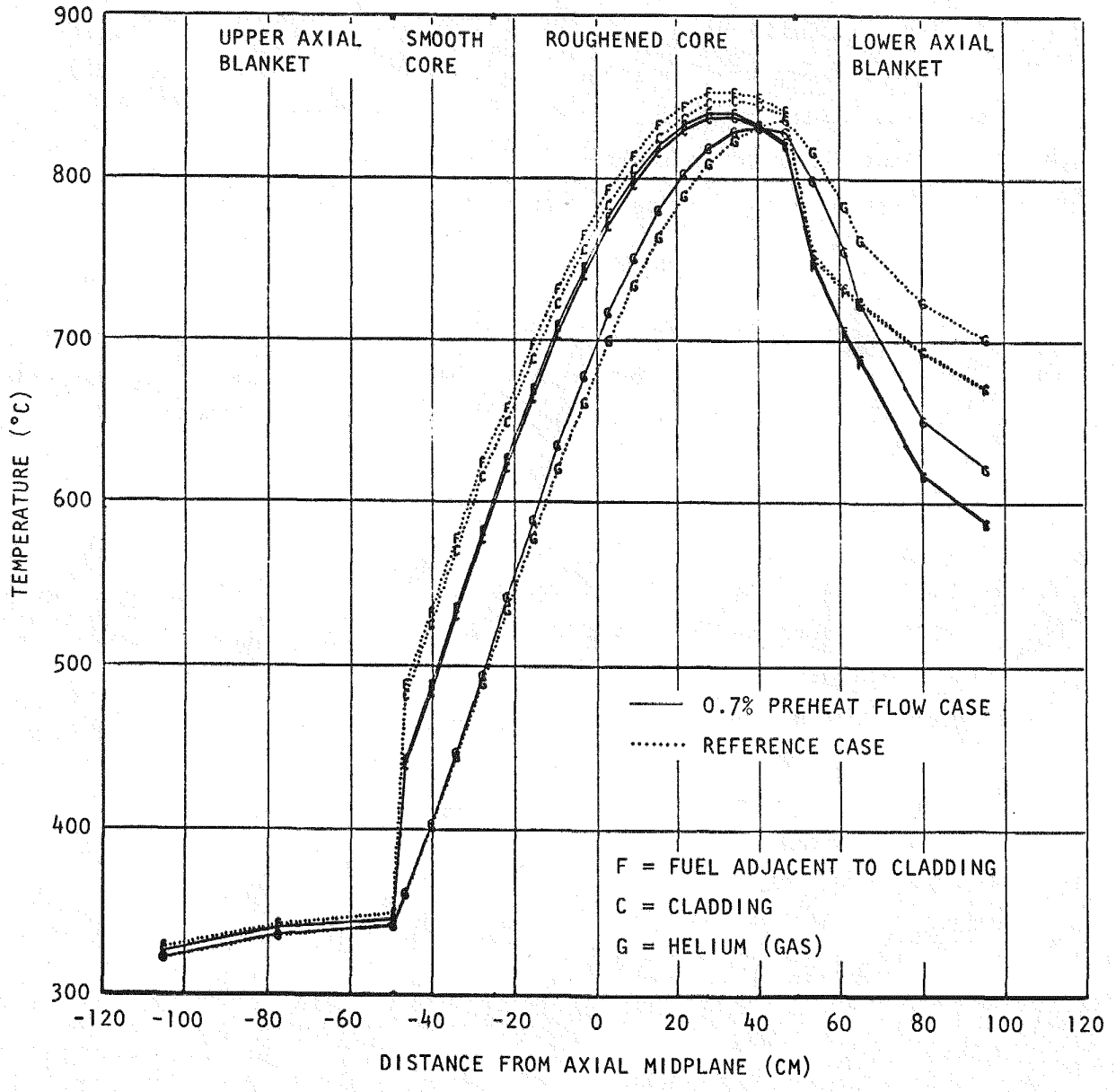

Fig. 13-4. Axial temperature distribution for the 0.7% flow preheat transient (at +60 s)

14. GCFR NUCLEAR ISLAND DESIGN (189a No. 00615)

14.1. GENERAL ARRANGEMENT AND SYSTEMS

The purpose of this subtask is to provide the general arrangement of the nuclear island so that the feasibility of several nuclear island concepts can be established together with the major dimensions of the buildings. Conceptual design information has been supplied for specific areas of the containment structure to enable preparation of preliminary piping and equipment layouts for the evaluation of alternate designs.

Plant arrangement studies have resulted in preliminary sketches showing the arrangement of major structures and a facility plan. These sketches were based on earlier work performed by Bechtel Corporation (Refs. 14-1 through 14-3) as well as review of other nuclear plant arrangements. The major changes from the Bechtel arrangement were

1. The reactor auxiliary building was combined with the reactor service building in a single Seismic Category I structure.

2. The procedure for removal and replacement of helium circulators and steam generators was modified and simplified.

The preliminary sketches are being reviewed by the applicable technical groups and will be issued upon resolution and/or incorporation of their comments.

14.2. STRUCTURAL DESIGN

The purposes of this subtask are to perform the necessary design of the nuclear island, participate in the layout of equipment in the containment,

service, and auxiliary buildings, and take part in the support efforts required for assuring the feasibility of the nuclear island.

During the previous quarter, a review was made of Bechtel's studies (Refs. 14-1, 14-2) to determine their recommendations for the nuclear island buildings. Equipment and component lists were compiled for each of the buildings. A preliminary plant layout criteria (PLC) list was reviewed by cognizant engineers for component identification and updating. Additional PLC drawings are being drafted, and the equipment and components for each of the buildings are being examined to determine requirements and locations. The requirements for the piping/instrumentation and process flow diagrams were evaluated to determine the diagrams which are necessary for the nuclear island facility.

Two PCRV design approaches have been taken: one with a resuperheater and one without. A cost study has been initiated to evaluate the two designs. A decision on the resuperheater is scheduled to be made in March 1977. At present, layouts and isometric drawings are being developed for the main steam piping loops with the resuperheater. A stress analysis of the piping loops has been initiated.

A contract was let on August 27, 1976 to Nuclear Services Corporation, Campbell, California, for a feasibility study of the access opening through the haunch of the containment building. This contract is due to be completed by January 15, 1977. Nuclear Services reports that the three-dimensional finite-element model for local analysis has been set up.

A contract was also let to Kellex Power Services, San Diego, California, a division of Pullman-Kellogg, on September 9, 1976 for a piping cost study of the resuperheater versus the nonresuperheater. The contract was completed September 30, 1976. Pullman-Kellog reported a $314 K saving using a nonresuperheater.

REFERENCES

14-1. "300 MW(e) Gas Cooled Fast Breeder Reactor Balance of Plant Preliminary Engineering and Cost Estimate," Bechtel Job 10437, August 1973.

14-2. "300 MW(e) Gas Cooled Fast Breeder Reactor Balance of Plant Follow-on Study," Bechtel Job 10437, November 1973.

14-3. "750 MW(e) Gas Cooled Fast Breeder Reactor Balance of Plant Preliminary Engineering and Cost Estimate," Bechtel Job 10437-004, October 1974.

15. GAS-COOLED REACTOR RELIABILITY DATA BANK (189a No. 00617)

The function of the data bank is to obtain, supply, and store reliability data estimates in support of the probabilistic accident analysis performed under the GCFR and HTGR probabilistic accident and risk analysis tasks.

15.1. GCFR CRITICAL DATA NEEDS

As a result of preliminary probabilistic risk studies on the GCFR, a list of components and subsystems which require reliability data for quantification of residual heat removal system reliability has been generated. This list is divided into two groups: (1) components and systems considered to be generic equipment in nuclear and fossil-fired power plants and other industries (principally secondary steam cycle equipment); (2) components and systems unique to gas-cooled reactors for which generic data assignments may be inappropriate. Reliability data for the first group of components are available from many sources, but the major sources for nuclear power plant risk assessment are Refs. 15-1 through 15-3 because of their large data base and updating. Reliability data for the second group are more difficult to obtain, and in many cases must be analyzed for their applicability to gas-cooled reactor conditions.

The steam-driven helium circulators and gas isolation valves have the least amount of long-term operating experience in the U.S., and special efforts are being made to obtain data from Systems Reliability Service (SRS) on British operating experience with some gas-cooled reactor components. One of the major accomplishments of the last quarter was a meeting with SRS personnel in England. Gas-cooled reactor reliability data needs were discussed, and SRS agreed to provide GA with specific information on primary coolant circulators and gas isolation valves. The output from this data

survey will be a data listing similar to the one in Ref. 15-1, Table III-1, which categorizes various reliability data sources and the total assessed value and range for a variety of components and subsystems found in gas-cooled reactor nuclear power plants. The failure rate median and range can then be combined with mean repair time and periodic test interval information to calculate system unavailabilities.

15.2. COMMON MODE FAILURE DATA

The other data need for GCFR evaluations is for information on common mode or dependent system failures. These data must be compared with normal operating data so that effective β factors (Ref. 15-4) can be determined for each redundant system. A review of data and operating experience with the equipment categories listed in Table 4-3 of Ref. 15-4 is underway; other equipment categories are also being examined.

15.3. DOCUMENTATION OF RELIABILITY DATA

Information from several data sources is maintained by the data bank, which requires updating as new information is received. Sources such as Ref. 15-3 provide periodically updated reports on equipment failures and nuclear power plant operating experience. These sources also supply material used to review and update reliability data estimates as operating experience in nuclear power plants increases. These documents are stored by the data bank for reference.

REFERENCES

15-1. "Reactor Safety - An Assessment of Accident Risks in U.S. Commercial Nuclear Plants," U.S. Nuclear Regulatory Commission Report WASH-1400 (NUREG-75/014), October 1975.

15-2. "Equipment Availability, Fossil, Component Cause Code Summary Report 1973," Edison Electric Institute, 1974.

15-3. "Operating Units Status Report, Licensed Operating Reactors: Data for Decisions," Nuclear Regulatory Commission Monthly Publication (NUREG-0020-1 to 12, 1976).

15-4. "HTGR Accident Initiation and Progression Analysis Status Report," v. II, ERDA Report GA-A13617, General Atomic, October 1975.